



**National Library
of Canada**

**Bibliothèque nationale
du Canada**

Canadian Theses Service

Service des thèses canadiennes

**Ottawa, Canada
K1A 0N4**

NOTICE

The quality of this microform is heavily dependent upon the quality of the original thesis submitted for microfilming. Every effort has been made to ensure the highest quality of reproduction possible.

If pages are missing, contact the university which granted the degree.

Some pages may have indistinct print especially if the original pages were typed with a poor typewriter ribbon or if the university sent us an inferior photocopy.

Reproduction in full or in part of this microform is governed by the Canadian Copyright Act, R.S.C. 1970, c. C-30, and subsequent amendments.

AVIS

La qualité de cette microforme dépend grandement de la qualité de la thèse soumise au microfilmage. Nous avons tout fait pour assurer une qualité supérieure de reproduction.

S'il manque des pages, veuillez communiquer avec l'université qui a conféré le grade.

La qualité d'impression de certaines pages peut laisser à désirer, surtout si les pages originales ont été dactylographiées à l'aide d'un ruban usé ou si l'université nous a fait parvenir une photocopie de qualité inférieure.

La reproduction, même partielle, de cette microforme est soumise à la Loi canadienne sur le droit d'auteur, SRC 1970, c. C-30, et ses amendements subséquents.

UNIVERSITY OF ALBERTA

NEUROMODULATORY MECHANISMS THAT REGULATE POTASSIUM
CONDUCTANCES IN AMPHIBIAN SYMPATHETIC GANGLIA.

BY

JEFFREY A. ZIDICHOUSKI

A THESIS SUBMITTED TO THE FACULTY OF GRADUATE STUDIES AND
RESEARCH IN PARTIAL FULFILLMENT OF THE REQUIREMENTS FOR
THE DEGREE OF DOCTOR OF PHILOSOPHY.

DEPARTMENT OF PHARMACOLOGY

EDMONTON, ALBERTA

FALL, 1990



**National Library
of Canada**

**Bibliothèque nationale
du Canada**

Canadian Theses Service Service des thèses canadiennes

**Ottawa, Canada
K1A 0N4**

The author has granted an irrevocable non-exclusive licence allowing the National Library of Canada to reproduce, loan, distribute or sell copies of his/her thesis by any means and in any form or format, making this thesis available to interested persons.

The author retains ownership of the copyright in his/her thesis. Neither the thesis nor substantial extracts from it may be printed or otherwise reproduced without his/her permission.

L'auteur a accordé une licence irrévocable et non exclusive permettant à la Bibliothèque nationale du Canada de reproduire, prêter, distribuer ou vendre des copies de sa thèse de quelque manière et sous quelque forme que ce soit pour mettre des exemplaires de cette thèse à la disposition des personnes intéressées.

L'auteur conserve la propriété du droit d'auteur qui protège sa thèse. Ni la thèse ni des extraits substantiels de celle-ci ne doivent être imprimés ou autrement reproduits sans son autorisation.

ISBN 0-315-64860-0

UNIVERSITY OF ALBERTA
RELEASE FORM

NAME OF AUTHOR: Jeffrey Anthony Zidichouski

TITLE OF THESIS: Neuromodulatory mechanisms that regulate potassium conductances in amphibian sympathetic ganglia.

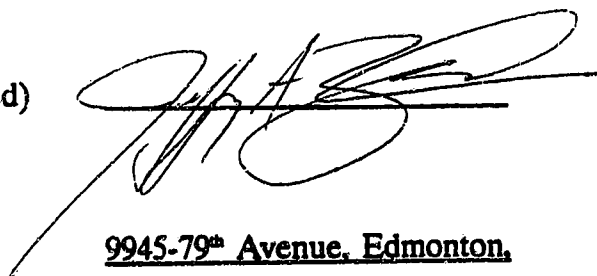
DEGREE: Doctor of Philosophy

DEGREE GRANTED: Fall, 1990

Permission is hereby granted to THE UNIVERSITY OF ALBERTA LIBRARY to produce single copies of this thesis and to lend or sell such copies for private, scholarly or scientific research purposes only.

The author reserves other publication rights, and neither the thesis nor extensive extracts from it may be printed or otherwise reproduced without the author's written permission.

(Signed)



9945-79th Avenue, Edmonton,

Alberta, CANADA T6E 1R3

Dated: September 27, 1990

THE UNIVERSITY OF ALBERTA
FACULTY OF GRADUATE STUDIES AND RESEARCH

The undersigned certify that they have read, and recommend to the Faculty of Graduate Studies and Research, for acceptance, a thesis entitled "Neuromodulatory mechanisms which regulate potassium conductances in amphibian sympathetic ganglia" submitted by Jeffrey A. Zidichouski in partial fulfillment of the requirements of the degree of Doctor of Philosophy in Pharmacology.

P. A. Smith

(Dr. P.A. Smith; supervisor)

[Signature]

(Dr. W.F. Colmers)

[Signature]

(Dr. K. Wong)

[Signature]

(Dr. D. Biggs)

[Signature]

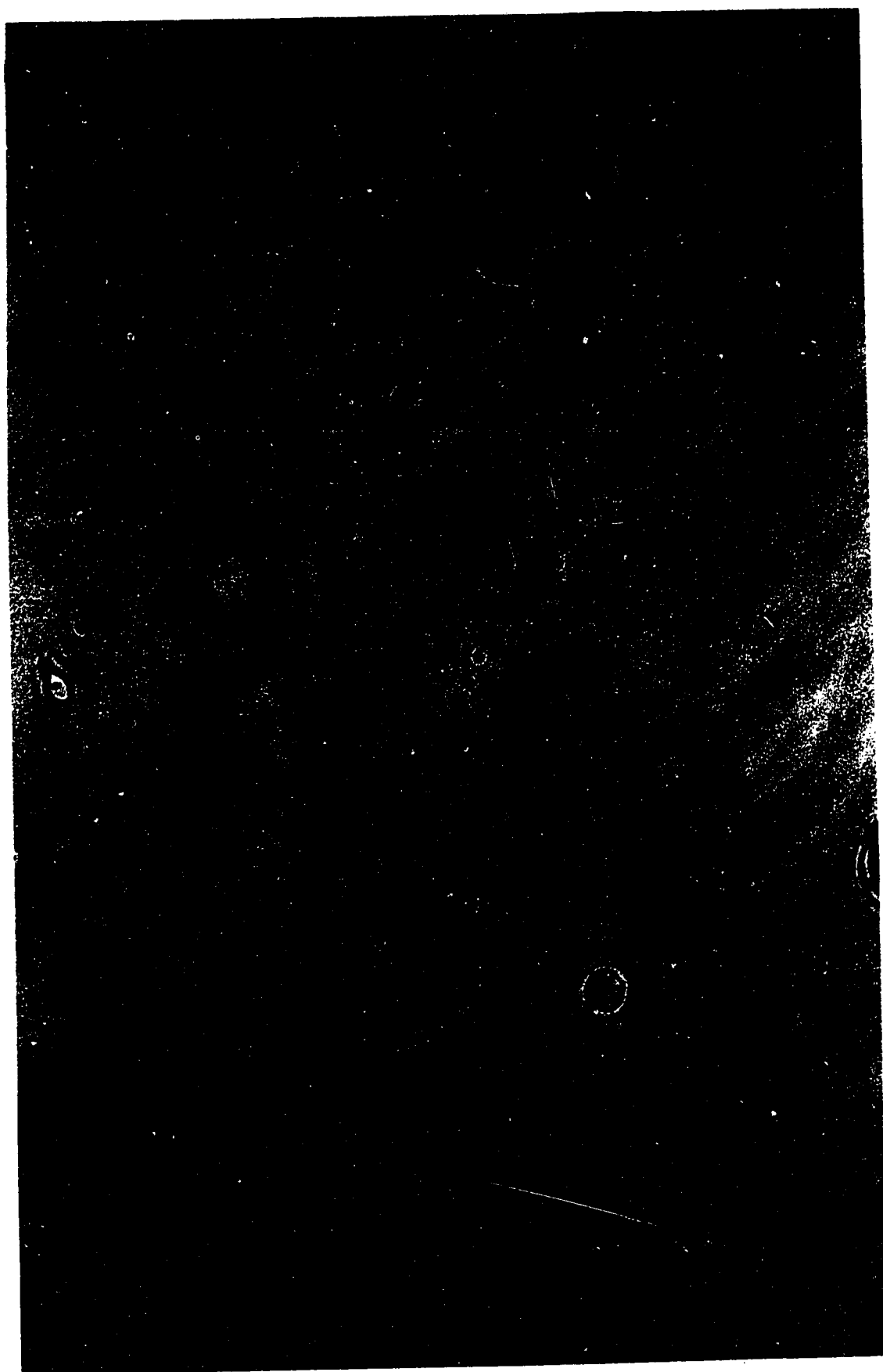
(Dr. W.R. Giles; external examiner)

[Signature]

(Dr. W.F. Dryden; committee chairman)

Date: August 9, 1990

Plate 1. Whole-cell recording from enzymatically dissociated sympathetic neuron. Patch electrode approaches neuron from top. Photograph taken just prior to the establishment of whole-cell recording. Drugs were applied by means of the U-tube (dark region located beneath the cell) method for drug application (Krishtal and Pidoplichko, 1980). 200X's magnification.



ABSTRACT

Whole-cell patch clamp recording (WCR), sucrose-gap recording and radioimmunoassay were used to investigate the mechanism of action of various neurotransmitters and peptides on neurons in Rana pipiens and/or Rana catesbeiana paravertebral sympathetic ganglia. Dissociated neurons were classified as C-cells or B-cells by their size, their responses to agonists and their electrophysiological characteristics.

C-cells were small and lacked a rapid transient outward K^+ current (I_A). Application of muscarine, adrenaline or neuropeptide Y (NPY) induced an inwardly-rectifying K^+ current via the same population of K^+ channels.

B-cells were larger than C-cells and exhibited I_A . Application of muscarine, chicken-II-luteinizing hormone releasing hormone (c-II-LHRH) or adrenaline produced an inward current due to the suppression of a non-inactivating K^+ current (I_M). Since the sum of I_M suppression by the independent addition of two agonists exceeded the available I_M , some M-channels were sensitive to more than one agonist. Isoprenaline and adrenaline augmented I_M in a few ($< 10\%$) B-cells probably via β -adrenoceptor activation.

The M-currents were similar in B- and C-cells; both activated at -75mV and had sigmoidal activation curves that reached a maximum at -30mV . However, the M-current density was greater in C-cells ($1495\mu\text{S}/\text{cm}^2$) than in B-cells ($1034\mu\text{S}/\text{cm}^2$). I_M in C-cells was suppressed by c-II-LHRH but not by muscarine.

The agonist-induced inwardly-rectifying K^+ current and I_M suppression were both generated via a pertussis toxin insensitive, GTP-binding protein. Since drugs that mimic or perturb the actions of cytosolic second messengers had little or no effect on these responses, both are likely mediated by the direct-coupling between the receptor-activated G-protein and the ion channel.

A slowly-inactivating, transient, 4-AP sensitive, Ca^{2+} -insensitive outward K^+ current (I_{SA}) developed during WCR from B- and C-neurons. The activation and inactivation curves for I_{SA} were similar to those for I_A ; however, I_{SA} inactivated about 80 times slower than I_A . Although I_{SA} was easily distinguished from I_A , it could not be clearly differentiated from the delayed rectifier ($I_{K(V)}$). Muscarine reversibly induced this current in cells that were devoid of a measurable I_{SA} . Therefore, effects of agonists on I_{SA} (or $I_{K(V)}$) must be considered when attempting to understand neuromodulatory mechanisms in autonomic ganglia.

ACKNOWLEDGEMENTS

There were many people who were instrumental in obtaining, processing, interpretation and production of the material presented in this thesis.

Firstly, I would like to express my sincerest thanks to Dr. Peter Smith for his belief in me as a scientific investigator, for his ongoing moral support, and for financial support provided during my early years in graduate school. Moreover, I thank for him for his enlightening teachings of the principles of electrophysiology and the scientific method for investigation.

My utmost gratitude to Dr. Alexander Selyanko his conveyance of the intricacies of whole-cell patch clamp recording and for his unselfish collaboration in a large number of experiments reported in this thesis. Again, to Dr. Smith for inviting Dr. Selyanko to work in our laboratory and to the Alberta Heritage Foundation for Medical Research for providing financial support through its Visiting Scientist Program.

To Ms. Mairead Kehoe and Mr. Vicky Wong for their skilled technical assistance in a number of sucrose-gap experiments. To Mr. Hysinyo Chen for his collaboration in the sympathomimetic study on the M-current and NPY experiments, Mr. Balvinder Jassar and Mr. Hysino Chen for performing the phosphatase inhibition experiments. Mrs. Tina Cho for producing graphics and labeling of figures. Greg Morrison for taking photographs, photoprocessing and for the use of his equipment and facilities. Mr. Darin Brox for his expert technical assistance with data and word processing. To the office staff of the Department of

Pharmacology for the use computer and photocopying equipment and particularly to Ms. Kimberley Strome for the typing of tables and equations included within. To the Pharmacology Workshop for ongoing electronic troubleshooting provided by Mr. David Ogden and detailed machine work performed by Mr. Nick Diakiw and Mr. Sam Grazziano.

To Dr. Ken Wong for the use of his laboratory and equipment and for providing useful discussions on the cAMP experiments. Also, to the University of Alberta Central Research Fund for granting necessary funds to support this project. Thanks to my supervisory committee for their suggestions, guidance and patience. I also am indebted to Dr. William Colmers for many useful discussions, for the use of computer and laser printer for reproducing later versions of the thesis and for the kind gift of neuropeptide Y.

Financial support was provided by the Department of Pharmacology through a Graduate Student Assistantship, by a studentship and independent research award from the Alberta Heritage Foundation for Medical Research and a studentship award from the Medical Research Council of Canada.

Last, but certainly not least, to my family. I thank my wife Valerie for her continuing and unconditional support during the course of these studies and for providing the detailed anatomical and schematic drawings contained within. To my son Aaron for inspiring the completion of this thesis. To my parents for instilling an inquisitive nature, the desire to discover, and the edification of others.

TABLE OF CONTENTS

<u>CHAPTER I</u> - INTRODUCTION	1
1. NEUROMODULATION	2
2. CHOICE OF MODEL FOR STUDY	3
3. PHYSIOLOGY AND PHARMACOLOGY OF SLOW POST-SYNAPTIC POTENTIALS IN SYMPATHETIC GANGLIA	4
3.1. SYNAPTIC ORGANIZATION	4
3.2. SYNAPTIC POTENTIALS IN AMPHIBIAN SYMPATHETIC GANGLIA	7
3.2.1. Slow Synaptic Potentials	8
a) s-EPSP	8
b) late-slow-EPSP	11
c) s-IPSP	13
4. THE ROLE OF K ⁺ CHANNELS IN NEUROMODULATION	15
4.1. DELAYED RECTIFIER	17
4.2. A-CURRENTS	17
4.3. I _M	19
4.4. CALCIUM-DEPENDENT K ⁺ CURRENTS	21
4.4.1. I _C	21
4.4.2. I _{AHP}	22
4.5. I _H	24
5. POSSIBLE TRANSDUCTION MECHANISMS FOR MODULATION OF ION CHANNEL FUNCTION	25

5.1.	G-PROTEINS	--
5.2.	TESTING AND IDENTIFICATION OF PUTATIVE TRANSDUCTION MECHANISMS	29
6.	RATIONALE AND STATEMENT OF THE PROBLEM ...	30
CHAPTER II - MATERIALS AND METHODS		34
1.	ELECTROPHYSIOLOGICAL TECHNIQUES	35
1.1.	SUCROSE-GAP EXPERIMENTS	35
1.1.1.	Theory	35
a)	Introduction	35
b)	Electrical modelling	37
1.1.2.	Experimental Preparation and Dissection	45
1.1.3.	Recording Chamber	46
1.1.4.	Solutions	51
1.1.5.	Solution Delivery System	52
1.2.	WHOLE CELL PATCH-CLAMP EXPERIMENTS ...	53
1.2.1.	Theory	53
a)	Introduction	53
b)	Whole cell recording	54
c)	Electronic design and circuitry for WCR ...	55
1.2.2.	The Dynamics Of Pipette- Cytoplasmic Fluid Exchange	63
1.2.3.	Dissociation Of Sympathetic Neurons	66

a)	External solutions	68
b)	Internal solution	68
1.2.5.	Experimental Apparatus	70
a)	Recording chamber and perfusion system	70
b)	Drug delivery system	75
c)	Recording system	75
1.2.6.	Patch Electrode Preparation	79
1.2.7.	Establishment of WCR	81
2.	BIOCHEMICAL ASSAYS	87
2.1.	RADIOIMMUNOASSAY	87
2.1.1.	Rationale	87
2.1.2.	cAMP Radioimmunoassay	87
2.1.3.	Tissue Preparation	88
2.1.4.	<u>In Vitro</u> Experimental Procedure	90
2.2.	Protein Assay	94
3.	DATA HANDLING AND STATISTICAL ANALYSIS	95
	<u>CHAPTER III - RESULTS</u>	97
1.	CHARACTERIZATION OF DISSOCIATED SYMPATHETIC GANGLION NEURONS	98
1.1.	MORPHOLOGY	98
1.2.	CELL IDENTIFICATION	101

1.2.1.	General	101
1.2.2.	Cell Characterization	101
1.2.3.	Currents Observed In Small And Large Neurons	105
1.2.4.	Role Of M-Conductance In The Generation Of The Slow Inward Relaxations.	109
1.2.5.	Re-Classification Of "Large" And "Small" Cells As B- And C-Cells	110
1.2.6.	Kinetic Analysis Of The M-Current In B- And C-Cells	111
a)	Rate of I_M deactivation	111
b)	Voltage-dependence of steady-state I_M conductance	112
1.3.	EFFECTS OF ADRENALINE ON SMALL AND LARGE NEURONS USING WCR	116
1.4.	INTERNAL SOLUTION REQUIREMENTS	117
2.	CHARACTERIZATION OF INTACT GANGLION RESPONSES	119
2.1.	CHARACTERIZATION OF THE WHOLE GANGLION RESPONSE TO MUSCARINE	120
2.1.1.	Pharmacology Of The Muscarine-Induced Hyperpolarization And Muscarine-Induced Depolarization In BFSG.	122
a)	Muscarinic agonists	123
b)	Muscarinic antagonists	125
2.1.2.	Muscarinic Response In <u>Rana Pipiens</u> Sympathetic Ganglia	125

2.2.	CHARACTERIZATION OF THE WHOLE GANGLION RESPONSE TO ADRENALINE	126
3.	EXAMINATION OF THE EFFECTS OF MUSCARINE AND ADRENALINE ON SYMPATHETIC GANGLION NEURONS	128
3.1.	EFFECTS OF MUSCARINIC AGONISTS ON C- CELLS	128
3.1.1.	Description Of Muscarine-Induced Conductance Changes Observed During WCR	128
3.1.2.	Quantitative Determination Of The E_R And The Ionic Basis For Muscarine- Induced, Inwardly-Rectifying Current . . .	133
3.1.3.	Kinetics Of The Inwardly-Rectifying K^+ Current	136
3.1.4.	Examination Of The Ca^{2+} Sensitivity Of Inwardly-Rectifying K^+ Channels	139
3.1.5.	Examination Of The Muscarinic Receptor Subtype Involved In The Generation Of The Muscarine-Induced Hyperpolarization In RPSG	142
3.1.6.	Evaluation Of The Involvement Of Second Messenger Systems In The Generation Of Muscarine-Induced, Inwardly-Rectifying K^+ Current	144
a)	Evidence for G-protein involvement	144
b)	The effects of phorbol ester on muscarine-induced, inwardly- rectifying K^+ current	150
c)	The effects of protein kinase inhibitors on muscarine-induced inwardly-rectifying K^+ current	152

	d)	The effects of protein kinase inhibitors on the phorbol ester-induced suppression of C-cell I_M	154
	e)	The effects of intracellular application of IP_3 and elevated $[Ca^{2+}]$ in C-cells	154
3.1.7.		Effects Of Luteinizing Hormone Releasing Hormone (LHRH) On C-Cells	158
3.2.		THE EFFECTS OF MUSCARINIC AGONISTS ON B-CELLS	158
3.2.1.		Description Of The Muscarine-induced I_M Suppression In Sympathetic B-Cells	158
3.2.2.		Over-Recovery of I_M	163
3.2.3.		Reversal Potential Of Muscarine-Induced I_M Suppression	163
3.2.4.		Is I_M Activated At Resting Membrane Potential?	165
3.2.5.		Examination Of Second Messenger Systems That May Be Associated with M-current Suppression	167
	a)	Confirmation of G-protein involvement in the suppression of I_M by muscarine	167
	b)	Evaluation of the involvement of a phosphatidylinositide-mediated transduction mechanism in the suppression of I_M	170
	c)	Effect of phosphatase inhibition on muscarine-induced I_M suppression	178
	d)	Effects of LHRH on B-cell I_M	182
3.3.		EFFECTS OF ADRENOCEPTOR AGONISTS ON C-CELLS	182

3.3.1.	Description Of Adrenaline-Induced Inwardly-Rectifying Current Occurring In C-Cells	182
3.3.2.	Reversal Potential For The Adrenaline-Induced Inwardly-Rectifying Current In C-Cells	187
3.3.3.	Does Adrenaline Occlude The Muscarine Effect In C-Cells?	187
3.3.4.	Is The Inhibition Of Adenylate Cyclase Involved In The Adrenaline-Induced Inhibition In C-Cells?	189
a)	Effects of increasing [cAMP] _i directly via WCR	189
b)	The effects of the elevation of [cAMP] _i in the intact isolated ganglion: An electrophysiological and biochemical analysis	190
3.4.	EFFECTS OF ADRENOCEPTOR AGONISTS ON B-CELLS	199
3.4.1.	Adrenaline-Induced Excitation In B-Cells	199
3.4.2.	Adrenaline-Induced Outward Currents In B-Cells	199
3.4.3.	Evaluation If Distinct Adrenoceptors Subtypes Mediate The Opposing Effects Of Adrenaline On I _M	201
4.	EFFECTS OF NEUROPEPTIDE Y ON SYMPATHETIC GANGLION NEURONS	205
4.1.	CHARACTERIZATION OF NPY EFFECTS ON B- AND C-CELLS	207
4.1.1.	Activation Of NPY-Induced, Inwardly-Rectifying K ⁺ -Current On C-Cells	211

4.1.2.	Does NPY Occlude The Muscarine Response In C-Cells?	211
5.	EXAMINATION OF A SLOW, TRANSIENT OUTWARD CURRENT REVEALED IN BOTH B- AND C-CELLS BY WCR.	214
5.1.	GENERAL	214
5.1.1.	Analysis Of The Onset And Development Of The Slow, Transient Outward Current	217
5.1.2.	Ionic Mechanism Of The Slow, Transient Outward Current	217
5.1.3.	Activation And Inactivation Kinetics Of The Slow, Transient Outward K^+ Current	220
5.2.	PHARMACOLOGY OF I_{SA}	224
5.2.1.	K^+ Channel Blockers	224
5.2.2.	Ca^{2+} -Dependence Of I_{SA}	227
5.3.	IS THE ONSET AND THE TIME-DEPENDENT DEVELOPMENT OF I_{SA} DUE TO A PROGRESSIVE LOSS OF SOME CYTOPLASMIC FACTOR?	227
5.4.	MODULATION OF I_{SA} BY MUSCARINE	227
5.5.	IS THE MUSCARINE-INDUCED ENHANCEMENT OF I_{SA} DUE TO AN IMPROVEMENT OF THE SPACE CLAMP?	229
5.6.	IS THE BINDING OF MUSCARINE VOLTAGE-DEPENDENT?	232
	<u>CHAPTER IV</u> - DISCUSSION	234
1.	GENERAL	235

2.	CHARACTERIZATION OF DISSOCIATED SYMPATHETIC NEURONS.	237
2.1.	ISOLATION OF CELLS FROM FROG PARAVERTEBRAL SYMPATHETIC GANGLIA ...	237
2.1.1.	Proposed Classification For Dissociated Sympathetic Ganglion Neurons	237
2.1.2.	Voltage-Dependent Currents In Putative B- And C-Cells	239
3.	CELL-SPECIFIC AND NON-SPECIFIC RESPONSES	242
3.1.	RESPONSES OCCURRING ONLY IN C-CELLS ...	243
3.1.1.	Nature Of The Agonist-Sensitive, Inwardly-Rectifying K^+ Channel	243
a)	Does I_{AIR} and I_{IR} flow through the same or distinct channel proteins?	244
b)	The nature of agonist-sensitive inwardly-rectifying K^+ current	246
c)	Agonist-sensitive inwardly-rectifying K^+ channels	247
3.1.2.	Examination Of The Transduction Mechanism For The Activation Of I_{AIR} ..	249
a)	General observations	249
b)	Evidence for G-protein involvement	249
c)	Analysis of the involvement of various signal transduction pathways in the generation of I_{AIR}	251
3.1.3.	Examination Of The Muscarinic Receptor Subtype Governing The C-Cell I_{AIR}	259
3.2.	RESPONSES OCCURRING ONLY IN B-CELLS ...	262

3.2.1.	Examination Of The Transduction Mechanism For I_M Suppression	262
a)	Ionic mechanism	262
b)	Examination of the involvement of various second messengers in I_M -suppression . . .	262
c)	Other more speculative possibilities for the transduction mechanism for I_M suppression	267
3.2.2.	Effects Of Adrenaline On B-Cells	269
a)	Adrenaline-induced I_M suppression in B-cells	269
b)	Adrenaline-induced I_M augmentation in B-cells	271
c)	Are sympathomimetic-induced I_M augmentation, I_M over-recovery and the slow development of I_M upon establishment of WCR related phenomena?	272
3.3.	EFFECTS OCCURRING IN BOTH B- AND C-CELLS	274
3.3.1.	I_M inhibition by LHRH	274
3.3.2.	I_{SA}	275
4.	SOME QUESTIONS FOR FUTURE STUDY	279
4.1.	I_{AIR} IN C-CELLS	279
4.2.	I_M	281
4.3.	I_{SA}	282
5.	SUMMARY	283
	<u>CHAPTER V</u> - REFERENCES	287

LIST OF TABLES

<u>Table 1.</u>	Characteristics of I_M	115
<u>Table 2.</u>	Effects of intracellular cAMP on agonist-induced effects	118
<u>Table 3.</u>	Effects of drugs on muscarine-induced hyperpolarization of <u>Rana pipiens</u> sympathetic ganglia	141
<u>Table 4.</u>	pA_2 determination for antagonism of muscarine-induced hyperpolarization in RPSG	143
<u>Table 5.</u>	The effects of various drugs to modify RIA measured [cAMP] and their ability to attenuate adrenaline-induced hyperpolarization measured physiologically	194
<u>Table 6.</u>	The ability of sympathomimetics to generate inward and outward current in RPSG B- and C-cells at -30mV	204
<u>Table 7.</u>	Effects of muscarine on I_{SA} in <u>Rana pipiens</u> sympathetic ganglion neurons	228

LIST OF FIGURES

<u>Figure 1.</u>	Anatomy and physiology of amphibian paravertebral sympathetic system	5
<u>Figure 2.</u>	Physiology of synaptic potentials in amphibian sympathetic ganglion	9
<u>Figure 3.</u>	Schematic representation of some of the signal transduction mechanisms thought to be involved in ion channel modulation	27
<u>Figure 4.</u>	Electrical modelling of sucrose-gap recording	39
<u>Figure 5.</u>	Schematic diagram of sucrose-gap recording chamber	47
<u>Figure 6.</u>	Circuit diagram of electronic apparatus used for sucrose-gap recording experiments	50
<u>Figure 7.</u>	Block diagram of the basic circuitry required for patch clamp recording	56
<u>Figure 8.</u>	Theory and operation of a frequency boost circuit for patch clamp recording	61
<u>Figure 9.</u>	U-tube methodology for external drug application	74
<u>Figure 10.</u>	Block diagram of electronic apparatus utilized for whole-cell patch clamp recording	76
<u>Figure 11.</u>	Comparison of the steady-state currents obtained from voltage-ramp paradigm and voltage-jump paradigm	78
<u>Figure 12.</u>	Method for the establishment of whole-cell recording of sympathetic neurons	84

<u>Figure 13.</u>	Basic theory for the Radioimmunoassay technique	89
<u>Figure 14.</u>	Experimental procedures for ganglionic cAMP determination by RIA	92
<u>Figure 15.</u>	Characteristics of 'small' and 'large' neurons dissociated from <i>Rana pipiens</i> sympathetic ganglia	104
<u>Figure 16.</u>	Characteristics of voltage-dependent currents of 'large' and 'small' neurons	108
<u>Figure 17.</u>	Kinetic analysis of I_M in B- and C-cells	112
<u>Figure 18.</u>	Range of muscarine-induced responses recorded by the sucrose-gap technique in intact BFSG	121
<u>Figure 19.</u>	Pirenzepine antagonism of muscarine-induced response in an isolated BFSG preparation (sucrose-gap recording)	124
<u>Figure 20.</u>	Steady-state current responses to application of muscarine (Musc; $10\mu\text{M}$) in a C-cell whilst holding at different command potentials (-30, -40, -50, and -60mV; $[\text{K}^+]_o = 6\text{mM}$)	129
<u>Figure 21.</u>	Typical muscarine-induced, inwardly-rectifying current in a sympathetic C-neuron	131
<u>Figure 22.</u>	Effect of $[\text{K}^+]_o$ on the reversal potential of agonist-induced currents on B- and C-neurons	134
<u>Figure 23.</u>	Onset of C-cell muscarine-induced inward-rectification	135

<u>Figure 24.</u>	The voltage-dependent activation kinetics of the muscarine-induced inwardly-rectifying current of a C-cell	138
<u>Figure 25.</u>	Effect of intracellularly-applied GTP-γ-S on muscarine-induced currents in a C-cell	146
<u>Figure 26.</u>	Effects of PTX pre-treatment on intact BFSG	149
<u>Figure 27.</u>	Effects of muscarine and phorbol-12-myristate- 13-acetate (PMA) on a C-cell	151
<u>Figure 28.</u>	Lack of effect of intracellularly applied H-7 on both muscarine-and PMA-induced effects of a C-cell	153
<u>Figure 29.</u>	Effects of intracellular application of IP₃ to a C-cell	155
<u>Figure 30.</u>	Comparison between the effects of muscarine and LHRH on a C-cell	157
<u>Figure 31.</u>	Effect of muscarine on a B-cell	160
<u>Figure 32.</u>	Over-recovery of I_M subsequent to the application of muscarine to a B-cell	162
<u>Figure 33.</u>	Reversal potential of muscarine-induced I_M suppression	164
<u>Figure 34.</u>	Effects of holding potential on muscarine-induced I_M suppression in a B-cell	166
<u>Figure 35.</u>	Effects of intracellular application of GTP-γ-S on muscarine-induced I_M suppression on a B-cell	168

<u>Figure 36.</u>	Effects of muscarine and phorbol-12-myristate-13-acetate (PMA) on a B-cell	171
<u>Figure 37.</u>	Lack of effect of intracellularly applied gold sodium thiomalate (GST) on response of a B-cell to muscarine and PMA	172
<u>Figure 38.</u>	Comparison of the effects of InsP₃ and muscarine on B-cells	174
<u>Figure 39.</u>	Effect of high [Ca²⁺]_i on muscarine-induced suppression of I_M on a B-cell	176
<u>Figure 40.</u>	Effects of intracellular application of GST, H-7, IP₃, and high [Ca²⁺]_i on available M-current in B-cells	177
<u>Figure 41.</u>	Effect of intracellular application of a phosphatase inhibitor on muscarine-induced I_M suppression in a B-cell	180
<u>Figure 42.</u>	Effects of muscarine and LHRH on a B-cell	181
<u>Figure 43.</u>	Steady-state current responses to adrenaline in a C-cell	184
<u>Figure 44.</u>	Effect of adrenaline on a C-cell	186
<u>Figure 45.</u>	Occlusion of muscarine-induced outward current by adrenaline on a C-cell	188
<u>Figure 46.</u>	Effects of drugs on [cAMP]_i accumulation determined by RIA from individual BFSG	192
<u>Figure 47.</u>	Comparison of the effects of drugs which elevate [cAMP]_i with their effects on the adrenaline-induced hyperpolarization	195

Figure 48.	Effects of 8-bromo-cAMP and IBMX on adrenaline-induced hyperpolarization recorded from isolated BFSG by means of the sucrose-gap technique	197
Figure 49.	Comparison of muscarine- and adrenaline-induced inward currents produced in a B-cell	200
Figure 50.	Adrenaline-induced potentiation and muscarine-induced inhibition of I_M in a B-cell	203
Figure 51.	Similar effects of muscarine and NPY on a C-cell	206
Figure 52.	Elevation of $[K^+]_o$ causes increase in NPY- and muscarine-induced inward rectification in a C-cell	208
Figure 53.	Similar effects of muscarine, adrenaline and NPY on the same C-cell	210
Figure 54.	NPY occludes the response to muscarine in a C-cell	213
Figure 55.	Time-dependent development of a slow, transient outward current in sympathetic neurons	216
Figure 56.	Ionic mechanism of the slow, transient outward current	219
Figure 57.	Kinetics of the slow, transient outward current	222
Figure 58.	Pharmacology of I_{SA}	226
Figure 59.	Muscarine-induced I_{SA} in the presence of Ba^{2+}	231
Figure 60.	Effect of holding potential on the binding of muscarine and suppression of I_M in a B-cell	233

LIST OF PHOTOGRAPHIC PLATES

<u>Plate 1.</u>	Whole-cell recording from an enzymatically dissociated single sympathetic neuron	preface
<u>Plate 2.</u>	Whole-cell patch clamp recording chamber design	72
<u>Plate 3.</u>	Dissociated sympathetic ganglion cells viewed at 200X magnification	100

ABBREVIATIONS

AA	arachidonic acid
AHP	after hyperpolarization
amp	amplifier
ASG	amphibian sympathetic ganglia
BFSG	bullfrog sympathetic ganglia
C_f	feedback resistor capacitance
C_{in}	input capacitance
C_t	total input capacitance
CV	conduction velocity
dB	decibels
dc	direct current
E_t	measured potential across sucrose-gap
E_K	potassium equilibrium potential
ΔE_m	microelectrode measurement of ΔV at the soma
ΔE_{pg}	pre-gap measurement of ΔV
E_r	actual resting membrane potential
f	feedback resistor
F	Faraday's constant
f-EPSP	fast excitatory postsynaptic potential
G	gigaohm (10^9)

g/l	grams per liter
G_K	potassium conductance
G_M	M-current conductance
G_{Na}	sodium conductance
Hz	Hertz
i_t	sodium/potassium current
i_b	sodium/potassium current
I_A	A-current (a potassium current)
I_{AHP}	slow Ca-activated potassium current
I_{AIR}	agonist-induced, inwardly-rectifying potassium current
I_C	fast calcium-activated potassium current
I_H	sodium/potassium current
I_{ss}	instantaneous current
I_{IR}	background inward rectifier (a potassium current)
$I_{K(V)}$	delayed rectifier (a potassium current)
I_M	M-current (a potassium current)
I_{SA}	slow A-current (a potassium current)
I_{ss}	steady-state current
$K_{(ATP)}$	ATP-sensitive potassium channel
K_d	dissociation constant
l	litre
ls-EPSP	late slow excitatory postsynaptic potential
mm	millimeter (10^{-3})

ms	millisecond
mM	millimolar
M	molar
nM	nanomolar (10^{-9})
MW	molecular weight
N	total number of axons
op-amp	operational amplifier
osm	osmolarity
pmol	picomoles (10^{-12})
pmol/tissue ww	concentration in picomoles/tissue wet weight
R	resistance (Ohms)
r	radius or radii
R_a	axoplasm resistance
R_s	post-sucrose gap axolemma resistance
R_f	feedback resistor resistance
R_i	internal resistance across sucrose-gap chamber
R_{ex}	gap external resistance
R_p	resistance due to microelectrode penetration
RIA	radioimmunoassay
R_{in}	input resistance
R_m	axonal membrane resistance
$R_{m'}$	post-gap axon membrane resistance
RMP	resting membrane potential

R_p	tip resistance of patch pipette or microelectrode
R_{ps}	series resistance sum of R_p , R_s and R_m
R_{post}	post gap axon resistance
RPSG	<u>Rana pipiens</u> sympathetic ganglia
R_s	series resistance of R_i and R_{soma}
R_{soma}	actual soma resistance
R_t	series resistance sum of R_{pp} , R_s and R_{post}
s-EPSP	slow excitatory post synaptic potential
s-IPSP	slow inhibitory post synaptic potential
SCG	superior cervical ganglia
SG	sympathetic ganglia
τ	time constant
τ_{amp}	op-amp time constant
τ_f	feedback resistor time constant
s	seconds
SG	sympathetic ganglia
μ	micro (10^{-6})
$V_{0.5, inact}$	voltage for half-inactivation (steady-state)
V_c	command voltage
V_H	holding potential
ΔV	actual slow voltage change at soma
Vol	volume

WCR	whole-cell recording
z	frequency
Z	frequency response
Z(z)	frequency response as a function of frequency
Z _c	derivative of frequency response function
ZZ _c	sum of frequency response and Z _c

DRUGS AND CHEMICALS

4-AP	4-aminopyridine
ACh	acetylcholine
ADP	adenosine diphosphate
AF-DX 116	a muscarinic antagonist
Ag/AgCl	silver/silver chloride
AMP	adenosine monophosphate
ARH-602	a muscarinic agonist
ATP	adenosine triphosphate
BaCl ₂	barium chloride
BAPTA	a calcium chelator
c-II-LHRH	chicken-II-LHRH (see LHRH)
CaCl ₂	calcium chloride
cAMP	cyclic adenosine monophosphate

cGMP	cyclic guanosine monophosphate
CTX	charybdotoxin
dTC	d-tubocurarine
DMI	desipramine
DMSO	dimethylsulphoxide
EGTA	a calcium chelator
GMP	guanosine monophosphate
GST	gold sodium thiomalate
GTP	guanosine triphosphate
GTP-γ-S	guanosine-5'-[3-thio]-triphosphate
H-7	1-(5-isoquinolinyI-sulphonyl)-2-methyl piperizine
HCl	hydrochloric acid
IBMX	isobutylmethylxanthine
INA	isoprenaline
IP₃	inositol triphosphate
KCl	potassium chloride
LHRH	luteinizing hormone releasing hormone
M^cN-343	a muscarinic receptor agonist (M₁)
MgCl₂	magnesium chloride
N₂₀	liquid nitrogen
NaCl	sodium chloride
NPY	neuropeptide tyrosine; europeptide Y
PE	phenylephrine

PKC	protein kinase C
PKIs	protein kinase inhibitors
PMA	phorbol-12-myristate-13-acetate, PKC activator
PTX	pertussis toxin
SP	substance P
TCA	trichloroacetic acid
TEA	tetraethylammonium
t-LHRH	teleost-LHRH
Tris-HCl	tris(hydroxymethyl)aminomethane-HCl

CHAPTER I

INTRODUCTION

1. NEUROMODULATION.

The electrical activity of all neurons results from the movement of ions through channels in the neuronal cell membrane. The flux of ions through such channels may be influenced by ligands interacting with 'intrinsic' or 'remote' sensors (Hille, 1984). In the first case, which is exemplified by the nicotinic acetylcholine (ACh) receptor, the ion channel and the agonist-binding site are located on the same macromolecule and activation of such receptors leads to electrical events in the millisecond range. In the later case, as exemplified by the muscarinic ACh receptor, the ion channel and ligand-binding site reside on separate macromolecules, and interaction between these two entities is effected by transduction mechanisms which usually involve GTP-binding proteins (G-proteins; Gilman, 1987) and sometimes cytosolic second messengers. Responses occurring through channels which use 'remote' sensors are generally of slow time course and are involved in neuromodulatory processes. Neuromodulation is defined by Kaczmarek and Levitan (1987) as:

"the ability of neurons to alter their electrical properties in response to intracellular biochemical changes resulting from synaptic or hormonal stimulation."

The time course of 'neuromodulatory effects' vary from a few hundred milliseconds to many years in duration. For instance, the pre- and postsynaptic effects of 'classical' neurotransmitters are examples of short-term neuromodulation

whilst the effect of a single exposure of a neuron to a trophic factor that influences differentiation is an example of long-term neuromodulation. Regardless of the time course, neuromodulation underlies the integrative power, the plasticity and the complexity of the entire nervous system.

2. CHOICE OF MODEL FOR STUDY.

Autonomic ganglia are widely used in the investigation of neuromodulatory phenomena. Sympathetic ganglia (SG) have proven to be an ideal model system for the study of slow muscarinic and peptidergic synaptic responses such as the slow inhibitory postsynaptic potential (s-IPSP), slow excitatory postsynaptic potential (s-EPSP) and the late-slow excitatory postsynaptic potential (ls-EPSP) (see Kaczmarek and Levitan, 1987). Although many investigations have been performed on mammalian sympathetic ganglia, such as the superior cervical ganglion (SCG), the organization of the amphibian sympathetic ganglia (ASG) provides a less complex model for study of synaptic transmission and neuromodulation (see Weight, 1974; Weight et al, 1979; Weight and MacDermott, 1981; Weight, 1983; Adams and Galvan 1986; Adams et al, 1986). For example: 1) ASG neurons are robust, spherical, and unipolar (lacking dendrites) and since synapses are located on the soma or axon hillock region (Taxi, 1976; Watanabe, 1980; Baluk, 1986), they are especially amenable to electrophysiological studies, 2) they have a simple synaptic organization which provides separate fiber tracts for the stimulation of two

distinct cell types (Skok, 1965; Nishi et al, 1965; Tosaka et al, 1968). This allows for the selective activation of s-IPSPs, s-EPSPs or ls-EPSPs (see below) and 3) they express a wide variety of pre- and postsynaptic receptors including those for biogenic amines, peptides and toxins, that are known to modify neuronal excitability (see below).

3. PHYSIOLOGY AND PHARMACOLOGY OF SLOW POSTSYNAPTIC POTENTIALS IN SYMPATHETIC GANGLIA.

3.1. SYNAPTIC ORGANIZATION.

In bullfrog sympathetic ganglia (BFSG), the neuronal population was initially divided into sympathetic B- and C-cells on the basis of differences in axonal (antidromic) conduction velocities (Nishi et al, 1965; Skok, 1965; Tosaka et al, 1968). This classification was re-examined by Dodd and Horn (1983a) who further subdivided the B-cell population into fast- and slow-B-cells. Fast B-cells are about $50\mu\text{M}$ in diameter and have antidromic and orthodromic conduction velocities (CV's) of 2 meters/second via myelinated B-fibers. Slow B-cells are similar to fast B-cells in size ($50\mu\text{M}$) and orthodromic-CV (2.4 meters/second) but the antidromic CV is only 0.6 meters/second (about 1/4 of that of fast-B-cell). C-cells are smaller in diameter ($30\mu\text{M}$) and orthodromic and antidromic CV's are both $< 0.3 \text{ m/s}$ via non-myelinated C-fibers.

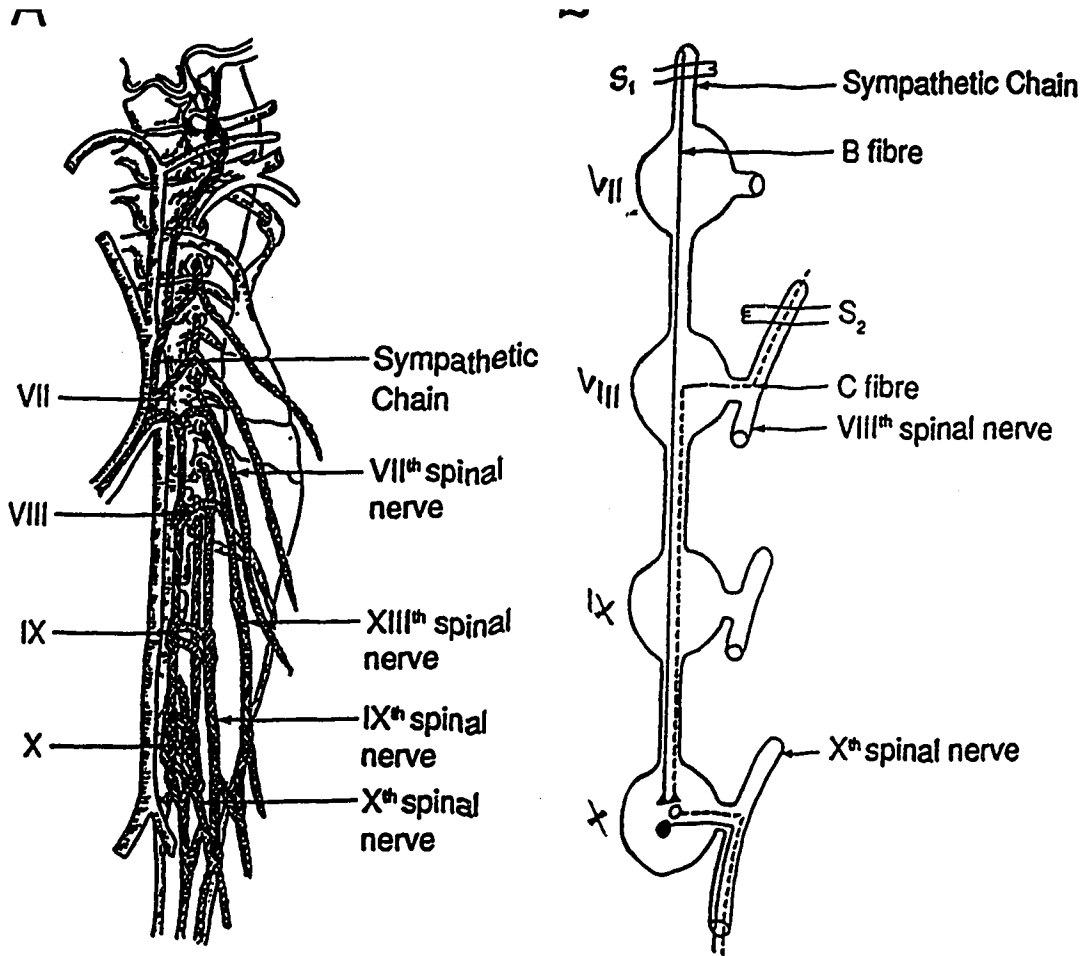


Figure 1. Anatomy and physiology of amphibian paravertebral sympathetic system. A. Drawing of the gross anatomy of the ventral surface of the spinal cord upon removal of viscera. The overlying paravertebral ganglia are numbered in a rostral to caudal direction from VII to X (left) and corresponding spinal nerves VII to X are indicated on right. B. Schematic showing B- and C-fiber tracts and stimulation sites, S₁ and S₂, for selective stimulation of B- and C-cells respectively within ganglion X. (Modified from Weight, 1983).

The anatomical organization of B- and C-fiber tracts permits independent synaptic activation of B- and C-neurons in the intact ganglion preparation. Figure 1A illustrates the gross anatomy of the amphibian paravertebral sympathetic ganglia *in situ*. Figure 1B schematically shows the different levels at which B- and C-fiber tracts enter the sympathetic chain. C-fibers enter the sympathetic chain via spinal nerves 7 and 8 whereas B-fibers enter the sympathetic chain via spinal nerves 4-6. Recently, Horn et al (1988) reported that post-ganglionic fibers arising from fast-B-, slow-B-, and C-fibers project to the skin via cutaneous nerve trunks, however C-fibers also selectively innervate striated muscle and the bladder via motor nerve trunks. It has also been shown that pre-ganglionic stimulation of C-fibers, but not B-fibers, causes vasoconstriction in skin and muscles suggesting that the vasculature is selectively innervated by C-cells (Yoshimura, 1979; Horn et al, 1987). Moreover, neuropeptide Y (NPY) -like immunoreactivity was observed in C-cells whereas B-cells were devoid of this peptide (Horn et al, 1987). These findings correlate well with the fact that NPY is known to have profound effects on cardiovascular function (Lundberg et al, 1982) and confirm a theory first proposed by Langley and Orbeli (1910) that differential projections of post-ganglionic nerve fibers to distinct target organs existed for specialized physiological functions in frogs (also see Honma, 1970; Yoshimura, 1979; Horn et al, 1986).

3.2. SYNAPTIC POTENTIALS IN AMPHIBIAN SYMPATHETIC GANGLIA.

In the three cell types described above, presynaptic release of acetylcholine (ACh) generates a f-EPSP which is similar to the end-plate potential at the nerve-muscle junction. The postsynaptic nicotinic-ACh receptors are concentrated in the area under the presynaptic bouton (Marshall, 1981). This accounts for the brief latency and time to peak (1-2ms) of the f-EPSP. The f-EPSP duration (30-50ms) is governed by the cell membrane time constant (Adams et al, 1986) and the current generated is usually of sufficient amplitude to evoke an action potential (Blackman et al, 1963; Nishi and Koketsu, 1968; Weitsen and Weight, 1977; Horn et al, 1988). In most instances, B- and C-cells are innervated by a single presynaptic fiber that forms many boutons over the soma and axon hillock region (Weitsen and Weight, 1977). The exact number of boutons has not been quantitated in frog sympathetic ganglion neurons, however, Sargent (1983) reported that about 40 boutons made contact on *Xenopus* cardiac ganglion cells. Presynaptic release of ACh and LHRH also activates slow postsynaptic potentials that facilitate ganglionic transmission via a s-EPSP and/or ls-EPSP, or inhibit transmission via a s-IPSP (Schulman and Weight, 1976; Dodd and Horn, 1983b; Kuffler and Sejnowski, 1983).

3.2.1. Slow Synaptic Potentials.

a) s-EPSP.

Stimulation of pre-ganglionic B-fibers induces a muscarinic s-EPSP in B-cells (see Figure 2) with a latency of 100-400ms. The response reaches a peak within 2s and lasts between 10-60s (Nishi and Koketsu, 1968; Tosaka et al, 1968; Weight and Votava, 1970; Blackman, 1981; Smith and Weight, 1986; Adams et al, 1986). Weight and Votava (1970) proposed that the s-EPSP was generated as a result of a decrease in resting potassium conductance (G_K). Voltage-clamp experiments performed over the last 10 years have confirmed the decreased conductance mechanism, but it is now believed that a voltage-sensitive G_K through M-channels is suppressed during muscarinic activation (Brown and Adams, 1980; Adams and Brown, 1982; Akasu and Koketsu, 1982; Jones, 1985). M-channels are unique in that they activate slowly at potentials positive to -60mV and do not inactivate (Adams et al, 1982a). Therefore, the M-current (I_M) is thought to contribute to the resting membrane potential (RMP; Adams et al, 1982a; but also see Jones, 1989). Suppression of this current, by synaptically released ACh, should enhance ganglionic transmission (Brown, 1983). This effect results from both the membrane depolarization and the increase in membrane resistance as M-channels close, such that the synaptic current due to ACh activation of nicotinic receptors results in an increased potential change (ie. a larger f-EPSP) (Schulman and

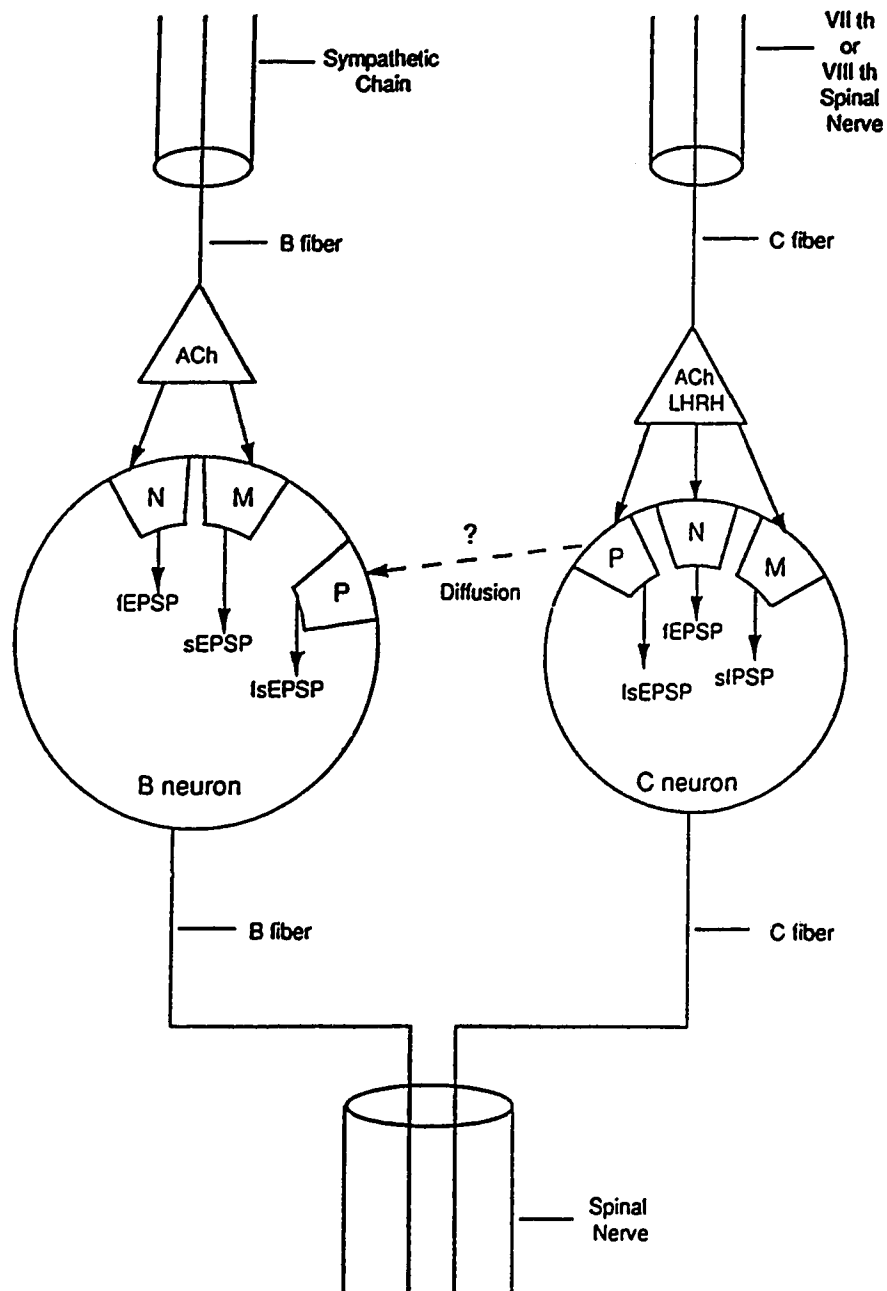


Figure 2. Physiology of synaptic potentials in amphibian sympathetic ganglion. Proposed fiber tracts, neurotransmitters, and receptors involved in the generation of f-, s- and Is-EPSP and the s-IPSP. N=nicotinic; M=muscarinic; P=peptidergic; LHRH=luteinizing hormone releasing hormone; ACh=Acetylcholine.

Weight, 1976). I_M suppression and the concomitant depolarization may cause sympathetic neurons to exhibit spontaneous action potentials. This may underlie the 'early afterdischarge' recorded in postganglionic fibers following tetanic stimulation of curarized ganglia (Nishi and Koketsu, 1966).

Although I_M was first identified in frog sympathetic B-cells, it has since been detected in a variety of vertebrate ganglion preparations (Brown and Selyanko, 1985; Brown et al, 1989; Selyanko et al, 1990a), rat hippocampal pyramidal neurons (Halliwell and Adams, 1982), human neocortex (Halliwell, 1986), dorsal horn spinal neurons (Murase et al, 1986) and intestinal smooth muscle cells (Sims et al, 1985).

Recently, an increase in conductance (probably to Na^+ and other cations; see Kuffler and Sejnowski, 1983; Akasu et al, 1984) has been proposed to provide an additional mechanism for excitation beyond the voltage sensitivity range of I_M (ie. negative to -60mV). High concentrations and long exposure to muscarine or LHRH increased the leakage current (see below) in bullfrog ganglion neurons (Jones et al, 1984; Jones, 1985; Adams et al, 1986). Furthermore, this effect persisted after I_M had fully recovered from the effect of muscarine. Therefore, the exact ionic mechanism for muscarinic excitation and facilitation of ganglionic transmission during the s-EPSP may be much more complicated than a suppression of I_M (see also Brown and Selyanko; 1985; Adams et al, 1986).

b) late-slow-EPSP.

High frequency stimulation of pre-ganglionic C-fibers (1-3s @ 50Hz) initiates another distinct excitatory postsynaptic potential in both B- and C-cells. This potential is termed the late-slow-EPSP (ls-EPSP) for its rather long latency (1-5s), slow time to peak and long duration (up to 10 minutes) (Nishi and Koketsu, 1968). However, B-fiber stimulation does not initiate a ls-EPSP. The response is not sensitive to atropine, adrenoceptor antagonists or nicotine (Nishi and Koketsu, 1968; Jan et al, 1980b; Jan and Jan, 1982). Jan and colleagues (1980 a & b) identified a peptide similar to mammalian luteinizing hormone releasing hormone (m-LHRH) as the neurotransmitter which generated ls-EPSP. This was the first unequivocal report that a peptide could function as a neurotransmitter. These authors showed that a LHRH-like peptide was released by a Ca^{2+} -dependent mechanism, LHRH-like immunoreactivity was present only within terminals which impinged on C-neurons, the ls-EPSP was mimicked by application of m-LHRH and blocked by LHRH antagonists. The latency for the appearance of a ls-EPSP in B-cells was longer than that observed in C-cells. The lack of LHRH immunoreactivity or release from B-fiber terminals lead to the finding that LHRH-like peptide was released from C-fiber terminals and that the peptide must diffuse to evoke a ls-EPSP in an adjacent B-cell (Jan et al, 1980b) (see Figure 2).

The ionic mechanism of the ls-EPSP appears to be similar to that underlying the s-EPSP. Schulman and Weight (1976) showed an increase in

membrane resistance during the ls-EPSP. Jan et al, (1980b) reported that m-LHRH and synaptic stimulation increased membrane resistance by a similar mechanism. Adams and Brown (1980) showed that m-LHRH reduced I_M in voltage-clamped B-cells. Similar effects of teleost-LHRH (t-LHRH) were also observed in C-cells suggesting that C-cells have a muscarine-insensitive I_M (Jones, 1987a). t-LHRH was used since the amino acid sequence of m-LHRH was reported to differ slightly from t-LHRH; amino acids 7 (leucine) and 8 (arginine) of m-LHRH are replaced with tryptamine and leucine in t-LHRH (Sherwood et al, 1983). Jones et al (1984) observed variability in the efficacy of LHRH isolated from different sources; this author found that t-LHRH (isolated from salmon brain) was more effective in suppressing I_M than m-LHRH suggesting that t-LHRH more closely resembled the endogenous peptide which is normally released from pre-ganglionic C-terminals.

Since synaptic release of peptides is enhanced by high frequency stimulation (Hökfelt et al, 1980), from a physiological perspective, the release of LHRH-like peptide during high sympathetic tone would initiate a long lasting facilitation of ganglionic transmission through both B- and C-cells whereas a minimal release of peptide might be observed during basal sympathetic tone. LHRH-like peptide could therefore play a significant neuromodulatory role during and after periods of intense sympathetic activation. Also, LHRH-like peptide is not subject to any significant degradation or uptake, suggesting that it may behave more like a local

hormone, which acts non-synaptically over large distances for a long duration, as well as a "classical" neurotransmitter.

c) s-IPSP.

Stimulation of presynaptic C-fibers causes release of ACh which generates a s-IPSP in C-cells. This response has a latency of 25-100ms, reaches a peak in about 1-2s and lasts 4-20s (for reviews see Kuba and Koketsu, 1978; Blackman, 1981; Weight, 1983). An ongoing debate continues to exist as to whether the s-IPSP is generated via a disynaptic pathway, as originally proposed by Eccles and Libet (1961), or via a monosynaptic pathway, as initially advanced by Weight and Padjen (1973b). In the disynaptic pathway, synaptically-released ACh was proposed to act on excitatory muscarinic receptors located on an interneuron. The muscarinic excitation caused the interneuron to release a catecholamine that generated a C-cell s-IPSP via adrenoceptors located on the C-cell soma. In the monosynaptic pathway, synaptically-released ACh is proposed to act directly on muscarinic receptors located on the C-cell (see Figure 2).

The disynaptic hypothesis has been strongly contested in amphibian sympathetic ganglia (Weight and Padjen, 1973 a & b; Weight and Weitsen, 1977; Weight and Smith, 1980; Horn and Dodd, 1981; Yavari and Weight, 1981; Dodd and Horn, 1983b; Weight, 1983; Smith and Weight, 1986; Rafuse and Smith, 1986; Yavari and Weight, 1988) and SCG (Dun and Karczmar, 1980; Gallagher et al,

1980; Cole and Shinnick-Gallagher, 1980 & 1984). The most convincing evidence for support of the monosynaptic hypothesis arises from studies that utilized adrenergic antagonists. Concentrations of phentolamine, yohimbine and idazoxan that antagonized adrenoceptor-mediated hyperpolarization failed to affect either the s-IPSP or hyperpolarizations induced by muscarinic agonists (Cole and Shinnick-Gallagher, 1980 & 1984; Rafuse and Smith, 1986). Furthermore, when release of adrenergic neurotransmitters from putative interneurons was blocked in low Ca^{2+} -high Mg^{2+} Ringer's solution, application of muscarinic agonists produced a hyperpolarization similar to the s-IPSP in both BFSG and SCG (Smith and Weight, 1981 & 1986; Cole and Shinnick-Gallagher, 1984).

Although the first extracellular recordings of a s-IPSP was reported about 40 years ago (in the turtle sympathetic ganglion; Laporte and Lorente de No, 1950), the exact ionic mechanism underlying its electrogenesis has been a contentious issue. The difficulty of successfully recording s-IPSPs with microelectrodes and the reliance on extracellular techniques has resulted in a number of proposed ionic mechanisms for the generation of this response. These include: 1) the activation of the sodium/potassium pump (Nishi and Koketsu, 1968) and 2) a decrease in sodium conductance (G_{Na}) (Weight and Padjen, 1973a). Weight (1983) later revised the hypothesis to include a concomitant increase in G_{K} with the decrease in G_{Na} . Presently, the most widely accepted hypothesis is that the s-IPSP is generated by a selective increase in G_{K} originally proposed by Horn and Dodd (1981). These authors used sophisticated optics to facilitate

microelectrode impalement of these small neurons and recorded large s-IPSPs which reversed at E_K (also see Horn and Dodd, 1983; Dodd and Horn, 1983b). Subsequently, a similar ionic mechanism for the s-IPSP was reported in SCG (Cole and Shinnick-Gallagher, 1984).

Although muscarinic agonists were shown to increase G_K and thereby mimic the s-IPSP in sympathetic C-cells, the identity of the specific population of K^+ channels involved was not determined (Horn and Dodd, 1983). Moreover, this issue was not addressed in comprehensive reviews published three years later on ganglionic transmission (Adams and Galvan, 1986; Adams et al, 1986). One object of this thesis is to identify and characterize the K^+ channels which underlie the generation of C-cell s-IPSP.

4. THE ROLE OF K^+ CHANNELS IN NEUROMODULATION.

Ca^{2+} and K^+ channels are the primary targets for neuromodulatory mechanisms. Generally, the release of neurotransmitter from synaptic terminals is governed by Ca^{2+} influx through voltage-dependent Ca^{2+} channels. The modulation of the excitability of the postsynaptic membrane is altered primarily by the flux of K^+ through a variety of potassium channels. All of the slow postsynaptic potentials described above involve the modulation of G_K that regulate integrative functions that modify transmission through the ganglion.

Of all the ion channels that exist within excitable cell membranes, none exhibit the diversity and ubiquity of K^+ channels (Rudy, 1988). To date, there have been 15 K^+ channels described in the literature (see Rudy, 1988; Castle et al, 1989). As it is obviously beyond the scope of this thesis to describe the distinguishing features and characteristics of all 15 K^+ channels, this introduction will be restricted to those presently known to exist in frog sympathetic ganglia neurons.

Six distinct potassium currents have been described in frog sympathetic neurons to date (Adams et al, 1982a; Adams et al, 1982c; Pennefather et al, 1985; Lancaster and Pennefather, 1987; Tokimasa and Akasu, 1990); these are i) the delayed rectifier $I_{K(V)}$, ii) the A-current (I_A), iii) I_M , vi) a voltage-dependent Ca-activated K^+ current (I_C), v) a slow voltage-insensitive Ca-activated K^+ current (I_{AHP}), vi) an inwardly-rectifying Na^+/K^+ -current (I_H) and another two K^+ currents will be described within this thesis (see Results), 1) an inwardly-rectifying agonist-sensitive K^+ current (I_{AIR}) and 2) a slow A-current (I_{SA}). Although the voltage-sensitivities of many of the K^+ currents overlap, they have distinct kinetic properties and pharmacological sensitivities which permit their isolation by recording in appropriate solutions and within certain voltage ranges.

In addition to the currents mentioned above, other voltage-insensitive leakage conductances exist that involve K^+ , Na^+ and perhaps Cl^- (Adams et al, 1982a; Jones, 1989). The 'leakage current' reverses at potentials positive to E_K and shifts with, but not exactly according to changes in E_K and indicates that more than one ion is involved (Jones, 1989).

4.1. DELAYED RECTIFIER.

The voltage-dependence of the delayed rectifier ($I_{K(V)}$) and its involvement in repolarization of action potential in squid axon was first described by Hodgkin and Huxley (1952). In bullfrog B-cells $I_{K(V)}$ activates between -25 and -20mV (Adams et al, 1982a) and the time constant for activation increases with depolarization ($\tau=20\text{ms}$ @ -40mV; 10ms @ 0mV; 2ms @ +50mV) (Adams et al, 1982a). $I_{K(V)}$ slowly inactivates (4-8s) and is sensitive to externally applied tetraethylammonium (TEA; $K_d=1\text{mM}$) but insensitive to 1mM 4-aminopyridine (4-AP) (Adams et al, 1982a; Adams and Galvan, 1986). Although, $I_{K(V)}$ exists in frog neurons, the activation kinetics are too slow to generate enough current to play a significant role in either spike repolarization or in the after hyperpolarization (AHP) (Adams et al, 1982a; Adams and Galvan, 1986).

4.2. A-CURRENTS.

I_A is a voltage-activated potassium current which was first described in neurons of the mollusc *Anisodoris* (Connor and Stevens, 1971; Neher, 1971). The I_A exhibited in bullfrog ganglion neurons is similar in most respects to molluscan I_A except the inactivation rate constant is not voltage-dependent (Adams et al, 1982a). The main characteristics that distinguish I_A from other K^+ currents in the frog are its rapid activation ($\tau = 5\text{ms}$) and inactivation kinetics ($\tau = 50\text{ms}$). The activation

(threshold = -60mV) and inactivation (complete inactivation > -40mV) curves overlap over a small voltage range about the RMP. The voltage for the steady-state half-inactivation ($V_{0.5,inact}$) occurs at -110mV. However, since I_A inactivation is removed by membrane hyperpolarization ($\tau = 150$ ms), the current briefly activates and inactivates upon the return to more positive potentials due to the 10 fold difference between activation and inactivation rate constants (see above).

Thompson (1977) showed that I_A was more sensitive than both $I_{K(V)}$ and I_C to 4-AP. Conversely, the I_A that occurs in BFSG is insensitive to 4-AP (up to 1mM; Adams et al, 1982a). This lack of effect is contradictory to 4-AP sensitivities reported in a variety of vertebrate ganglionic, hippocampal, sensory and central neurons which all have K_d values between 1-2mM (see Rudy, 1988).

Recently, other " I_A -like" currents have been reported to occur in a number of vertebrate neurons that have the following general characteristics (for review see Rudy, 1988): fast activation kinetics (1-20ms), activation threshold -40 to -60mV and the midpoint for steady-state inactivation (-60 to -70mV). However, there are also distinct differences from I_A : 1) the rate of inactivation is in the order of seconds, 2) complete blockade by 30 μ M to 500 μ M 4-AP is observed, and 3) the $V_{0.5,inact}$ in hippocampal neurons is 40 to 50mV more positive (hippocampal neurons; -60 to -70mV). Rudy (1988) noted that the effect of 4-AP on A-channels in general may be directly related to the rate of inactivation since 4-AP exhibits both a voltage-dependent closed channel block, that is reduced by depolarization, and

an open channel block (Thompson, 1982). This may account for the increased affinity of 4-AP for the more slowly inactivating A-like currents.

4.3. I_M .

I_M was first described in frog ganglion B-neurons by Adams and Brown (1980) as a muscarine-sensitive K^+ current with unusual properties. Most notably, once I_M is activated, the M-channels remain open at potentials positive to -60mV and are closed by muscarinic agonists. Moreover, since RMP reported in a number of studies were all positive to the activation threshold for I_M (Nishi and Koketsu, 1960; Tosaka et al, 1968; Tokimasa, 1984) and it is thought to provide a steady outward K^+ current that contributes to the RMP. However, Jones (1989) has recently provided evidence that B-neuron RMP is about -75mV as measured by whole-cell recording (WCR) thus questioning its contribution to the RMP. However, it is possible that I_M activation curve shifts to the more negative potentials during WCR (Selyanko et al, 1990a; see Discussion).

Although the conductance of single M-channels has not yet been unequivocally measured, data from noise analysis suggests that this value is very low (1.6pS) in SCG neurons (Owen et al, 1989) and only 3pS in neuroblastoma hybrid cells (Neher et al, 1988). Gruner et al (1989) obtained recordings from 15pS K^+ channels in BFSG which had similar deactivation characteristics to M-

--

channels. These preliminary reports on ganglion neurons also suggested that M-channels had three distinct conductance states.

The most significant property of I_M is that it is reduced by synaptically-released ACh and LHRH-like peptide in frog sympathetic ganglion neurons. The actions of these two neurotransmitters are thought to contribute to the generation of s-EPSP and ls-EPSP (see above) to facilitate ganglionic transmission. However, I_M is also modulated by a number of other pharmacological agents. There is a growing list of peptides, other than LHRH, which reduce I_M . These include substance P (SP), bradykinin, substance K, eledoisin, kassinin, angiotensin and atrial natriuretic factor (Constanti and Brown, 1981; Adams et al, 1983; Akasu et al, 1983; Jones, 1985; Higashida and Brown, 1986; Pant and Smith, 1989). Nucleotides such as uridine triphosphate (Adams et al, 1982b) and adenosine triphosphate (ATP; Akasu et al, 1982) reduced I_M , as well as compounds totally unrelated to peptides or nucleotides such as phorbol esters (Higashida and Brown, 1986). Unfortunately, there is no high-affinity ligand currently available, such as a toxin, for M-channels which could be used to isolate and study the channel protein.

It is not yet understood why such a wide variety of compounds suppress I_M via independent receptors (in most instances). However, the hypothesis that slow modulatory responses are generated by multistep second messenger systems is a central theme. Pharmacological intervention could therefore occur at a number of sites and may account for the wide variety of structurally unrelated compounds to modulate the same physiological response.

4.4. CALCIUM-DEPENDENT K^+ CURRENTS.

The general characteristic that separates these particular currents from other K^+ currents is a dependence on $[Ca^{2+}]_i$ for activation. The source of Ca^{2+} can be external, via voltage-dependent Ca^{2+} channels, or internal from Ca^{2+} release from intracellular stores. At present, two major subtypes of Ca-activated K^+ channels ($I_{K(Ca)}$) are known to exist in vertebrate neurons: 1) large conductance, voltage-sensitive, Ca-sensitive K^+ (Maxi-K or BK) channels that underlie I_c and 2) small conductance, voltage-independent calcium-sensitive K^+ channels (SK channels) that underlie the action potential after-hyperpolarization (Pennefather et al, 1985). These currents are particularly well understood in rat skeletal muscle (Romey and Lazdunski, 1984; Blatz and Magleby, 1986) and bullfrog sympathetic ganglion neurons (Pennefather et al, 1985) where these two Ca^{2+} -dependent K^+ channels co-exist.

4.4.1. I_c .

A fast, Ca-sensitive-K current (I_c) was first reported in chromaffin cells by Marty (1981) and subsequently characterized in rat skeletal muscle (Pallotta et al, 1981) and bullfrog B-cells (Adams et al, 1982c). I_c in all three tissues has the essentially the same properties (Lancaster and Pennefather, 1987). The single channel conductance of Maxi-K channels lies between 100 - 250 pS. I_c is strongly

voltage-dependent such that the probability of channel opening increases about 2.3-fold for each +10 to +15 mV shift. This is likely due to voltage-dependent binding of Ca^{2+} to the Maxi-K channel (Moczydlowski and Lattore, 1983). I_c is sensitive to externally applied TEA ($K_d < 1\text{mM}$), barium (Ba^{2+}), quinine (Habermann, 1984) and requires a pCa of 5 or 6 for activation. Recently, nanomolar (nM) concentrations of charybdotoxin (CTX), a scorpion venom toxin, were reported to block both reconstituted skeletal muscle Maxi-K channels ($K_d = 3\text{nM}$) (Miller et al, 1985) and I_c in bullfrog neurons (Goh and Pennefather, 1987).

The activation of I_c underlies rapid spike repolarization in BFSG neurons since the rate of activation of $I_{K(V)}$ is not fast enough to contribute to action potential repolarization. I_c channel kinetics are well suited for this function since these channels rapidly activate upon depolarization and deactivate at peak after-hyperpolarization (Adams and Galvan, 1986). I_c also provides a negative feedback on voltage-dependent current through Ca^{2+} channels since the action potential duration is increased by TEA (Adams and Galvan, 1986) and CTX (Storm, 1988).

4.4.2. I_{AHP}

The existence of slow, Ca-activated K^+ channels (SK), which were apamin-sensitive and TEA-insensitive, was first reported in reconstitution experiments on channels from rat skeletal muscle (Hughes et al, 1982; Romey and Lazdunski, 1984). Thereafter, Pennefather and coworkers (1985) reported that apamin, a bee

venom toxin, selectively blocked a similar population of channels in BFG neurons that were responsible for the action potential after-hyperpolarization. This apamin-sensitive current was therefore termed I_{AHP} . The characteristics and function of SK channels differ dramatically from Maxi-K channels. The single channel conductance is only about 10pS and the probability of channel opening depends only on $[Ca^{2+}]_i$ (Blatz and Magleby, 1986). Since activation is independent of voltage, I_{AHP} can influence the membrane potential over wide voltage range as long as $[Ca^{2+}]_i$ requirement is satisfied (200-500nM for half maximal activation) (Blatz and Magleby, 1986). In BFG neurons, slow activation of I_{AHP} channels is due to Ca^{2+} influx during the action potential. This modulates after-hyperpolarization duration and thereby controls repetitive discharge (in a similar manner to I_M , see above) (Pennefather et al, 1985).

The appearance and duration of I_{AHP} is markedly affected by the quality of recording. Adams and Galvan (1986) describe a model in which both the duration and longevity of after-hyperpolarization depend directly on the damage rendered by microelectrode impalement since I_{AHP} durations were very brief in cells that had low input resistances.

I_{AHP} is similar to I_M (see above) in that they both deactivate slowly, are relatively small currents which limit repetitive discharge and display similar sensitivities to agonists such as muscarine, oxotremorine (Tokimasa, 1984), and t-LHRH (Adams et al, 1986). However, I_{AHP} markedly differs from I_M in its sensitivity to Ca^{2+} and voltage-dependence.

4.5. I_H .

I_H is the most recently described current reported in frog sympathetic neurons (Tokimasa and Akasu, 1990) and is similar to I_b in dorsal root ganglion neurons (Mayer and Westbrook, 1983), I_Q in hippocampal neurons (Halliwell and Adams, 1982), I_b in sino-atrial node cells (Yanagihara and Ishawa, 1980) and i_f in Purkinje fibers (DiFrancesco, 1981 a&b). In frog neurons, I_H was described as a non-inactivating, inwardly-rectifying K^+/Na^+ conductance that was progressively activated by hyperpolarization. The voltage activation range is -60mV to -130mV with a half-activation potential of -90mV and reverses at potentials positive to E_K (ie. I_H reversed at -24mV in 20mM [K], where E_K was approximately -40mV). I_H was isolated by elimination of all other ionic conductances in B-neurons (G_{Na} , G_{Ca} , and the other 5 G_K 's). Under these conditions, a K^+ current remained that was blocked by Cs^{2+} . Furthermore, the Cs^{2+} block was enhanced by hyperpolarization suggesting an open channel blocking mechanism. I_H was modulated by a cAMP-dependent process since increases in cAMP, due to the addition of forskolin or cAMP analogues, shifted the I_H activation curve to the right (Tokimasa and Akasu, 1990). Similar effects of β -adrenoceptor activation and forskolin that are attributed to effects on i_f were shown on sino-atrial node cells (Tsien et al, 1972; DiFrancesco et al, 1986) and an opposite effect, a hyperpolarizing shift of the i_f activation curve, was induced by muscarine in the same tissue (DiFrancesco and Tromba, 1987, 1988 a&b).

5. POSSIBLE TRANSDUCTION MECHANISMS FOR MODULATION OF ION CHANNEL FUNCTION.

In the most general terms, modulation of ion channel function is accomplished by an interaction between a receptor, a membrane-bound transducer and an effector. In the case of the 'intrinsic sensor' model, all entities are located on the same macromolecule; most often, however, the three components are distinct entities and the ion channel function is modulated by the production of a 'messenger' generated as a result of stimulation of an 'extrinsic sensor' or receptor.

There are at least five distinct signal transduction pathways that have been implicated in the transduction and amplification of external signals that could alter neuronal excitability, these include: 1) activation, and perhaps, inhibition of adenylate cyclase pathway (Tsien et al, 1972; Andrade and Aghajanian, 1985), 2) Guanylate cyclase pathway (Light et al, 1989), 3) Phosphatidylinositide pathway (Berridge and Irvine, 1984; Nishizuka, 1984), 4) Direct pathway (Yantani et al, 1987; Codina et al, 1987) and 5) Arachidonic Acid pathway (Kim et al, 1989). A simplified schematic of some of these transduction mechanisms is illustrated in Figure 3.

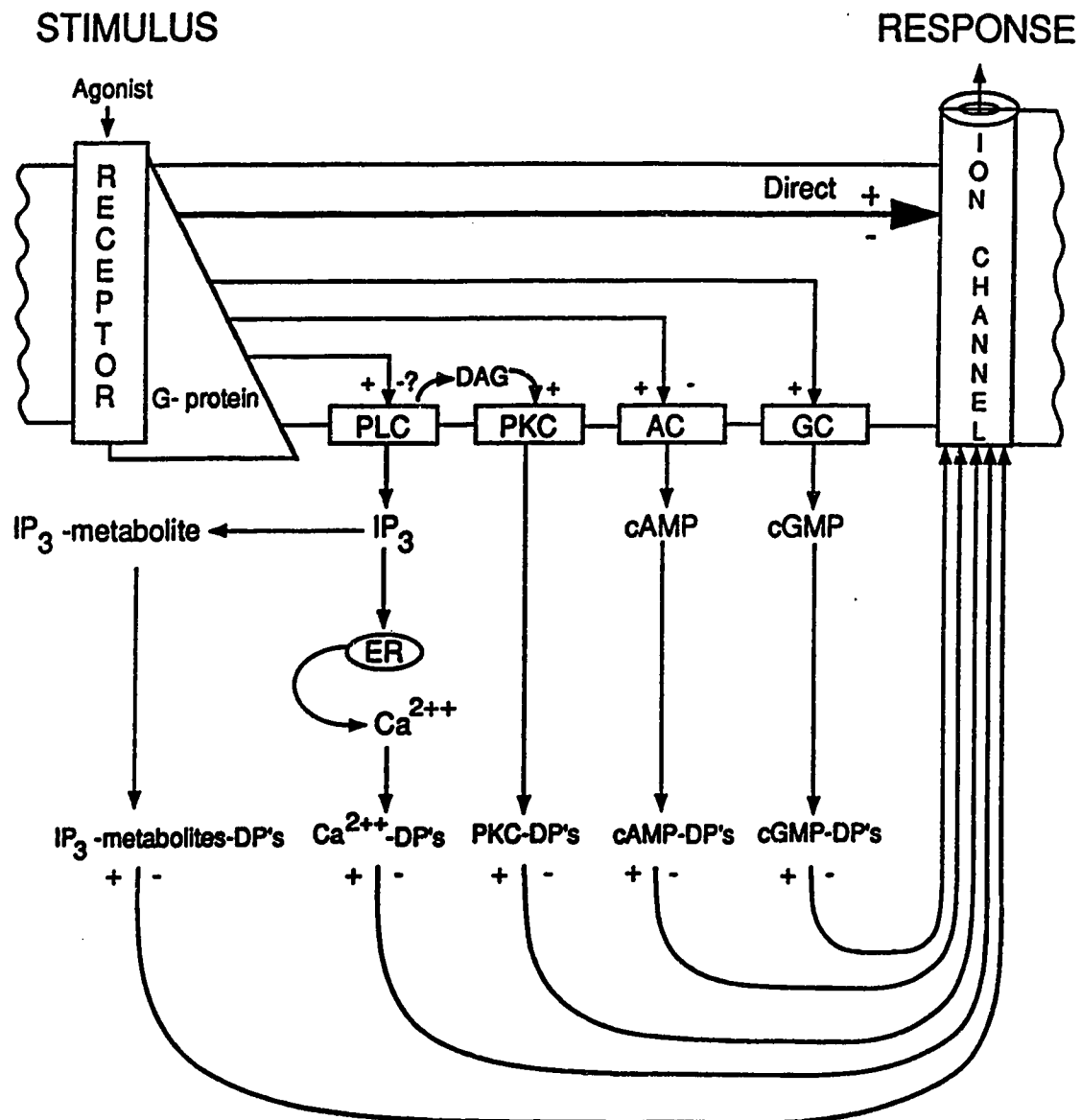
3. Schematic representation of some of the signal transduction mechanisms thought to be involved in ion channel modulation. Subsequent to G-protein activation, the following pathways may be activated and thereby alter ion channel function (+ denotes stimulation and - denotes inhibition).

Phosphatidylinositol pathway includes: phospholipase C (PLC), protein kinase C (PKC), diacylglycerol (DAG), inositol trisphosphate (IP_3), its metabolites and dependent processes (DP's), endoplasmic reticulum (ER), calcium (Ca^{2+}) and Ca^{++} -DP's.

Adenylate cyclase pathway consists of membrane-bound adenylate cyclase (AC) which modulates cytoplasmic cyclic adenosine-3',5'-monophosphate (cAMP) levels and cAMP-DP's.

Guanylate cyclase pathway includes: membrane-bound guanylate cyclase (GC) which increases intracellular concentration of cyclic guanosine-3',5'-monophosphate (cGMP) and modulate cGMP-DP's.

Direct pathway, whereby a specific subunit of the G-protein directly modulates the ion channel.



5.1. G-PROTEINS.

It is well established that GTP-binding-proteins are specialized membrane-bound proteins that, upon the binding of guanosine triphosphate (GTP), interact with a number of effector enzymes or channels implicated in the regulation of cellular functions (Gilman, 1987). The G-protein activity is regulated by GDP/GTP exchange. The binding of a drug to its receptor induces the exchange of GDP with GTP and the G-protein dissociates into 2 distinct subunits, G_α and $G_{\beta\gamma}$. The GTP binding site is located on the α -subunit and the $\beta\gamma$ dimer is thought to act as a regulatory subunit, similar to the protein kinase A regulatory subunit (Ross, 1989). However, the $G_{\beta\gamma}$ subunit may also directly regulate an atrial K^+ channel (Logothetis et al, 1987). Inherent GTPase activity hydrolyses the GTP that is bound to the activated G_α . This allows for the re-association of the subunits, and the G-protein returns to the inactive GDP-bound state.

There are probably in excess of 100 different receptors that exert their biological effect through G-proteins. These specialized proteins amplify external signals and process information within the neuron membrane to activate the appropriate effector system. The role of G-proteins in signal transduction is somewhat underestimated because these regulatory proteins direct numerous external signals by converging, diverging or simple networks (Ross, 1989).

The suppression of I_M by a variety of agents, including neurotransmitters, neurotransmitter-like substances, nucleotides and a number of peptides (see above) is an excellent example of a complex convergent transduction mechanism. How do all of these unrelated agents cause a similar response? Furthermore, why is there variability in the degree to which an agent suppresses I_M ? The most logical answer is that a convergence of the various transduction mechanisms probably occur and the coupling efficacy is variable at the locus of convergence.

5.2. TESTING AND IDENTIFICATION OF PUTATIVE TRANSDUCTION MECHANISMS.

Many of the experiments described within this thesis are designed to identify which second messenger systems are involved in the mechanism of action of muscarine, adrenaline, LHRH and NPY in amphibian sympathetic ganglion neurons. Stimulation of muscarinic, adrenergic and peptidergic receptors result in responses that are mediated by G-proteins which either couple directly to an effector mechanism (ion channel) or couple indirectly via a transduction mechanism involving a cytosolic second messenger. Therefore, the aim of the present study was to evaluate the effects of various drugs that interfere with or mimic the particular transduction mechanisms involved in the generation of the slow modulatory mechanisms described above. There are certain problems with this approach which must be considered in the design of such experiments: 1) Many of the drugs used

to probe transduction mechanisms are non-specific; for example, the protein kinase C (PKC) inhibitor, H-7 (Hidaka et al, 1984; Kikkawa and Nishizuka, 1986) can also inhibit other protein kinases, 2) Divergent pathways may exist between receptor and effector, for example, in atria, muscarinic receptors are coupled directly to K^+ channels via a G-protein (Pfaffinger et al, 1985) but may also be coupled indirectly via arachidonic acid metabolites (Kim et al, 1989). The 'pleiotropic' aspect of receptor activation has recently been emphasized by Hille (1989), 3) Some components of transduction mechanisms can exert negative modulatory effects on the agonist-receptor, for example PKC can affect adrenoceptor function (Kikkawa and Nishizuka, 1986), and 4) There are numerous interactions between second messenger pathways (Ross, 1989). In order to minimize these problems a wide variety of pharmacological probes were utilized to investigate transduction mechanisms and caution has been taken in drawing conclusions. It is easier to conclude which transduction mechanisms are *not* involved rather than to provide positive evidence in support of a given process.

6. RATIONALE AND STATEMENT OF THE PROBLEM.

The focus of this thesis is to study postsynaptic modulation of neuronal excitability which would be of an intermediate time course, (100 ms to several minutes in duration) and that is associated with the activation and generation of slow postsynaptic potentials (s-EPSP, s-IPSP and ls-EPSP). A variety of

experimental techniques, including whole-cell recording (WCR), sucrose-gap recording and biochemical techniques were used. The general mechanism thought to underlie these particular changes in neuronal excitability involves the activation of a distinct (muscarinic or peptidergic) receptor that triggers a transduction mechanism to alter ion channel function. Although the responses have a slower time course than those mediated via ligand-gated ion channels with 'intrinsic sensors', each step of the transduction mechanism introduces a means for signal amplification. Moreover, since each step is a discrete biochemical process, it provides an additional locus for neuromodulation and for pharmacological intervention to elucidate the underlying transduction mechanism.

Therefore, the following questions were asked at the beginning of this study in order to evaluate logically neuromodulatory actions that are related to the generation of postsynaptic potentials in amphibian sympathetic ganglia.

- 1) Can ganglionic slow postsynaptic potentials (s-IPSP, s-EPSP and ls-EPSP) and responses due to agonists which mimic these PSPs be emulated by exogenous application of drugs onto enzymatically dispersed B- and C-cells isolated from frog paravertebral sympathetic ganglia.
- 2) Can criteria be established to characterize dispersed sympathetic neurons into putative B- and C-cells based on differences between the two cell types as determined electrophysiologically via WCR?

- 3) Can the currents that are thought to underlie the above mentioned PSPs and agonist-induced responses be recorded and maintained during WCR so as to permit pharmacological investigations?
- 4) What is the nature of the ionic channels involved in such responses and which messengers are involved (or not involved) in the generation of these responses?
- 5) Can exogenous application of agonists that are unrelated to the synaptically-released transmitters evoke similar changes in membrane conductances in ASG B- and C-cells? Do these agents utilize the same signal transduction mechanism and if so, where does the convergence occur?

During the course of this study, some of these questions were concurrently addressed by various other workers, particularly with respect the transduction mechanism of the M-current by WCR (see Brown and Adams, 1987; Pfaffinger, 1988; Pfaffinger et al, 1988; Brown 1988; Bosma and Hille, 1989; Brown et al, 1989; Bley and Tsien, 1990; Simmons et al, 1990) but none of these studies were successful in unequivocally identifying the means by which M-channels were suppressed by agonists. The studies reported here on muscarinic inhibition observed

in C-cells and cell type characterization on dissociated ASG neurons are believed to be the first in depth investigation of these matters by WCR. Some of this work has previously appeared in abstract and paper form (Zidichouski et al, 1987; Zidichouski et al, 1989a; Zidichouski et al, 1989b; Zidichouski et al, 1989c; Selyanko et al, 1990; Selyanko et al, 1990; Zidichouski et al, 1990).

CHAPTER II

MATERIALS AND METHODS

1. ELECTROPHYSIOLOGICAL TECHNIQUES.

The electrophysiological properties of amphibian sympathetic ganglion cells were studied using two techniques:

- 1.1. Whole ganglion responses, or population responses, were studied using the sucrose-gap recording method.
- 1.2. Electrophysiological properties of single cells isolated from the same tissue were evaluated using the whole-cell patch-clamp recording technique.

1.1. SUCROSE-GAP EXPERIMENTS.

1.1.1. Theory.

a) Introduction.

The basic theory for the sucrose-gap recording technique was developed from the observation that an isotonic sucrose solution applied to a region of membrane, located between two extracellular recording electrodes, resulted in an increased amplitude of an observed electrical response (Stampfli, 1954). The technique has been widely used on muscle and nerve preparations to study the

propagation of both active and passive electrical events (see Wallis et al, 1975). The practical design of a sucrose-gap recording chamber attempts to maximize the effectiveness of the seal between the low resistance electrolyte solution and the high resistance sucrose solution. Also, the design of the recording chamber must accommodate the geometry of the particular preparation under study. The use of sucrose in the gap is superior to air, mineral oil or a glass sleeve because it penetrates the area between the axons and more effectively increases gap resistivity, thus minimizing current leakage (see Electrical modelling, next section). Seals are produced by surrounding the nerve bundle with a mixture of vasoline and wax at the Ringer's solution/sucrose interface to eliminate fluid mixing. The consequences of inadequate seal formation and the subsequent electrical shunting that occurs will be discussed below (see Electrical Modelling).

The sucrose-gap method has proven to be an useful method to study direct current (dc) or slow potentials and was the principal means by which many of the slow synaptic potentials were first studied in the sympathetic ganglia (Eccles, 1943). McAfee (1982), has referred to this method as a "poor man's microelectrode", since the cut axon provides direct intracellular access analogous to a microelectrode. However, the total potential recorded is subject to attenuation due to principles discussed in the next section.

b) Electrical modelling.

The potential recorded using the sucrose-gap technique is essentially the average potential difference of a population of neurons. It is not equivalent to the actual membrane potential, nor do the recorded potential changes reflect the actual voltage change occurring at the soma, or distal to the soma. However, the electrical changes occurring due to synaptic events or receptor-mediated events and their modification by exogenously-applied agents can be recorded and interpreted by comparison with controls. Therefore, the results compiled utilizing this technique are reported as the relative percent change compared to control rather than an actual change in the membrane potential.

As stated earlier, the method utilizes the cut axon to act as an intracellular electrode. However, the axon also has distinct passive membrane properties and the voltage difference measured from a single neuron by sucrose-gap recording is less than that obtained via a microelectrode. A transmembrane difference can be best recorded by means of sucrose-gap recording if the cell body is as close to the sucrose interface as possible. However, in the whole ganglion only a very limited number of cells would be positioned as such and the majority of cells would have a short axonal segment from which current would leak prior to entering the high resistance sucrose solution.

Figure 4. Electrical modelling of sucrose-gap recording. A) Equivalent circuit representing a single neuron to compare microelectrode recording and sucrose-gap recording. B) Thevenin equivalent circuits for recording from the soma (S), soma-axon (S-A), soma-axon-sucrose gap interface (S-A-G) and soma-axon-sucrose-gap-post-gap (S-A-G-PG). C) Thevenin equivalent circuit for whole nerve containing N-axons. Modified from M'Affee (1983) and Rafuse (1985).

ΔE_s measured potential change across sucrose gap

ΔE_m measured potential change in soma

ΔE_{pg} measured change at ~~post-gap~~ sucrose interface

N total number of axons

R resistance (ohms)

R_a axoplasm resistance

R_p post-sucrose gap axolemma resistance

R_s internal resistance across sucrose-gap chamber

R_{pg} gap external resistance

R_i resistance due to microelectrode penetration

R_m axonal membrane resistance

$R_{m'}$ post-gap axon membrane resistance

R_{pg} sum of pre-gap R_a , R_p and R_m

R_{pg} post-gap resistance

R_{post} post-gap axon resistance

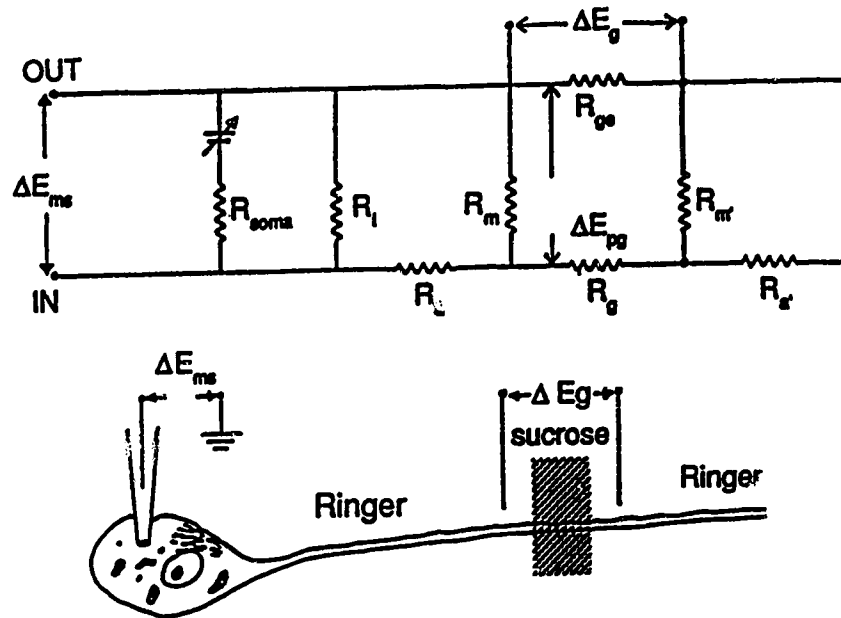
R_i sum of R_i and R_{soma} (input R)

R_{soma} actual soma resistance

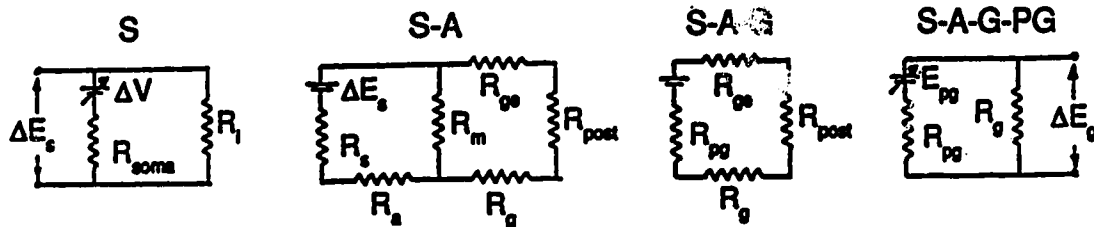
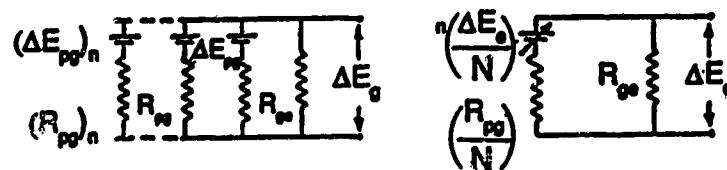
R_i total resistance; sum of $R_{pg} + R_s + R_{post}$

ΔV actual slow voltage change occurring at the soma

A



B Soma and axon (single)

C Whole nerve (N - axons)

It is important to note that the electrical events measured by this technique are attenuated and probably represent 10-25% of the actual voltage change occurring at the cell body. The technical reasons for this reduction are due to the positioning of the cell body relative to the wax/vaseline seal, the quality of the seal, the number of cells responding, and the cable properties of the axons involved in the propagation of graded responses (McAfee, 1982).

An explanation of the differences between an actual potential change occurring at the soma and that recorded by the sucrose-gap technique can be obtained by converting the physical characteristics of the neuron to an electrical correlate (Thevenin equivalent circuit) (see Grob, 1977). The following theoretical modelling is adapted from McAfee's comprehensive paper (1982).

The Thevenin equivalent of an amphibian sympathetic ganglion neuron is illustrated in Figure 4. The potential at the soma (E_s) is the actual resting membrane potential and R_{soma} is the soma membrane resistance. However, the soma voltage, as measured by a microelectrode (E_m), is dependent on the quality of the soma-electrode seal. The better the seal, the closer E_m is to E_s .

In the event of a slow voltage change (ΔV) occurring at the soma, the voltage change measured by the microelectrode (ΔE_m) is also dependent on the leakage due to penetration injury (R_i) as indicated by equation (1).

$$(1) \quad \Delta E_m = \frac{\Delta V R_i}{R_{soma} + R_i}$$

Again, if the penetration injury is minimal, R_i is larger, thus ΔE_m approaches ΔV . The total resistance of two resistors in parallel is the sum of their inverse and resistances contributed by R_i and R_{soma} can be reduced to a single resistance (R_s), which is the measured input resistance of the cell (see equation (2)).

$$(2) \quad \begin{aligned} a) \quad & \frac{1}{R_s} = \frac{1}{R_{soma}} + \frac{1}{R_i} \\ b) \quad & R_s = \frac{R_{soma} R_i}{R_{soma} + R_i} \\ c) \quad & \frac{R_s}{R_{soma}} = \frac{R_i}{R_{soma} + R_i} \end{aligned}$$

If (2) c) is substituted into equation (1), the result (3) will represent the change in voltage observed when recording from the soma via a microelectrode. The Thevenin circuit equivalent is shown in Figure 4B, S.

$$(3) \quad \Delta E_m = \frac{\Delta V R_s}{R_{soma}}$$

However, in sucrose-gap recording, as a voltage change travels along an axon, it is reduced according to the cable properties of the axon. Axons have a high resistance component across its membrane (R_m) and a comparatively lower axolemma resistance (R_a) along its axis. Therefore, the pre-gap membrane potential

change (ΔE_{pg}) must be less than ΔE_m , due to the voltage drop contributions of both R_m and R_s (Figure 4B, S-A).

$$(4) \quad \Delta E_{pg} = \frac{E_m R_m}{R_s + R_a + R_m}$$

Again, the contribution of R_s , R_a and R_m can be reduced to a single pre-gap single resistance R_{pg} .

$$(5) \quad a) \quad R_{pg} = \frac{R_m (R_s + R_a)}{R_s + R_a + R_m}$$

$$b) \quad \frac{R_{pg}}{R_s + R_a} = \frac{R_m}{R_s + R_a + R_m}$$

Substituting equation (5) into (4) gives the pre-gap potential change (ΔE_{pg}) represented by (6) and Figure 4B, S-A-G.

$$(6) \quad \Delta E_{pg} = \frac{\Delta E_m R_{pg}}{R_s + R_a}$$

The measured potential change measured across the sucrose gap (ΔE_g) is represented by the Thevenin equivalent.

$$(7) \quad \Delta E_g = \frac{\Delta E_{pg} R_g}{R_g + R_t}$$

Where R_t is the total resistance contributed by the pre-gap (R_{pg}), plus the internal resistance of the gap (R_g) and the post-gap axon resistance (R_{post}) as shown in equation 8 where R_a is the post-gap axoplasm resistance and R_m is the post-gap axolemma resistance.

$$(8) \quad a) \quad R_t = R_{pg} + R_g + R_{post}$$

$$b) \quad R_t = \frac{R_m(R_a + R_m)}{R_a + R_m + R_m} + R_g + \frac{(R_a \cdot R_b)}{R_a + R_b}$$

E_g is about 80-95% of E_{pg} because the external resistance of the gap (R_{pg}) is generally many times higher than R_g . The consequence of leaky seals diminishes R_{pg} and results in a large amount of signal shunting. From equation (7), the potential across the sucrose-gap must be less than the pre-gap potential. Therefore, the rank order of the potential recorded from a neuron is: $E_i > E_m > E_{pg} > E_g$. Clearly, any ΔV occurring at the soma will be progressively diminished due to the array of resistances encountered during as the signal proceeds along the axon.

The above discussion takes into account the behavior of only one neuron. When these methods are employed in the study of ganglionic tissue, the contribution of many neurons are monitored. However, under normal conditions the propagated potential of an active axon can be attenuated by shunting to an adjacent, inactive, axon. It is therefore important to ascertain how many neurons are active. Equation 9 and Figure 4C represents ΔE_g due to the activity of "n axons" of the total axonal population (N).

$$(9) \quad \Delta E_g = \frac{n(\Delta E_{po}/N) (R_g)}{R_g + (R_i/N)}$$

The magnitude of ΔE_g is directly proportional to the number of active axons. Another factor to consider is the relative distance that the cell bodies are situated prior to their entry into the high resistance sucrose-gap. McAfee (1982) calculated that the distance ranged from a minimum of 0.5 to 2.5 millimeters in rat SCG and the ratio of E_m/E_g of a whole ganglion was about 11% of the soma-dendritic potential if all the neurons contained in the ganglion changed membrane potential at exactly the same instant. When drug-induced voltage changes are being studied, diffusion must be considered since neurons on the outside of the ganglion respond before the more centrally located neurons. Therefore, a synaptically-evoked response would be considered more synchronous compared to a drug-induced effect.

Sucrose-gap recording may however be a better method for recording voltage changes compared to microelectrode recording if the following circumstances occur:

- 1) Many small cells remain refractory to microelectrode recording due particularly to the damage which impalement inflicts on the cell membrane, resulting in a large degree of shunting.
- 2) Since the sucrose-gap records a potential across an axonal segment, signals that are initiated at the axon hillock, or the axon itself, may

not be detected by a microelectrode placed in the soma. This is due to the signal attenuation which occurs in the soma membrane due its low impedance compared to that of the axon (Jack et al, 1975).

- 3) Many neuronal tissues under study are not homogeneous in their cellular make-up. In the amphibian sympathetic ganglion, there exists at least 3 neuronal subtypes (Dodd and Horn, 1983a). A neuron impaled with a microelectrode may not even be activated by a particular agent or pre-synaptic stimulus, however, under sucrose-gap recording conditions, an output would be detected if a response occurred in the population of the other cell types.

1.1.2. Experimental Preparation and Dissection.

Rana catesbeiana (8-12 cm body length) or Rana pipiens (4-6 cm body length) purchased from Anilab Canada (St. Foy, Quebec) were stored in a large inclined plastic bath at room temperature and continuously supplied with fresh running tap water. Generally, the animals remained unfed under these conditions for an average of two to three weeks prior to experimentation. Experiments were attempted throughout the year but it was found that responses from animals obtained between May and September often deteriorated rapidly. It was obviously impossible to collect data from such animals.

The animals were either pithed or decapitated and pinned to a dissecting board so as to expose the ventral surface and then viewed under a dissecting microscope (Wild type M3). The skin and rectus abdominis muscles were removed to expose the viscera. The cloaca was severed and the entire viscera, except for the kidneys, were removed by gently lifting and cutting of the connective tissue. The abdominal cavity was irrigated with frog Ringer's solution so as to remove blood. The kidneys were carefully separated from the underlying aorta. Ganglia 7 through 10 were removed with the sympathetic chain intact as well as a small segment of the 8th, 9th and/or 10th spinal nerves. The preparation was transferred and pinned to a layer of 'Sylgard®' in the bottom of a petri dish. The remaining connective tissue was carefully removed from the best ganglion-ramus communis combination for recording. This was chosen on the basis of the size of the ganglia, ramus length and ramus thickness. It should be noted that successful recording could be obtained from the 8th, 9th, or 10th ganglia and that it was necessary to remove the majority of the connective tissue from the chosen ganglion as well as from its respective ramus.

1.1.3. Recording Chamber.

The apparatus consists of a recording chamber adapted from the Nishi and Koketsu design (1968). The modified chamber with the experimental preparation in place is shown in Figure 5A. The ramus had to be a minimum of 2mm in length in order to span the sucrose compartment and be sealed properly. Therefore, if a

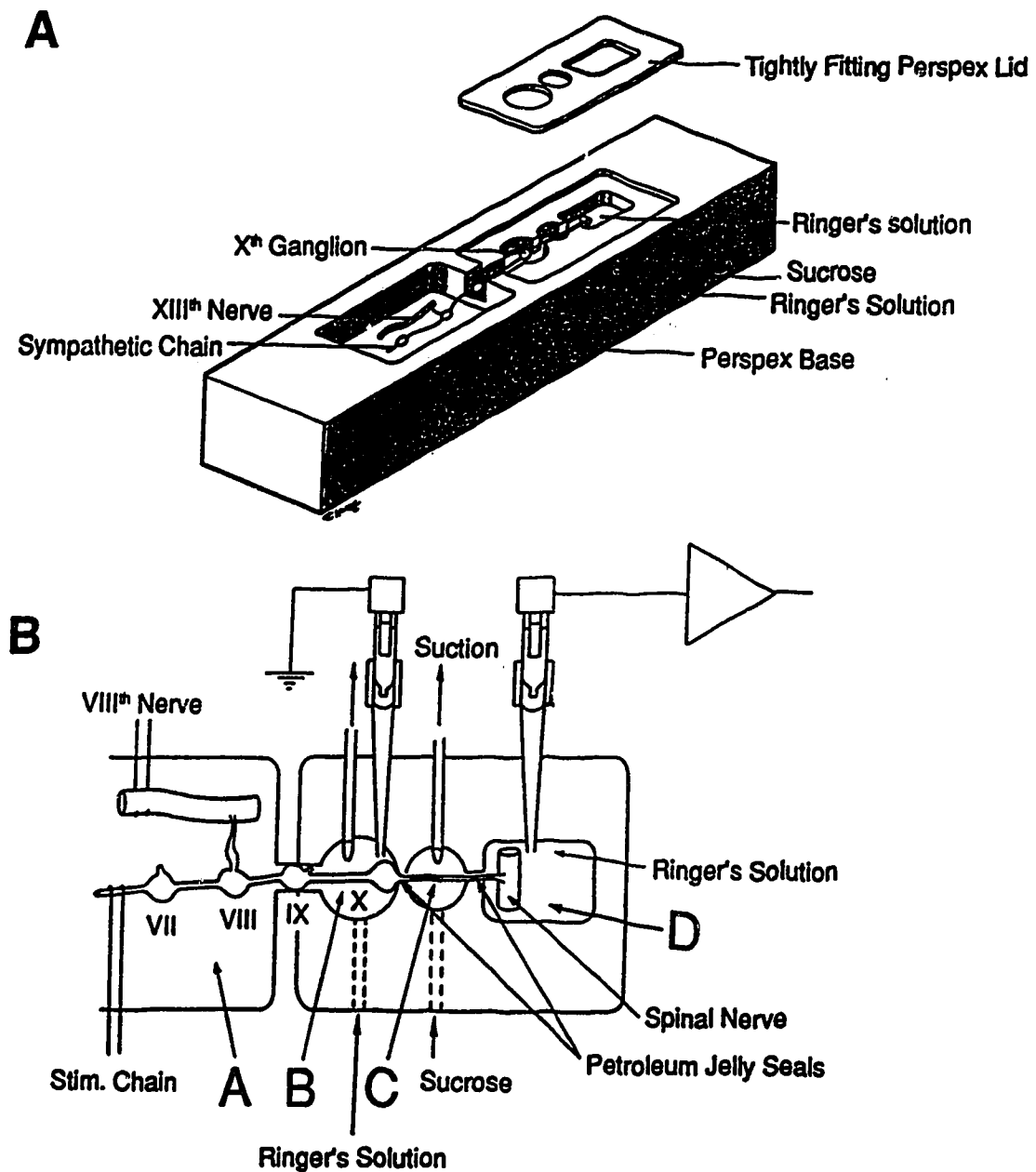


Figure 5. Schematic diagram of sucrose-gap recording chamber. **A.** Illustration of the recording chamber. **B.** Schematic diagram of top view showing a properly placed preparation for recording from the Xth ganglion. Also shows locations of compartments A (mineral oil), B (Ringer's), C (sucrose) and D (Ringer's).

preparation of marginal length was mounted, the recording was compromised due to inadequate seal formation and possible neuronal damage due to over-stretching of the post-ganglionic axons.

Figure 5B schematically illustrates the recording chamber, which consists of four different fluid compartments that are isolated from each other by vaseline-wax seals. Compartment A (300 μ l) contains the sympathetic chain and the eighth spinal nerve which are bathed in mineral oil. Compartment B (20 μ l) contains the 8th, 9th or 10th ganglion and is continually perfused with frog Ringer's solution. The whole ganglion is electrically isolated from compartment D by the perfusion of a poorly-conducting, isotonic sucrose solution (76 g/l in deionized water) through compartment C. The perfusing fluids are removed from the top of compartments B and C by syringe needles connected to separate vacuum sources. A short section of the spinal nerve at the end of the ramus is immersed in frog Ringer's solution in compartment D (120 μ l). The fluid in Compartment D is not perfused and is sealed completely with wax film-vaseline combination for the entire experiment to eliminate fluid loss by evaporation. The axons in the ramus communicans conducted whole ganglia electrical activity (attenuated due to the various shunts described in the previous section). This was measured as a potential difference between the recording electrode located in compartment D and the ground electrode located in compartment B. The resulting signal represents the population response of the whole ganglion. Experiments were carried out at room temperature (range 20-25°C).

Standard platinum bipolar stimulating electrodes (located in compartment A) were used to independently evoke synaptic potentials. Orthodromic, single pulse supramaximal stimulation of the sympathetic chain, rostral to the 8th ganglion, selectively activated sympathetic B-fibers and stimulation of the 9th spinal nerve selectively activated C-fibers (see Figure 1B in Introduction). Synaptic potentials were used to normalize values to compare control versus pertussis toxin treated groups (see Results). In some experiments, the C-cell f-EPSP was attenuated with 70 μ M dTC so as to monitor s-IPSP. This slow synaptic potential could be recorded using a single stimulus, however, it was best recorded using a supramaximal stimulus train of 1ms pulses at 10 Hz for 1s.

Figure 6 illustrates a block diagram of the components used for sucrose-gap recording. The electrical potential was measured using Fisher Calomel Reference Electrodes (Model E-6A) filled with concentrated potassium chloride (KCl). These electrodes were fitted with a modified Pasteur pipette tip containing 2% agar in glucose-free Ringer's solution which electrically coupled the electrode with the bath Ringer's solution. Signals were amplified 2.5 or 10 times using a high-impedance amplifier which was custom built in the Department of Pharmacology workshop. Data were recorded on a Gould 2400 rectilinear chart recorder and filters were set to -3 dB at 5 Hz. Fast signals (f-EPSP) were observed on an Iwatsu SS 5802 storage oscilloscope. In some cases, signals were captured using a Gould 13-4616-10 Single Channel Waveform Recorder which is capable of digitizing and storing a 20msec - 5s signal in a 2048 bit memory. The stored signal was removed

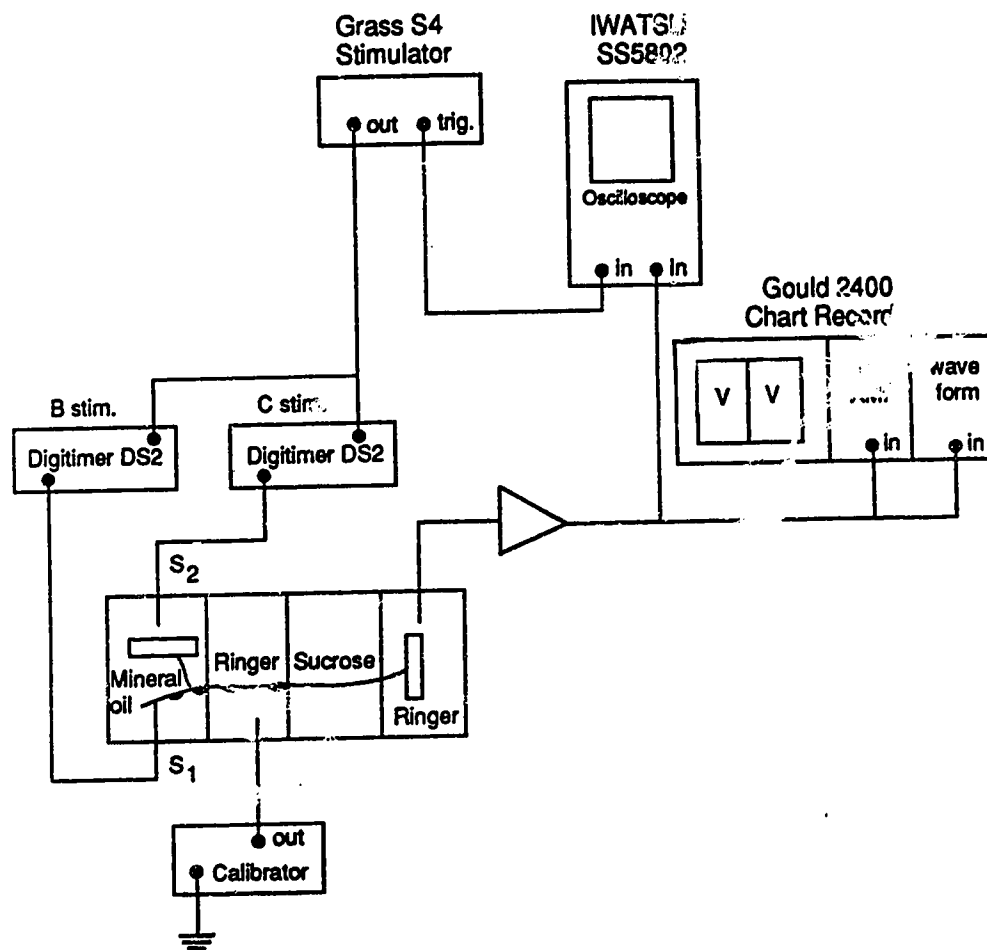


Figure 6. Circuit diagram of electronic apparatus used for sucrose-gap recording experiments. Signal amplified 2.5 or 10X. (Modified from Rafuse, 1985.)

from the memory, at a rate within the frequency response range of the chart recorder, thus reconstructing the entire analogue signal.

1.1.4. Solutions.

Unless otherwise stated, frog Ringer's solution of the following composition was used in all sucrose-gap experiments: NaCl:100mM, CaCl₂:1.3mM, KCl:2mM, Tris(hydroxymethyl)aminomethane HCl (Tris-HCl) (pH 7.2):16mM and d-glucose:5.5mM in deionized, distilled water. The building distilled water supply was deionized by filtration through a series of five Barnstead cartridges (1 organic removal, 2 high capacity and 2 ultrapure mixed-bed) resulting a resistivity of about about 20 M Ω /cm².

Except as stated below, all drugs were dissolved directly in Ringer's solution. In all of the cases where the effect of adrenaline was studied, 500nM of the uptake 1 blocker desipramine (DMI) was added. Forskolin and dantrolene and were initially dissolved in dimethylsulphoxide (DMSO) prior to the further dilution with Ringer's. The maximum concentration of DMSO used was 2% by volume and the vehicle was included in all of the solutions used in these particular experiments. It has been previously established that this concentration of DMSO does not attenuate the drug responses recorded by means of the sucrose-gap technique (Rafuse, 1985). The muscarinic blocker 11-[[2-[(diethylamino)methyl]-1-piperidinyl] acetyl]-5,11-dihydro-6H-pyrido [2,3-b] [1,4]benzodiazapine-6-one) (AF-DX 116) was initially

dissolved in 1M HCl. AF-DX 116 stock solution did not exceed 0.01% by volume upon dilution by Ringer's and did not affect the pH. In experiments where pertussis toxin (PTX) was used, a stock solution was made using sterile, glucose-free Ringer's solution and stored at 4 °C prior to dilution in frog Ringer's. It was not necessary to pre-activate the pertussis toxin since experiments were always performed on intact cells and require the entire protein for activity (Moss et al, 1983).

1.1.5. Solution Delivery System.

The whole ganglion and ramus compartments were continuously superfused. Solutions were delivered by gravity from glass dripper bottles fixed to a Travenol JC0002 solution administration set (60 drops = 1ml). Four, three-way valves were inserted in the Ringer's feed line to permit uninterrupted drug delivery to the ganglion compartment. The flow rate, of about 1ml/min, was determined by a needle valve located downstream of the three-way valve system. A latency of about 20 seconds existed between the turning on of the three-way valve and the delivery of the agent to the ganglion chamber.

In experiments where the effect of PTX was studied, the toxin solution was recycled at a rate of 1ml/min to the whole ganglion chamber using a mini-perfusion pump (Pharmacia Peristaltic Pump P-3). Recording during this application time was not feasible because of the electrical noise introduced by the pump. Also, the

positioning of the tube carrying the return flow did not permit the reference electrode to be properly placed.

In some experiments the effects of the peptides, LHRH and the bee venom toxin, apamin, and other expensive agents were studied. Due to the relative cost of such chemicals, small volumes were delivered by slow injection via a 1 ml syringe through a three-way valve located just upstream from the needle valve.

1.2. WHOLE-CELL PATCH-CLAMP EXPERIMENTS.

1.2.1. Theory.

a) Introduction.

The first report of single ion channel currents were described by Neher and Sakmann (1976) in frog muscle fibre. Measurable currents were detected through the patch of membrane encircled beneath a recording pipette. A strong chemical interaction between the heat-polished glass pipette and the muscle membrane resulted the formation of an electrical seal, in the order of about 50 M Ω , which significantly improved the signal to noise ratio. Furthermore, the accuracy of current measurement through a membrane patch could be improved by increasing the quality of the seal between the glass pipette and the membrane. Sigworth and Neher (1980) showed that by using very clean polished pipettes (2-5 M Ω) and the

application of a small amount of negative pressure to the interior of the pipette, after contact with the membrane, electric seals in the order of 10-100 G Ω could be attained in many biological membranes. This resulted in an order of magnitude increase in current detection compared to M Ω seals. Moreover, the voltage across the patch of membrane was more accurately controlled due to minimizing current leakage between the electrode and the membrane. This permitted the voltage-clamp study of many cells without damage caused by the use of conventional single electrode voltage clamp method. The introduction of "giga-seal" recording technique offered a significant improvement in frequency response of recording which permitted the accurate studies on channel kinetics that, prior to this advance, were purely speculative (Hamill et al, 1981).

The formation of a "Giga-seal" cell-attached patch also resulted in a high degree of mechanical stability that enabled other recording configurations such as Cell-Attached, Whole-Cell Recording (WCR), Outside-Out patch and Inside-Out patch to be attained by simple manipulations (see Hamill et al, 1981).

All experiments described within this thesis utilized the whole-cell recording technique and the theory described hereafter will address the aspects involved with this mode of recording.

b) Whole-cell recording.

The WCR technique was first described by Hamill et al (1981). These authors reported that when short pulse of suction was applied to the interior of the

patch pipette, after a G_{Ω} seal was established in the cell-attached mode, the small area of membrane encircled by the pipette tip could be disrupted without compromising the quality of the seal. This provided a low resistance pathway to the interior of the cell with a minimum of damage and permitted high fidelity current recording from the whole cell membrane rather than a small membrane patch. This is somewhat similar in principle to the "Kostyuk method" of recording from dialysed snail neurons (Kostyuk and Krishtal, 1977), however the recording resolution of that technique is lower than WCR since seal resistance as high as only $1 G_{\Omega}$ could be attained.

WCR provides distinct advantages over conventional microelectrode recording. The main advantage of WCR is the ability to record from small cells which were previously refractory to electrophysiological methods (due to cell damage upon microelectrode impalement). The second advantage is gained due to the low series resistance of the patch electrode which allows better voltage control of the membrane (Marty and Neher, 1983).

c) Electronic design and circuitry for WCR.

The design of the circuitry must provide the means to successfully record small signals at an inherently low noise level with a wide bandwidth. A simplified schematic of the basic components involved, shown in Figure 7, are as follows: A)

I/V converter, E) Frequency boost, C) Fast and slow pipette capacitance cancellation, D) Whole-cell RC compensation, and E) Series resistance compensation.

I/V converter allows the measurement of small currents by monitoring the voltage drop across a resistor. The resistor used for these purposes must be large so as to minimize error the current drawn from the voltage sources and generally ranges from $500\text{ M}\Omega$ - $50\text{ G}\Omega$ for typical patch-clamp amplifiers. The voltage is controlled by an operational amplifier (op-amp) which compares the source voltage with a reference voltage. If a voltage difference exists, the current output from the amplifier is fed back through the resistor until the voltage at the two inputs are equal (current through a resistor = Voltage).

The mathematical derivations of the following functions are complex and require the solving of first and second order differential equations as well as an understanding of Laplace transformation to describe the design and frequency response for an ideal patch-clamp I/V converter. The discussion below will describe important factors involved in the design and one can refer to Sigworth (1983) for a more in-depth mathematical explanation.

The optimal design of an I/V converter suitable for patch-clamp recording must incorporate the following dynamic characteristics. The frequency response (Z) of an op-amp acting instantaneously at a certain frequency, z , is governed by feedback resistors resistance (R_f) and capacitance (C_f) as indicated by (1).

$$(1) \quad Z(z) = R_f / (R_f C_f z + 1)$$

As z increases, the amplifier will have a unity output until the response begins to roll-off. The feedback resistor time constant (τ_f) can be minimized by choosing a resistor with a very low shunt capacitance.

However, under normal circumstances, the op-amp has a finite speed as well as an input capacitance (C_{in}) that must be incorporated in the equation to properly describe the frequency response characteristics of the I/V converter. The time constant of the op-amp (τ_{amp}) is the inverse of the gain-bandwidth product and the total input capacitance ($C_i = C_f + C_{in}$) and the frequency response as a function of z ($Z(z)$), is described by equation (2).

$$(2) \quad Z(z) = R_f / (\tau_{amp} R_f C_i z^2 + (\tau_{amp} + \tau_f) z + 1)$$

This equation can be reduced to the following quadratic equation (3) that is similar to (1), but has an additional component to describe the finite speed of the op-amp.

$$(3) \quad Z(z) = R_f / ((\tau_{amp} z + 1)(\tau_2 z + 1))$$

$$\text{where: } \tau_1 = \tau_f \text{ and } \tau_2 = \tau_{amp} (C_f / C_i)$$

One may think that the cutoff frequency could be maximized by simply reducing the stray capacitance across the feedback resistor, however, since $\tau_1 = C_f R_f$, any decrease in τ_1 will result in an equal increase in τ_2 . If the two time constants are equivalent ($\tau_0 = \tau_1 = \tau_2$), the frequency response can be described as a dampened harmonic oscillator (4).

$$(4) \quad Z(s) = R_f / (\tau_0^2 s^2 + 2\xi\tau_0 s + 1)$$

where ξ = damping factor.

The problem that arises from the above discussion is that the components required to design an op-amp with a reasonable bandwidth require an ultra-fast op-amp as well as a feedback resistor with a very low stray capacitance. For example, a natural high frequency I/V converter (ie. bandwidth = 10KHz, $R_f = 10 \text{ G}\Omega$ and $C_m = 10\text{pF}$) would require an amplifier gain-bandwidth product of 60 MHz ($\tau_A = 2.6 \times 10^{-9} \text{ s}$) and at the same time the stray capacitance would have to be in the 10^{-15} range (Sigworth, 1983).

Since the design of such an op-amp is not feasible, an alternative is to select components for which τ_2 is smaller and roll-off occurs beyond useful frequency range of the op-amp. Such a system will therefore act instantaneously in the range of frequencies required for patch-clamp study. This is accomplished by choosing

a large enough R_f and a fast enough op-amp so $\tau_1 \gg \tau_2$ and the frequency response reduces to equation 1. As a consequence of selecting a large feedback resistor, the increase in stray capacitance significantly reduces the bandwidth. This can be compensated for by incorporating a correction circuit to increase the frequency response.

Frequency correction circuit. The amplifier used in these studies (Axopatch 1-B, Axon Instruments) has a τ_1 of 0.25 ms ($R_f=500\text{ M}\Omega$ and $C_f=0.5\text{ pF}$). Therefore, the first roll-off (0.707 of unity gain) of the signal from the op-amp, due entirely from the feedback resistor, occurs at 4500 Hz. This bandwidth range is inadequate and must be improved by a frequency boost or correction circuit. Figure 8A shows a simplified correction circuit that ~~increases~~ the recording bandwidth of the Axopatch 1-B. The circuit essentially takes the derivative of the input from the I/V converter (Z_c) and adds it back to the input (ZZ_c). This markedly improves the frequency response. However, the boost circuitry must be tuned properly so that the time constant of the I/V converter (τ_1) matches the time constant of the correction circuit (τ_c). The limit of correction is governed by the τ_2 value which is beyond the useful frequency response range for patch clamp recording. Figure 8B shows the three functions and the resulting improvement of frequency response of the amplifier by the correction circuit.

Frequency Boost circuit

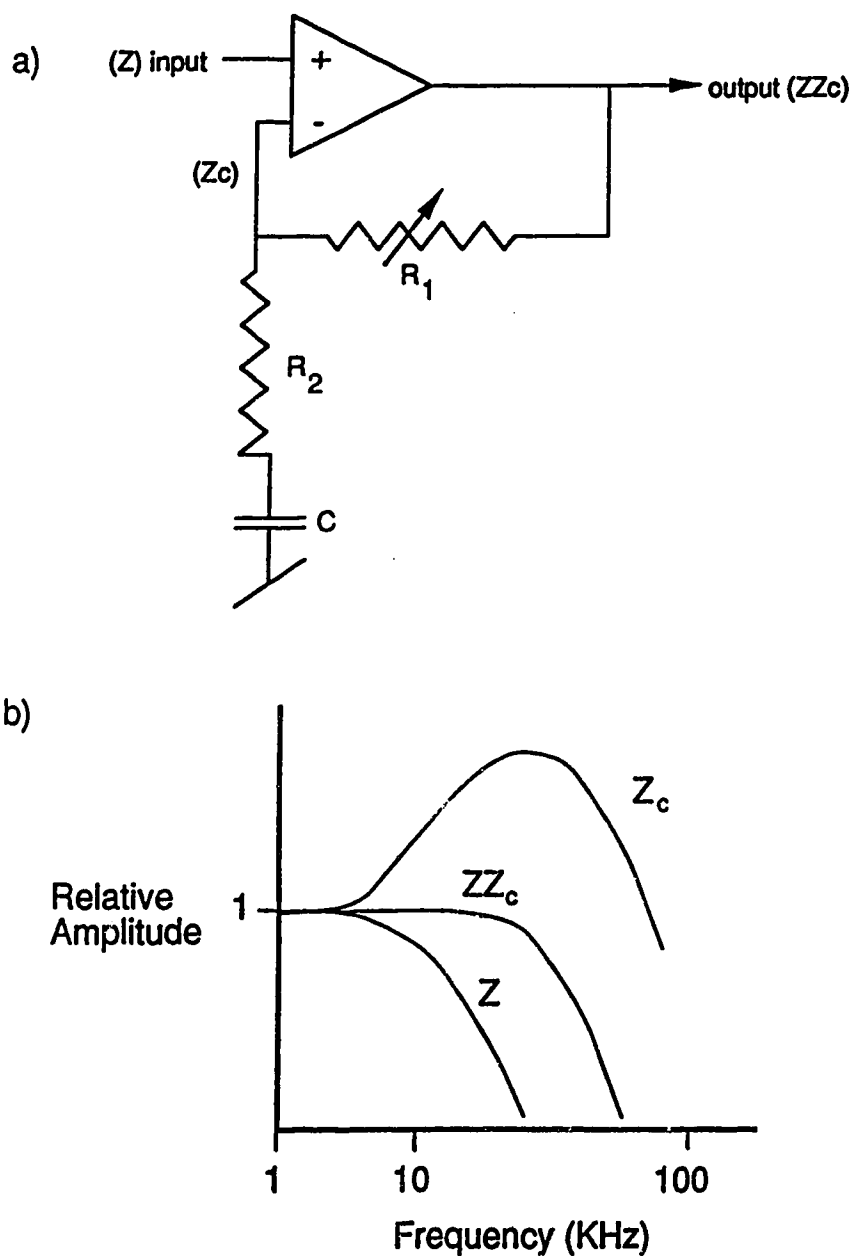


Figure 8. Theory and operation of a frequency boost circuit for patch clamp recording. **A.** Simplified circuit diagram of a frequency correction circuit which boosts amplifier bandwidth. **B.** The bandwidth is increased from 4000Hz (Z) to about 40KHz (ZZ_c) by summing Z with its derivative (Z_c). Modified from Sigworth (1983).

The actual behavior of the Axopatch 1-B feedback resistor does not follow a first order function as depicted by Z in Figure 8B, thus the boost circuitry is some what more complicated. However, the concept that the correction circuit adds the appropriate function to the I/V converter output to increase the frequency response remains universal.

Fast and slow pipette capacitance compensation. The principal method for obtaining useful voltage clamp information is to set the command potential and monitor the current flow from the previously described circuitry. During any voltage change, current flows through the feedback resistor and charges the pipette capacitance. If this current is not corrected for a large transient current appears can saturate the I/V op-amp and/or the frequency correction circuit and result in a significant distortion of the current recorded. Moreover, the voltage clamp is lost due to the breakdown of the feedback loop of the op-amp. Proper compensation of the pipette capacitance is important for single-channel currents and for large whole-cell currents. Since the currents studied in this thesis were small, it was not necessary to use this circuit to compensate for the pipette capacitance.

Whole-cell capacitance compensation circuit. Upon the establishment of whole-cell recording, the additional capacitance component provided by the cell membrane must be compensated. This current is much slower compared to the electrode capacitance because the membrane is charged through the cell series

resistance. Proper adjustment of the whole-cell compensation is described in detail below (See Methods section 1.2.7; Establishment of WCR).

Series resistance compensation. The series resistance compensation circuit for patch clamp recording is a feedback circuit used to correct the voltage drop that occurs as current flows through the tip resistance of the patch pipette. In WCR, the voltage drop may be significant. For example, if the whole-cell current under study was 2 nA and the series resistance was 15 M Ω , the voltage error would be 30 mV. However, the series resistance compensation circuit was not utilized in obtaining the data contained in this thesis because the whole-cell potassium currents from the largest cell studied did not exceed 300 pA and a series resistance did not exceed 15 M Ω . This would result in a maximum voltage error of 4.5 mV.

1.2.2. The Dynamics Of Pipette-Cytoplasmic Fluid Exchange.

Successful WCR using electrodes with tip resistances as low as 0.5 M Ω has been reported. However, as a consequence of the large diameter of the electrode tip, the fluid contained within the pipette can rapidly exchange with the cytoplasmic contents (see below). It is therefore important that the ionic composition of the internal solution is similar to that contained in cytoplasm. The rate of exchange depends on the mobility of the various components is related to basic diffusion principles. The Stokes radius is proportional to the rate of diffusion such that the

exchange of Na^+ ions will exchange much faster ($\tau \approx 5\text{s}$) than a globular protein with a Stokes radius of 50 Angstroms ($\tau \approx 3\text{min}$) (Marty and Neher, 1983). Also, the affinity which various cytoplasmic components have for ions, such as Ca^{2+} or H^+ , may result in sequestration and effectively slow the rate of exchange. Furthermore, large vesicles and organelles, such as mitochondria and endoplasmic reticulum, are not able to pass through the typical range of tip openings utilized.

A study of the relationship among these various factors has concluded that the rate of diffusion of ions or higher molecular weight compounds can be determined mathematically (Pusch and Neher, 1988). Formulae (1 & 2) were derived to illustrate the dependence of the molecular weight (MW in Daltons), the diffusion coefficient (D, in $10^7\text{cm}^2\text{s}^{-1}$) of compounds, and the pipette access resistance (R_p) on the rate of pipette-cellular content exchange (τ) using bovine chromaffin cells (Pusch and Neher, 1988).

$$(1) \quad \tau = 78.4 (R_p/D)$$

or

$$(2) \quad \tau = 0.60 (R_p \times \text{MW}^{1/3})$$

It is important to note that these results were obtained from bovine chromaffin cells, which are spherical in shape, with an average whole cell capacitance of 5.9 pF. If other cells are used that are geometrically similar, the

appropriate τ value (τ_2) can be obtained by a simple scaling formula derived from the relationship between the two cells radii (r), volume (Vol), or whole cell capacitance (C_m) as shown in (3).

$$(3) \quad \tau_2/\tau_1 = (r_2/r_1)^3 = (\text{Vol}_2/\text{Vol}_1) = (C_{m1}/C_{m2})^{1/3}$$

One disadvantage of the rapid exchange is that it is probably responsible for the "run-down" effect wherein the recorded ionic currents progressively diminish during WCR. This limits the available recording time of many cells under study. This phenomenon is particularly evident in the study of calcium currents (Belles et al, 1988) and suggests that an intracellular factor may be responsible for the maintenance of ion channel function (Catterall, 1988).

Investigators have included various substances such as nucleotides or protease inhibitors in attempts to preserve ionic currents. Some have gone to extreme lengths to mimic cytoplasmic intracellular contents. For example, actually extracting cytoplasm from the particular cell type under study for use as the internal solution. However, after this rather tedious extraction the pipette blocks quite easily.

On the other hand, there are certain advantages to the fast exchange of the pipette solution with the cytoplasmic contents because the low resistance recording pipette provides an excellent means by which various chemicals can be applied directly to the intracellular compartment. This is a distinct advantage over

conventional methods that allow agents with high lipid solubility or those that are transported by membrane bound carrier systems to gain access to the intracellular milieu.

Therefore, WCR provides significant technological advances that enable accurate electrophysiological studies to be performed on many small cells for the first time. Also, it provides an excellent means for the delivery of agents that affect cell biochemistry while enabling the experimenter to study the electrophysiological consequences of such manipulations.

1.2.3. Dissociation Of Sympathetic Neurons.

The method used in these experiments was developed from the descriptions of the enzymatic dissociation of snail ganglion neurons (Kostyuk et al, 1974) and from Rana catesbeiana paravertebral sympathetic neurons (Kuffler and Sejnowski, 1983; Schofield et al, 1988).

The paravertebral sympathetic ganglia were excised from 2-3 Rana pipiens as described earlier in this chapter. It was not necessary to remove the preparation with the spinal nerves intact; however, removal as such provided suitable sites for proper pinning to the petri dish. The remaining connective tissue surrounding the ganglia was removed under 40X magnification. Each ganglion was cut in a ribbon-like manner by making about ten deep cuts almost through the body, five from each side, with fine iridectomy scissors. The sectioned ganglion bodies were

dissected free from the sympathetic chain and placed in a 50ml plastic tissue culture vessel (Nuclon 20/160) that contained 3 ml of 3mg/ml of trypsin (Sigma type III) in external solution (see next section in Methods for composition).

The culture vessel containing the ganglia was mechanically agitated at 2 Hz in a temperature-controlled water bath at 37°C for 35-50 minutes. The trypsin solution was carefully removed with an Eppendorff pipette and replaced with 3mls of 1mg/ml collagenase (Sigma type 1a) in external solution. The vessel was then agitated, under the same conditions, for another 20-25 minutes. The collagenase solution was slowly removed, such that the loss of visible tissue was minimized, and replaced with 4 mls of external solution. The final dissociation was accomplished by gently drawing and expelling the tissue-solution suspension four or five times into a 1000 μ l Eppendorff pipette. The cells were then transferred to 35mm plastic petri dishes and either stored in the refrigerator at 4°C, or superfused with fresh external solution to remove residual enzymes. There was no discernable effect between the refrigerated unsuperfused cells and those cells which were used immediately. In some cases, the stored, refrigerated cells appeared more viable than cells that were superfused immediately. In all cases, the cells were permitted to adhere to the bottom of the plastic petri dish for 60-90 minutes prior to experimentation. Fresh cells were prepared each day and experiments were performed at room temperature.

1.2.4. Solutions.

a) External solutions.

The composition of the external solution was: NaCl:117mM, KCl:2mM, CaCl₂:2mM, MgCl₂:2mM, Hepes/NaOH (pH7.2):5mM and d-glucose:10mM. In those cases where [KCl]_o was increased to 6mM, 20mM or 60mM, the appropriate osmolarity (248 mOsm) was maintained by reducing the [NaCl] to 113mM, 99mM or 59mM respectively. The external solution was usually prepared for each experiment in a quantity sufficient for an entire experiment to ensure constant experimental conditions. All external solutions were filtered through a 0.22 μ m filter (Millipore) to remove particulate matter found in typical laboratory grade chemicals that can impair electrode-membrane seal formation (Hamill et al, 1981).

b) Internal solution.

As previously mentioned, it was important that the 'experimental internal solution' mimicked the 'actual internal solution' composition of frog sympathetic ganglion cells as well as possible. The composition of internal solution for all experiments was KCl:110mM, NaCl:10mM, MgCl₂:2mM, CaCl₂:0.4mM, EGTA:4.4mM², Hepes/KOH (pH 7.2):5mM and d-glucose:5mM. The osmolarity (Osm) of the above solution was measured to be 248 mOsm using an osmometer

(Westcor 5500). The rate of use of the internal solution was very slow and thus served as the standard to which the external solution osmolarity was compared. The external solution was deemed acceptable if the difference in osmolarity did not exceed 4 mOsm (2% difference).

The free Ca^{2+} in the 'internal solution', measured with a Ca^{2+} selective electrode, was about 100nM. The free Ca^{2+} was buffered by the ratio of added CaCl_2 : EGTA. Under control conditions this ratio was 1 : 11. In experiments where the effects of raising intracellular $[\text{Ca}^{2+}]$ were studied, 4mM CaCl_2 : 4.4 mM EGTA buffered the free Ca^{2+} to about $1\mu\text{M}$ (Portzehl et al, 1964). However, the exact concentration of internal calcium in B-and C-neurons was not determined.

Early experiments utilized the above internal solution, however, the inclusion of various nucleotides or cyclic nucleotides have been proposed to play a role in the maintenance of whole cell currents (Lee and Tsien, 1984; Pfaffinger et al, 1985; Belles et al, 1988). Therefore, the majority of the experiments were conducted with either cyclic adenosine monophosphate (cAMP; $100\mu\text{M}$), adenosine triphosphate (ATP; 1.5mM), or guanosine triphosphate (GTP; 1.5mM) included in the internal solution (all Na^+ salts).

The electrodes were filled with internal solution by backfilling with a syringe. The solution was filtered through a $0.22\mu\text{m}$ in-line needle filter to remove particulate matter that could impair pipette-membrane seal formation. The electrode was filled to about 5mm from the top and the outside of the electrode was dried to minimize noise generated by solution leakage inside the electrode

holder. Bubbles were removed by gentle tapping of the electrode. It was important to fill the electrodes with polyethylene tubing rather than a metal hypodermic needle because EGTA will chelate metal ions from the inside of the needle that alters the EGTA/free Ca^{2+} ratio as well as decrease the pH of the internal solution (see Corey and Stevens, 1983).

1.2.5. Experimental Apparatus.

a) Recording chamber and perfusion system.

The recording chamber, shown in Plate 2, was designed to accommodate a 35mm plastic petri dish containing the dissociated cells. Three holes, 3/8" in diameter, surrounding the petri dish provided small reservoirs for the placement of syphons for inflow and outflow of bath solutions. This arrangement facilitated the adjustment of fluid level with minimal disturbance to the dissociated cells. The external solution was superfused through the petri dish and removed by a vacuum located opposite the inlet site. The third hole contained the sintered silver-silver chloride (Ag-AgCl) ground reference electrode (A-M systems, cat. # 5330) that was electrically coupled to the petri dish by a third syphon tube.

Plate 2. Whole-cell patch clamp recording chamber design. Positioning of the inflow, outflow, and ground chambers and their syphons to and from the bath.

headstage

patch pipette

u-tube

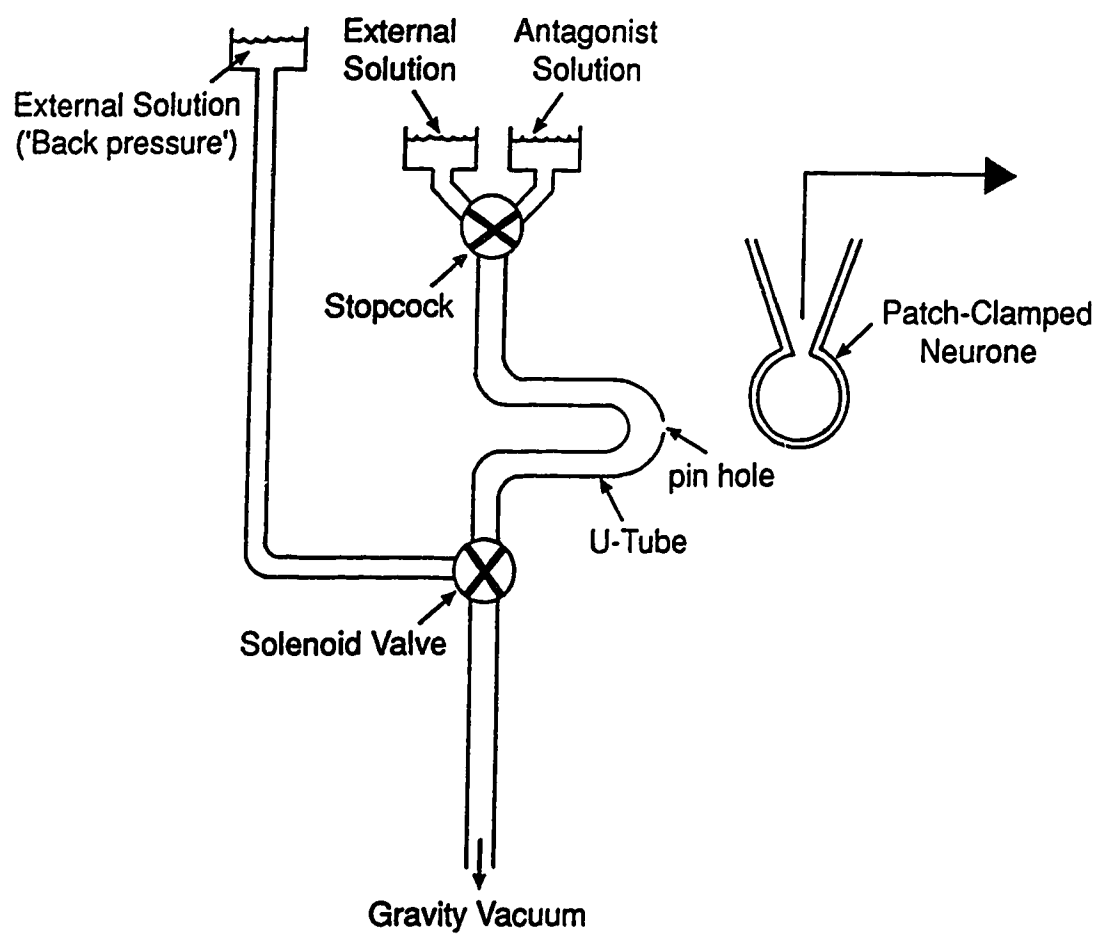
bath perfusion inlet

siphon inflow to bath

dissociated neurons

plexiglass base

Figure 9. U-tube methodology for external drug application. The drug solution is continuously perfused through the polyethylene tubing by gravity feed. Note the pinhole at the apex of the U-tube. When the gravity drain is switched, by means of an electrically controlled 3-way solenoid valve, to a positive pressure head, the only remaining path for the fluid is to be ejected into the bath through the pinhole. This provides rapid and local application of the agent directly onto the cell without noticeable effect on the recording. When the gravity feed switched back to the gravity drain, the fluid is no longer ejected. In this mode, the fluid flowing through the tubing, past the pinhole, creates small pressure gradient which removes fluid from the bath. This action acts as a convenient drug uptake system and one does not have to rely on slow bath perfusion to remove the drug from the area surrounding the cell.



b) Drug delivery system.

Drug solutions were applied by the U-tube method (Krishtal and Pidoplichko, 1980). Figure 9 illustrates the hydrodynamics of this method. The U-tube was positioned about 300 μ m from the neuron under study. There existed a latency of about 0.2s between the turning on of a drug solution and the actual response. This latency was measured by examining the delay for the initiation of inward current following the switching to an external solution containing 20mM K⁺. Latency time was variable and depended on the back pressure, the positioning of the tube relative to the cell and the pin hole diameter, particularly if the pin hole was blocked with cellular debris collected as bath solution was drawn into the U-tube. The U-tube method provided economical, reproducible, and local drug application and removal as well as the flexibility to apply many agents onto the same cell.

c) Recording system

The recording chamber was mounted on a steel plate affixed to the base of a Nikon 'DIAPHOT-TMD' inverted microscope. The patch electrode was secured within an electrode holder (Axon Instruments model #HL-1-12) that was inserted directly into the headstage amplifier. The positioning of the electrode was controlled by a three dimensional hydraulic microdrive (Narashige Model MO-103M).

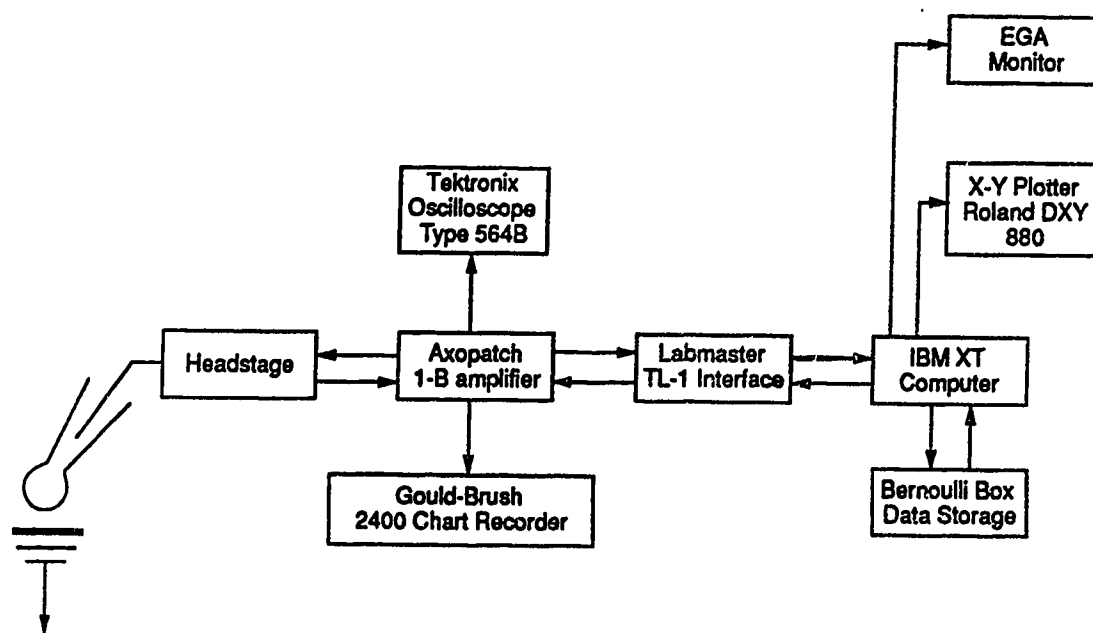


Figure 10. Block diagram of electronic apparatus utilized for whole-cell patch clamp recording.

The WCR electronic apparatus block diagram is shown in Figure 10. Whole cell patch-clamp recordings were obtained using an Axopatch-1B amplifier (Axon Instruments) interfaced with an IBM-XT computer by an Analogue to Digital (A/D) converter (Axon Instruments Labmaster TL-1 Interface). The amplifier was also connected to an oscilloscope (Tektronix Type 564B Storage Oscilloscope) that was used to monitor seal formation, membrane rupture, and to properly adjust the capacitance compensation. Most of the recordings performed were obtained in the voltage-clamp mode, however, an accurate measurement of the resting membrane potential was obtained in current-clamp mode. Software-generated voltage protocols and the resulting current responses were obtained and analyzed using the 'Pclamp' computer program (Axon Instruments).

The currents obtained from the two principal voltage protocols utilized are illustrated in Figure 11. Voltage-jumps, shown in panel A, were generated by 'Pclamp' software to deliver a series of voltage steps for a pre-determined time interval and then return to the holding potential (filtered at 500 Hz). The voltage-ramp protocol utilized a 5s ramp of voltage from the holding potential (-30mV) to a desired voltage (usually -110mV; filtered at 200 Hz). The steady-state currents measured from the voltage jumps (●) are superimposed on the whole-cell current obtained from a ramp of voltage in B, indicating that the ramp protocol is an excellent approximation of steady state I/V curves in the -30 to -110 mV range. The 'Pclamp' software also digitally acquired data in a 2048 point buffer, therefore, the resolution of the currents obtained using voltage jumps was ranged from 1.46

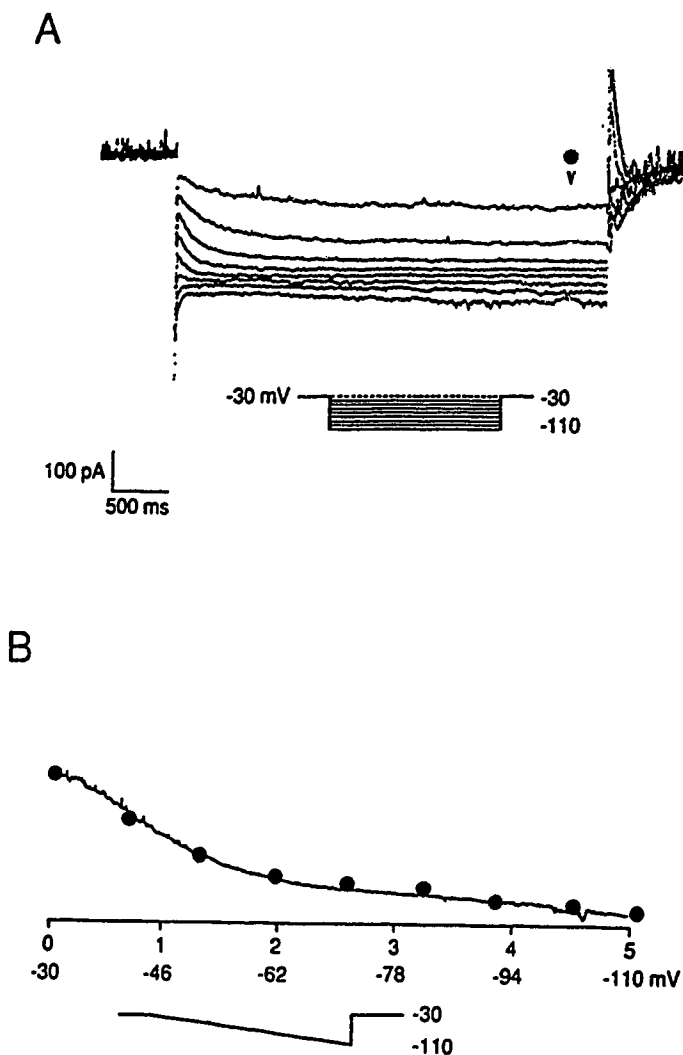


Figure 11. Comparison of the steady-state currents obtained from voltage-ramp paradigm and voltage-jump paradigm. **A.** Series of inward current relaxations produced by successive 10mV hyperpolarizing voltage commands applied from -30mV to -110mV. **B.** Current response, in the same cell, to a slow voltage gradient (-16mv/sec) from -30 to -110mV for 5s. The steady-state currents flowing at the point marked (●) in A correspond with the points marked (●) in B. Traces from x-y plotter.

ms/point for typical I/V curves to 12 ms/point. Currents obtained from the voltage-ramp protocols were usually resolved at 2.44 ms/point.

All data was stored on removable hard discs in an Iomega 10+10 megabyte 'Bernoulli' box (Iomega Corporation). On occasion, voltage parameters were generated by a pulse generator (Dagan S-900 stimulator) that was attached directly to the Axopatch-1B amplifier. On-line signals were recorded on a dc rectilinear pen recorder (Gould Instruments 2400: pen rise time < 8ms). Hard copies of computer stored data were obtained using a Roland DXY 880 x-y plotter.

1.2.6. Patch Electrode Preparation.

The patch pipette electrodes were prepared from borosilicate glass tubing (hard glass), 1.5 mm outer diameter (OD) and 0.8 mm inner diameter (ID) (Hilgenberg Glass), by the following method. Initially, the uncleaned tubing was cut to about 10 cms in length and the ends were gently flame polished. The electrodes were pulled on a typical 2-stage patch pipette puller (Narashige PP-83). The tubing was mounted vertically in the puller with the upper part fixed and with the lower portion free so that it could move along the vertical axis upon sufficient heating of the tubing. During the first pull, the nichrome heater coil was set at 54 (arbitrary scale). The glass tube elongates to a pre-determined length, controlled by a microswitch, producing an hour-glass like thinning the heated region to about 200-400 μ m OD. The coil is adjusted to a position just below the center of the thinnest

region and a second pull was initiated (coil setting at 60) that narrowed the glass to the point where it separated into two electrodes of about 1-2 μ m OD.

At this stage, a silicon based elastomer (Sylgard® 184, Dow Corning) was applied to the shank of the electrode, taking care not to occlude the tip opening. The production of the electrode increases the capacitance of the glass tubing and if uncorrected it will introduce a large amount of background noise to the system. The capacitance observed between two conducting fluids separated by concentric cylinders is proportional to logarithm (inner diameter/outer diameter). Therefore, increasing the outer diameter with 'Sylgard' reduced the electrode capacitance, typically, to less than 1 pF. A small amount of 'Sylgard' was prepared for each experiment by mixing 0.5mls of the elastomer with 2 or 3 drops of hardener. The mixture was stored in a thermoelectric cooling device prior to use (Cambion Thermo-Electric Assembly Model # 806-1001-01-00-00). Once applied to the electrode, the mixture was heat-cured with a 'sylgarding jig' (see Corey and Stevens, 1983). Care was taken not to leave the electrode tip near the curing coil for more than about five seconds because the tip can be polished closed and render the electrode useless. The electrodes were protected from dust by storage in a covered petri dish.

The final step in electrode preparation involved the polishing of the tip of the electrode using a microforge similar to that described by Corey and Stevens (1983). The electrode was viewed at 400X magnification under a compound microscope with a calibrated eye piece (American Optical, Polanret model # 120).

The electrode was carefully advanced to about 60 μ m from a heating coil, that was made from a single length of platinum-iridium wire, with the aid of a 3-way micromanipulator. Tip polishing was accomplished by a brief activation of a foot switch that applied 40 V across the wire. A gentle air stream directed towards the shank ensured rapid electrode tip cooling. Upon filling the electrode with the appropriate solution, resistances of 5-20 M Ω were observed.

There are many factors associated with the making of proper electrodes. The experimenter must adjust certain subjective aspects of the general process and with practice will produce consistent patch-pipette electrodes.

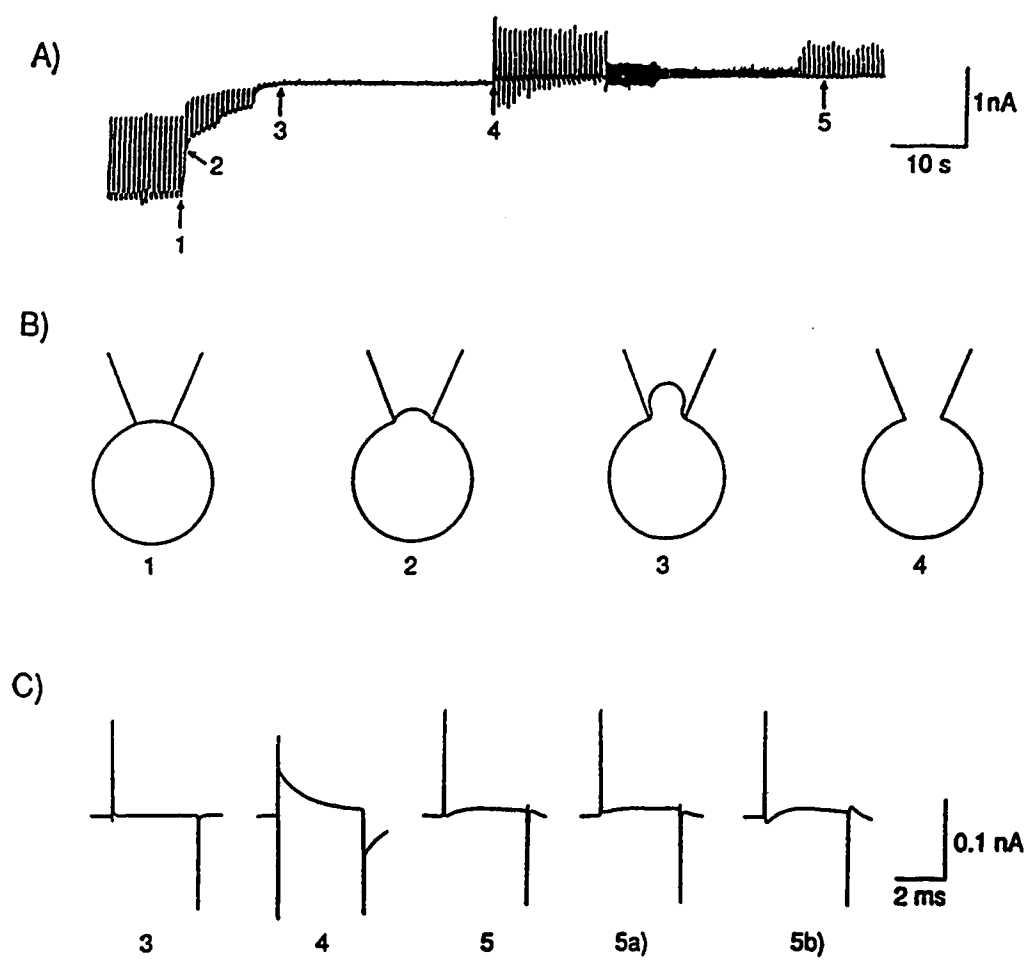
1.2.7. Establishment of WCR.

The enzymatic dissociation described above normally gave rise to a large number of suitable cells for the whole-cell recording. An appropriate cell was chosen and U-tube was correctly positioned for each neuron prior to seal formation. The pipette, filled with "internal solution", was secured in a low noise electrode holder and inserted directly into the headstage. The current output was zeroed to a virtual ground, ensuring the utilization of the entire dynamic range of the op-amp. The electrode was lowered into the bath using the microdrive. The pipette junction potential was zeroed and drift was compensated for using an Auto-Junction Null-Hold mode feature on the Axopatch-1B which maintains the pipette current at the zeroed level. This compensates for the offsets caused by the liquid-

liquid and liquid-metal junctions in the bath and the electrode holder respectively. However, it does not compensate for any change due to seal formation or junction potential drift caused by loss of cell contents during pipette-cytoplasm fluid exchange (Marty and Neher, 1983). If the silver wire was changed or re-chlorided, the manual junction null was used to adjust the pipette current to zero the amplifier was then zeroed and the mode switched back to the Auto-junction Null mode.

Figure 12 illustrates the establishment of whole-cell recording from a frog sympathetic ganglion neuron. Brief, 20mV test pulses were applied at 100Hz across the recording electrode. The pipette was positioned just above the neuron and then contact was established by slowly moving the pipette towards the cell. As the pipette contacted the membrane (indicated by 1), the current deflections to the test pulses reduced in amplitude since the effective resistance at the tip of the pipette is increased (Ohm's Law). The next step was to establish a $G\Omega$ seal, a small amount of suction was applied (indicated by 2) to the interior of the pipette by means of a polyethylene tube attached to the pipette holder. A high quality seal was formed when the current deflections to the test pulse disappeared (at 3) indicating the establishment of an electrical seal of tens of $G\Omega$ s. The seal formation was facilitated by clamping the pipette to negative potentials (-60 to -100 mV). The next step was to rupture the membrane, prior to which the holding potential was roughly adjusted to the anticipated resting membrane potential. Applying negative pressure to the pipette interior promoted membrane rupture as illustrated by 4. At

Figure 12. Method for the establishment of whole-cell recording of sympathetic neurons. **A)** is a real-time current record. **B)** illustrates the events occurring at the pipette-cell membrane interface and **C)** shows fast current records produced by 20mV test pulses to monitor seal formation, 'break-in' and to compensate whole-cell capacitance. The brief current interruptions are generated from 20mV test pulses for 3.3ms at 100 Hz to the patch electrode. 1-5 denotes the following events occurring in panels **A)**, **B)** and **C)**: 1. pipette contact with the cell membrane, 2. application of negative pressure to increase seal resistance, 3. G Ω seal established, 4. breaking of membrane contained within the pipette and 5. whole-cell capacitance compensation adjusted properly. Panel **C)** contains fast records of currents observed during the 20mV test pulses to illustrate the high resistance seal (3), the additional capacitance contributed by the cell membrane subsequent to break in (4), proper compensation (5) and improper series resistance adjustments, **5a)** series resistance too low and **5b)** series resistance too high.



this point the resistance dropped and current responses to the 20mV step commands re-appeared. The current deflections now contained additional transient components due to the current flow through the membrane capacitance.

This additional current (I) is given by the relationship:

$$I = C_m(\partial V/\partial t),$$

where C_m is the membrane capacitance and $\partial V/\partial t$ is the rate of change of voltage with respect to time. For an instantaneous change in voltage, $\partial V/\partial t$ would approach infinity and the resulting current would be very large.

Biological membranes have both capacitive and resistive properties, therefore the membrane must charge and discharge at a rate determined by these two factors. The rate of capacitance charging was further slowed by the series resistance. Cell resistance and capacitance were compensated for by adjustment of a variable RC circuit on the amplifier. These controls were adjusted so that both the current rise time function and the current decay were exponential. Note that the amplitude of the current deflections, properly corrected, should be less than that observed prior to cell contact because the a typical cell input resistance of about 2 G Ω which compared to the open tip patch pipette resistance of about 10 M Ω .

Figure 12C shows fast current records to illustrate proper compensation of the additional membrane capacitance observed subsequent to membrane rupture as well examples of over- and under-compensated series resistance.

C_m was obtained from the whole-cell capacitance compensation adjustment and was proportional to the cell size. Assuming a specific capacitance of $1\mu\text{F}/\text{cm}^2$, the relationship for spherical cells was $C_m = \pi d^2/100$, where d was the cell diameter in micrometers (see Marty and Neher, 1983).

The voltage-drop across the series resistance was not compensated for due to the rather small currents that were studied. The maximum currents obtained from the largest cell about 300 pA, combined with a series resistance of about 15 M Ω would result in a maximum voltage error of 4.5 mV. Moreover, most of the currents were in the 20-200 pA range and the voltage drop at the series resistance would be considerably less.

The RMP was measured by noting the voltage when the amplifier was switched to current-clamp mode (in this mode the pipette current is clamped to zero). It was important to ensure that no additional holding potentials were generated by the software or directly applied through the amplifier when this measurement was taken and that the holding potential was re-applied prior to switching back to the voltage-clamp mode.

2. BIOCHEMICAL ASSAYS.

2.1. RADIOIMMUNOASSAY.

2.1.1. Rationale.

A Radioimmunoassay (RIA) for cAMP was performed to test the hypothesis that a reduction in ganglionic cAMP content was directly involved with inhibitory adrenergic responses which were observed electrophysiologically.

2.1.2. cAMP Radioimmunoassay.

The cAMP radioimmunoassay was performed utilizing the RIANEN® cAMP [¹²⁵I] RIA kit (Dupont Cat. # NEK-033). RIA theory is based on the following events (illustrated in Figure 13): the cAMP isolated from each sample acts as an unlabelled antigen and competes with a labelled-cAMP complex (Succinyl cAMP Tyrosine Methyl Ester [¹²⁵I]) for a specific antibody. After equilibrium conditions are established, the labelled-antigen-antibody complex is then separated from the free-labelled antigen. This is accomplished by the addition of an excess amount of a second antibody that is specific for the antigen-antibody complex. The resulting tertiary structure precipitates from the solution and the ¹²⁵I radioactivity is determined for each sample. The results are quantitated by interpolation from a

standard curve. Therefore, the results are based on an inverse competition curve whereby the tissue derived cAMP content is inversely proportional to the number of counts observed by a gamma counter (see Yalow and Berson, 1971).

2.1.3. Tissue Preparation.

The ninth and tenth paravertebral sympathetic ganglia and the connecting length of sympathetic chain were excised from pithed Rana catesbeiana (bullfrogs) in the manner described in the previous section. Since the cAMP content of each whole ganglion was expressed on a picomole/tissue wet weight basis (pmol/tissue w.w.), it was important to remove as much of the connective tissue and axonal material as possible. Each ganglion was carefully weighed and transferred into individually marked reaction vessels containing Ringer's solution. The average weight of these ganglia was usually about 1mg wet weight. However, in a few instances it was necessary to include two smaller ganglia in a single reaction vessel to obtain enough material to assay.

The reaction vessels were made by securing a small piece of nylon mesh between two pieces of tubing. This arrangement permitted the bathing solution to flow through the mesh and also facilitated the transfer of the ganglia from solution to solution.

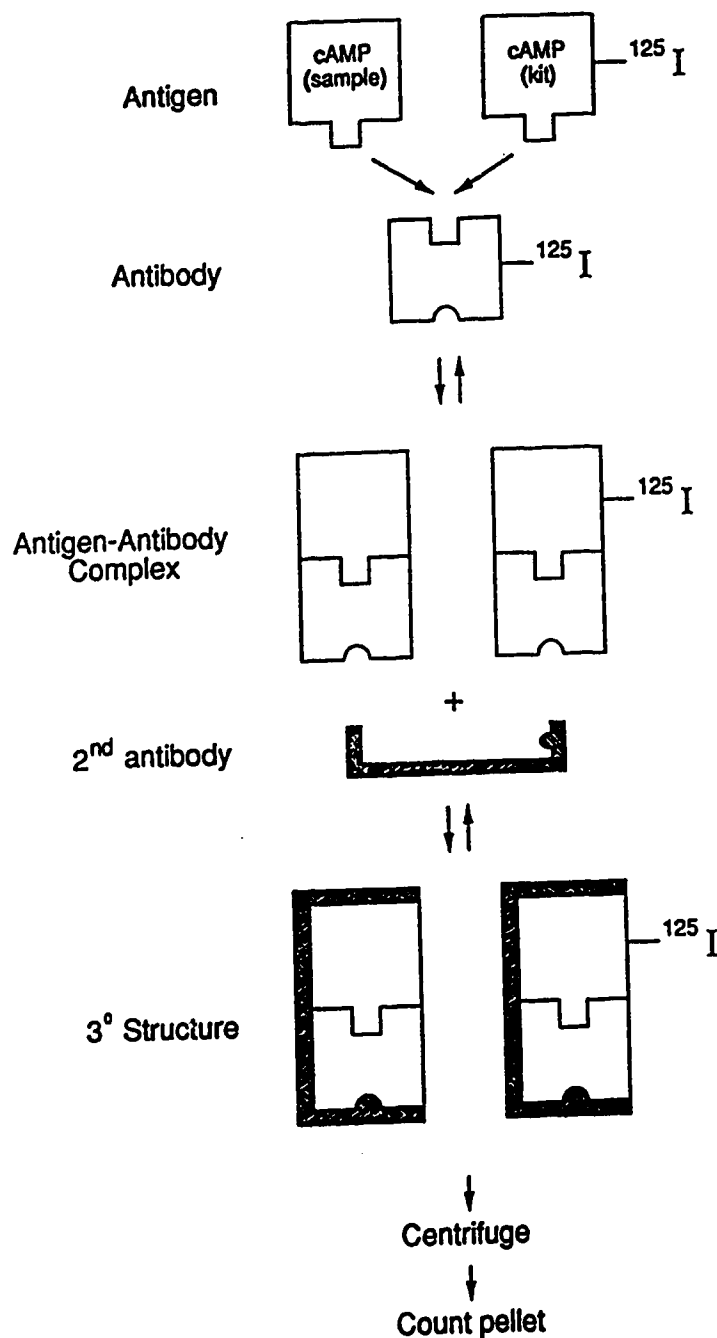


Figure 13. Basic theory for the Radioimmunoassay technique. A schematic representation of an antibody-antigen interaction whereby the experimentally derived cAMP sample competes with ^{125}I -cAMP for the same binding site. Upon the establishment of equilibrium conditions, a second antibody is added which is specific for the cAMP-antibody complex. The antibody-antigen-antibody structure then precipitates out of solution and ^{125}I is measured by a gamma counter.

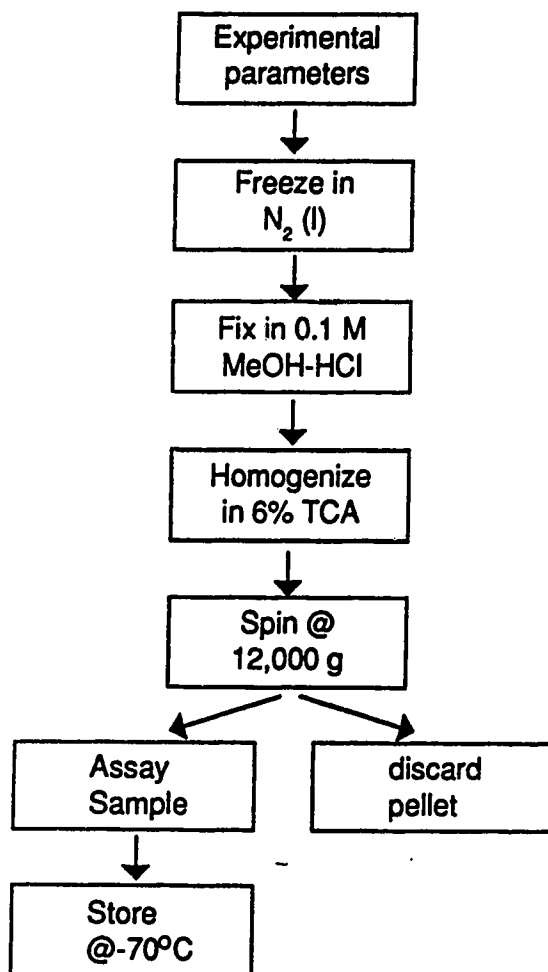
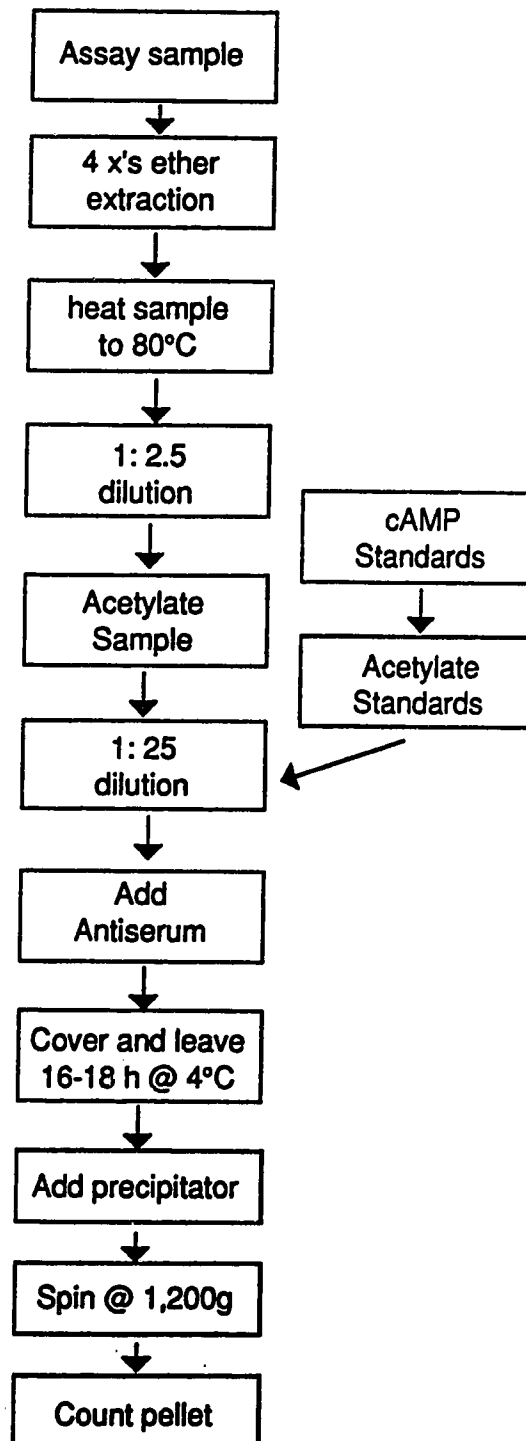
2.1.4. In Vitro Experimental Procedure.

The experiments were conducted at room temperature as these results were compared with the results from sucrose-gap experiments. It was important to allow the tissues to equilibrate in Ringer's solution for at least 2 hours prior to the start of the experiment. This facilitated reproducible assay measurements because cAMP levels are elevated by handling during tissue preparation (Smith et al, 1979).

Groups of six reaction vessels were placed in a 3" plastic petri dish which had its bottom removed and replaced with nylon mesh. Each group (n=6) was transferred to various test drug solutions contained in 6" plastic petri dishes, for a pre-determined time interval. All preparations were handled in the exactly the same manner so as to control for any cAMP elevation caused by the transfer of the ganglia from solution to solution (i.e. the controls were lifted out and replaced into the same solution whilst the test ganglia were transferred a test solution). Following drug exposure, each sample was blotted to remove excess Ringer's solution and frozen in liquid nitrogen.

Each tissue sample was fixed in a marked polypropylene mini-centrifuge tubes (1.5µl, Bio-Rad, Cat. # 2239501) containing 0.5ml of 90% methanol - 0.1M HCl solution for two hours at -20°C. After fixation, the remaining sample preparation was carried out at 4°C. Individual tissue samples were homogenized in 0.5 mls of 6% trichloroacetic acid (TCA), particulate and cell debris were removed by a 4 minute centrifugation at 12000 times gravity (Eppendorf Model 5414) and

Figure 14. Experimental procedures for ganglionic cAMP determination by RIA. **A.** Method by which each ganglion was prepared for subsequent cAMP content determination. **B.** Step-by-step procedure for cAMP RIA as per kit manufacturer (New England Nuclear).

A. Sample Preparation**B. RIA**

the supernatant was stored in liquid nitrogen ($N_{2(l)}$) (see [Figure 14A](#)).

The acetylated method was utilized to take advantage of about a 20 fold increase in assay sensitivity (Frandsen and Krishna, 1976). [Figure 14B](#) illustrates the step-by-step procedure for the complete method. Initially, each sample underwent 4 successive ether extractions. The sample was diluted four fold by ether, mixed in a vortex and the organic layer was carefully removed by suction. This extraction removed residual TCA left over from the homogenization process. The ether was then evaporated off and proteases were destroyed by heating each sample in a hot block to 80°C for 10min. All reagents were added using calibrated Eppendorff pipettes and solutions were mixed with a standard vortex. The acetylation reagent (a solution of triethylamine and acetic anhydride) was then added to each sample as well as cAMP standards. The "working tracer solution" (^{125}I -cAMP + carrier serum) and the antiserum complex was added to all the samples (in duplicate) and standards with exception of the total counts and the blank tubes that were used to determine the endpoints of the standard curve. All the tubes were left to incubate overnight (16-18 hrs @ 4 °C).

The following day a second antibody was added to each tube and vortexed, except the total counts tube, and the precipitate was spun at 1200 times gravity in a refrigerated swing bucket centrifuge for 15 minutes (Sorval RC-3B Refrigerated Centrifuge @ 2300 rpm @ 4°C). The tubes were decanted and left upside down to drain on blotting paper and were then counted using an automated gamma counter (LBK-Wallac 1272 CliniGamma). Samples were counted for 300s. The

gamma counter determined its counting efficiency and generated a standard curve (SPLINE METHOD) upon which the cAMP content of duplicate samples was determined by interpolation. The sensitivity reported by the manufacturer (Dupont) was < 0.2 pmol cAMP/ml. Specificity studies determined by kit manufactures (Dupont) report cross-reactivity values of less than 0.01% for cyclic guanosine monophosphate (cGMP), guanosine monophosphate (GMP), ATP, and adenosine diphosphate (ADP), less than 0.02% to adenosine monophosphate (AMP) and less than 0.0001% to theophylline.

2.2. Protein Assay.

Protein content was determined by the Bradford method (Bradford 1976). Upon binding to protein, Coomassie Brilliant Blue G-250 changes from red to blue in color and observed using a standard spectrophotometer. The dye-protein complex forms readily in a few minutes and is stable for a few hours. The results are quantified by interpolation on a protein content curve of bovine serum albumin standards. This particular method was selected since it is more sensitive than the Lowry method (Lowry et al, 1954), less time consuming, is not affected by K^+ and Mg^{2+} , and displays less interference from nucleic acids and short peptides which are present in crude membrane preparations.

Since the experiment was designed to assess the changes in cAMP content of individual ganglion samples to compare with the physiological effects observed

using sucrose-gap recording, the biochemistry was performed on individual whole ganglia. As mentioned above, the initial wet weight of each sample was about 1 mg. The protein assay was performed on the crude membrane preparation because most of the measurable protein was removed by the first spin after the homogenization of the whole ganglia.

A 100 μ l sample was hydrolysed by adding an equivalent amount of 1N NaOH and immersion in hot water for 10 minutes. The sample was then neutralized by the addition 100 μ l of 0.5 M HCl and then 800 μ l of Tris-buffer pH to give a 1:11 dilution. The protein content was then determined using a Beckman spectrophotometer measuring the absorbance at 595nm and quantified by comparison to a standard curve prepared from bovine serum albumin.

3. DATA HANDLING AND STATISTICAL ANALYSIS.

Unless otherwise indicated values are reported as mean \pm standard error followed by the number of experimental observations ($\bar{x} \pm \text{s.e.}, n$). The Student's t-test was used to compare between two groups of data with an equal number of observations and the General-t test was utilized to establish the statistical significance between two groups of data with an unequal number of observations. Electrophysiological data obtained from sucrose-gap recording were normalized to control values. A number of controls were usually taken to establish steady-state conditions prior to drug challenges. The effects observed were calculated as a

percent depression of control (% of control) unless otherwise stated and recovery also is reported as a percent of control. If a second experiment was performed on the same tissue, a new control value was established since tissue responsiveness can run-down over time. Dose-response curves were visually fit and EC_{50} values were obtained by extrapolation. Most slope values were calculated by linear regression however some pA_2 values were visually fit after data was plotted on semilog paper. EC_{50} values were determined by calculating the geometric mean of the measured EC_{50} values obtained from individual experiments.

CHAPTER III

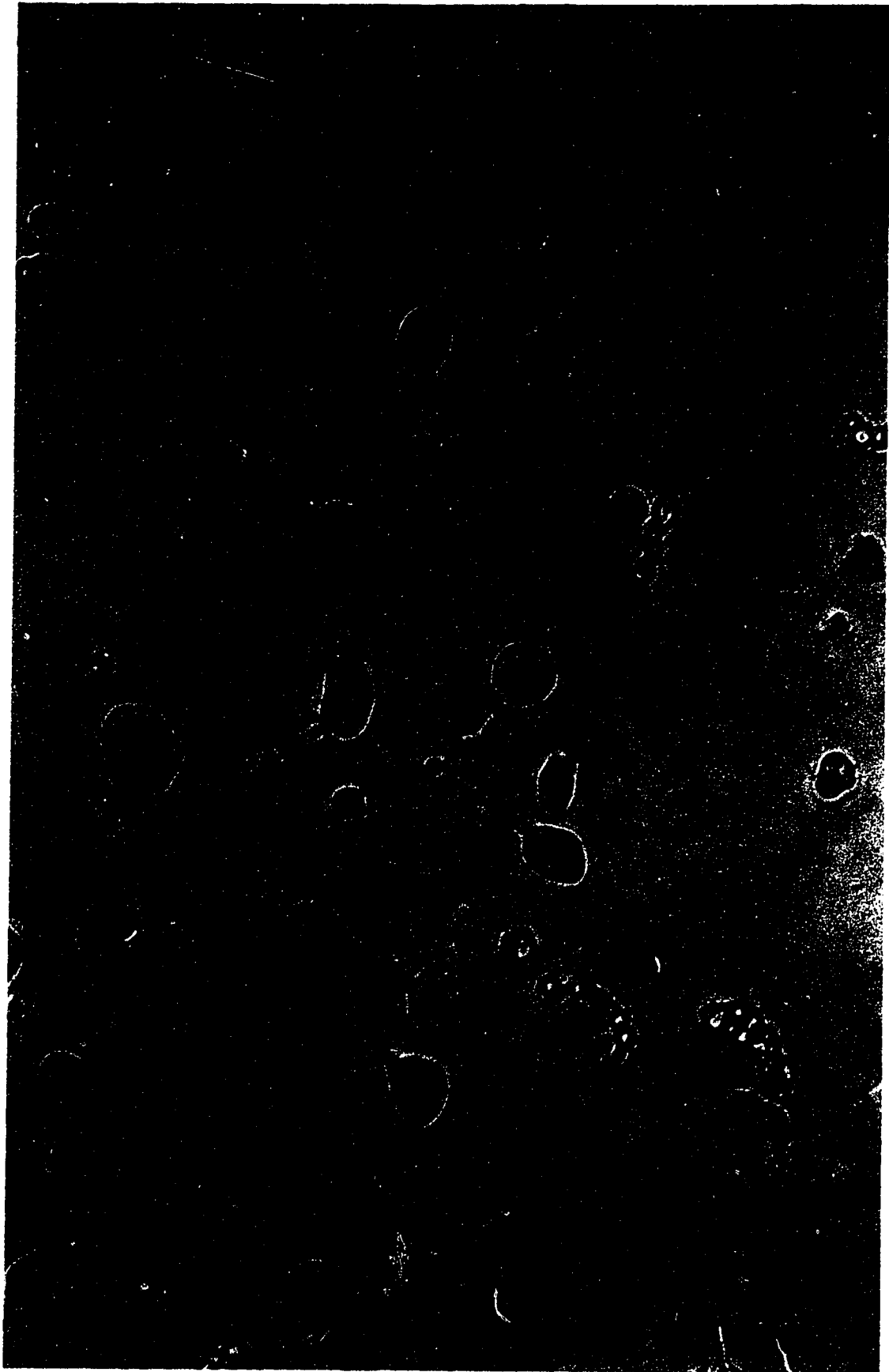
RESULTS

1. CHARACTERIZATION OF DISSOCIATED SYMPATHETIC GANGLION NEURONS.

1.1. MORPHOLOGY.

Plate 3 shows neurons that were successfully dissociated from Rana pipiens sympathetic ganglia, visualized at 200 X's magnification. These unipolar neurons had cell bodies that were round, pear-like, or ellipsoid in shape, had well defined nuclei, and compared well with previous electron micrographic descriptions of BFGG neurons (Taxi, 1976; Weight, 1983; Baluk, 1986). The degree to which neurons were spherical was inversely related to the length of axonal material remaining after the dissociation procedure. Also evident from Plate 3, is the variability in cell body diameter. There existed a large number of small diameter cells that, if an axon stump was intact, were ellipsoid in shape. Conversely, the larger neurons which had an axon stump were pear-like in shape. Occasionally, pre-ganglionic fibers were observed spiralling around the axon hillock as well as the appearance of small, distinct, dark regions on the cell body, close to the axon hillock, where synaptic boutons may have made contact, again similar to electron-micrographic reports (Taxi, 1976; Weight, 1983). This indicated that the cells that had an axonal segment were similar morphologically to those contained in the intact ganglia and should therefore be better candidates for WCR than the more spherical neurons.

Plate 3. Dissociated sympathetic ganglion cells viewed at 200X magnification. Note the variability in cell size and that the largest neurons ($\approx 40\mu\text{M}$) seem to lack axonal processes as compared to the smaller neurons ($\approx 20\mu\text{M}$).



1.2. CELL IDENTIFICATION.

1.2.1. General.

The variability in cell diameter and shape indicated that the population of neurons may not have been homogeneous. Since axonal material was all but removed, neurons could not be identified as fast-B, slow-B or C-cells according to criteria put forward by Dodd and Horn (1983a).

One aspect of the present study was to test whether the "small" neurons corresponded to "C-cells" and whether the "large" neurons corresponded to "B-cells". Exogenously-applied muscarinic agonists induced a hyperpolarization in C-cells (Weight and Padjen, 1973b; Dodd and Horn, 1983b) whilst the same type of agonist caused a depolarization when applied to B-cells (Koketsu et al, 1968; Schulman and Weight, 1976), thus if the small cells corresponded to the C-cells, they should respond with an outward current and if the large cells correspond to B-cells, they should respond with an inward current to the application of muscarinic agonists.

1.2.2. Cell Characterization.

Figure 15A relates the frequency of observation of outward currents to the measured C_m , obtained when 1.5mM GTP, 1.5mM ATP, or 100 μ M cAMP was

included in the internal solution. There was an inverse relationship between the frequency of observation of muscarine-induced outward currents and the cell size. Muscarine exclusively produced outward currents in all cells with $C_m < 18\text{pF}$.

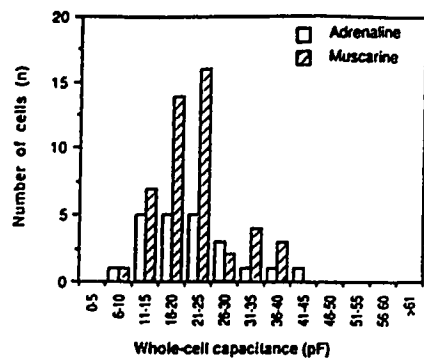
The histogram illustrated in Figure 15B relates the frequency of observation of inward currents (cell depolarization in current clamp) to C_m under the same recording conditions described above. The majority of large cells studied displayed an inward current in response to $10\mu\text{M}$ muscarine. All cells with $C_m > 40\text{ pF}$ exhibited inward current in response to this agonist.

The input resistances (R_m) of a number of neurons were calculated and plotted against C_m to see if a relationship between cell size and R_m existed (see Figure 15C). The R_m was the slope of steady-state current over -80 to -90 mV portion of the voltage-ramp generated I/V plot (recorded in $6\text{mM } [\text{K}^+]_o$). Although there was a tendency for the R_m to increase as the cell size decreased, the mean R_m of the small cells that exhibited outward currents ($1.65 \pm 0.22\text{ G}\Omega$, $n=22$) was not significantly different from the R_m ($1.26 \pm 0.15\text{ G}\Omega$, $n=48$) of large cells that exhibited inward currents. The R_m measured in the resting potential range (-50mV) was approximately an order of magnitude less than that in the -80 to -90mV range indicating the presence of voltage-sensitive conductances.

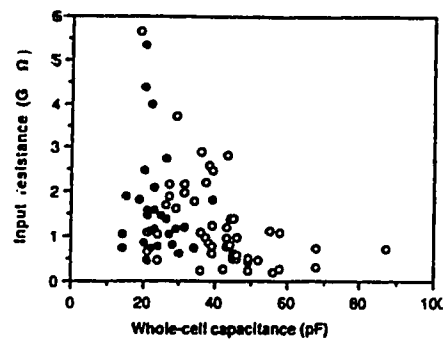
Figure 15D illustrates the resting membrane potential plotted against the C_m measured in $6\text{mM } [\text{K}^+]_o$. The mean RMP was $-49.50 \pm 0.64\text{mV}$, $n=82$. There was no significant difference in the measured RMP of cells that exhibited inward currents

Figure 15. Characteristics of 'small' and 'large' neurons dissociated from Rana pipiens sympathetic ganglia. Cell size, which is proportional to whole-cell capacitance (C_m), is plotted on the ordinate of all graphs. Distribution histograms for outward (A) and inward currents (B) in response to $10\mu\text{M}$ muscarine and $100\mu\text{M}$ adrenaline. C. Graph of input resistance (R_m) versus C_m for 'small' (●) and (○) 'large' neurons. D. Graph of the measured resting membrane potential (r.m.p.) versus C_m for small (●) and large (○) neurons. E. Distribution histogram of neurons exhibiting I_A where 'n' refers to the number of cells examined in each capacitance category.

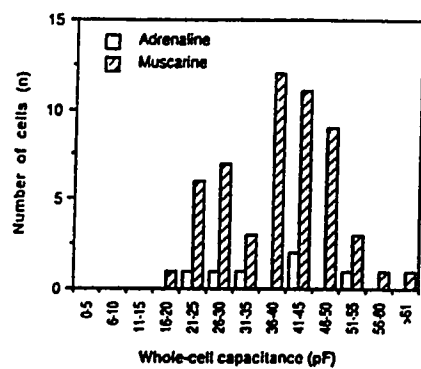
A Outward Currents



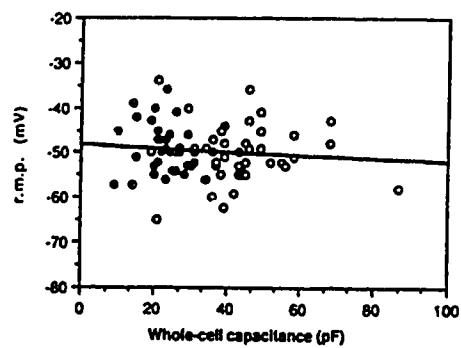
C



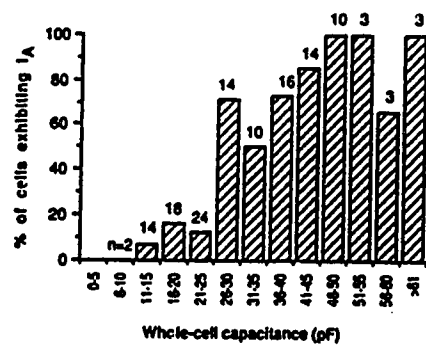
B Inward Currents



D



E



($-49.80 \pm 0.87 \text{ mV}$, $n=48$) or cells that exhibited outward currents ($-48.94 \pm 0.97 \text{ mV}$, $n=34$).

One other disparity between the two types of cells was the presence or absence of a rapid, transient outward current, I_A (Adams et al, 1982a). Figure 15E clearly shows that cell capacitance (size) is proportional to the percentage of cells that display I_A . I_A was present in $\approx 95\%$ of the cells with $C_m > 40 \text{ pF}$ but was only observed in $\approx 12\%$ (7/58) of the cells with an C_m of $< 26 \text{ pF}$. This compared well with the 7/68 ($\approx 10\%$) of the cells with $C_m < 26 \text{ pF}$ in which an inward current to muscarine was observed (see Figure 15B). There were no instances where I_A was observed in cells with $C_m < 10 \text{ pF}$.

1.2.3. Currents Observed In Small And Large Neurons.

A holding potential of -30 mV and voltage command (V_c) range of -30 to -110 mV was selected to attempt to isolate the M-current (Adams et al, 1982a). This holding potential ($V_H = -30 \text{ mV}$) was selected to minimize the contribution of most of the other ionic conductances previously characterized in amphibian sympathetic ganglion neurons, such as the delayed rectifier ($I_{K(V)}$) and voltage-sensitive calcium-dependent K^+ current (I_C) that are both activated at potentials positive to -25 mV (Adams et al, 1982a), sodium currents (Jones, 1987b) and Type-L Ca^{2+} currents which are both activated at potentials positive to -20 mV (Adams, 1981). The

remaining currents that contribute to the resting membrane conductance in the selected range are the M-current (Adams et al, 1982a) and voltage-independent leak current (Jones, 1989). The transient A-current was usually inactivated or only briefly activated. However, it should be noted that activation curves may be shifted to more negative potentials due a loss of intracellular constituents and/or by an improvement in voltage control afforded by WCR (Marty and Neher, 1983).

I_M was first described to occur in amphibian sympathetic ganglion B-neurons by Adams et al (1982a) as a non-inactivating, slowly-deactivating potassium conductance that activated at voltages positive to -60mV and was inhibited by muscarine. This current was shown to exist in amphibian sympathetic C-neurons but was insensitive to muscarine (Jones, 1987a). Since the results of these studies were obtained using conventional microelectrode recording, one objective of this investigation was to determine if I_M could be maintained in Rana pipiens sympathetic ganglion neurons during WCR.

Figure 16a) shows currents observed from large (A) and small (B) dissociated neurons upon the application of a series of voltage hyperpolarizations from a holding potential of -30mV. The experiments were performed in 2mM $[K^+]_o$ (calculated E_K was -101mV). Three current components were observed under these conditions, an instantaneous current (I_{im}), a time dependent relaxation (*) and a steady-state current (I_{ss}). These events can be described as follows:

- 1) I_{im} reflected the membrane conductance (leak and voltage-activated) just prior to the change in membrane conductance at the new voltage.

- 2) The slow relaxations (*) were due to the time- and voltage-dependent reduction in conductance at each hyperpolarized level. The reduced conductance and not the activation of an inward current was observed since there was a decrease in the I_{m} at the termination of each voltage step indicating an increased membrane resistance during the voltage step.
- 3) A new I_{m} was attained during each voltage step upon the completion of the relaxations. This reflected the resting steady-state membrane conductance at that particular voltage.

The relaxations were due to the finite time that channels took to close (deactivate) under voltage conditions outside their optimal range. The rate of relaxation was voltage-dependent such that the rate of relaxation increased with respect to hyperpolarization (also see Table 1). The amplitude of the relaxation was also dependent on the driving force of the particular ion(s) involved. Note that the relaxations were very small at -90mV and reversed at -110mV. As previously stated, the E_{K} in this experiment was -101mV and the potential at which current reversal occurred indicated that K^+ was most likely the charge carrying ion. The time constants of current relaxation and activation, occurring at the voltage onset and offset, were similar. Furthermore, the kinetics of the conductance observed likely follow a simple, reversible, voltage-dependent activation-deactivation model.

The I/V characteristics of I_{m} and I_{h} in both small and large neurons are shown in Figure 16b). Note that the conductance observed in both cell types

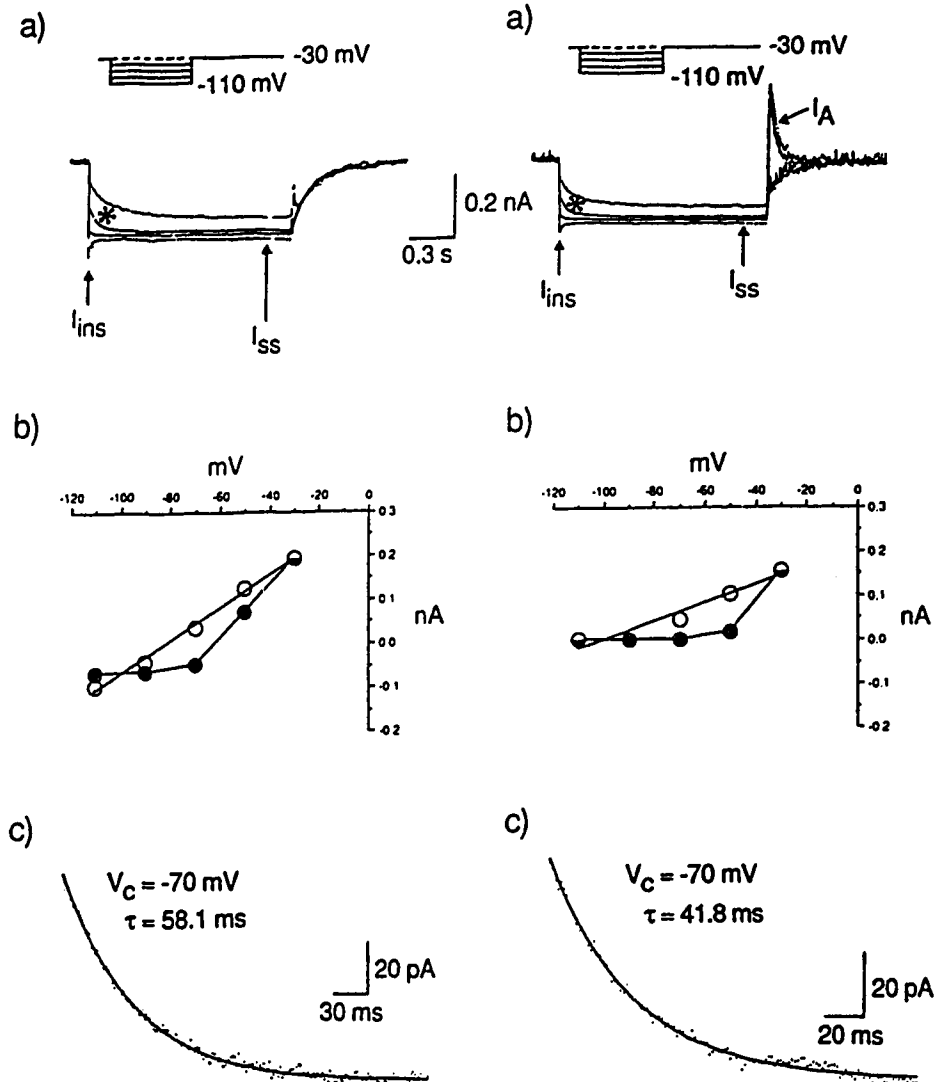


Figure 16. Characteristics of voltage-dependent currents of 'large' and 'small' neurons. Response of A, a small and B, a large neuron to a series of hyperpolarizing voltage commands (-50, -70, -90, and -110 mV) from a holding potential of -30 mV. ($[K^+]_o = 2$ mM). a) original data records, b) instantaneous (O) and steady state (●) I/V relationships plotted from I_{ins} and I_{ss} values from the data records in a). c), computer fitted curves (single exponential) of the inward current relaxations (*in a)) of a command potential from -30 to -70 mV. Traces from x-y plotter.

changed very little below -70mV and the intersection of I_{m} and I_{s} occurred at about -100mV, coinciding with the calculated E_{K} in 2mM $[\text{K}^+]_o$. The voltage-dependent currents observed from the two cells illustrated are comparable, however, currents observed from small cells were generally less than those observed from large cells (see Table 1).

Figure 16c) compares the time course of the relaxations recorded from a single voltage step from -30 to -70mV. The first point of each trace occurred at the end of the I_{m} and the last points occurred well after I_{s} was attained. Each trace was fitted with a computer-generated single exponential. At -70mV, τ of the "small" neuron (58.1 ms) was slower than that measured in the "large" neuron ($\tau=41.8$ ms).

1.2.4. Role Of M-Conductance In The Generation Of The Slow Inward Relaxations.

The slow inward relaxations described in the previous section were identified as I_{M} relaxations on the basis the following similarities to I_{M} relaxations described in the existing literature (also see Table 1):

- 1) The reversal potential shows that the conductance was due to K^+ ions.
- 2) The slope conductance observed in the I/V plots for both small and large cells was constant at potentials negative to -70mV and voltage-dependent at potentials positive to -70mV.

- 3) The activation and deactivation time constants were similar indicating a simple activation-deactivation model in the voltage range studied.
- 4) The current did not inactivate in its activation range.
- 5) The relaxation time constants increased as hyperpolarization increased.
- 6) Large cell relaxation time constants were faster than those observed in small cells.
- 7) Muscarine suppressed this current in large cells (cf Adams et al, 1982a) but not in small cells (cf Jones, 1987a). The current was suppressed by c-II-LHRH in both cell types.

1.2.5. Re-Classification Of "Large" And "Small" Cells As B- And C-Cells.

These data convincingly show that distinctions existed between "small" and "large" neurons. The mean C_m for small cells that exhibited outward currents in response to muscarine was $21.3 \pm 0.8 \text{ pF}$ ($n=70$) and was $40.5 \pm 1.5 \text{ pF}$ ($n=66$) for large cells that displayed inward currents. Although conduction velocities could not be determined from dissociated cells, the following results obtained from the present study showed a strong correlation with previous reports in the literature and allowed large cells to be identified as B-cells and the small cells as C-cells.

A neuron under study was identified as a B-cell if it satisfied the following criteria:

- 1) The observation of an inward current upon the application of muscarine when the cell was held positive to E_K .
- 2) The I_M was clearly and reversibly reduced in the presence of muscarine.
- 3) The presence of the fast, transient I_A following repolarization to -30mV from a hyperpolarized command.
- 4) $C_{in} > 20\text{pF}$.

The cell under study was determined to be a C-cell if the following criteria were satisfied:

- 1) The cell responded to muscarine with an outward current if $V_H > E_K$ (see below).
- 2) The muscarine-induced current displayed a reversible inward-rectification at voltages negative to E_K (see below).
- 3) An absence of the fast transient I_A upon return of command voltage to -30mV from hyperpolarized levels.
- 4) The presence of a muscarine-insensitive I_M .
- 5) $C_{in} < 20\text{pF}$.

1.2.6. Kinetic Analysis Of The M-Current In B- And C-Cells.

- a) Rate of I_M deactivation.

The rate of deactivation of I_M was directly related to the membrane potential. Figure 17A shows the voltage-dependence of the rate of I_M deactivation. The I_M occurring in the smaller C-cells deactivates at a slower rate than the B-cells for every command voltage potential studied.

Table 1 shows the raw data used in Figure 17A. Note that the rate of B-cell I_M deactivation was twice that of C-cells over the -50 to -80mV range. The omissions in Table 1 were due to the difficulty in measuring the time constants for I_M deactivation close to E_K in 2mM $[K^+]_o$.

b) Voltage-dependence of steady-state I_M conductance.

The steady-state I_M observed at each potential was studied using a voltage ramp protocol rather than a voltage step protocol. Figure 11 (see Methods) illustrates that when a slow hyperpolarizing voltage ramp (16mV/s) was applied to a neuron, the resulting current was equivalent to the steady-state current measured at each voltage jump.

The net current observed at each potential was the sum of I_M and the leakage current (assuming that no other voltage-activated conductances were altered). Therefore, if the leakage current, which was always assumed to be a linear function, was subtracted from the I/V ramp, the remaining current was attributed to conductance through M-channels. The leakage current was calculated by measuring the slope of the I/V ramp at potentials negative to the activation of I_M

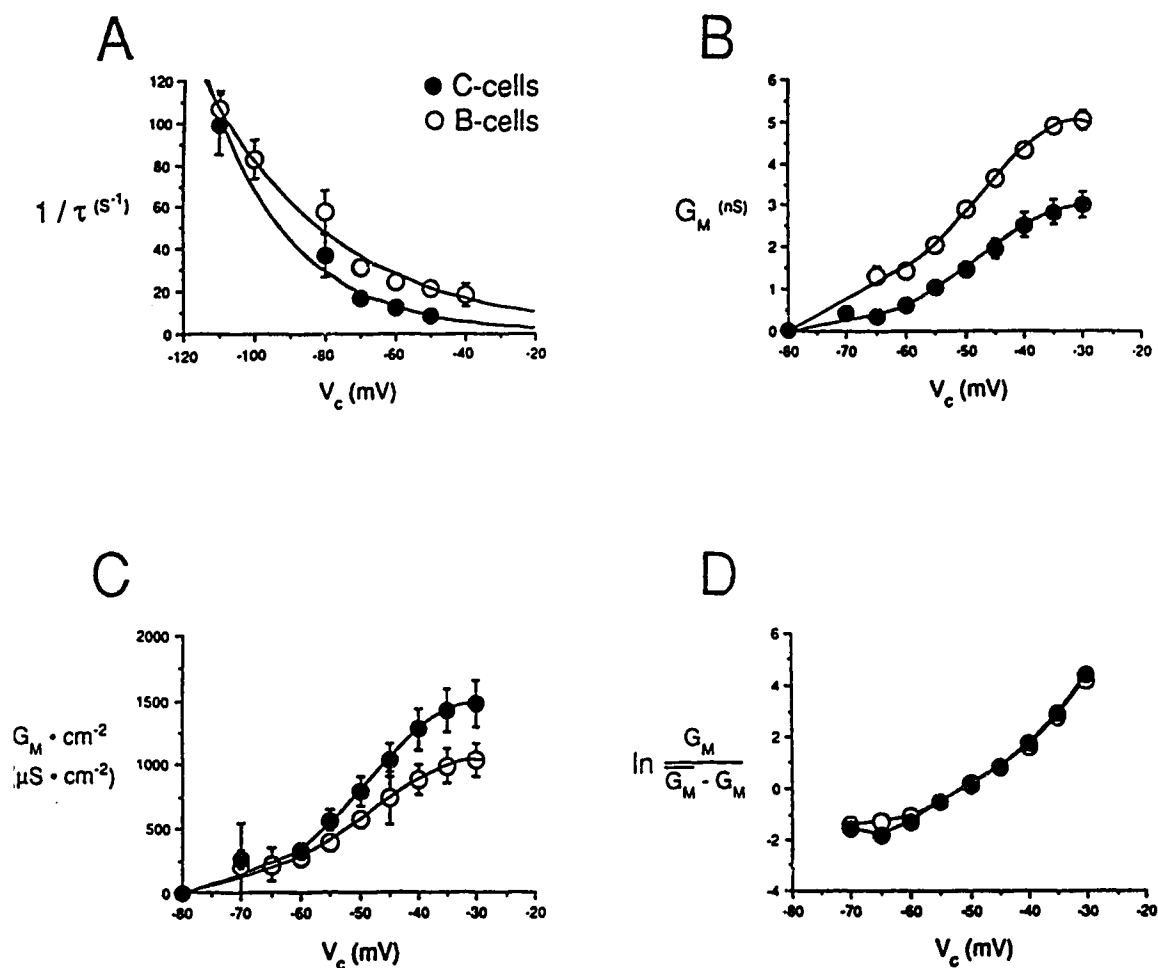


Figure 17. Kinetic analysis of I_M in B- and C-cells. **A.** Plot of $1/\tau$ versus command voltage (V_c) to show the voltage-dependence of the rate of I_M deactivation in C- and B-cells. Number of observations per point varied from 3 for C-cells at -60mV to 16 for B-cells at -70mV. **B.** Graph of V_c versus G_M obtained from 15 B-cells and 21 C-cells. **C.** Voltage dependence of G_M normalized in terms of $\mu\text{S}/\text{cm}^2$ of cell membrane. **D.** Graph of $\ln (G_M / \overline{G_M} - G_M)$ versus V_c to show voltage dependence of G_M . In all graphs, (O) represents data from B-cells and (●) data from C-cells. Error bars show s.e.m. and where absent, the error was smaller than the data points.

(-80 to -95mV) and was then digitally subtracted from the entire trace. The whole-cell M-channel conductance (G_M) at any given voltage (V) was calculated using the following relationship:

$$G_{M(V)} = (I_{M(V)} - I_{M(-80mV)}) / (V(V) - E_K),$$

The numerator is the steady-state current measured at each voltage, less the current observed outside the voltage-activated range of the M-channels, divided by the effective driving force for K^+ at each potential.

Figure 17B shows the relationship between the whole cell M-channel conductance (G_M) and the command voltage (V_c). The average G_M measured in C-cells ($n=21$) studied was less than that observed in B-cells ($n=16$) at every command voltage. Although, the half maximal activation voltage estimated in both cell types occurred at about -52mV, the mean maximum G_M found in B-cells was 5nS compared to 3nS in C-cells.

The G_M per unit area was calculated assuming a membrane capacitance of $1\mu F/cm^2$. Figure 17C illustrates that when cell size was taken into account, the mean whole cell G_M/cm^2 of C-cells was greater than that observed in B-cells over the entire voltage range. Therefore, the C-cells had a larger M-channel density ($1477 \pm 168 \mu S/cm^2$, $n=21$) than B-cells ($1034 \pm 125 \mu S/cm^2$, $n=13$), provided that the same single channel conductance existed.

The voltage dependence of G_M for both B- and C-cells was determined from the slope of a plot of $\ln(G_M / (\bar{G}_M - G_M))$ vs V_c (see Figure 17D). There was an

Table 1Characteristics of I_M

	<u>Characteristics of I_M</u>		<u>Microelectrode voltage-clamp recording</u>	
	<u>B-cells</u>	<u>C-cells</u>	<u>B-cells¹</u>	<u>C-cells²</u>
τ deactivation				
-40 mV	81.2 \pm 15.8 ms (n=8)	-	-	-
-50 mV	63.7 \pm 10.9 ms (n=17)	119.0 \pm 7.2 ms (n=6)	-	-
-60 mV	44.6 \pm 4.8 ms (n=8)	81.9 \pm 6.5 ms (n=3)	-	-
-70 mV	37.2 \pm 4.6 ms (n=16)	66.1 \pm 5.9 ms (n=9)	\approx 50 ms	\approx 100 ms
-80 mV	20.5 \pm 3.4 ms (n=7)	39.4 \pm 10.2 ms (n=6)	-	-
-90 mV	-	-	-	-
-100 mV	13.2 \pm 2.2 ms (n=6)	-	-	-
-110 mV	10.3 \pm 2.8 ms (n=14)	11.5 \pm 1.5 ms (n=8)	-	-
activation threshold	\approx -75 mV	\approx -75 mV	\approx -60 mV	\approx -60 mV
\bar{G}_M per cell	\approx 5 nS	\approx 3 nS	\approx 84 nS	\approx 77 nS
potential for \bar{G}_M	\approx -30 mV	\approx -30 mV	\approx 0 mV	-
half max activation	\approx -52 mV	\approx -52 mV	\approx -35 mV	-
voltage change for e fold \uparrow \bar{G}_M	7 mV	7 mV	10 mV	-
G_M per cm ²	\approx 1050 μ S.cm ⁻²	\approx 1495 μ S.cm ⁻²	-	-

¹ Data from Adams *et al.*, (1982b)² Data from Jones (1987a)

exponential-fold change in G_M for each 7mV change in voltage. The fact that these two curves superimpose indicate that the voltage-sensitivities of B- and C-cell M -channels are similar.

Table 1 summarizes the I_M kinetics and compares the results obtained with microelectrode studies of the M -current reported from studies on Rana catesbeiana B-cells (Adams et al, 1982a) and C-cells (Jones, 1987a). There were discrepancies between the activation kinetics, where the WCR I_M activation curves were shifted to more negative potentials. I_M relaxations also were faster in WCR. The maximum G_M obtained from these studies were significantly less than the currents observed by microelectrode recording. These differences and the possible relation to the loss of cytoplasmic factors will be addressed in the Discussion.

1.3. EFFECTS OF ADRENALINE ON SMALL AND LARGE NEURONS USING WCR.

Although there is little evidence for the presynaptic release of adrenaline from presynaptic terminals in the amphibian sympathetic ganglia, exogenous application of adrenaline has been reported to induce both presynaptic and postsynaptic effects (Kuba et al, 1981; Koketsu and Nakamura, 1976). Adrenaline hyperpolarized the whole ganglion preparation via a postsynaptic α_2 -adrenoceptor (Rafuse and Smith, 1986) and induced a depolarization in bullfrog B-cells (Akasu and Koketsu, 1987; Akasu, 1988a&b). Therefore, the effects of adrenaline were

studied to determine whether there existed a similar division of hyperpolarization and depolarization responses associated with 'small' and 'large' cells respectively.

Each cell included in Figure 15 was also tested with 100 μ M adrenaline to compare with the muscarine response. The frequency histogram in Figure 15A shows that outward current responses to adrenaline occur less frequently than outward current responses to muscarine. Only about 47% (21/45) of the cells studies responded with an outward current to application of both muscarine and adrenaline. The histogram also shows that small cells were more likely to respond to adrenaline with an outward current.

Figure 15B shows the incidence of adrenaline-induced inward current was less than the incidence of muscarine-induced inward current. Both agents induced an inward current in the same cell only about 11% (6/54) of the time and the amplitude of the adrenaline-induced inward current was always much smaller than that induced by muscarine (See Figure 49 for example). It cannot be determined from the histogram whether there was an increased likelihood of observing an inward current to adrenaline if the cell was large in size, since the frequency of observation was evenly distributed for cells with $C_m > 20$ pF. However, adrenaline never produced inward current in C-cells ($C_m < 20$ pF).

1.4. INTERNAL SOLUTION REQUIREMENTS.

The importance of the composition of the internal solution was briefly addressed in the methods section. The rapid fluid exchange that occurs between

Table 2

Effects of intracellular cAMP on agonist-induced effects.

		<u>Large-cells</u>		<u>Small-cells</u>	
Capacitance (pF, $\bar{x} \pm \text{SEM}$, n)		40.5 \pm 1.5, 66		21.3 \pm 0.8, 70	
A Current*		63/69		5/69	
		I_i	I_o	I_i	I_o
Musc 10 μM^*	no cyclic AMP	8/8	0/8	0/16	10/16
	100 μM cyclic AMP	49/52	1/52	0/46	39/47
Adr 100 μM^*	no cyclic AMP	1/7	1/7	0/14	3/14
	100 μM cyclic AMP	7/13	1/14	0/23	17/23

*number of responding cells
number of cells tested

the contents of the patch pipette and the cytoplasmic contents can dilute various nucleotides that are thought to be important in the maintenance of ion channel function (Catterall, 1988; Pfaffinger, 1988). Therefore, various nucleotides were added to the internal solution and the effects on currents recorded from both large and small cells were monitored. The inclusion of ATP (1.5mM), GTP (1.5mM) were ineffective in increasing the amplitude of inward or outward currents. However, inclusion of cAMP (100 μ M) dramatically increased the probability of observing adrenaline-induced effects in both large and small cells. Table 2 compares effects of the presence or absence of cAMP on the frequency of observation of inward and outward currents in large and small neurons. The rank order as a percentage of the increase in frequency of observation was: small cell adrenaline-induced outward current (+53%) > large cell adrenaline-induced inward current (+40%) > small cell muscarine-induced outward current (+20.5%) > large cell muscarine-induced inward current (-6%). The inclusion of 100 μ M cAMP in the internal solution (for composition see Methods) was adopted for all the WCR experiments unless otherwise indicated.

2. CHARACTERIZATION OF INTACT GANGLION RESPONSES.

In the previous section, it was reported that responses evoked by application of muscarine and adrenaline in dissociated neurons appeared to be cell specific. However, when muscarine is applied to an intact ganglion (consisting of 100's of

neurons) and recorded by means of the sucrose-gap technique, the response usually appears more complex since the output is representative of the total population of cells that responded, or in other words, the integrative sum of cells that were hyperpolarized and depolarized by muscarine.

2.1. CHARACTERIZATION OF THE WHOLE GANGLION RESPONSE TO MUSCARINE.

Figure 18A shows the effects of muscarine on an intact bullfrog sympathetic ganglion (BFSG). The response is biphasic; a brief hyperpolarization precedes a long sustained depolarization. This reflects the hyperpolarization of the C-cells followed by the depolarization of the B-cells (Smith and Weight, 1986). The apparent change in membrane potential, as measured by the sucrose-gap, is due to the integrative contribution of the cells contained within the ganglion. On a temporal basis, the hyperpolarization always precedes the depolarization. This was consistent with WCR studies where the outward current latency and time to peak response was significantly less than those values measured for the inward current (see below). However, additional considerations must be included in the evaluation of population responses recorded from the whole ganglion. There likely exists some overlap of the two phases of the response that could attenuate the hyperpolarization. This may be due to existing diffusion barriers and relative location of the cell types; a B-cell depolarization occurring near the outer portion

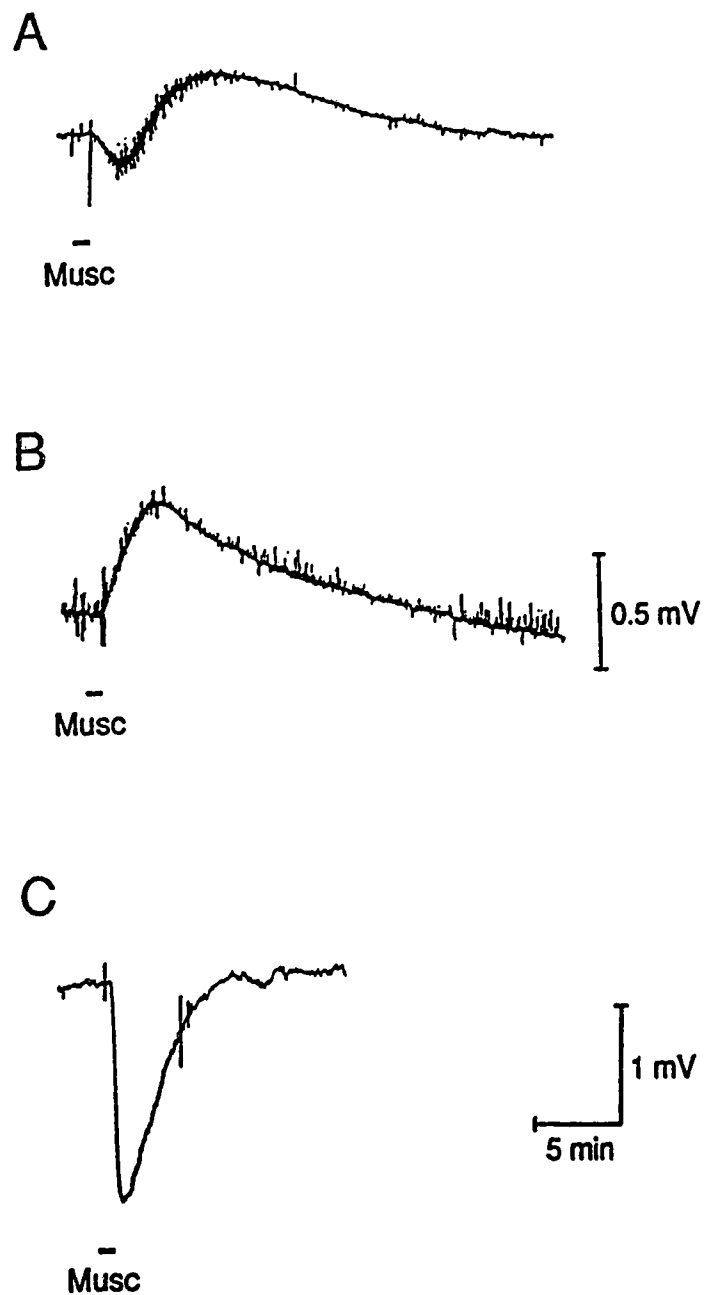


Figure 18. Range of muscarine-induced responses recorded by the sucrose-gap technique in intact BFGS. Three different responses to the addition of $10\mu\text{M}$ muscarine to three different BFGS preparations. A. Biphasic. B. Pure depolarization. C. Pure hyperpolarization. 1mV voltage calibration refers to both A and C. Traces obtained on a rectilinear chart recorder.

of the ganglion may attenuate a concomitant C-cell hyperpolarization occurring in the centre of the ganglion, even though the drug was applied at the same time. The exact percentage and temporal contribution of each cell type was difficult to determine quantitatively, however a relative contribution could be estimated. Figures 18B & C shows the range of variability of muscarine-induced responses ($10\mu\text{M}$) obtained from different isolated bullfrog ganglia preparations. B shows a monophasic depolarization and C shows an example of a pure hyperpolarization due to the application of the same concentration of muscarine. There was no correlation between the likelihood of observing any of the three muscarine-induced responses and the particular ganglion selected (ie. 8th, 9th or 10th ganglion). However, in most experiments a biphasic response was observed. This is consistent with a heterogeneous cell population.

2.1.1. Pharmacology Of The Muscarine-Induced Hyperpolarization And Muscarine-Induced Depolarization In BFG.

It would be advantageous to develop a method in which the muscarinic hyperpolarization and depolarization could be separated for independent study. This would permit non-invasive examination of the transduction mechanism for each response in an intact preparation and should compliment results obtained from the more intrusive single-cell WCR studies. Monophasic responses would also permit quantitative pharmacological studies for receptor subtype identification. Therefore,

experiments were undertaken to examine the actions of selective muscarinic agonists and antagonists to determine whether these responses could be segregated on a pharmacological basis.

a) Muscarinic agonists.

A study was first performed to assess the muscarine-sensitivity for each phase of the response. The mean EC_{50} value of muscarine-induced hyperpolarization was $2.14 \mu\text{M}$ (geometric range of $0.67\mu\text{M} \leq x \leq 6.84 \mu\text{M}$, $n=7$) and was not significantly different from muscarine-induced depolarization EC_{50} of $0.78 \mu\text{M}$ (geometric range of $0.45 \mu\text{M} \leq x \leq 1.35 \mu\text{M}$, $n=8$). Therefore, neither response could be preferentially activated by simply selecting an appropriate concentration of muscarine.

Various muscarinic agonists were screened for selective activation of a depolarization or a hyperpolarization in isolated BFSG. However, these attempts were unsuccessful since bethanechol ($10\mu\text{M}$), carbachol ($10\mu\text{M}$), and methacholine ($100\mu\text{M}$) all induced biphasic responses (data not shown), ARH-602 (0.1mM) caused a small depolarization which was not blocked by atropine. M^cN-343 (10 - $100\mu\text{M}$) caused a depolarization that was reversed to a hyperpolarization by $70\mu\text{M}$ dTC but the hyperpolarization was insensitive to pirenzepine ($1\mu\text{M}$) (data not shown).

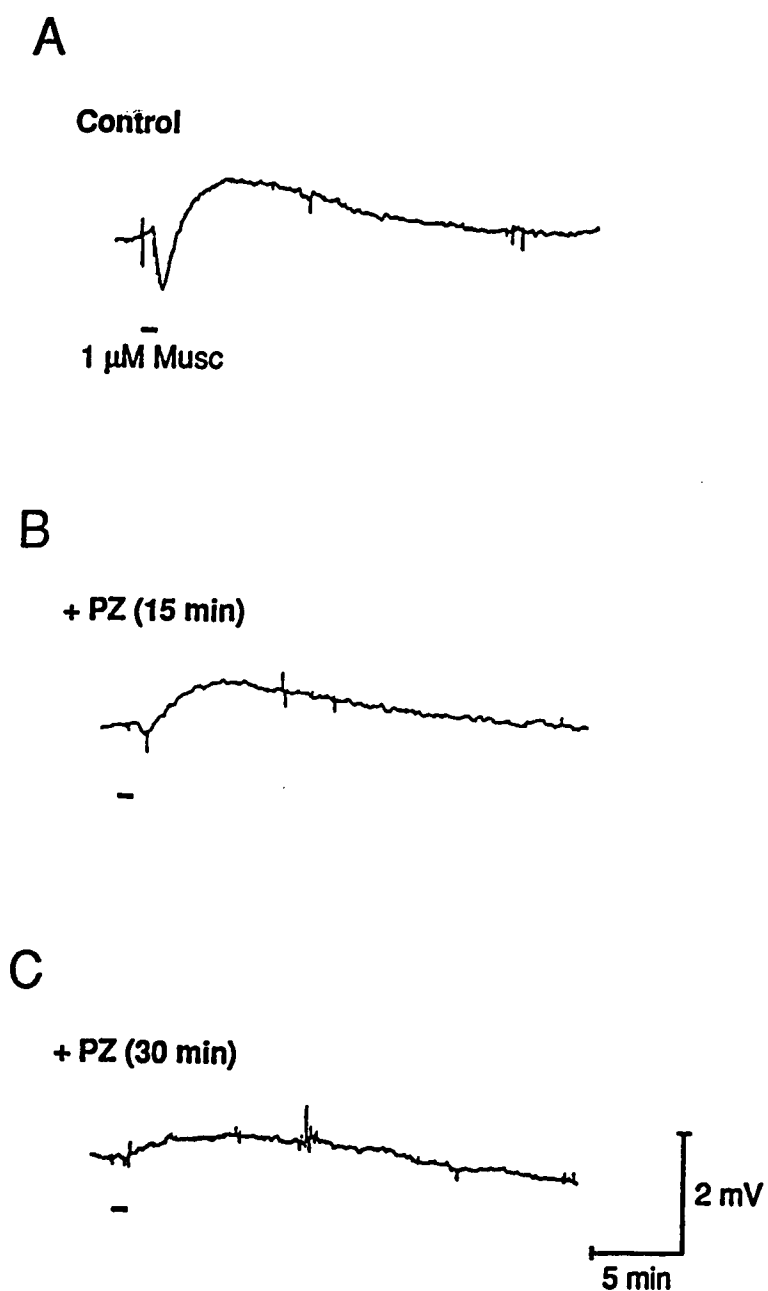


Figure 19. Pirenzepine antagonism of muscarine-induced response in an isolated BFSG preparation (sucrose-gap recording). Panel A shows a biphasic response to a 20s application 10 μ M muscarine. Muscarine-induced response in the presence of 0.1 μ M pirenzepine after 15 min of exposure (B) and 30 min exposure (C) to pirenzepine. Traces from a rectilinear chart recorder.

b) Muscarinic antagonists.

Muscarinic antagonists were screened in an attempt to isolate the two phases because distinct muscarinic receptor subtypes likely govern each of the cell specific responses (Nathanson, 1987; Hoss and Messer 1986; Jones, 1987a). Low concentrations of the M_1 antagonist pirenzepine have been reported to block muscarinic depolarizations in the SCG and muscarinic hyperpolarizations are selectively blocked by gallamine (an M_2 antagonist; Newberry et al, 1985). However, in BFSG both pirenzepine and gallamine preferentially reduced the s-IPSP (Yavari and Weight, 1988). Figure 19 A & B shows a seemingly selective antagonism of the muscarine-induced hyperpolarization by $0.1\mu M$ pirenzepine. However, panel C shows that prolonged exposure to pirenzepine also markedly attenuates the muscarine-induced depolarization. Therefore, attempts to use pirenzepine to dissociate the muscarine-induced biphasic response in an isolated BFSG preparation were unsuccessful.

2.1.2. Muscarinic Response In Rana Pipiens Sympathetic Ganglia.

Rafuse (1985) and Rafuse and Smith (1986) recorded monophasic methacholine-induced hyperpolarizations from Rana pipiens sympathetic ganglia (RPSG). It was first necessary to test whether muscarine-induced hyperpolarizations observed in RPSG were comparable to those observed in BFSG. The EC_{50} of

muscarine-induced hyperpolarization observed in RPSG was $1.48\mu\text{M}$ (geometric range $1.05\mu\text{M} \leq x \leq 2.09\mu\text{M}$, $n=13$) and was not significantly different from the muscarine-induced hyperpolarization in BFSG ($\text{EC}_{50} 2.14\mu\text{M}$, geometric range $0.67\mu\text{M} \leq x \leq 6.84\mu\text{M}$, $.4 > p > .3$). Since muscarine consistently produced a pure hyperpolarization in RPSG, this suggested a predominant contribution of C-cells to the response. Occasionally, the muscarine-induced hyperpolarization was followed by a small depolarization if high concentrations of muscarinic agonists were applied (mM range). However, the response was assumed to be a relatively pure hyperpolarization in the concentration range that was used in these studies. The muscarine-induced hyperpolarization in Rana pipiens was blocked by atropine, pirenzepine, AF-DX 116 and gallamine without unmasking a depolarization. The pharmacological characterization of the receptor that mediates the muscarine-induced hyperpolarization using the above mentioned antagonists is reported below (see Table 4). Therefore, the isolation of muscarine-induced hyperpolarization from muscarine-induced depolarization was accomplished by selecting another experimental species rather than the use of pharmacological intervention.

2.2. CHARACTERIZATION OF THE WHOLE GANGLION RESPONSE TO ADRENALINE.

The application of adrenaline to an isolated BFSG results in a monophasic hyperpolarization (cf Libet and Kobayashi, 1974; Koketsu and Nakamura, 1976;

Weight and Smith, 1980; Rafuse and Smith, 1986). Although on occasion, there have been reports of adrenaline-induced depolarizations measured by sucrose-gap recording (Koketsu and Nakamura, 1976; Rafuse 1985; Smith et al, 1990). The recorded response, however, remained representative of the activation of a heterogeneous population of neurons contained within each ganglion. The responsiveness of single B- and C-neurons studied by WCR indicated that the responses to adrenaline were observed less frequently than responses to muscarine (see above). Furthermore, C-cells were more likely than B-cells to respond to adrenaline (see above). This may explain why a monophasic hyperpolarization was usually observed in response to the addition of adrenaline and the occasional adrenaline-induced depolarization may be accounted for on the basis of a larger proportion of B-cells than C-cells contained within a particular whole ganglion preparation.

The monophasic hyperpolarization observed in the bullfrog has been reported to be due to the activation of an α_2 -adrenoceptor that ultimately caused an increase in K^+ conductance (Rafuse and Smith, 1986). From the WCR data reported above, the α_2 -adrenoceptor presumably resides on the C-cells. The sucrose-gap method was used to help elucidate the transduction mechanism that underlies this response. These results obtained from both the biochemical and WCR techniques are reported in subsequent sections of the results.

3. EXAMINATION OF THE EFFECTS OF MUSCARINE AND ADRENALINE ON SYMPATHETIC GANGLION NEURONS.

The preliminary characterization of various agonist-induced responses occurring in the sympathetic ganglion formed the basis for the following studies where a series of experiments were performed to elucidate the ionic and signal transduction mechanisms involved in their generation. The results will be reported as follows:

- 3.1. Effects of Muscarinic Agonists on C-cells.**
- 3.2. Effects of Muscarinic Agonists on B-cells.**
- 3.3. Effects of Adrenaline on C-cells.**
- 3.4. Effects of Adrenaline on B-cells.**

3.1. EFFECTS OF MUSCARINIC AGONISTS ON C-CELLS.

- 3.1.1. Description Of Muscarine-Induced Conductance Changes
Observed During WCR.**

A series of steady-state currents induced by the application of $10\mu\text{M}$ muscarine, in $20\text{mM } [\text{K}^+]_o$ at various holding potentials between -30 and -110 mV are shown in Figure 20. Note that the muscarine-induced current is outward at

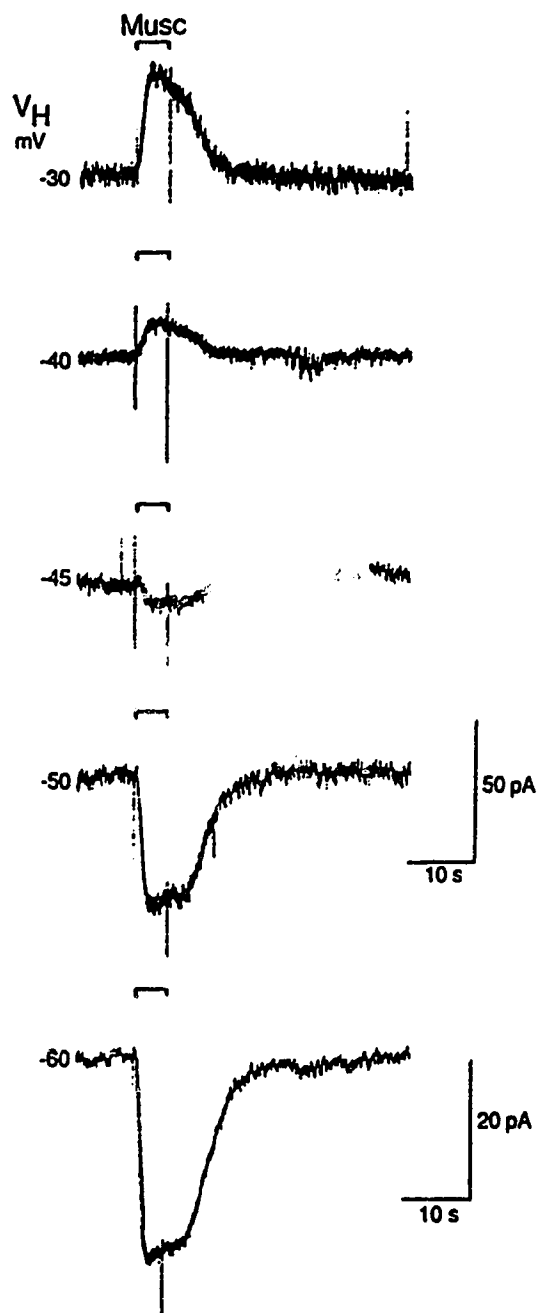


Figure 20. Steady-state current responses to application of muscarine (Musc; $10\mu\text{M}$) in a C-cell whilst holding at different command potentials (-30 , -40 , -50 , and -60mV ; $[\text{K}^+]_o = 6\text{mM}$). The polarity of the muscarine-induced current reverses between -40 and -45mV . This corresponds well to the calculated E_{K} of -43mV . The Musc-induced current displays pronounced inward-rectification at potentials negative to current reversal. (Note change in calibration for $V_{\text{H}} = -60\text{mV}$).

potentials positive to E_K (calculated to be -43mV). The current reverses at E_K and displays a strong inward rectification at more negative potentials. The apparent latency for onset of muscarine-induced outward current measured at -30mV was $0.39 \pm 0.01\text{s}$ ($n=13$) and since the solution exchange time in the U-tube was about 0.2s , the biological latency for the initiation of the response was about 0.2s . Peak outward current was reached in $2.61 \pm 0.45\text{s}$ ($n=20$) and recovery to the resting current level occurred $22.96 \pm 5.57\text{s}$ ($n=17$) after the removal of muscarine.

The steady-state currents at various voltages were also studied using a voltage ramp protocol rather than a voltage jump protocol because the entire I/V curve could be determined within 5s . This protocol also reduced drug application time and thereby decreases the likelihood for receptor desensitization. Figure 21 illustrates a typical C-cell response to the application of $10\mu\text{M}$ muscarine in 6mM $[\text{K}^+]_o$. The whole-cell currents were recorded at a holding potential of -30mV . In panel A, the slow record shows the change in steady-state currents evoked when 5s voltage ramp from -30 to -110mV was applied before, during, and after the application of $10\mu\text{M}$ muscarine. Muscarine promoted a small steady-state outward current when the cell was held at -30mV . The voltage ramp was initiated at the peak outward current response. The most noticeable difference between the current responses to the 5s voltage ramp in the presence of muscarine is the distinct increase in peak inward current at the most hyperpolarized voltage (@ -110mV).

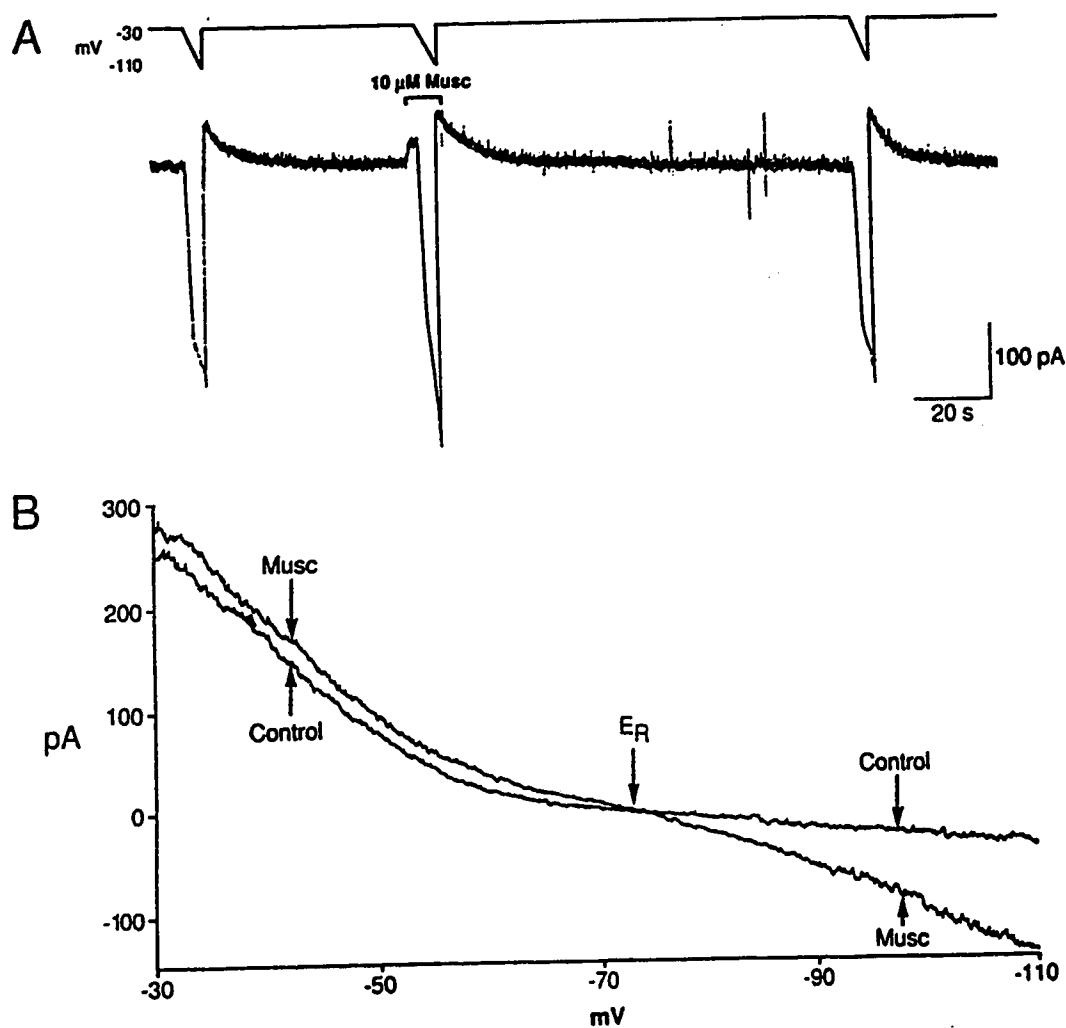


Figure 21. Typical muscarine-induced, inwardly-rectifying current in a sympathetic C-neuron. **A.** Steady-state currents observed in 6mM $[K^+]_o$ at $V_H = -30$ mV. Brief downward deflections are current responses to 5s voltage ramp from V_H to -110 mV. **B.** Fast records of I/V relationships obtained before and during the action of 10μ M muscarine. Note reversal potential (E_R) and the small outward current in response to muscarine above E_R and large inward current at hyperpolarized potentials (inward rectification). Traces in A from rectilinear pen recorder and B from x-y plotter.

The I/V characteristics are better illustrated in panel B, where the digitized record of the whole-cell current observed during the voltage ramps in the absence and presence of muscarine are shown (the first two downward deflections from panel A). The control I/V curve shows an increase in conductance at voltages positive to -50mV (due to I_M activation) and little change, other than a linear leakage current, negative to -60mV. In the presence of muscarine, an increase in conductance occurs but the I/V curve remains almost parallel to the control curve between -30 to -55mV. The difference between the two curves diminishes as the reversal potential (E_R) is approached. However, at potentials negative to E_R , the muscarine-induced current displays a strong inward-rectification. The reversal potential occurs at the calculated E_K (-73mV), indicating that the conductance change was consistent with the opening of a population of channels that are selective for K^+ ions.

The observation of inward rectification was an excellent indicator of the activation of this particular current. In most experiments where the external potassium concentration was elevated to 20mM or 60mM, outward currents evoked at -30mV were small since the driving force for K^+ was reduced. Although there are reports that the inwardly-rectifying K^+ current is dependent on external $[K^+]$, (Williams et al, 1988a; Pennefather and Cohen, 1990) the amount of inward rectification was also dramatically increased and the use of a lower amplifier gain was necessary to obtain the full extent of the muscarine-induced inward current at potentials negative to E_R .

3.1.2. Quantitative Determination Of The E_K And The Ionic Basis For Muscarine-Induced, Inwardly-Rectifying K^+ Current.

The reversal potential was determined in 2, 6, 20, and 60mM $[K^+]_o$. Figure 22 includes data from averaged C-cell drug responses measured in 2, 6, 20, and 60mM $[K^+]_o$. The estimated reversal potentials shifted in accordance with the calculated E_K 's of -101, -73, -43, and -12 mV respectively. The slope of the line was about 58mV per log unit change in external K^+ .

The filled circles (●) represent the $[K^+]_o$ plotted against the average reversal potential observed on muscarine-activated C-cells. The mean E_K values were 100.9 ± 1.1 mV in 2mM ($n=3$), 73.9 ± 1.9 mV in 6mM ($n=9$), 48.1 ± 1.9 mV in 20mM ($n=6$) and 17.7 ± 1.5 in 60mM ($n=4$). The lack of any significant deviation of the reversal potential from the calculated E_K provided irrevocable evidence that the muscarine-induced conductance occurring in C-cells resulted from the flow of potassium ions through K^+ selective channels. Under physiological conditions, muscarine would induce a small hyperpolarization (outward current) that corresponded with the whole-ganglion population response.

Figure 23 illustrates the I/V effects of the application of 10 μ M muscarine in 6 and 20mM $[K^+]_o$ on two separate C-cells. The subtractions of control current from muscarine-induced current indicate that inward-rectification occurs at about E_K and also shifts according to the change in extracellular K^+ .

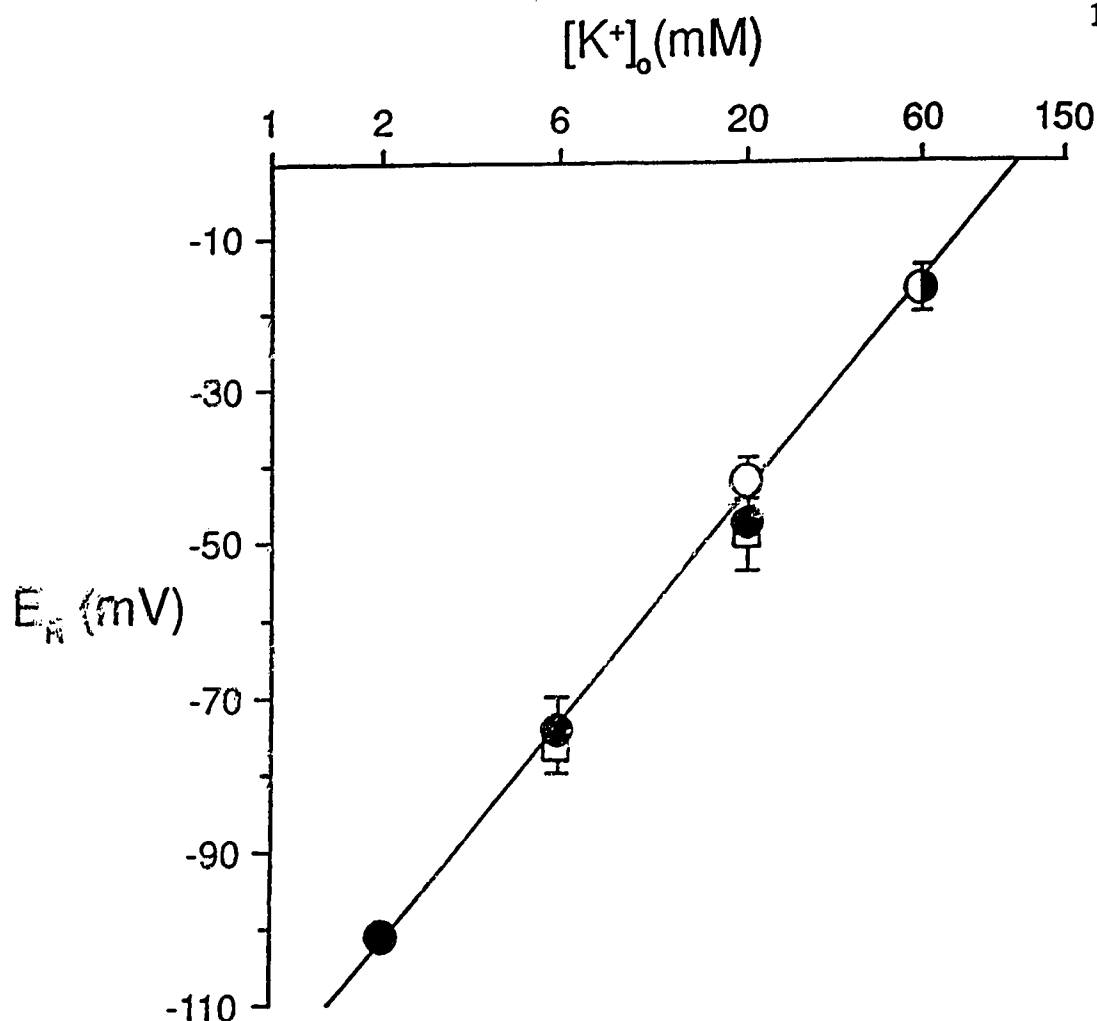


Figure 22. Effect of $[K^+]_o$ on the reversal potential of agonist-induced currents on B- and C-neurons. Effect of $[K^+]_o$ on reversal potential (E_R) for muscarine- (●) and adrenaline- (□) induced outward currents in C-cells and muscarine-induced inward currents in B-cells (○). E_R for adrenaline-induced inward current in B-cells was only determined in 60mM $[K^+]_o$ and was -17.4 ± 1.5 mV ($n=3$). This point was omitted for clarity. The line has a slope of 55mV per ten-fold change of $[K^+]_o$. This is consistent with a prediction by the Nernst equation. All data points obtained from 3 (muscarine-induced outward currents in 2mM $[K^+]_o$) to 9 experiments (muscarine-induced outward currents in 6mM $[K^+]_o$). In some cases, error bars are occluded by graph symbols.

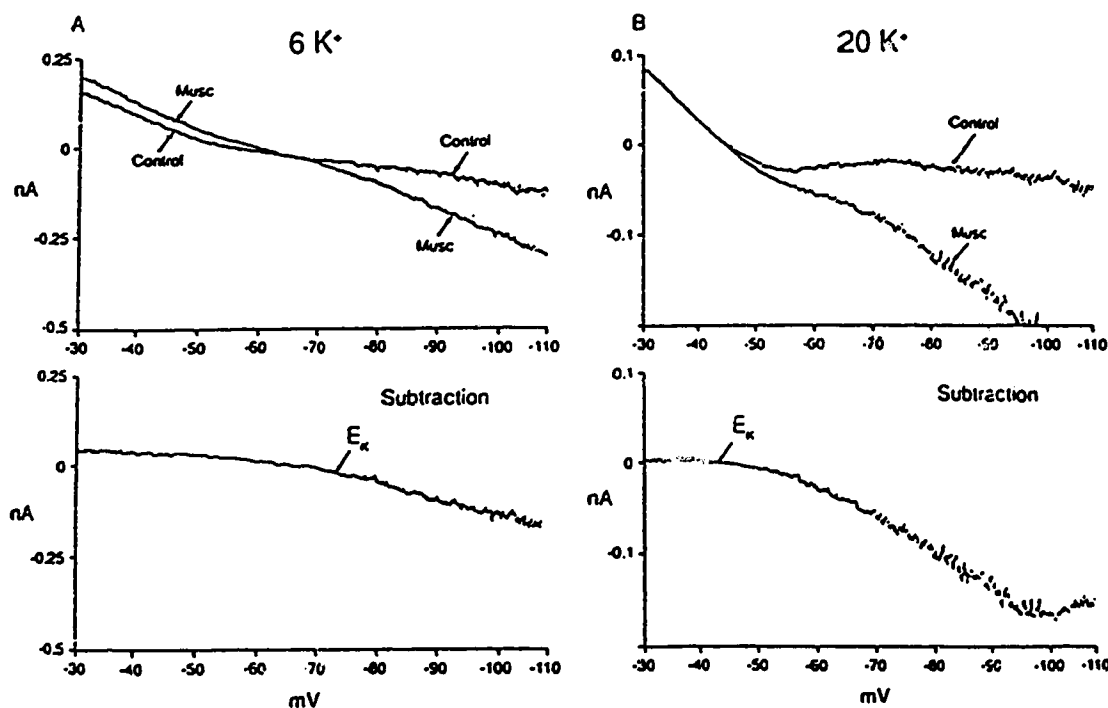
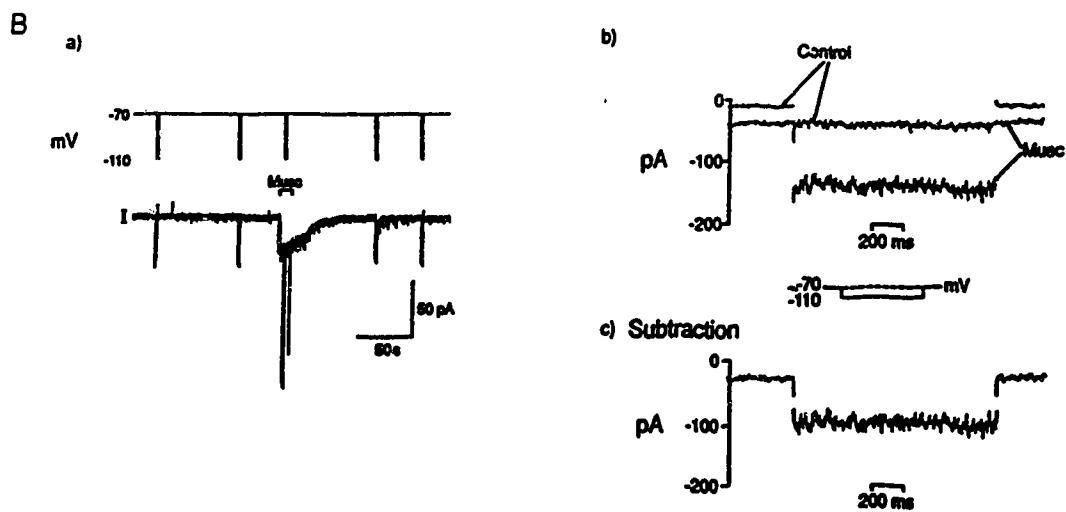
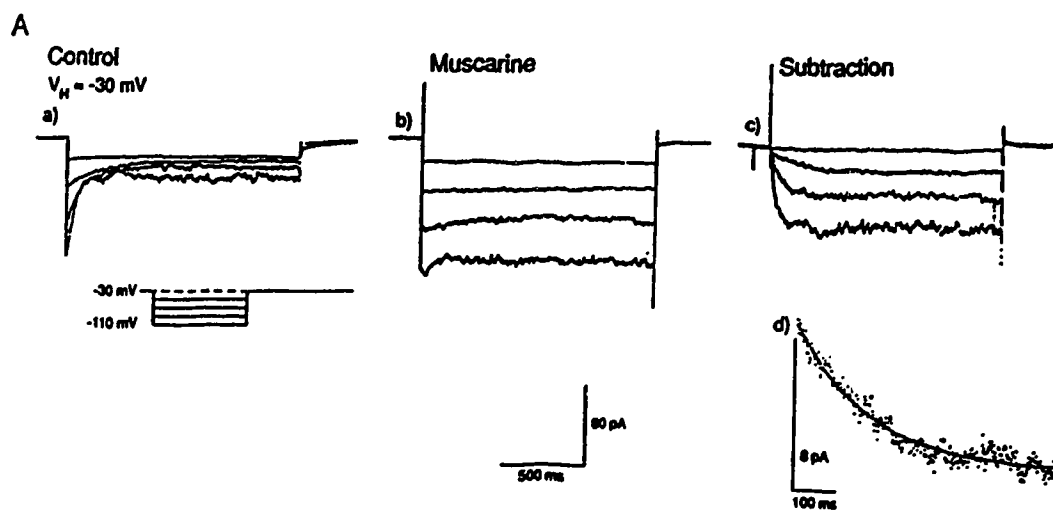


Figure 23. Onset of C-cell muscarine-induced inward-rectification. I/V plots of control and muscarine-induced conductance changes in 6mM[K⁺]_o (A) and in 20mM[K⁺]_o (B) (data from two separate C-cells). $V_H = -30$ mV in both experiments. The net muscarine-induced change in conductance was obtained by subtracting the control I/V from the muscarine-induced I/V. The muscarine-induced currents recorded in 6 and 20mM [K⁺]_o reverse and begin to rectify at their respective E_K 's (located below A and B respectively). They also increase in magnitude at potentials negative to E_K as K⁺ driving force increases. All traces obtained from x-y plotter.

3.1.3. Kinetics Of The Inwardly-Rectifying K^+ Current.

The currents obtained using a voltage ramp paradigm represented the steady-state effects of muscarine. This protocol, however, did not permit the analysis of the rate of current activation. This information was obtained using a voltage step protocol. Figure 24A illustrates the muscarine-induced currents observed using a series of voltage steps from a holding potential of -30mV to -110mV measured in 20mM $[K^+]_o$. The strong rectification induced by 10 μ M muscarine is clearly evident during the three most hyperpolarized step commands and little occurs during the first step to -50mV (Figure 24 A b). The calculated E_K was -43mV and driving force during the first step was only -7mV but increased by an increment of 20mV for each subsequent hyperpolarizing step. The subtractions of muscarine-induced currents from control currents are shown in Figure 24 A c). The currents appear to slowly activate in a voltage-dependent manner. The computer-fitted single exponential time constant for a single step to -70mV was 172 ms (Figure 24 A d). The mean τ values for the apparent rate of activation in 20mM $[K^+]_o$ were 213.5 ± 30.3 ms at -70mV (n=4), 107.2 ± 35.2 ms at -90mV (n=5), and 61.5 ± 14.5 ms at -110mV (n=5). However, the large transient inward tails (due to K^+ flowing through open M-channels prior to their deactivation at negative membrane potentials) might alter space clamp and thereby influence the apparent time constants of activation. Simmons and Hartzell (1987) reported slow activation of

Figure 24. The voltage-dependent activation kinetics of the muscarine-induced inwardly-rectifying current of a C-cell. **A.** Current responses of voltage steps from $V_H = -30\text{mV}$ to -50 , -70 , -90 , and -110mV in the absence, a), and the presence, b), of $10\mu\text{M}$ muscarine; $[\text{K}^+]_o = 20\text{mM}$. The net muscarine-induced current, c), is obtained from the subtraction of b) from a). Note the slow, time-dependent activation of the current recorded under these conditions. The time constant (computer fitted to a single exponential) determined from a single step from V_H to -70mV was 172ms . **B.** Activation kinetics of muscarine-induced inwardly-rectifying K^+ current determined from a second C-cell when $V_H = -70\text{mV}$ (20mM $[\text{K}^+]_o$). a) Steady-state currents in the absence and presence of $10\mu\text{M}$ muscarine. Note, under these conditions, muscarine induces an inward current, since V_H is negative to E_K . Brief interruptions of the current trace are due to 1s hyperpolarizing pulses from -70 to -110mV . The fast records of the first two pulses, in the absence and presence of muscarine, are shown in b) and the net muscarine-induced current is shown in c). Note that muscarine-induced current recorded under these conditions is virtually instantaneous. All records were obtained from x-y plots of computer stored data, except B a), which is a chart record obtained from a rectilinear pen recorder.



ACh-induced inwardly-rectifying K^+ currents in isolated frog atria cells at depolarized potentials, but instantaneous activation at negative holding potentials. Therefore, the experiment was repeated at command voltages of -70mV to eliminate possible artifacts from space-clamp alterations accompanying M-current deactivation. Figure 24 B shows the muscarine-induced inward-rectification in another C-cell in $20\text{mM}[K^+]_o$. The subtraction of the currents (Figure 24 B c) obtained from a brief hyperpolarization to -110mV in the presence of muscarine from those obtained during the control show the inward-rectification is fully activated within 5ms (cf Williams et al, 1988a; Simmons and Hartzell, 1987). These channels did not appear to inactivate during the 1 second hyperpolarizing step commands.

3.1.4. Examination Of The Ca^{2+} -Sensitivity Of Inwardly-Rectifying Channels.

Muscarinic agonists have been reported to increase conductance through calcium-activated K^+ channels as a result of IP_3 production and Ca^{2+} release from intracellular stores in the lacrimal gland (see Hille, 1989). However, it has not been determined whether the C-cell muscarinic-inhibition was due to an increase in $[\text{Ca}^{2+}]_i$ to activate a similar calcium-dependent current. The possibility that the source of Ca^{2+} was extracellular would be remote since voltage-dependent L- Ca^{2+} channels are activated by depolarization and muscarine never depolarized C-cells

(Adams, 1981). The source of Ca^{2+} may, however, be internal where Ca^{2+} release is facilitated by a receptor-mediated liberation from intracellular stores (Cole and Shinnick-Gallagher, 1984; Smith and Weight, 1986).

Therefore, muscarinic agonists may induce the rise in intracellular Ca^{2+} that could activate a calcium-dependent current and conceivably lead to an inhibitory action. If this were the case, the potassium channels involved in the generation of muscarine-induced hyperpolarization should be sensitive to drugs that block calcium-sensitive K^+ channels or interfere with the intracellular Ca^{2+} release process. The effects of apamin (Banks et al, 1979; Pennefather et al, 1985; Galvan and Behrends, 1985), d-tubocurarine (dTC; Nohmi and Kuba, 1984), dantrolene (Van Winkle, 1976) and 4-aminopyridine (4-AP) on the muscarine-induced hyperpolarization are summarized in Table 3. Very little or no antagonism of the muscarine-induced hyperpolarization was observed in the presence of apamin ($1\text{-}10\mu\text{M}$) or dTC ($70\mu\text{M}$), both of which have been proposed to block calcium-sensitive K^+ conductances, or by dantrolene ($60\mu\text{M}$) that block Ca^{2+} -release processes. However, 1mM 4-AP, which does not affect this class of K^+ channels (Cook, 1988) was the most potent antagonist of muscarine-induced hyperpolarization.

Table 3

Effects of drugs on muscarine-induced hyperpolarization
of Rana pipiens sympathetic ganglia.

Drug	Attenuation of Musc _H ¹ (% of control, \pm sem ²)	n	Apparent change of membrane potential (mV \pm sem)
Apamin (1-10 μ M)	76.0 \pm 8.0	5	no change
d-tubocurarine (70 μ M)	78.2 \pm 4.1	6	1.44 \pm .38
Dantrolene (60 μ M)	94.2 \pm 4.1	6	0.45 \pm .20
4-aminopyridine (1 mM)	10.3 \pm 4.48	6	no change ³

¹Musc_H - muscarine-induced hyperpolarization

²sem - standard error and mean

³ transient depolarization occurred; however, baseline returned to control level prior to challenge with muscarine.

3.1.5. Examination Of The Muscarinic Receptor Subtype Involved In The Generation Of The Muscarine-Induced Hyperpolarization In RPSG.

Muscarine induces a seemingly pure hyperpolarization in RPSG and a Schild analysis of the antagonism of this response could therefore be performed. These quantitative receptor studies were accomplished using the sucrose-gap recording technique. The WCR technique was not utilized since muscarine-induced outward currents in C-cells could not be maintained for the time required to perform pA_2 determinations.

The effect of atropine was initially screened to verify the involvement of a muscarinic receptor in the generation of the muscarine-induced hyperpolarization. Low nanomolar concentrations of atropine effectively blocked the response and was rapidly reversible (data not shown). pA_2 values resolved for pirenzepine, and AF-DX 116 are shown in Table 4. Both antagonists were highly selective blockers of the muscarine-induced hyperpolarization. However, ~~tests~~ for competitiveness showed that pirenzepine antagonism was competitive whilst AF-DX 116 antagonism was not.

The pA_2 value for gallamine was not determined since it uncompetitively blocks muscarinic receptors (Stockton et al, 1983; Dunlap and Brown, 1983; Nedoma et al, 1985; Jagadeesh and Sulakhe, 1985; Birdsall et al, 1987), however, the muscarine-induced hyperpolarization was rapidly and reversibly blocked by

Table 4

pA_2 determination for antagonism of muscarine-induced hyperpolarization in RPSG.

Drug	pA_2	n	K_D , geometric mean (nM)
Pirenzepine	7.98 ¹	7	10.6, $5.6 \leq x \leq 15.5$
AF-DX 116	7.78 ²	7	17.1, $9.9 \leq x \leq 28.6$

¹ slope = 1.02

² $pA_2 - pA_{10} = 1.13$

50 μ M gallamine and was reduced to 18% of control by 10 μ M gallamine (n=1, data not shown).

3.1.6. Evaluation Of The Involvement Of Second Messenger Systems In The Generation Of Muscarine-Induced, Inwardly-Rectifying K⁺ Current.

The involvement of established signal transduction mechanisms in the generation of muscarine-induced inwardly-rectifying K⁺ current was tested by using various chemical agents that impair or stimulate certain elements of the signalling pathway. The cumulative data should provide evidence that could lead to the identification of the signalling process involved, or at the least, eliminate transduction mechanisms that are not directly involved the generation of this particular response.

a) Evidence for G-protein involvement.

The effects of guanosine-5'-[3-thio]-triphosphate (GTP- γ -S) on muscarine-induced, inwardly-rectifying K⁺ current. The involvement of G-proteins in any given signal transduction mechanism can be studied by using agents that are known to affect G-protein function. Dialyzing neurons with non-hydrolyzable GTP analogues, such as GTP- γ -S, has provided strong evidence for G-protein involvement in the

coupling to muscarinic receptors leading to the suppression of ganglionic M-currents (Pfaffinger et al, 1985; Pfaffinger, 1988; Brown et al, 1989). If muscarinic inhibition is G-protein coupled, the addition of GTP- γ -S should activate an inwardly-rectifying current. Furthermore, the activation should persist since the thiol group attaches to the third phosphate group impairs GTPase and inhibits the 'off-reaction'.

The effect of the addition of 50 μ M GTP- γ -S via the patch pipette to a C-cell is shown in Figure 25. $[K^+]_o$ was elevated to 20mM so as to increase the amount of inward K^+ current at negative potentials. The cell membrane conductance was measured at -110, -90, -70, -50, and -10mV, before, during and after the application of 10 μ M muscarine ($V_H = -30$ mV). Note that I/V characteristics do not change prior to the first application of muscarine. The results indicate that, under these conditions, the activation of muscarine-induced current required the addition of an appropriate agonist to activate the G-protein, even in the presence of GTP- γ -S (Dolphin et al, 1987). The application of muscarine (10 μ M) induced a small outward current (indicated by an arrow) at -30mV and the conductance is increased during all voltage steps negative to the holding potential. The conductance change is better illustrated in the middle traces, where the fast records corresponding to the first step from -30 to -110mV (●) in the upper trace, before, during and after application of muscarine are shown. Note that the muscarine-induced rectification persists. This indicates that the activated K^+ channels remain open in the absence of muscarine. The lower traces best illustrate

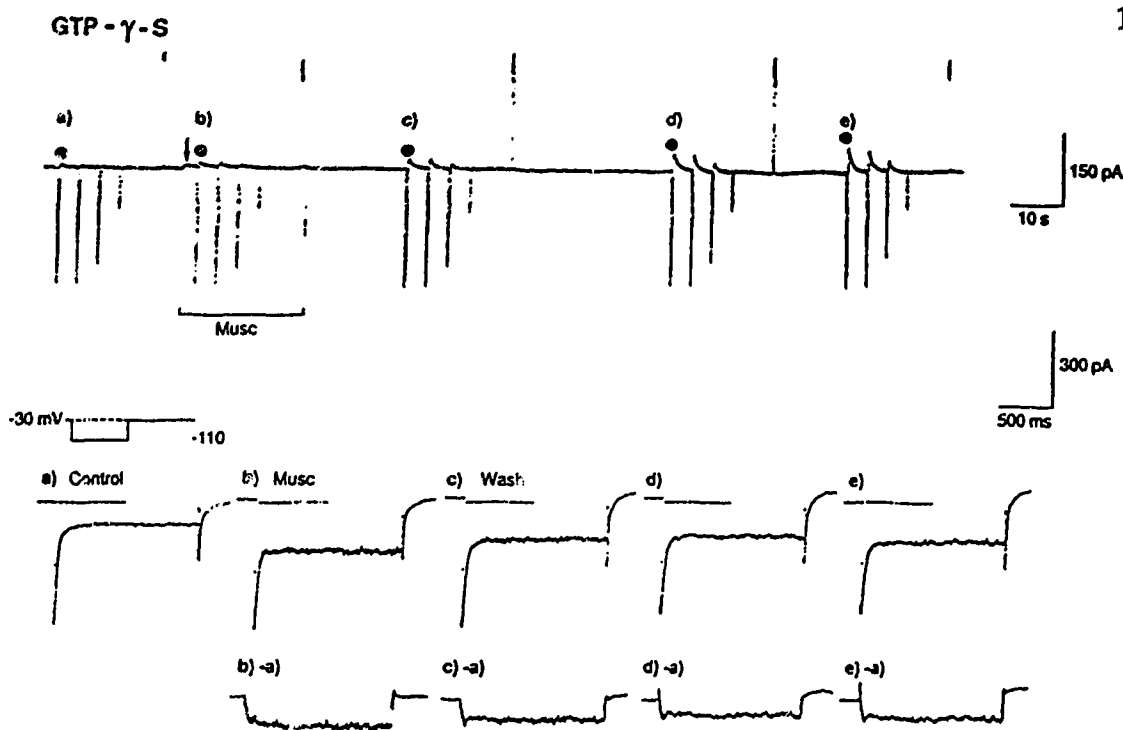


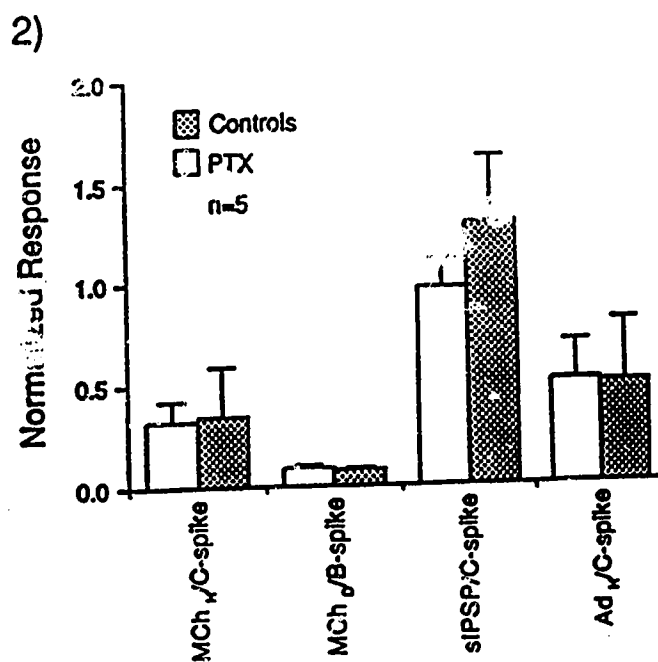
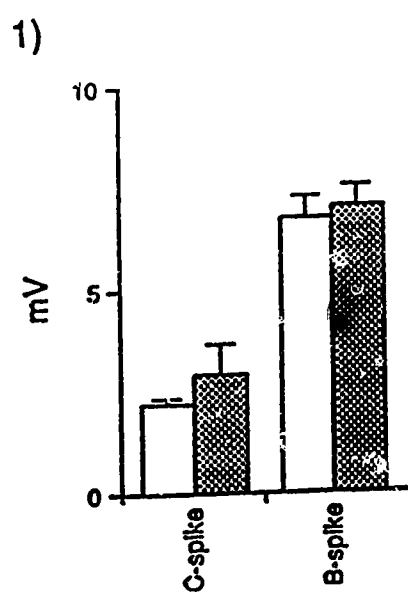
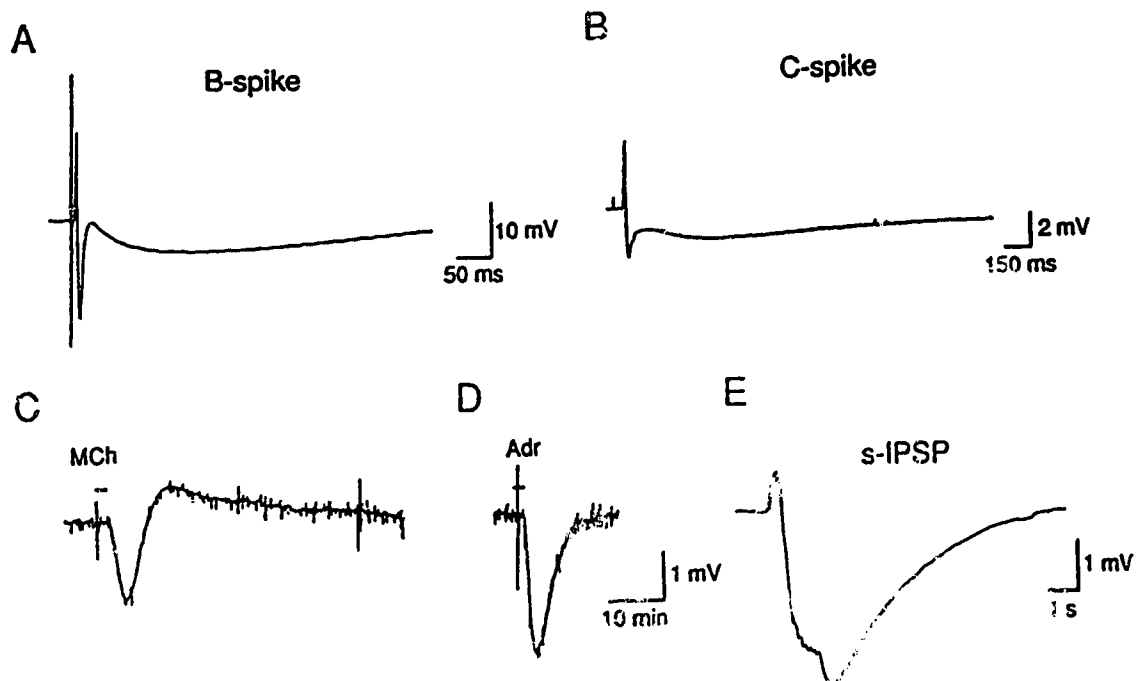
Figure 25. Effect of intracellularly-applied GTP- γ -S on muscarine-induced currents in a C-cell. Upper record. Slow chart record of currents recorded at $V_H = -30$ mV; $[K^+]_o = 20$ mM. Brief downward and upward deflections are current responses to step commands to -110, -90, -70, -50 and +10 mV. (Voltage command trace omitted for clarity). Arrow indicates small outward current produced by application of 10μ M muscarine (Musc). Middle record. Faster speed records of the current responses from V_H to -110 mV (indicated by \bullet in upper trace). Traces obtained from x-y plot of computer-stored data. Records a) to e) in this portion of the figure corresponding to records a) to e) in the upper trace. Dotted line indicates steady-state current level prior to the application of muscarine. Lower records. Currents observed at -110 mV during and after the application of muscarine. The persistence of muscarine-induced inward-rectification is better illustrated by the records obtained by subtracting the control current response in a) from those obtained in b) to e).

the persistence of the muscarine-induced current where the control current (a) is subtracted from each of the middle traces (b to e). Note that muscarine-induced current increased about 2 fold and did not return to the control current during the wash. It appears as if some recovery occurs during the wash, between c-a and d-a, however, the net current is larger in e-a. This contrasts with the muscarine-induced effects observed in control C-cells, where the current normally abates and returns to its original level within 25s after the application of muscarine is stopped (see Figures 21, 27A, 28A, 30A).

The slow, transient outward current that appears following command voltage hyperpolarizations in this figure, also appears in many other figures presented within this thesis (see Figures 21, 27, 28B, 30A, 32, 37A, 41A, 42A, 44, and 52). This phenomenon occurs in both B- and C-cells and is thought to be due to the activation of a slow, transient, 4-AP-sensitive outward K^+ current (for full description and analysis, see Results section 5).

Evaluation of G-protein sensitivity to pertussis toxin. If the transduction mechanism of muscarinic inhibition involves a PTX-sensitive G-protein, the response to a muscarinic-agonist should be attenuated when compared to an untreated, or control response to the same agonist. There was no significant effect of on the methacholine-induced hyperpolarization or the s-IPSP in isolated bullfrog whole ganglia which were pre-treated for about 16 hours in $5\mu\text{g/ml}$ PTX at 4°C . Figure 26B shows the averaged data obtained from 5 control-matched experiments. The

Figure 26. Effects of PTX pre-treatment on intact BFSG. Typical responses observed in RPSG: (A) orthodromically-activated B-cell action potential, (B) orthodromically-activated C-cell action potential, (C) methacholine-(MCh; 10 μ M) induced biphasic response, (D) adrenaline- (Adr; 1 μ M) induced hyperpolarization, and (E) s-IPSP observed in 70 μ M dTC. 1) Comparison between orthodromically-activated C- and B-cell action potentials (C- and B-spikes) obtained from 5 control ganglion preparations versus 5 PTX pre-treated preparations (5 μ g/ml for 18h @ 4°C). 2) compares effects of PTX pre-treatment on various 'slow responses'. Responses were normalized to the C-spike amplitude where comparisons were made between the two experimental groups and methacholine-induced hyperpolarization (MCh_H), s-IPSP, or adrenaline-induced hyperpolarization (Ad_H). The methacholine-induced depolarization (MCh_D) was normalized to the B-spike.



data from each ganglion was normalized to the orthodromically-activated C-fiber action potential. Note that the averaged orthodromically-activated action potentials in control and PTX-treated preparations were quite comparable. This indicated that PTX-pre-treatment did not have an adverse affect on f-EPSP's and comparisons between the two groups should therefore be valid.

- b) The effects of phorbol ester on muscarine-induced, inwardly-rectifying K^+ current.

If the addition of muscarine increased the production of diacylglycerol leading to activation of protein kinase C (PKC) via the phosphatidylinositol pathway (Berridge and Irvine, 1984), then superfusion of phorbol esters, which directly activate PKC (Nishizuka, 1984), should mimic the application of muscarine on a C-cell.

Figure 27 illustrates a typical experiment that tested this hypothesis. The experiment was performed in 6mM $[K^+]_o$ so as to increase the amplitude of the drug-induced inward rectification. Panel A shows a typical C-cell response to muscarine (10 μ M) and the I/V plots for control and muscarine responses. Panel B shows the effect of 2 μ M phorbol-12-myristate-13-acetate (PMA) to the same C-cell. In all 3 experiments, PMA induced a slow and persistent inward current which did not abate during the washout. The I/V plots indicate that PMA does not induce

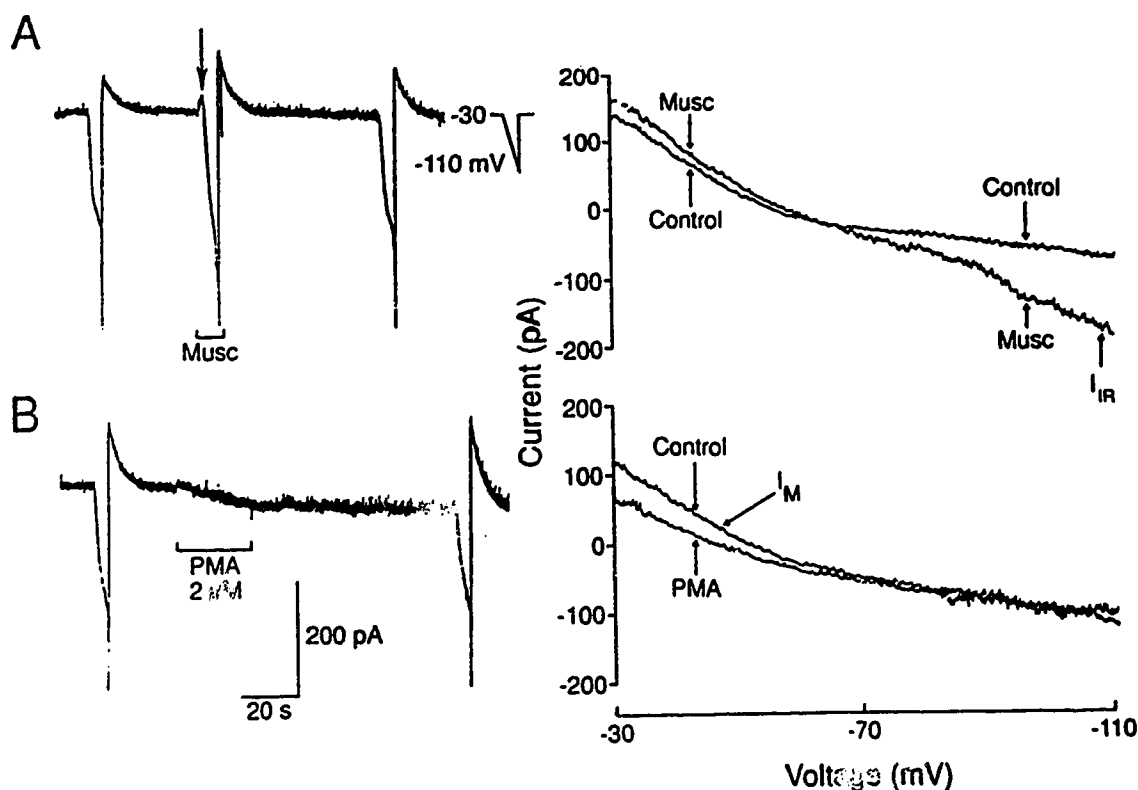


Figure 27. Effects of muscarine and phorbol-12-myristate-13-acetate (PMA) on a C-cell. Current deflections result from 5s hyperpolarizing ramp commands from -30 to -110mV before and during the application of drugs; $[K^+]_o=6\text{mM}$. **A.** (left) The application of $10\mu\text{M}$ muscarine (Musc) evokes a small, steady-state outward current at -30mV (indicated by arrow). The I/V plot, located to right, shows that muscarine produces an outward current which reverses and rectifies (I_{IR}) at potentials negative to E_R . **B.** Effect of $2\mu\text{M}$ PMA. Slow chart record (left) shows that PMA-induces a slowly developing inward current. The I/V plot (located to the right) shows that conductance is reduced in the I_M range. Traces on the left obtained from rectilinear pen recorder and right hand traces are x-y plots of computer stored data.

a K^+ current similar to that induced by muscarine in C-cells and suppressed the muscarine-insensitive I_M to $62 \pm 5\%$ of control ($n=3$).

- c) The effects of protein kinase inhibitors on muscarine-induced inwardly-rectifying K^+ current.

Another method which tested whether PKC was involved in the transduction mechanism for muscarine-induced currents in C-cells was to examine the effects of protein kinase inhibitors (PKIs) 1-(5-isoquinoliny-sulphonyl)-2-methyl piperazine (H-7; Hidaka et al, 1984) and gold sodium thiomalate (GST; Parente et al, 1989).

The appearance of a muscarine-induced current was not affected by the inclusion of either $50\mu M$ H-7 or $50\mu M$ GST in the patch pipette. Figure 28A shows a normal C-cell response to the application of $10\mu M$ muscarine when $50\mu M$ H-7 was included in the patch pipette. The density of the muscarine-induced current measured in C-cells dialyzed with GST or H-7 was $3.02 \pm 0.25\mu A/cm^2$ ($n=4$, measured @ $-110mV$) and was indistinguishable from that measured in control C-cells ($4.54 \pm 1.21\mu A/cm^2$, $n=16$, $p > 0.2$). Therefore, the phorbol ester-induced attenuation of I_M appears, from these data, to be independent of PKC activation (cf Bosma and Hille, 1989; see Discussion).

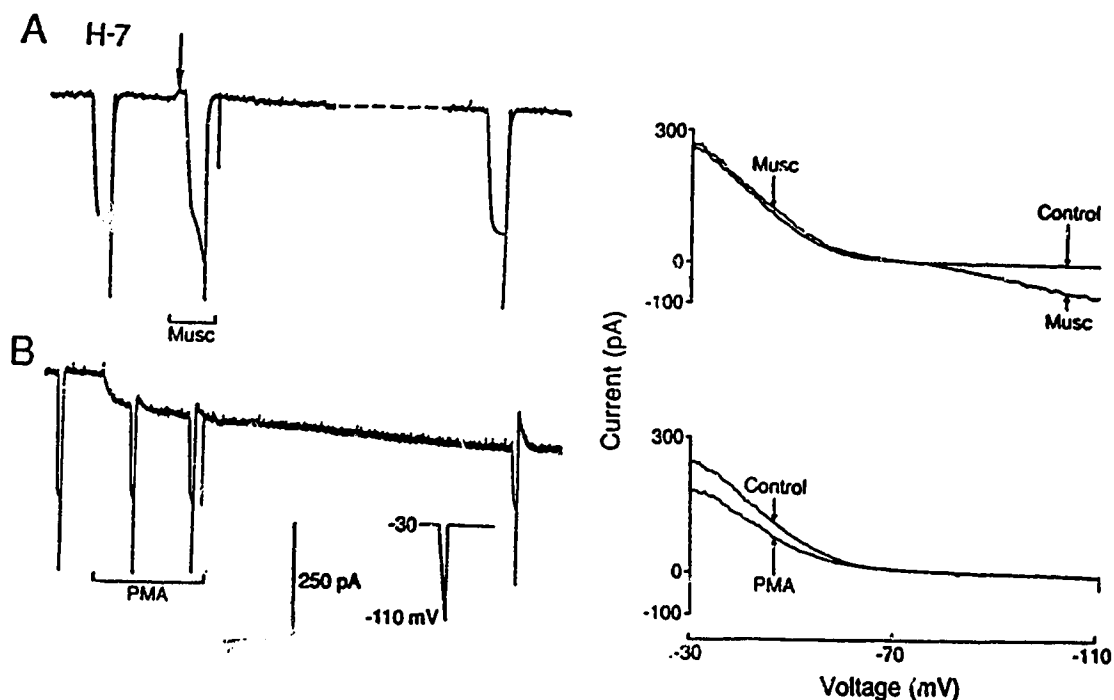


Figure 28. Lack of effect of intracellularly applied H-7 on both muscarine- and PMA-induced effects of a C-cell. A. $[K^+]_o = 6\text{mM}$, $V_H = -30\text{mV}$. Hyperpolarizing voltage-ramp commands (as shown in inset; next to calibration bars) to -110mV were applied before, during, and after the application of drugs. The resulting I/V plots are shown on the right hand side of the figure. A. Typical inwardly-rectifying current evoked by $10\mu\text{M}$ muscarine; although H-7 ($50\mu\text{M}$) is included also included in the patch pipette. B. Effect of PMA ($2\mu\text{M}$). Note steady-state, slowly-developing inward current which, from the I/V plot, involves a decreased conductance of I_M (in the presence of H-7). Left hand series of records from rectilinear pen recorder, right hand records obtained from x-y plot of computer-stored data. Data illustrated in this figure are almost identical to data obtained without H-7 in the patch-pipette (see [Figure 27](#)).

- d) The effects of protein kinase inhibitors on the phorbol ester-induced suppression of C-cell I_M .

Phorbol esters have been reported to affect non-PKC substrate, therefore specificity of PMA should be verified (Nishizuka, 1984; Katada et al, 1985; Kikkawa and Nishizuka, 1986). Figure 28B shows that $2\mu\text{M}$ PMA reduced I_M in the presence of H-7. There was no significant difference between the I_M suppression measured in C-cells dialyzed with either $50\mu\text{M}$ GST or $50\mu\text{M}$ H-7 ($48.4 \pm 16.4\%$, $n=4$) and PMA effect in the absence of PKI's ($61.5 \pm 5.0\%$, $n=3$). There was also no significant difference between capacitance-corrected I_M measured prior to application of PMA at -30mV of control C-cells ($1809 \pm 168 \mu\text{S}/\text{cm}^2$, $n=21$) versus C-cells dialyzed with either GST or H-7 ($1816 \pm 487 \mu\text{S}/\text{cm}^2$, $n=4$). The phorbol ester attenuation of I_M appears, from these data, to be independent of PKC activation (cf Bosma and Hille, 1989; see Discussion).

- e) The effects of intracellular application of IP_3 and elevated $[\text{Ca}^{2+}]$ in C-cells.

If the muscarine-induced, inwardly rectifying K^+ current is mediated by an IP_3 -induced intracellular Ca^{2+} -release or by a direct effect of IP_3 to activate calcium

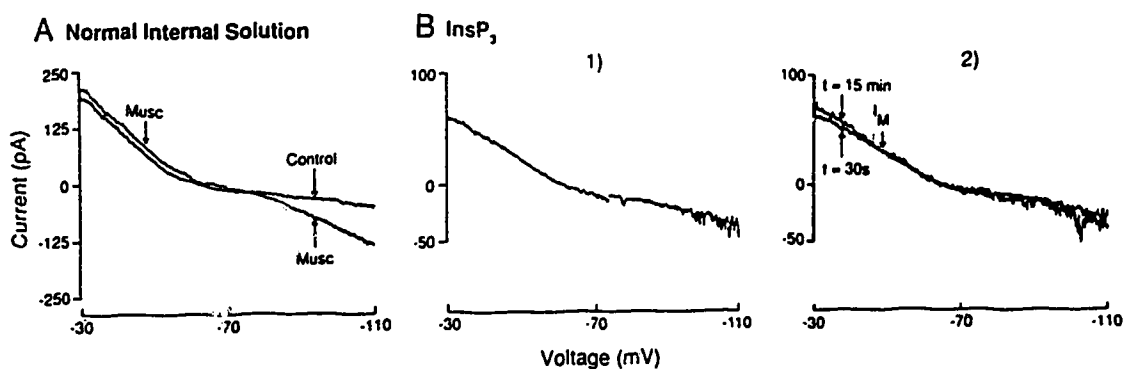


Figure 29. Effects of intracellular application of IP₃ to a C-cell. [K⁺]_o; V_H = -30 mV. **A.** Response of a control C-cell to the addition of 10 μM muscarine. Note the muscarine-induced increase in conductance at -110 mV. **B.** Effects of the inclusion of 0.5 mM IP₃ in the patch pipette on another C-cell. **B 1).** I/V plot obtained 30s after the establishment of WCR (break-in). **B 2).** I/V plot obtained 15 minutes after the establishment of WRC and compared to that obtained after 30s (**B 1**). All I/V plots obtained from computer stored data of current responses to 5s voltage ramp commands from -30 mV to -110 mV. Note difference in current scale in traces **A** compared with those in **B**.

channel in the cell membrane (see Dutar and Nicoll, 1988), an inwardly-rectifying K^+ current should slowly activate as IP_3 dialyses into the cell.

Figure 29 compares the I/V characteristics of a typical C-cell response to $10\mu M$ muscarine when dialyzed with normal 'internal solution' (A) to a second C-cell that was dialyzed with $0.5mM$ IP_3 (B). The I/V relation illustrated in panel B 1) was obtained 15s after WCR was established and shows no mimicry of a muscarine-induced, inwardly-rectifying K^+ current. A second I/V relation was obtained after 15 minutes of dialysis and is compared to the 15s I/V in panel B 2). Note that prolonged exposure to IP_3 did not induce a delayed effect or have any deleterious effects on C-cell currents. Panel B 2) also shows the characteristic increase in I_{Na} that occurs in C-cells after the establishment of WCR, is not affected by the inclusion of IP_3 in the pipette.

Since the release of Ca^{2+} from internal stores has been implicated as the principal mechanism of action for the receptor-induced liberation of IP_3 (Berridge, 1984; Berridge and Irvine 1984), a direct elevation of $[Ca^{2+}]_i$ to about $1\mu M$ was attempted to test whether C-cells would exhibit inward rectification under these conditions. The ratio of EGTA to $CaCl_2$ was adjusted to buffer the internal solution $pCa^{2+}=6$ (see Methods). Although I/V curves were obtained as soon as possible upon the establishment of WCR, C-cells were too leaky to determine if high $[Ca^{2+}]_i$ conditions could induce an effect similar to a muscarine-activated inwardly-rectifying K^+ current (data not shown).

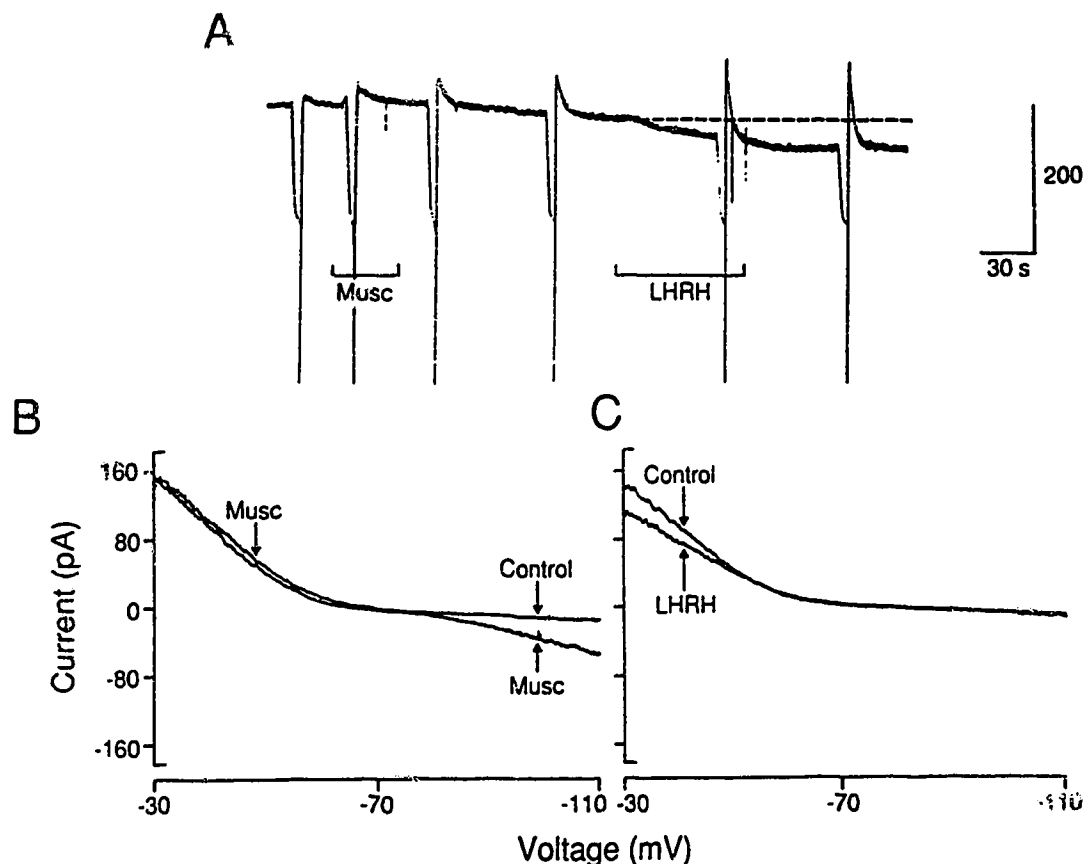


Figure 30. Comparison between the effects of muscarine and LHRH on a C-cell. **A.** Slow chart record of steady-state responses. Note outward current due to application of $10\mu\text{M}$ muscarine (Musc) and the slowly developing inward current due to application of $100\mu\text{M}$ chicken- γ -LHRH. Note the muscarine effect returns to control level within 30s whilst the LHRH effect persists. The LHRH effect did not recover after prolonged wash out. Brief interruptions in **A** are current responses to 5s voltage ramps from -30 to -110 mV. **B** and **C** are fast records of currents obtained from voltage ramps before and during the application of muscarine and LHRH respectively. Muscarine induces conductance change over the entire voltage range whilst LHRH affects conductances in I_M activation range. Voltage protocol omitted for clarity. Traces in **A** from rectilinear pen recorder and **B** and **C** are x-y plots.

3.1.7. Effects Of Luteinizing Hormone Releasing Hormone (LHRH) On C-Cells.

In frog sympathetic ganglia, synaptically released LHRH-like peptide from C-fiber terminals (Jan and Jan, 1982) induces 1s-EPSP in both B- and C-cells that is thought to involve I_M suppression (Adams and Brown, 1980; Adams et al, 1983).

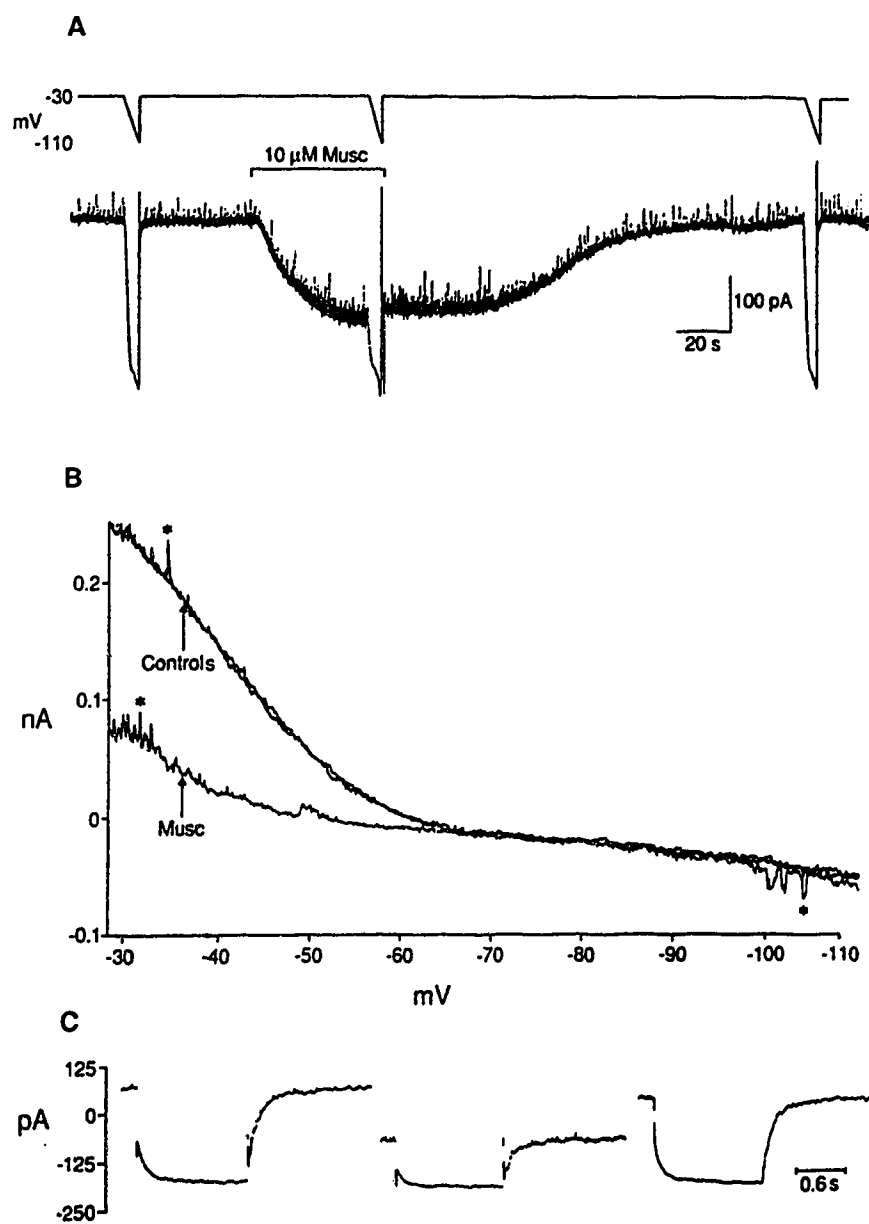
Figure 30A shows a continuous slow chart record of responses to $10\mu\text{M}$ muscarine and chicken-II-LHRH (c-II-LHRH; $100\mu\text{M}$). The I/V characteristics of the agonist-induced currents are better seen in panels B and C where the current responses to a 5s voltage ramp from -30 to -110mV are shown. In Figure 30B, muscarine evokes a typical inwardly-rectifying K^+ current, whereas c-II-LHRH only affects whole-cell currents in the I_M range (Figure 30C).

3.2. THE EFFECTS OF MUSCARINIC AGONISTS ON B-CELLS.

3.2.1. Description Of The Muscarine-Induced I_M Suppression In Sympathetic B-Cells.

A typical B-cell response to $10\mu\text{M}$ muscarine is illustrated in Figure 31. The slow chart records in Figure 31A show current responses to voltage ramps from -30 to -110 before, during, and after application of muscarine. Muscarine produces a large, reversible, steady-state inward current. The apparent latency between drug

Figure 31. Effect of muscarine on a B-cell. **A.** Steady-state inward current produced by 10 μ M muscarine (Musc) in a B-cell; 6mM [K⁺]_o and V_H=-30mV. Upper record; voltage command, lower record; current response. 5s hyperpolarizing ramp commands promote inward currents before, during and after response to muscarine. **B.** I/V relationships obtained from voltage ramp commands in **A** on faster time (voltage) scale. The small upward and downward deflexions marked with an asterisk are thought to represent spontaneous miniature outward currents ('smocs', Satin & Adams, 1987). **C.** Inward current relaxations produced by a hyperpolarizing voltage command from -30 to -70mV, before, during, and after the application of 10 μ M muscarine to another B-cell. Voltage trace omitted for clarity. Traces in **A** from rectilinear pen recorder and in **B** and **C** from x-y plotter.



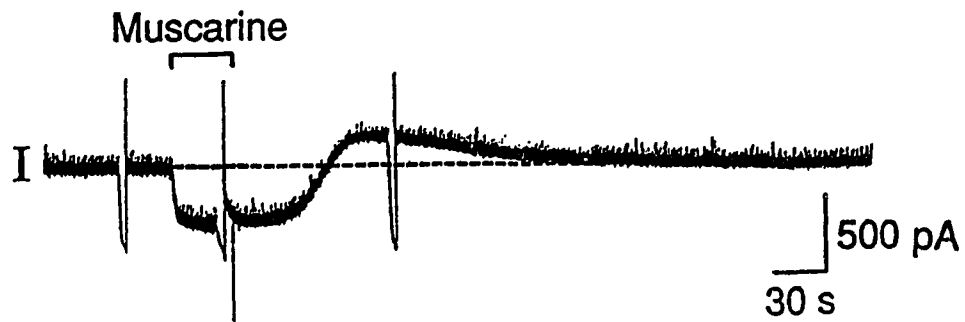
application and the appearance of inward current was 2.2 ± 0.6 s ($n=16$). This was about ten-times slower than the latency of muscarine-induced outward current observed in C-cells (about 0.2s; see Results: section 3.1.1.). The time to peak of the muscarine-induced inward current was 30.9 ± 3.0 s ($n=16$). The current recovered to the resting level 88.5 ± 9.6 s ($n=15$) after the termination of drug application from the U-tube. The currents evoked by the voltage ramp paradigm in the presence of muscarine were always less than those recorded during its absence. This is consistent with an agonist-induced decrease in membrane conductance.

Figure 31B better illustrates the decrease in B-cell conductance. Fast records of the current response to voltage ramps, before and during the application of muscarine are superimposed. Muscarine ($10\mu\text{M}$) reduces conductance in the I_M voltage range (-65 to -30mV) and the whole-cell I_M , measured at -30mV, is decreased to 38% of control. The mean I_M suppression by $10\mu\text{M}$ muscarine was $54.9 \pm 7.2\%$ ($n=11$) (cf Jones, 1985; Pfaffinger, 1988).

Figure 31C shows a single voltage step from -30 to -70mV in another B-cell before, during, and after the application of $10\mu\text{M}$ muscarine. Muscarine reduces the following current components: 1) the steady-state outward current, 2) the initial ohmic step (that represents the contribution of both the I_M and leak current), 3) the inward relaxation, and 4) the outward current associated with I_M reactivation (cf Brown and Adams, 1980; Adams et al, 1982a).

A)

162



B)

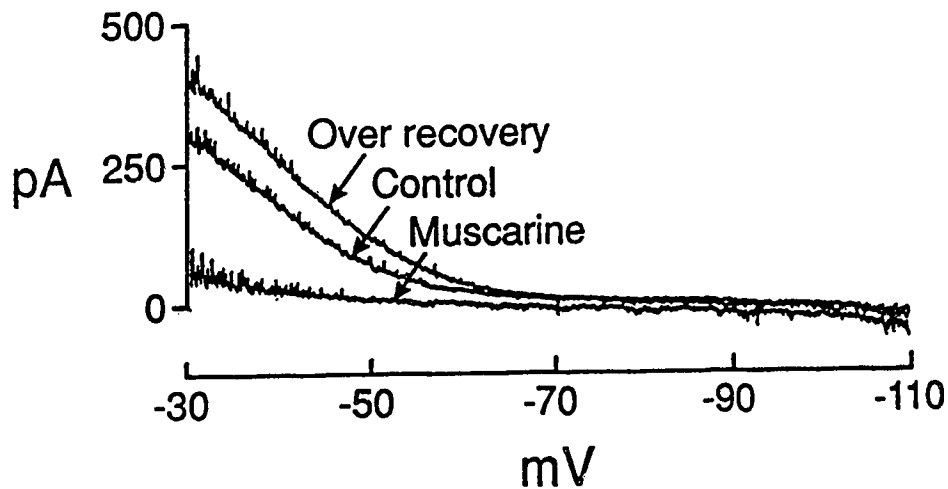


Figure 32. Over-recovery of I_M subsequent to the application of muscarine to a B-cell. **A.** Steady-state inward current due to the application of $10\mu\text{M}$ muscarine; $[\text{K}^+]_o = 6\text{mM}$ and $V_H = -30\text{mV}$. Note the large, transient increase in steady-state current which occurs during recovery. Inward current deflections represent the current response to 5s voltage ramp commands from V_H to -110mV (voltage trace omitted for clarity). **B.** Fast records of the current responses to voltage ramp commands from **A**. Note that both effects are restricted to the I_M voltage range. Traces in **A** from rectilinear pen recorder and **B** is an x-y plot of computer stored data.

3.2.2. Over-Recovery of I_M .

In a large number of B-cells studied, I_M transiently increased during the washout of muscarine and eventually returned to the control level. Figure 32A shows the chart record of steady-state current (@-30mV) observed before, during and after application of 10 μ M muscarine. Note that the steady-state current recovers beyond control current level, peaks, and then returns to the control baseline. In Figure 32B, fast records of current responses to hyperpolarizing voltage ramps shows that both suppression and potentiation of I_M are attributable to the application of muscarine.

3.2.3. Reversal Potential Of Muscarine-Induced I_M Suppression.

The reversal potential of the muscarine-induced effect is not readily observed in Figure 31B because E_K (-73mV) occurs at a potential where M-channels are completely deactivated (see Table 1). The E_K was therefore adjusted to depolarized potentials (-43 or -12mV) by increasing the $[K^+]_o$ to 20mM or 60mM. In Figure 33A, the muscarine-induced inward current reverses at about -45mV. Note that a small outward current appears between the E_R and about -60mV. This results from outward current flowing through M-channels prior to their complete deactivation at -60mV (ie. driving force for K^+ is in the outward direction at these potentials).

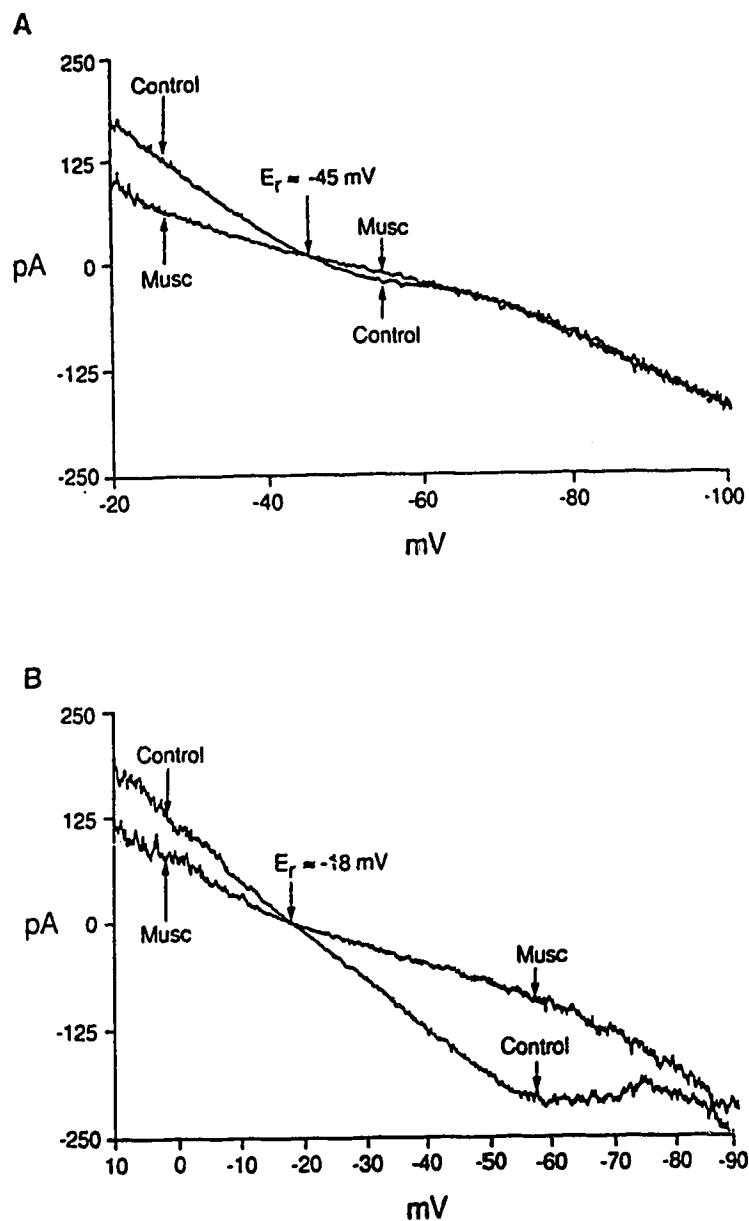


Figure 33. Reversal potential of muscarine-induced I_M suppression. I/V plots are x-y plots of computer-stored data of current responses to voltage ramp commands in the presence and absence of $10\mu\text{M}$ muscarine (Musc). **A.** I/V plots obtained from a B-cell in $20\text{mM } [\text{K}^+]_o$; 5s voltage ramps from $V_H = -30$ to -110mV . **B.** I/V plots acquired from another B-cell in $60\text{mM } [\text{K}^+]_o$; 5s voltage ramps from $V_H = +10$ to -90mV . Note the muscarine-induced outward current which occurs at potentials negative to E_r but positive to -60mV where I_M is deactivated.

Figure 33B shows the E_r is shifted to about -18mV in $60\text{mM } [\text{K}^+]_o$. In this experiment, the 5s voltage ramp ranged from $+10$ to -90mV .

In experiments where $60\text{mM } [\text{K}^+]_o$ was used, it was necessary to hold B-cells @ $+10\text{mV}$ so as to observe agonist-induced current reversal. The small negative deviations of the observed E_r from calculated E_K may be explained by the activation of other voltage-dependent conductances (see Adams, 1981; Adams et al, 1982a; Jones, 1987b). A plot of the average muscarine-induced reversal potential vs the E_K in B-cells is shown in Figure 22 (open circles, \circ). The mean E_r in $20\text{mM } [\text{K}^+]_o$ was $-42.5 \pm 1.5\text{mV}$ ($n=3$) and $-17.6 \pm 1.1\text{mV}$ ($n=6$) in $60\text{mM } [\text{K}^+]_o$ and the slope of 58mV per $\log [\text{K}^+]_o$ confirms that muscarine initiates a decrease in K^+ conductance in sympathetic ganglion B-cells.

3.2.4. Is I_M Activated At Resting Membrane Potential?

Since muscarine normally depolarizes intact BFSG (see Figure 18 A & B) and always depolarized B-cells that were studied by means of conventional microelectrode techniques (Smith and Zidichouski, unpublished observations), it was necessary to show that muscarine causes an inward current by suppression of I_M whilst holding a B-cell at the normal RMP. The mean RMP measured in $6\text{mM } [\text{K}^+]_o$ was $-48.94 \pm 0.97\text{mV}$ ($n=34$). Figure 34 shows that $10\mu\text{M}$ muscarine causes I_M suppression at holding potentials positive to -60mV (also in $6\text{mM } [\text{K}^+]_o$). It was also

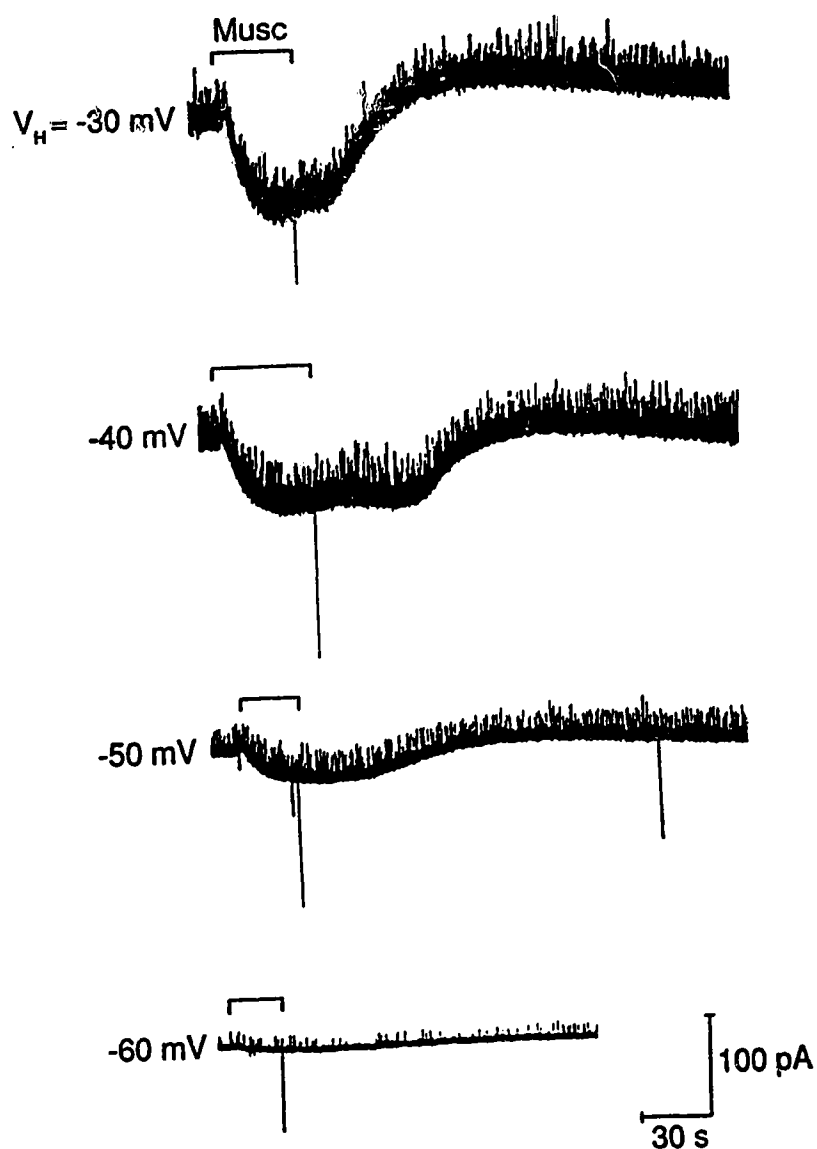


Figure 34. Effects of holding potential on muscarine-induced I_M suppression in a B-cell. A series of muscarine-induced ($10\mu M$) steady-state inward currents whilst holding the same B-cell at -30, -40, -50, and -60 mV. Note that a transient over-recovery occurs during the traces where inward current is clearly generated by the addition of muscarine ($V_H = -30, -40, \text{ and } -50 \text{ mV}$) and is not evident when $V_H = -60 \text{ mV}$. Traces from rectilinear pen recorder.

noted that I_M was depressed to the same endpoint (current level) due to the application of muscarine, irrespective of the holding potential (leak current in this particular cell was negligible). This observation would be consistent with the notion that, subsequent to muscarine receptor stimulation, the same proportion of M-channels are suppressed.

3.2.5. Examination Of Second Messenger Systems That May Be Associated with M-current Suppression.

- a) Confirmation of G-protein involvement in the suppression of I_M by muscarine.

Effects of GTP- γ -S dialysis on B-cells. The involvement of a G-protein would be verified if the addition of GTP- γ -S irreversibly reduced I_M in B-cells. Figure 35 shows that this effect occurs when 50 μ M GTP- γ -S is included in the patch pipette. Prior to the application of 10 μ M muscarine, there was no progressive change in either the steady-state current measured at -30mV or current responses to a series of voltage step commands to -110, -90, -70, -50 and -10mV. The first application of muscarine causes an inward current. The apparent recovery is likely augmented by the over-recovery phenomenon since steady-state current subsequently diminishes during the wash (time course compares with Figure 34). The second application of muscarine further reduces steady-state current and little recovery occurs even after

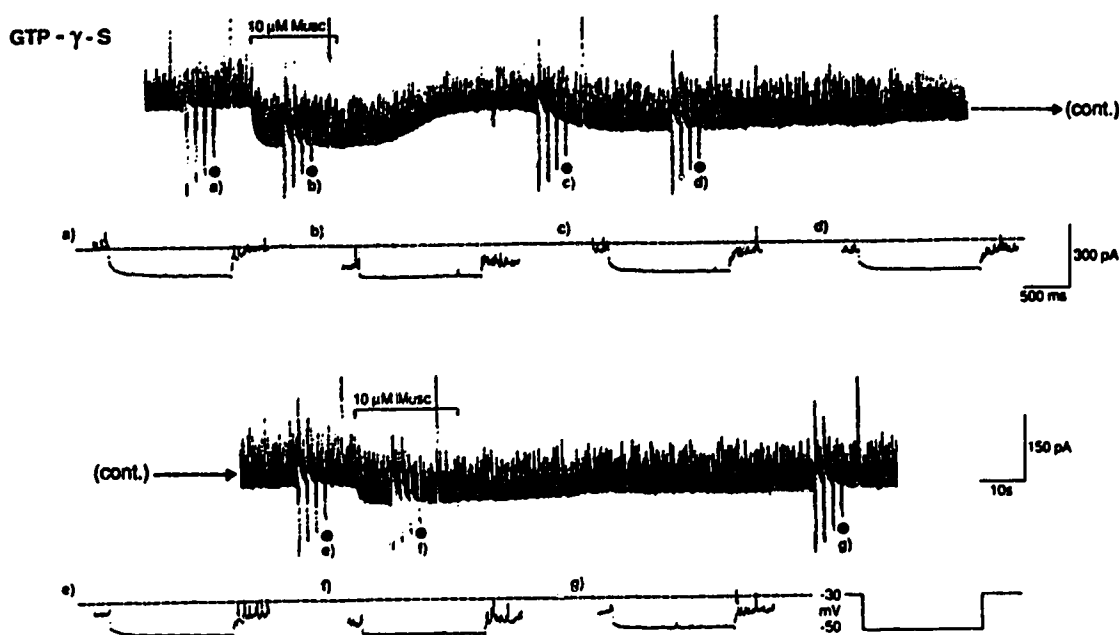


Figure 35. Effect of intracellular application of GTP- γ -S on muscarine-induced I_M suppression on a B-cell. Upper record. Continuous slow-speed chart record of steady-state current; $V_H = -30\text{mV}$ and $[K^+]_o = 6\text{mM}$. Brief downward and upward current deflections are in response to a series of 1.5s voltage step commands from V_H to -110 , -90 , -70 , -50 , and $+10\text{mV}$. The first application of $10\mu\text{M}$ muscarine (Musc) evokes an inward current which starts to abate following the removal of agonist, but never returns to the control level. Prior to the second application of muscarine, a spontaneous inward current develops and a new steady-state current is attained. The second application of muscarine promotes an irreversible inward current. Lower traces (a) to g) are fast current records of single voltage steps from -30 to -70mV . These traces show that the drug effect is on I_M . Also I_M never recovers to the control level (indicated by broken line). Upper traces from rectilinear pen recorder and lower traces are x-y plots of computer stored data.

100s of wash. The lower traces show that the effect of both muscarine and GTP- γ -S are restricted to the M-current. Traces a) to g) compare fast current records of single steps from -30 to -70mV (taken from upper traces indicated by ●). The dashed line represents the steady-state current at -30mV prior to the initial application of muscarine. Note that the second application of muscarine completely inhibits the residual I_M not yet affected by GTP- γ -S. Under control conditions, when B-cells were dialyzed with 'normal internal solution', I_M usually returned to control or a potentiated value 90s after the removal of muscarine (see [Figure 31](#) for example).

Pertussis toxin sensitivity of the G-protein involved in I_M suppression. The effect of overnight incubation with 5 μ g/ml PTX (@ 4°C) was tested on methacholine-(MCh) induced depolarization. [Figure 26B](#) shows the lack of effect of PTX in 5 control-matched experiments when MCh-depolarizations are normalized to orthodromically-activated B-fiber action potentials (0.075 ± 0.015 , n=5) and compared to normalized control responses (0.087 ± 0.016 , n=5). There were also no deleterious effects on PTX-treated preparations, since both B- and C-fiber action potentials (6.8 ± 0.48 mV, n=5; 2.2 ± 0.12 mV, n=5) were not significantly different from control B- and C-fiber action potentials (7.04 ± 0.56 mV, n=5; 2.98 ± 0.78 mV, n=5).

- b) Evaluation of the involvement of a phosphatidylinositide-mediated transduction mechanism in the suppression of I_M .

The involvement of the phosphatidylinositide pathway was investigated by examining whether I_M suppression was mimicked by the addition of IP_3 , phorbol esters, or increasing $[Ca^{2+}]_i$ in Rana pipiens B-cells.

The effects of phorbol ester on I_M . Figure 36 illustrates the effect of external application of $2\mu M$ PMA on a B-cell. In panel A, application of $10\mu M$ muscarine produces a reversible inward current due to inhibition of I_M (see corresponding I/V plot). The subsequent application of PMA onto the same cell causes a slowly developing inward current to appear that did not abate upon prolonged washing. The effect of PMA appears to be selective for I_M , since whole-cell conductance is only reduced over the -30 to -70mV range. Although a relatively high concentration of PMA was used, I_M was only suppressed an average of $33.5 \pm 5.5\%$. These results confirm recent reports of the phorbol ester effect on I_M by Pfaffinger et al (1988) and Bosma and Hille (1989).

Effects of protein kinase inhibitors on muscarine-induced I_M inhibition. If activation of PKC underlies I_M suppression, then protein kinase inhibitors (PKIs) should antagonize the muscarine-induced I_M suppression. Figure 37A shows that this

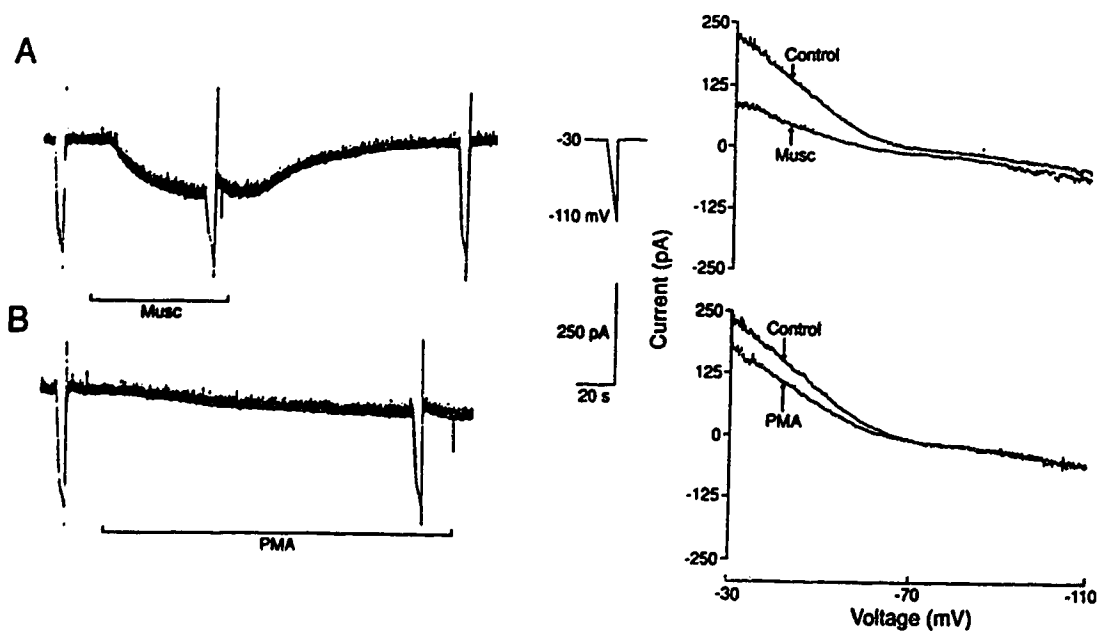


Figure 36. Effects of muscarine and phorbol-12-myristate-13acetate (PMA) on a B-cell. Left-hand records are steady-state current responses to the addition of $10\mu\text{M}$ muscarine (A) and $2\mu\text{M}$ PMA (B) on the same B-cell; $[\text{K}^+]_o = 6\text{mM}$. Downward deflections in left hand records are current responses to 5s voltage ramps from $V_H = -30$ to -110mV . Right. I/V plots of voltage ramp responses in the presence and absence of muscarine (top right) and PMA (bottom right). Note that both agents reduce whole-cell conductance in the I_M range. Left-hand traces from rectilinear chart recorder and right traces are x-y plots of computer-stored data.

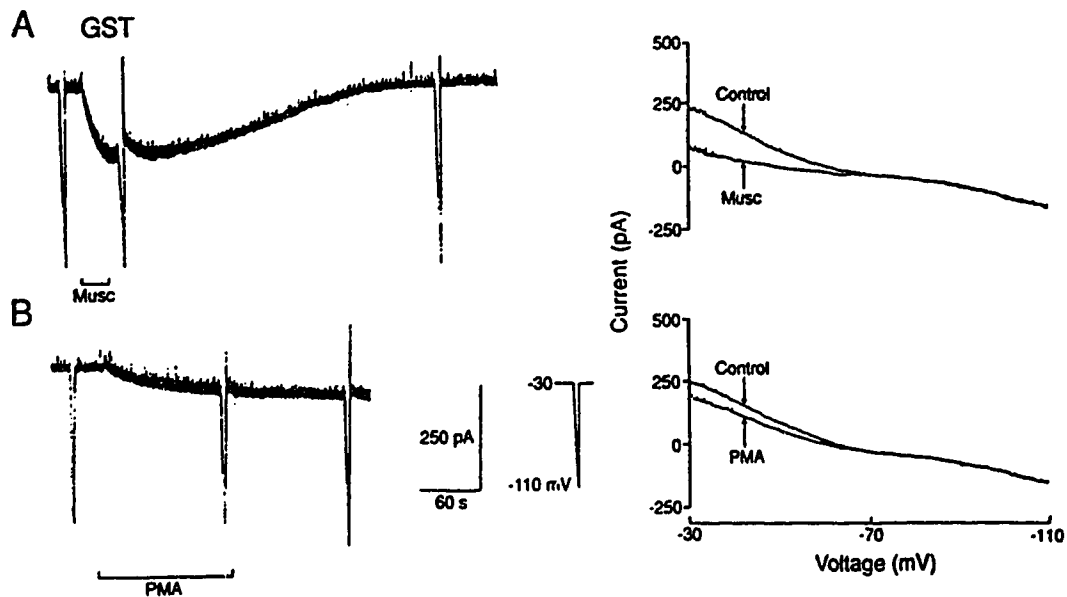
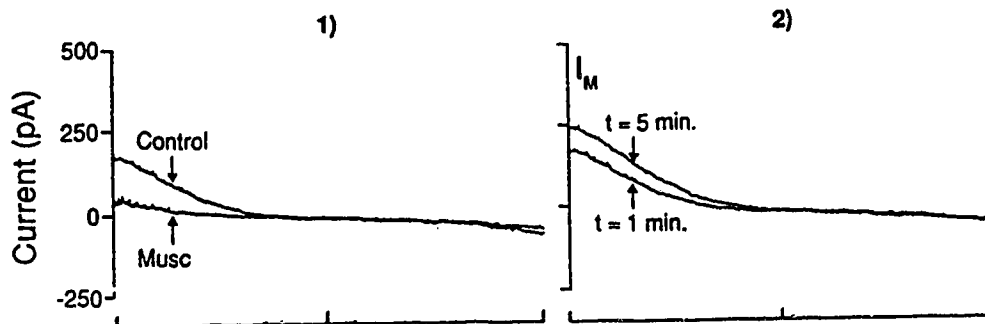


Figure 37. Lack of effect of intracellularly applied gold sodium thiomalate (GST) on B-cell response to application of muscarine and PMA. $[K^+]_o = 6\text{mM}$; $V_H = -30\text{mV}$. Left-hand records are steady-state responses. I/V plots, obtained from hyperpolarizing ramp commands, are shown on right. A. Effect of 10 μ M muscarine. B. Effect of 2 μ M PMA. Note that both drugs produce inward current associated with I_M suppression in the presence of 50 μ M GST. Left-hand records from rectilinear pen recorder; right-hand records from x-y plots of computer-stored data.

should antagonize the muscarine-induced I_M suppression. Figure 37A shows that this was not the case since muscarine effectively reduces I_M when GST ($50\mu\text{M}$) was included in the patch pipette. The average muscarine-induced depression of I_M in the presence of $50\mu\text{M}$ GST or $50\mu\text{M}$ H-7 was $42.7\pm6.2\%$ ($n=7$) and $51.2\pm6.7\%$ ($n=10$) respectively and this was statistically indistinguishable from those values observed in control cells ($54.9\pm7.2\%$, $n=11$, $p > 0.8$ for H-7; $p > 0.95$ for GST). Figure 40 shows the available I_M (per cm^2 ; measured @ -30mV) was not altered by GST ($1127\pm271 \mu\text{S}/\text{cm}^2$, $n=10$) or H-7 ($1237\pm224 \mu\text{S}/\text{cm}^2$, $n=4$) when compared to that observed in control cells ($1034\pm125 \mu\text{S}/\text{cm}^2$, $n=13$).

Protein kinase inhibitors did not attenuate the PMA-induced I_M suppression in B-cells (similar to C-cells, see above; cf Bosma and Hille, 1989). Figure 37B shows that application of $2\mu\text{M}$ PMA still reduced B-cell I_M when $50\mu\text{M}$ GST was included in the pipette. The lack of effect can be appreciated by comparing Figures 37B and 36B where a similar PMA-induced effect is observed in the presence or the absence of GST. Inclusion of $50\mu\text{M}$ H-7 also failed to antagonize the PMA effect (data not shown). PMA reduced I_M in B-cells dialyzed with GST or H-7, by $43.8\pm7.5\%$ ($n=4$). This was statistically indistinguishable PMA-induced I_M suppression in control B-cells ($33.5\pm5.5\%$, $n=3$). Therefore, the lack of effect of GST or H-7 on muscarine-induced I_M suppression as well as their inability to attenuate the PMA-induced effect suggests that activation of PKC is not directly involved in the closure of M-channels.

A Normal Internal Solution



B InsP₃

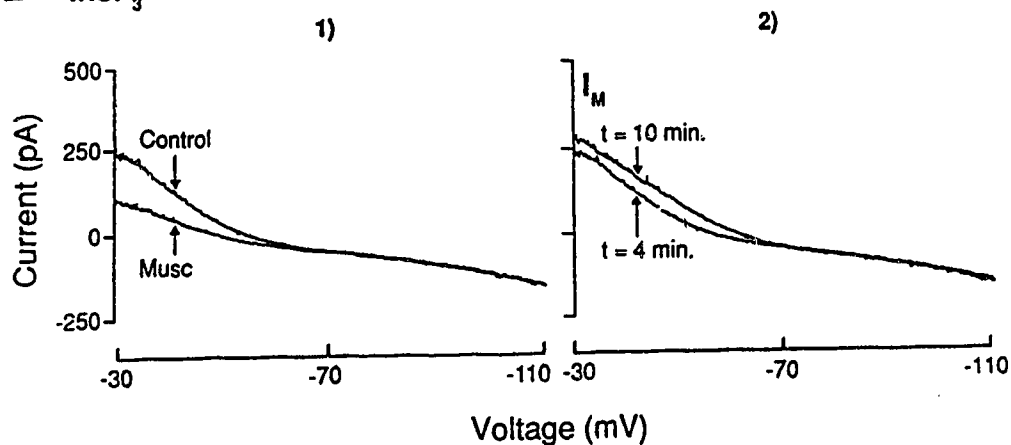


Figure 38. Comparison of the effects of IP₃ and muscarine on B-cells. Data presented as I/V plots obtained from 5s ramp commands from $V_H = -30$ to -110 mV; $[K^+]_o = 6$ mM. **A.** Control B-cell; patch pipette contains 'normal internal solution'. 1) Suppression of I_M by 10μ M muscarine. 2) Comparison of I/V plots 1 and 5 min after establishing whole-cell recording to illustrate progressive development of I_M . **B.** Another B-cell; pipette contains 0.5 mM IP₃ (InsP₃). 1) Suppression of I_M by 10μ M muscarine. 2) Comparison of I/V plots to show progressive development of I_M during whole-cell recording despite the presence of 0.5 mM IP₃. Records obtained from x-y plots of computer-stored data.

Effects of inositol 1,4,5-trisphosphate on B-cell I_M . If muscarine-induced I_M suppression is mediated by an increase of intracellular $[IP_3]$, then inclusion of IP_3 in the patch pipette should mimic the effect of muscarine. Figure 38 compares the whole-cell currents observed in a control B-cell (A) with currents obtained in a second B-cell that was studied using a patch pipette containing 0.5mM IP_3 (B). Note that amplitude of I_M and the sensitivity to muscarine in the IP_3 -treated cell are comparable to the control B-cell. Furthermore, a progressive increase in I_M was observed under both conditions (see A 2) and B 2)) subsequent to the establishment of WCR. This suggests that even high concentrations of IP_3 did not affect the normal early development of this current. Figure 40 shows the mean I_M (per unit area; @-30mV) measured in IP_3 -dialyzed cells ($1382 \pm 114 \mu S/cm^2$, $n=4$) was significantly different from that observed in control cells ($1034 \pm 125 \mu S/cm^2$, $n=13$).

The effects of elevation of $[Ca^{2+}]_i$ on I_M in B-cells. In a parallel series of experiments, the effect of the elevation of $[Ca^{2+}]_i$ on I_M was directly tested since it was possible that dialysis with 'internal solution' could deplete or affect Ca^{2+} storage sites and therefore might account for the lack of IP_3 -induced effect. However, Figure 39 shows a muscarine-induced inhibition of I_M is still observed when $pCa^{2+}=6$. Figure 40 shows that I_M was unaffected by this increase in $[Ca^{2+}]_i$ since the available I_M measured at -30mV ($1287 \pm 161 \mu S/cm^2$, $n=4$) was similar to that measured in control cells ($p > 0.4$) where $pCa^{2+}=7$ ($1034 \pm 125 \mu S/cm^2$, $n=13$).

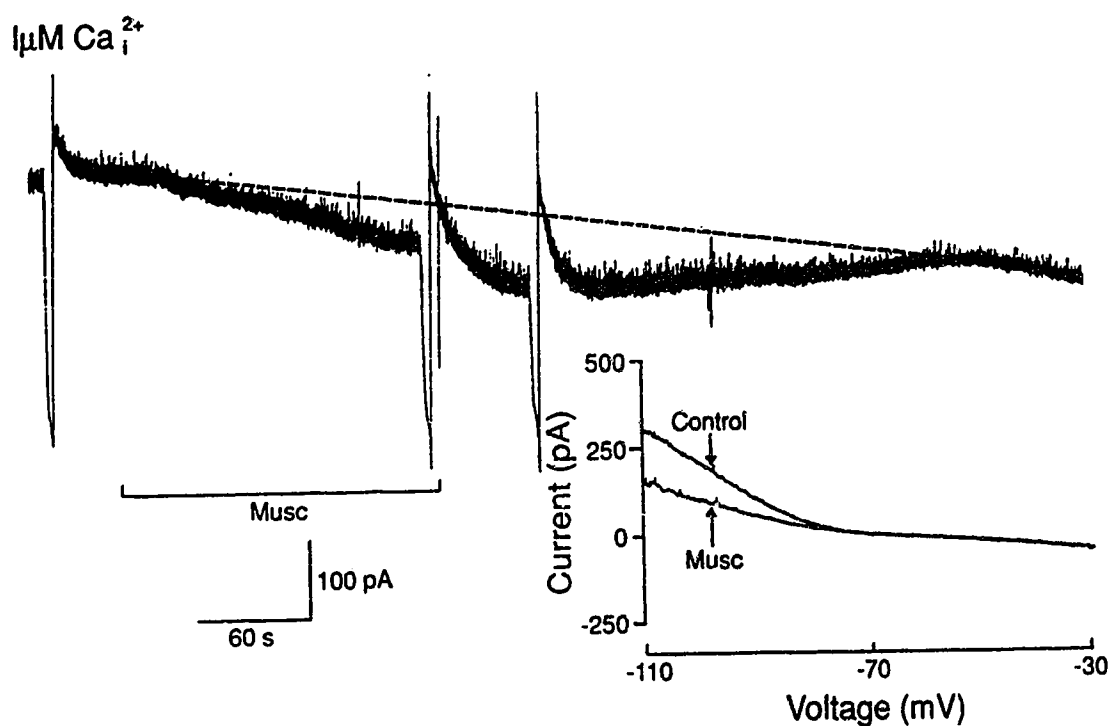


Figure 39. Effect of high $[\text{Ca}^{2+}]_i$ on muscarine-induced suppression of I_M on a B-cell. Upper record. Slow chart record of steady-state inward current produced by the application of $10\mu\text{M}$ muscarine on a B-cell. Recording obtained with a patch pipette containing 'internal solution' with $p\text{Ca}^{2+}=6$; $[\text{K}^+]_o=6\text{mM}$. Lower record is I/V plot of currents obtained during 5s voltage ramps from -30 (V_H) to -110mV (first two downward deflections in upper record). Note that muscarine produced a strong suppression of I_M under these recording conditions. Upper records from rectilinear pen recorder; lower traces from x-y plot of computer-stored data.

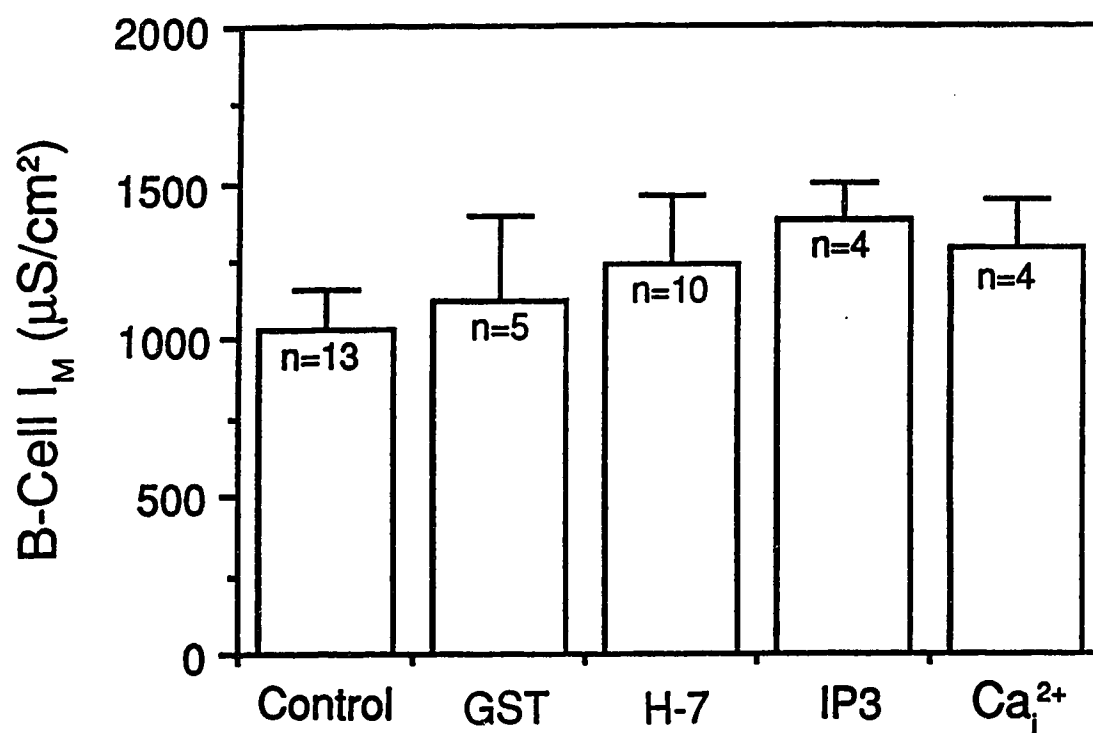


Figure 40. Effects of intracellular application of GST, H-7, IP₃ and high [Ca²⁺]_i on available M-current in B-cells. Histogram compares the mean I_M normalized to cell size. 'n' indicates the number of cells in each category. Mean values $\mu S/cm^2 \pm s.e.m.$; Control=1034 \pm 125, 50 μ M GST=1127 \pm 271, 50 μ M H-7=1237 \pm 224, 0.5mM IP₃=1382 \pm 114, and pCa²⁺=6 Ca²⁺=1287 \pm 161.

- c) Effect of phosphatase inhibition on muscarine-induced I_M suppression.

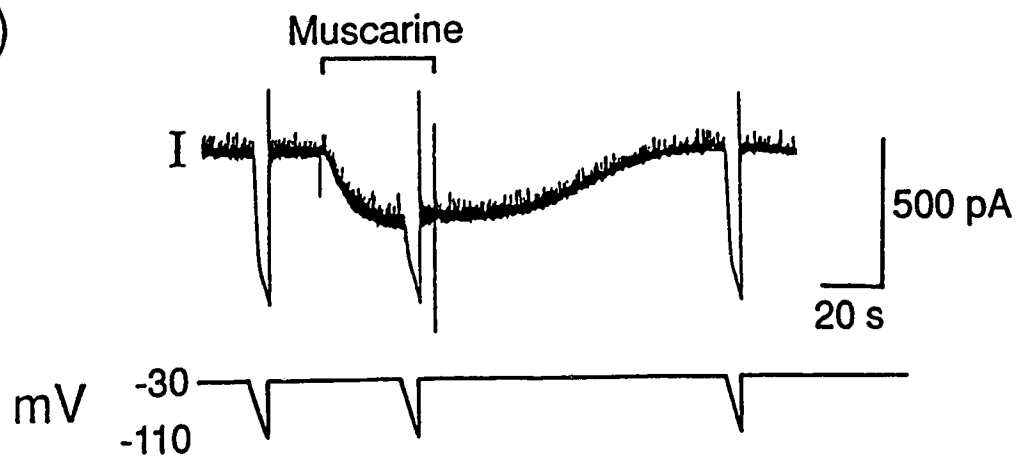
Pfaffinger (1988) suggested that the suppression of I_M by agonists could involve a dephosphorylation mechanism. He suggested that M-channels were maintained in an open state by phosphorylation and channel closure occurred upon the hydrolysis of a phosphate group from the cytoplasmic portion of the channel protein. This process would presumably involve the activation of a phosphatase.

This hypothesis was tested examining the effects of an intracellularly-applied phosphatase inhibitor, 2,3-diphospho-D-glyceric acid (DPG; 1mM), on muscarine-induced I_M suppression. If muscarinic agonists promoted activation of a phosphatase such that a phosphate group was removed from the M-channel, then the inclusion of DPG should render the M-channels insensitive to external application of muscarine. Figure 41 shows however that this was not the case, 10 μ M muscarine strongly suppresses I_M and the response is similar to that recorded in control cells (for comparison, see Figures 31, 32, 34, 36A, 37A, 38). This argues against closure of M-channels directly regulated by dephosphorylation. Furthermore, the *duration* of the muscarine-induced response is not increased by the presence of DPG. These are significant observations because they are consistent with the notion that muscarine-induced I_M suppression and the subsequent re-activation are totally independent of phosphorylation mechanisms (see Discussion).

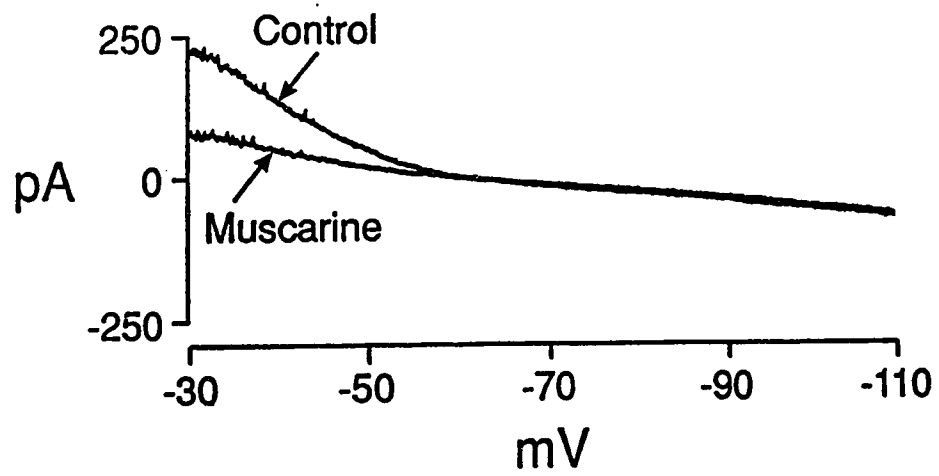
Figure 41. Effect of intracellular application of a phosphatase inhibitor on muscarine-induced I_M suppression in a B-cell. **A)** Upper trace. Slow chart record of steady-state current responses to application of $10\mu\text{M}$ muscarine with diphosphoglyceric acid (DPG; 1mM) included in the patch pipette; $[\text{K}^+]_o = 6\text{mM}$. **A)** lower trace. Command voltage trace where $V_H = -30\text{mV}$ is interrupted by 5s ramp commands to -110mV before, during, and after application of muscarine. **B)** Fast records of ramp commands before and during application of muscarine. Note that neither the ability of muscarine to suppress I_M , nor the time course of recovery from drug application are affected by dialysis with DPG. Traces in **A** from rectilinear pen recorder and **B** is an x-y plot of computer stored data.

ImM DPG

A)



B)



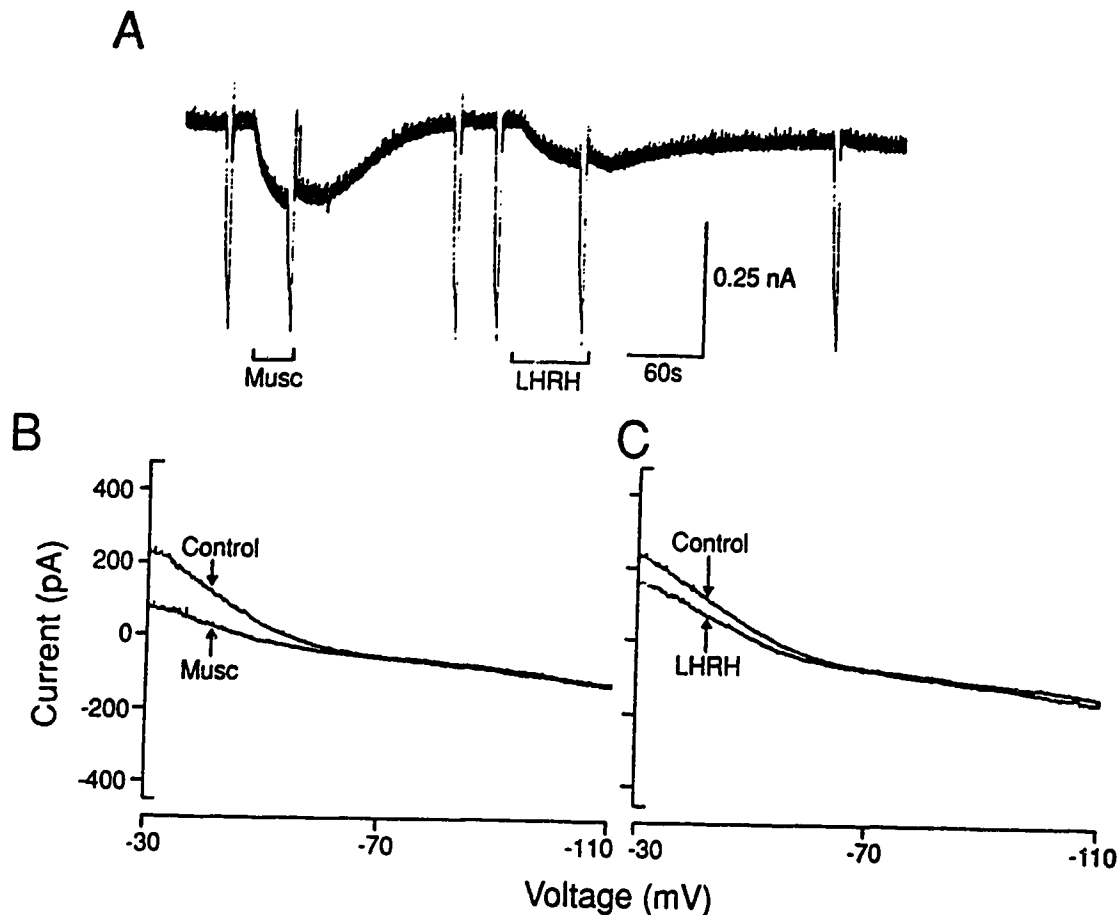


Figure 42. Effects of muscarine and LHRH on a B-cell. **A.** Continuous chart record of steady-state current responses due to application of $10\mu\text{M}$ muscarine and $100\mu\text{M}$ c-II-LHRH on the same B-cell; $V_H = -30\text{mV}$ and $[\text{K}^+]_o = 6\text{mM}$. Downward deflections are current responses to 5s voltage ramp commands from V_H to -110mV (voltage trace omitted for clarity). Lower traces. I/V plots of current responses to voltage ramp commands (in A) in the absence and the presence of muscarine (B) and LHRH (C). Note that the decrease in whole-cell conductance induced by both agents is restricted to I_M voltage activation range. Traces in A from rectilinear pen recorder; B & C are x-y plots of computer stored data.

d) Effects of LHRH on B-cell I_M .

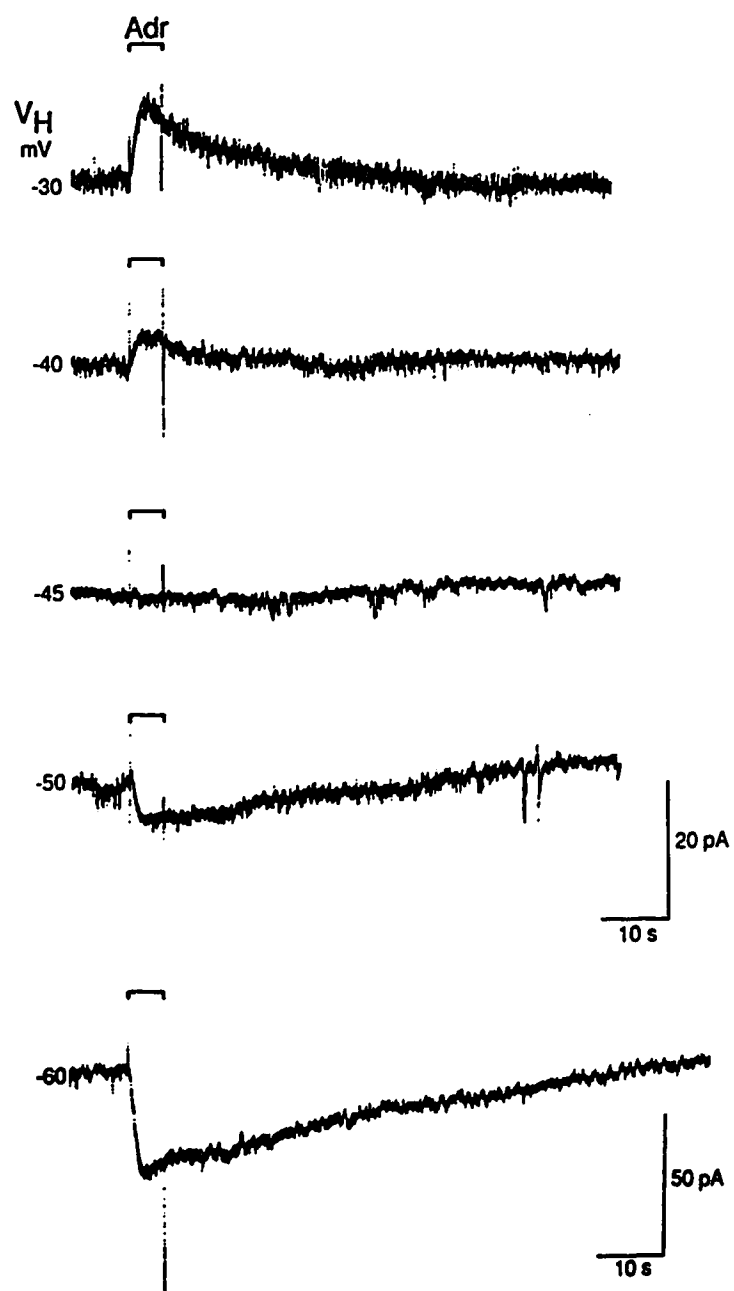
The effects of muscarine ($10\mu\text{M}$) and LHRH ($100\mu\text{M}$) on a B-cell are shown in Figure 42. In panel A, the slow speed chart record illustrates a typical muscarine-induced I_M suppression (69%). I_M suppression by the addition of c-II-LHRH induces a less dramatic effect (36% suppression) and the recovery is slower and incomplete when compared to muscarine. However, both muscarine and c-II-LHRH affect the whole-cell conductance over an identical voltage range (panels B & C), confirming that I_M is affected by both agonists. In this experiment the sum of I_M inhibition exceeded 100%. Therefore, some M-channels were sensitive to both agonists and provides support for the convergence of transduction mechanisms subsequent to the muscarine and LHRH receptors.

3.3. EFFECTS OF ADRENOCEPTOR AGONISTS ON C-CELLS.

3.3.1. Description Of Adrenaline-Induced Inwardly-Rectifying Current Occurring In C-Cells.

Figure 43 shows the steady-state currents elicited by application of $100\mu\text{M}$ adrenaline on a C-cell held at potentials between -30 and -60mV in 20mM $[\text{K}^+]_o$. The current reverses at about -45mV which corresponds to the calculated E_K (-43mV) and inwardly rectifies at potentials negative to E_K . The absolute latency

Figure 43. Steady-state current responses to adrenaline in a C-cell whilst holding at different command potentials (-30, -40, -45, -50, and -60mV; $[K^+]_o=6mM$). The adrenaline- (100 μ M Adr) induced current is negligible at -45mV and reverses in polarity at more negative potentials. This corresponds well to the calculated E_K of -43mV. Note the pronounced inward-rectification of adrenaline-induced current (note 2.5 fold decrease in current gain) at $V_H=-60mV$. 20pA calibration refers to currents obtained when $V_H= -30, -40, -45$ and -50mV. 50 pA calibration refers to bottom current record ($V_H=-60mV$). All traces obtained on a rectilinear pen recorder.



for the adrenaline-induced outward current measured at -30mV (assuming that the time equals zero when the U-tube is switched on) were $0.30 \pm 0.03\text{s}$ ($n=13$) for the appearance of the current, $2.46 \pm 0.24\text{s}$ ($n=14$) to reach peak outward current, and $23.83 \pm 5.95\text{s}$ for the current to return to the control level. These currents are strikingly similar to the muscarine-induced outward currents observed in C-cells (see Figure 20). In fact the same C-cell provided the data shown in Figures 20 & 43.

The downward deflections in the chart record shown in Figure 44A are current responses to a 5s voltage ramp from -30 to -110mV before, during, and after application of $100\mu\text{M}$ adrenaline (in $6\text{mM } [\text{K}^+]_o$). Adrenaline induces a small outward current at -30mV , the ramp of voltage is initiated when the largest outward current is observed so as to examine the agonist-induced changes over a wide voltage range when the conductance is maximally activated. The current quickly returns to control level after adrenaline application was stopped. The adrenaline-induced effects are better illustrated by Figure 44B where the fast records of current responses to voltage ramps before and during the application of adrenaline (the recovery was complete and was omitted for clarity). A small outward current of surprisingly constant amplitude is observed at all voltages positive to E_r whereas at potentials negative to E_r , the conductance increases with hyperpolarization (inward rectification).

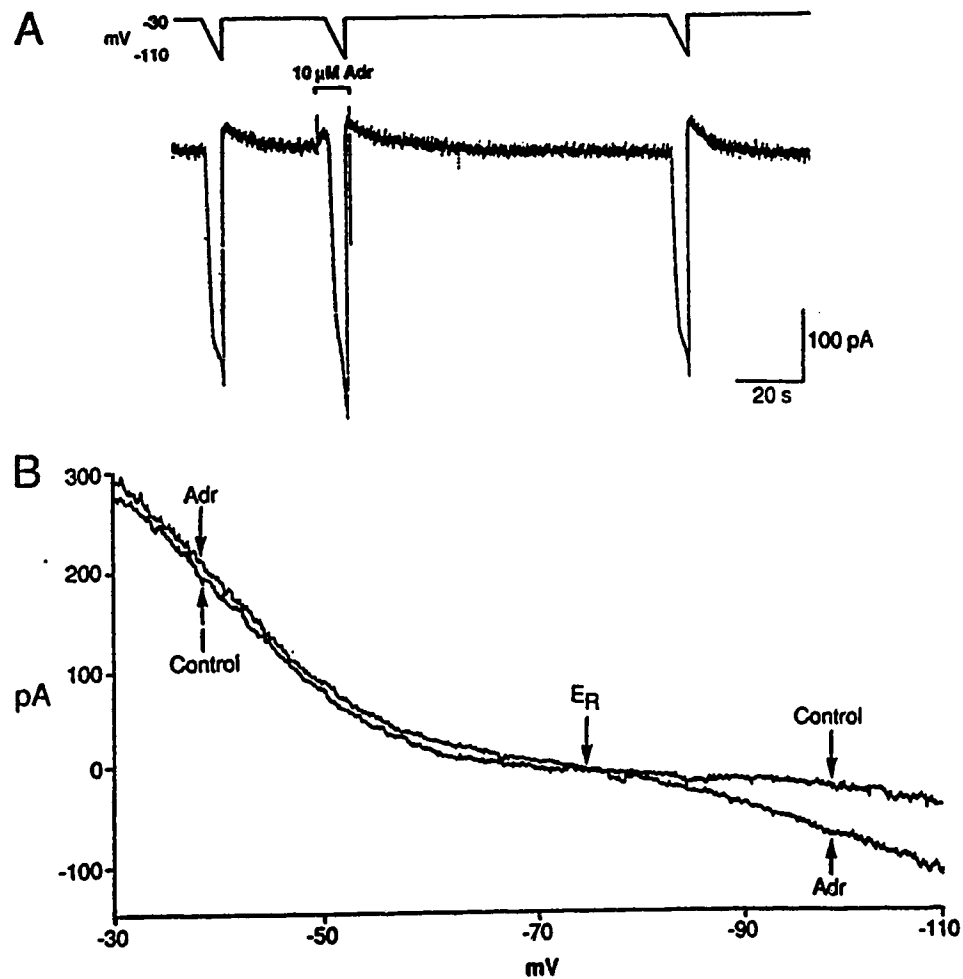


Figure 44. Effect of adrenaline on a C-cell. **A.** Steady-state response observed at $V_H = -30$ mV in 6 mM K^+ . Voltage ramp commands from V_H to -110 mV are applied before, during, and after application of adrenaline (100 μ M Adr). **B.** I/V plots of current response to the first two 5 s ramp commands shown in A. Note the adrenaline-induced current reverses at about -74 mV, small outward current produced at potentials positive to E_R and large inward current (rectification) at hyperpolarized commands. Data in A from rectilinear pen recorder and in B x-y plot of stored data.

3.3.2. Reversal Potential For The Adrenaline-Induced Inwardly-Rectifying Current In C-Cells.

In Figures 43 and 44B, the reversal of the adrenaline-induced conductance occurs near E_K , suggesting that adrenaline, like muscarine, increases K^+ conductance. In Figure 22, the average E_r of the adrenaline-induced currents observed from C-cells are plotted against $[K^+]_o$ (represented by open squares, \square). The mean E_r values in 6mM and 20mM $[K^+]_o$ were $-48.74 \pm 3.27\text{mV}$ ($n=5$) and $-75.77 \pm 1.41\text{mV}$ ($n=5$) respectively. There is not any noticeable deviation from the slope of 58mV for each 10 fold shift in $[K^+]_o$. This confirms that the adrenaline-induced current results from the opening of a population of K^+ -selective channels.

3.3.3. Does Adrenaline Occlude The Muscarine Effect In C-Cells?

If adrenaline and muscarine induce an inwardly-rectifying K^+ conductance in C-cells through the same population of K^+ channels then, providing a significant number of the available receptors are activated, the effects of both agonists should not be additive (North, 1986).

Figure 45 shows steady-state currents induced by $10\mu\text{M}$ muscarine and $100\mu\text{M}$ adrenaline do not sum. Both of these responses are initiated by the activation of distinct receptor sites on the C-cells; adrenaline via α_2 -adrenoceptor



Figure 45. Occlusion of muscarine-induced outward current by adrenaline on a C-cell. Steady-state chart record showing successive application of agents to the same C-cell; $V_H = -30\text{mV}$ in 6mM $[\text{K}^+]_o$. Separate application of $10\mu\text{M}$ muscarine (Musc) and $100\mu\text{M}$ adrenaline (Adr) produce outward currents of comparable magnitude. However, no additive effect occurs when both agonists are applied simultaneously. Records from rectilinear pen recorder.

(Rafuse, 1985) and muscarine through a pirenzepine-sensitive receptor (see Results section 3.1.5.).

3.3.4. Is The Inhibition Of Adenylate Cyclase Involved In The Adrenaline-Induced Inhibition In C-Cells?

The α_2 -adrenoceptor is thought to be negatively coupled to adenylate cyclase via an inhibitory G-protein (Gilman, 1987). Aghajanian and Wang (1987) have suggested that a reduction in cAMP may be involved in the generation of the inhibitory response observed subsequent to the activation of locus ceruleus α_2 -receptors. This hypothesis was based on experiments where an α_2 -mediated inhibition was attenuated by the superfusion of membrane permeable cAMP analogues, such as 8-bromo-cAMP, that presumably elevated intracellular [cAMP] ([cAMP]_i).

a) Effects of increasing [cAMP]_i directly via WCR.

The whole-cell recording technique provided an uncomplicated means to address whether inhibition of adenylate cyclase was involved in the generation of the adrenaline-induced inwardly-rectifying K⁺ currents in C-cells. Using patch pipettes containing 100 μ M cAMP, adrenaline-induced responses could be tested and

compared to C-cells which 'normal internal solution' was used. The additional $[cAMP]_i$ should reduce the likelihood of observing an adrenaline-induced inwardly-rectifying K^+ current if inhibition of adenylate cyclase is directly involved in the generation of this particular response.

Table 2 summarizes data that examined whether the addition of $100\mu M$ cAMP via the patch pipette affected the frequency of observation of agonist-induced currents in B- and C-cells. In the absence of $100\mu M$ cAMP, adrenaline ($100\mu M$) induced an inwardly-rectifying K^+ current in only 3/14 small cells. The unresponsive cells were assumed to be C-cells on the basis of their input capacitance (C_m), lack of a muscarine-induced inward current and the absence of I_A . However, in the presence of cAMP, 17/23 small cells exhibited an adrenaline-induced, inwardly-rectifying K^+ current.

- b) The effects of the elevation of $[cAMP]_i$ in the intact isolated ganglion: An electrophysiological and biochemical analysis.

The involvement of cAMP was also evaluated using intact BFSG since there is a possibility that intracellular dialysis with artificial cytoplasmic solution (internal solution) may alter cellular biochemistry and therefore obscure WCR results. Furthermore, since multiple pathways for cellular processes are known to exist (Ross, 1989), cross-talk between second messenger systems could lead to false positive results.

These caveats were addressed by using an intact ganglion preparation and performing a series of manipulations which are thought to increase $[cAMP]_i$ by affecting different loci of the adenylate cyclase signal transduction pathway. These studies tested whether the adrenaline-induced hyperpolarization, which is mediated by an α_2 -receptor (Rafuse, 1985), was attenuated by drugs that elevate $[cAMP]_i$. Moreover, the order of potency of such drugs should correlate with their ability to increase cAMP as measured by radioimmunoassay (RIA).

Effect of adrenaline on forskolin-stimulated cAMP accumulation. If α_2 -adrenoceptor agonist inhibits adenylate cyclase, a concomitant reduction of $[cAMP]_i$ should be observed. The activity of membrane-bound adenylate cyclase was increased by the addition of forskolin (Seaman, 1985) because the inhibition of the relatively low basal $[cAMP]_i$ is difficult to quantitate (Dunman and Enna, 1986). Figure 46 shows that $50\mu M$ forskolin increased basal $[cAMP]_i$ from 3.44 ± 0.64 ($n=16$) to 34.00 ± 3.08 ($n=17$) pmol/mg protein wet weight, ($p < 0.001$) and a 30s exposure to $1\mu M$ adrenaline decreased cAMP accumulation in forskolin pre-treated ganglia by about 35% (21.96 ± 2.26 pmol/mg protein wet weight, $p < 0.005$). $1\mu M$ propranolol and $500nM$ DMI were included in the bathing solutions, since adrenaline also can promote cAMP accumulation via β -adrenoceptor stimulation (Brown et al, 1979) and can be readily removed by uptake mechanisms into the terminals (Rafuse and Smith, 1986).

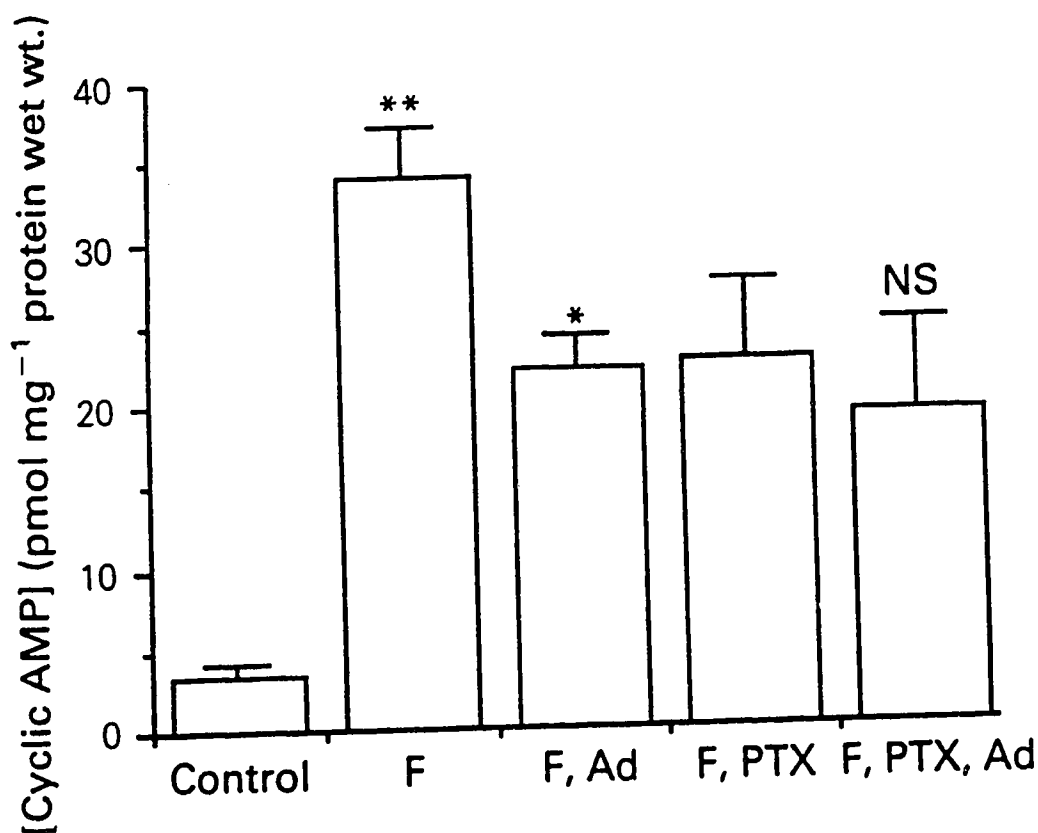


Figure 46. Effects of drugs on [cAMP]_i accumulation determined by RIA from individual BFGS. Histogram compares drug effects on the accumulation of [cAMP]_i in groups of individual ganglia (n=6 or more) subjected to the following conditions: 1) 50μM forskolin (F) for 15min, 2) 50μM F for 14min 30s then to 1μM adrenaline (Ad) in 50μM F for a further 30s. In experiments which tested the effects of pre-exposure to PTX, the groups of ganglia were subjected to the same manipulations as above, except tissues were pre-incubated with 5μg/ml PTX for 2h at 20°C prior to drug challenges (PTX was included in all drug solutions). Error bars indicate s.e. of mean. Ringer's solution contained both 500nM DMI and 1μM propranolol.

Effect of pertussis toxin on adrenaline-induced inhibition of cAMP accumulation. If the α_2 -adrenoceptor is coupled to adenylate cyclase via G_i , then pre-treatment with PTX should prevent the adrenaline-induced inhibition of cAMP accumulation. In Figure 46, it appears as if a 2 hour pre-treatment with $5\mu\text{g/ml}$ PTX did not prevent adrenaline from reducing the cAMP content. However, PTX pretreatment alone reduced cAMP content to a similar value.

Effects of phosphodiesterase inhibitors and simulators of adenylate cyclase on cAMP level measured by RIA and on the adrenaline-induced hyperpolarization. The lack of a G-protein PTX-sensitivity in the frog may have been due the absence of the cysteine 354 ADP-ribosylation site (Ross, 1989), since adrenaline reduced cAMP accumulation in forskolin treated tissue. Therefore, the ability of drugs to elevate cAMP, as measured by RIA, should correlate with their ability to attenuate the adrenaline-induced hyperpolarization in the isolated bullfrog sympathetic ganglion.

Table 5 shows the effects of isobutylmethylxanthine (2mM IBMX) and caffeine (5mM) that block phosphodiesterase hydrolysis of cAMP to 5'-AMP by phosphodiesterase, and the effects of the adenylate cyclase activators fluoride (2 & 5mM) and forskolin on cytosolic cAMP accumulation measured by RIA. The order of potency determined for these various agents to increase basal levels of cAMP was forskolin >> fluoride (5mM) > fluoride (2mM) > IBMX > caffeine. The order of potency for the effect of these same drugs to attenuate the adrenaline-

Table 5

The effects of various drugs to modify RIA measured [cAMP] and their ability to attenuate adrenaline-induced hyperpolarization measured physiologically.

Drug	[Cyclic AMP] (pmol mg ⁻¹ protein, wet wt)	Increase in cyclic AMP (% of control) ^{1,5}	P value for cyclic AMP increase	Attenuation ¹ of Ad _h (%)	Depolarization (mV)
IBMX (2 mM)	5.3 ± 1.3 (6)	155.2	> 0.2	63.5 ± 5.5 (6)	+0.96 ± 0.22 (6)
Fluoride (5 mM)	7.2 ± 0.8 (6)	208.7	< 0.005	46.2 ± 10.2 (4)	+0.20 ± 0.13 (2)
Fluoride (2 mM)	6.4 ± 1.3 (6)	185.5	< 0.05	7.2 ± 4.4 (6)	+0.27 ± 0.09 (3)
Caffeine (5 mM)	4.8 ± 0.8 (6)	139.0	> 0.2	38.2 ± 7.3 (5)	+0.91 ± 0.29 (5)
8-Br-cyclic AMP (1 mM)	—	—	—	21.8 ± 7.2 (8)	+0.93 ± 0.35 (3)
Pertussis ² toxin (5 µg ml ⁻¹)	—	—	—	2.2 ± 11.3 (4)	—
Forskolin ⁴ (1–100 µM)	34.0 ± 3.1 (17)	985.5	< 0.001	–6.6 ± 11.4 (5 ³)	+1.01 ± 0.09 (5)

¹ Ganglia exposed to all drugs (except pertussis toxin) for 15 min.

² Ganglia exposed to pertussis toxin for 2 h.

³ In the presence of forskolin, the Ad_h was potentiated to 106.6 ± 11.4% of control.

⁴ For cyclic AMP determinations, all ganglia were exposed to 50 µM forskolin.

⁵ Control [cyclic AMP] = 3.44 ± 0.65 pmol mg⁻¹ protein wet wt. s.e.mean, n = 16.

Number of observations (n) given in parentheses; values are ± s.e.mean.

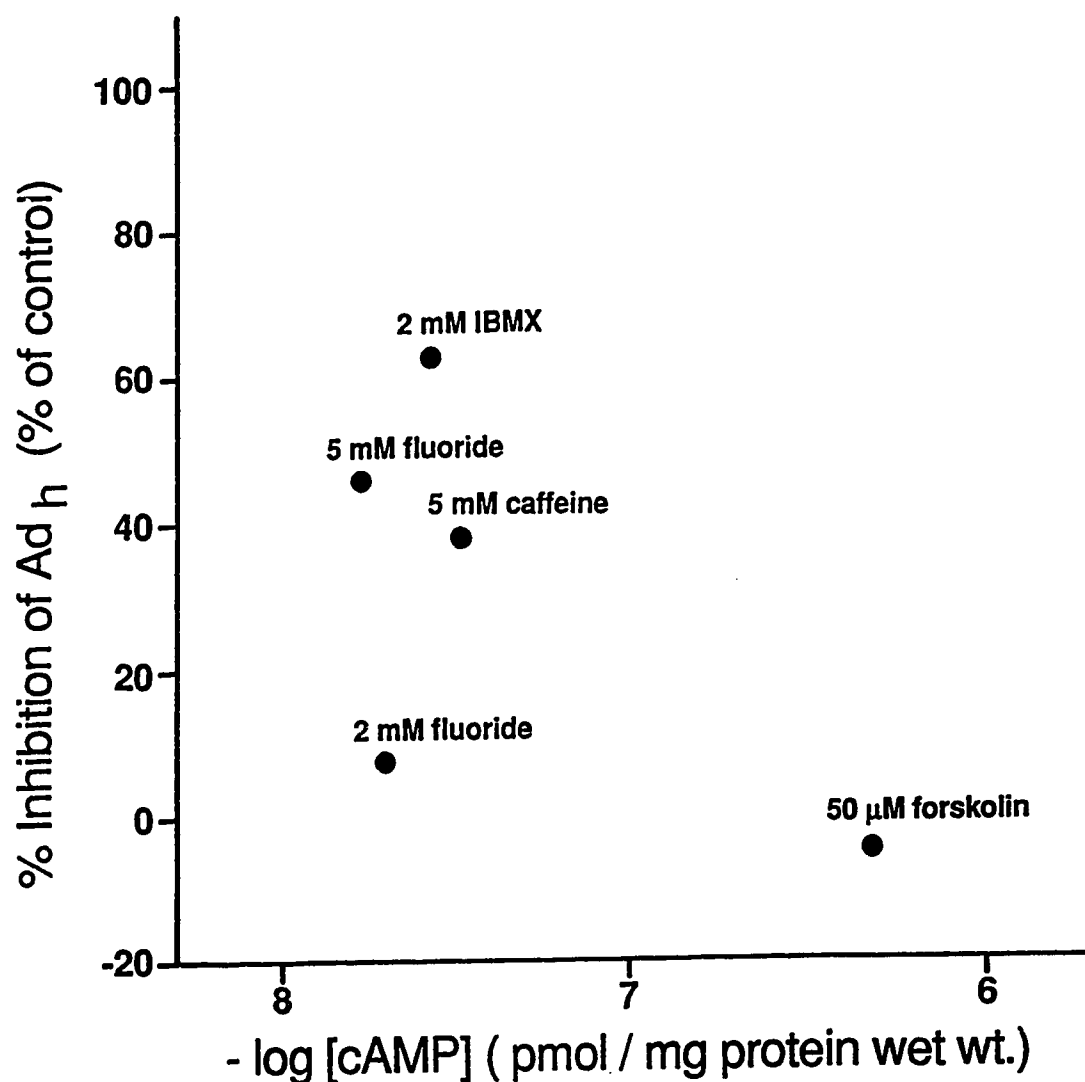


Figure 47. Comparison of the effects of drugs which elevate $[cAMP]_i$ with their effect on the adrenaline-induced hyperpolarization. Abscissa: mean cAMP content of groups of ganglia (minimum $n=6$) upon 15min exposure to 2mM IBMX, 2 and 5mM fluoride, 5mM caffeine, or 50 μ M forskolin (see Table 5 for actual data). Ordinate: mean percentage inhibition of adrenaline-induced hyperpolarization determined from sucrose-gap experiments (minimum $n=5$) to the same drugs (same concentrations and duration) used in RIA experiments (see Table 5 for actual data).

induced hyperpolarization was IBMX > fluoride (5mM) > caffeine >> fluoride (2mM) > forskolin.

Table 5 also shows that all of the drugs depolarized ganglia to some extent. If an increase in membrane conductance caused the depolarization, a reduction the amplitude of the adrenaline-induced hyperpolarization might be explained by an electrical shunt (Kuba and Nishi, 1976). This was not the case since the adrenaline-induced hyperpolarization was not attenuated by forskolin (n=5) although it induced the most dramatic depolarizing effect ($1.01 \pm 0.1 \text{mV}$, n=5) and conversely, 5mM fluoride (n=4) strongly attenuated the adrenaline-induced hyperpolarization whilst the depolarization was insignificant and was only observed in 2 of 4 fluoride experiments ($+0.20 \pm 0.13 \text{mV}$, n=2).

The lack of correlation between drugs that elevate cAMP and the attenuation of the adrenaline-induced hyperpolarization is illustrated in Figure 47.

Effects of extracellular application of 8-bromo-cAMP on the adrenaline-induced hyperpolarization. Application of membrane permeable cAMP analogues has been shown to reduce the α_2 -adrenoceptor mediated hyperpolarization in rat locus ceruleus neurons (Andrade and Aghajanian, 1985). A similar effect is shown in Figure 48A where superfusion of $1 \mu\text{M}$ 8-bromo-cAMP reversibly reduces the adrenaline-induced hyperpolarization in isolated BFSG preparation. The mean attenuation observed in 8 experiments was $21.8 \pm 7.2\%$ and depolarization was observed in only 3 experiments (see Table 5). To ensure that the observed

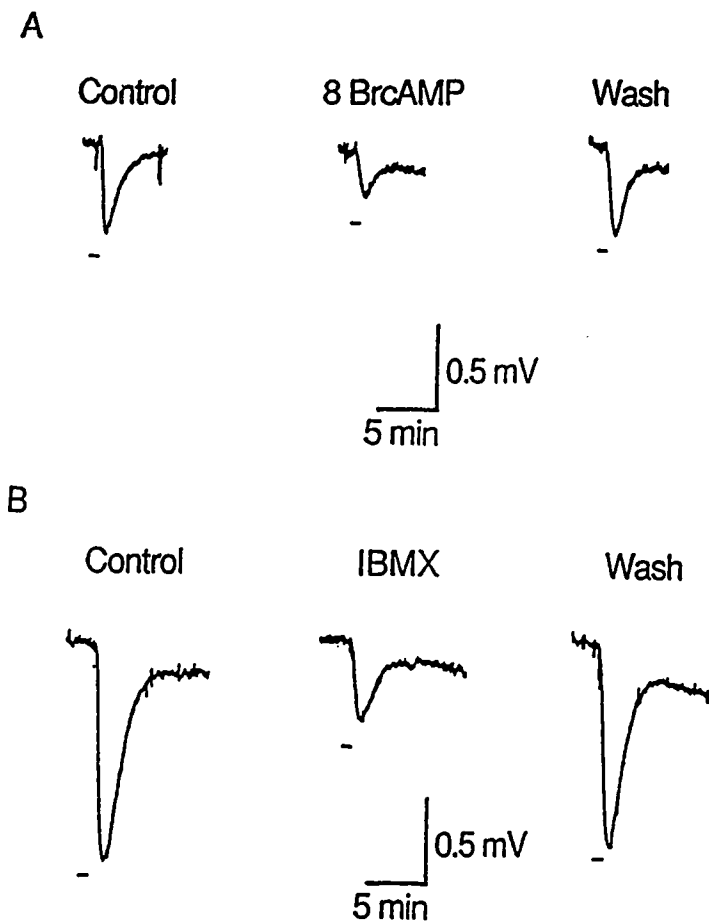


Figure 48. Effects of 8-bromo-cAMP and IBMX on adrenaline-induced hyperpolarization recorded from isolated BFSG by means of the sucrose-gap technique. All traces shown are hyperpolarizations in response to 30s superfusion with 1 μ M adrenaline (indicated by $_$). A. Left record: control, middle record: response after 15 min exposure to 1 μ M 8-Bromo-cAMP (8 BrcAMP), and right trace: recovery response obtained after 40 minutes of wash. B. Left record: control response, middle record: response after 15min superfusion with 2mM IBMX, and right trace: recovery obtained upon 30min of wash. All traces from rectilinear pen recorder.

antagonism was not due to stimulation of adenosine receptors, the effect of the adenosine receptor agonist, 2-chloro-adenosine ($10\mu\text{M}$ - 1mM) was examined on the adrenaline-induced hyperpolarization. This substance failed to attenuate the adrenaline-induced hyperpolarization (data not shown).

The effect of pertussis toxin on the adrenaline-induced hyperpolarization in isolated bullfrog sympathetic ganglia. α_2 -adrenoceptor mediated inhibition in the CNS have been previously reported to be PTX-sensitive (Aghajanian and Wang, 1986; Aghajanian and Wang, 1987). The question of PTX-sensitivity was addressed by an acute exposure of $5\mu\text{g/ml}$ PTX to the ganglion for 2h at room temperature (see Methods) for comparison with ganglia exposed to PTX ($5\mu\text{g/ml}$) overnight (@ 4°C). This approach was taken since Holz et al (1986) reported that PTX transport into the dorsal root ganglion was strongly temperature-dependent.

There was no significant effect of PTX under either experimental condition. The data obtained from control matched overnight PTX incubation are included in Figure 26B. There was no significant difference between normalized, adrenaline-induced hyperpolarizations (normalized to the C-fiber action potential) measured in the control (0.51 ± 0.20 , $n=5$) and PTX-treated preparations (0.50 ± 0.31 , $n=5$) ($p > 0.98$).

In experiments where $5\mu\text{g/ml}$ PTX was applied directly to the ganglion for 2 hours, the mean amplitude of the adrenaline-induced hyperpolarizations were

virtually unchanged ($2.2 \pm 11.3\%$ $n=4$) when compared to responses obtained prior to PTX exposure (see table 5).

3.4. EFFECTS OF ADRENOCEPTOR AGONISTS ON B-CELLS.

3.4.1. Adrenaline-Induced Excitation In B-Cells.

Adrenaline has been reported to excite bullfrog ganglion B-cells by suppression of I_M (Akasu and Koketsu, 1987; Akasu, 1988b). An adrenaline-induced reduction in whole cell current was found in 40% (8/20) of B-neurons. Figure 49 illustrates the effects of the application of $100\mu\text{M}$ adrenaline (A) and $10\mu\text{M}$ muscarine (B) to the same B-cell. Although the muscarine-induced effect is more evident (90% inhibition) than that induced by adrenaline (20%), Figure 49C clearly shows that I_M is reduced by both agonists. Since the sum of I_M inhibition produced by both agonists exceeds 100%, some M-channels must be sensitive to both muscarine and adrenaline. This is consistent with a convergence of the two transduction mechanisms at a locus subsequent to the receptor.

3.4.2. Adrenaline-Induced Outward Currents In B-Cells.

The activation of β -adrenoceptors and subsequent increase in I_M has been reported in isolated toad smooth muscle cells, (Sims et al, 1988). A similar I_M

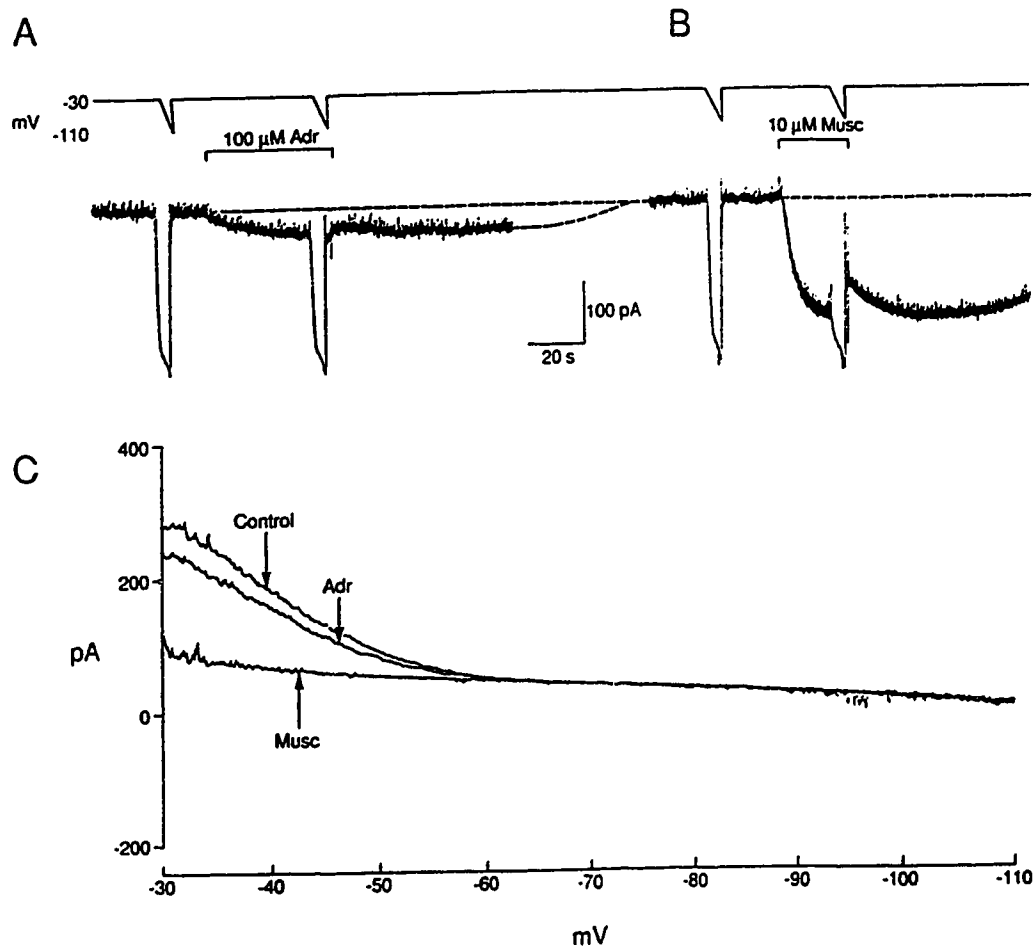


Figure 49. Comparison of muscarine- and adrenaline-induced inward currents produced in a B-cell. A & B. Steady-state inward currents produced by agonists in 6 mM $[K^+]_o$ and $V_H = -30$ mV. C. I/V relationships obtained from 5s voltage ramp commands to -110 mV before and during the action of agonists. Note that the effects of 100 μ M adrenaline (Adr) and 10 μ M muscarine (Musc) are confined to potentials positive to -60 mV (I_M activation range). Traces in A & B from rectilinear pen recorder and in C from x-y plots of computer stored data.

augmentation by catecholamines has not yet been reported in neurons. However, in the present study, adrenaline increased I_M in about 10% of the B-cells examined.

A particularly strong adrenaline-induced I_M enhancement is shown in Figure 50. Muscarine ($10\mu\text{M}$) typically suppresses I_M (panel A), whereas application of $100\mu\text{M}$ adrenaline induces a strong, reversible increase in whole cell current (panel B). Panel C better illustrates adrenaline- and muscarine-induced changes in I/V characteristics and clearly shows that adrenaline increases conductance between -30 and -60mV corresponding to an effect on I_M .

3.4.3. Examination If Distinct Adrenoceptor Subtypes Mediate The Opposing Effects Of Adrenaline On I_M .

β -adrenoceptor stimulation has been implicated to cause both an increase in I_M (Sims et al, 1988) and a decrease in I_M (Akasu and Koketsu, 1987). Smith et al, (1990) reported that an adrenaline-induced depolarization observed in BFSG was mediated by an α_1 -receptor. Therefore, the effects of α - and β -agonists were tested on I_M .

Table 6 compares the responses to $100\mu\text{M}$ adrenaline with those produced by the β -adrenoceptor agonist, isoprenaline (INA; $25\mu\text{M}$), and the α_1 -agonist, phenylephrine (PE; $25\mu\text{M}$). Each cell was pre-tested with $10\mu\text{M}$ muscarine to ensure that it was indeed a B-cell. In the cells that responded to the addition of

Figure 50. Adrenaline-induced potentiation and muscarine-induced inhibition of I_M in a B-cell. **A** & **B.** Steady-state responses to the application of $10\mu\text{M}$ muscarine (Musc) and $100\mu\text{M}$ adrenaline (Adr); $V_H = -30\text{mV}$ in $6\text{mM } [\text{K}^+]_o$. Note the agonist-induced conductance changes are similar in absolute magnitude and duration, but opposite in polarity. **C.** I/V plot of current response to 5s voltage ramp from V_H to -110mV in the absence and presence of adrenaline and muscarine (second control trace omitted for clarity). Note decrease in conductance in the I_M range produced by muscarine and increase in conductance in the same range produced by adrenaline. Traces in **A** and **B** from rectilinear pen recorder and **C** from superimposed x-y plots of computer stored data.

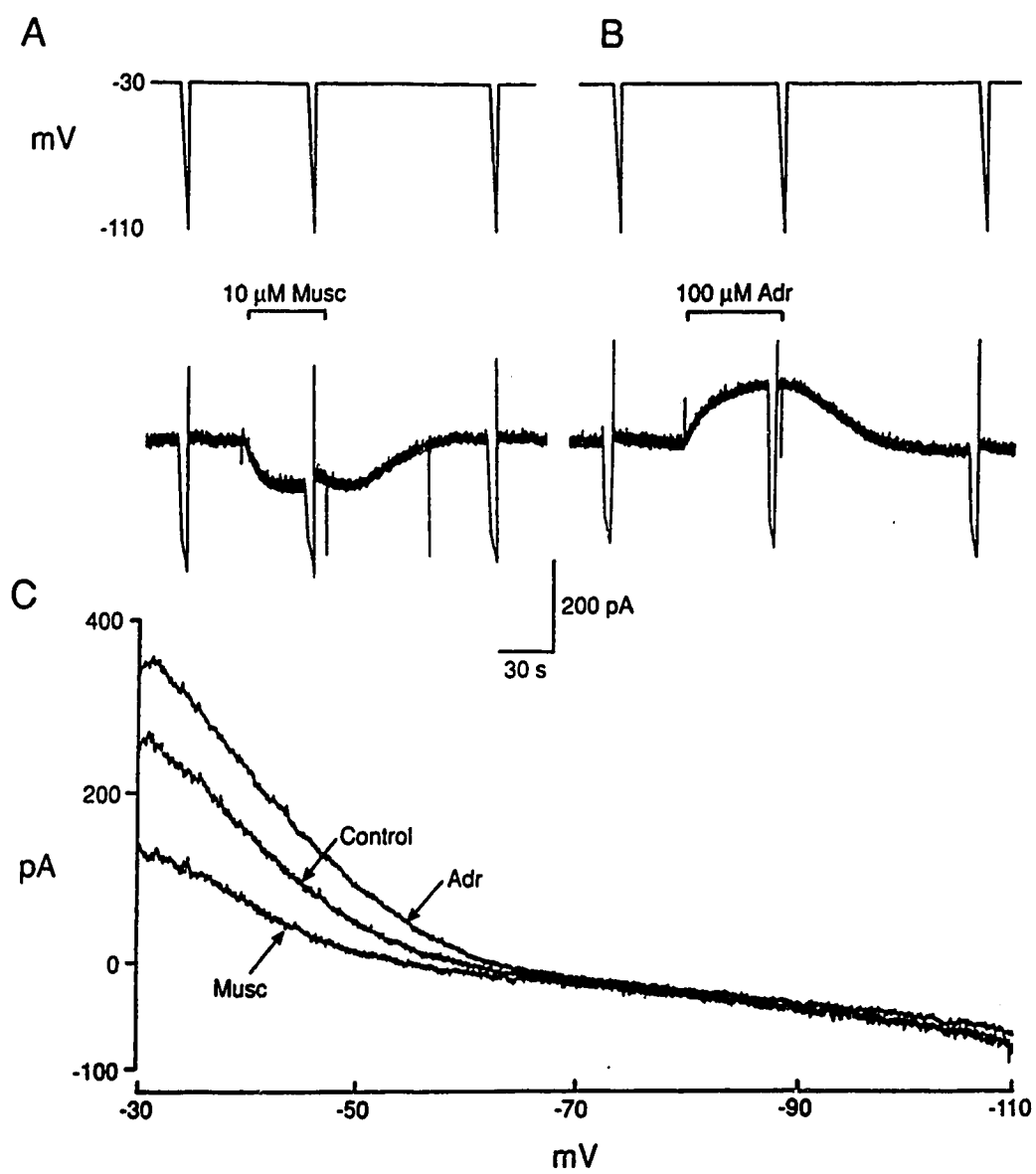


Table 6

The ability of sympathomimetics to generate inward and outward current
in RPSG B- and C-cells at -30mV.

	B-cells		C-cells	
	I _{in}	I _{out}	I _{in}	I _{out}
Adr (0.1mM)	7/14	1/14	0/37	20/37
PE (2.5x10 ⁻⁵)	6/10	1/10	NT	NT
INA (2.5x10 ⁻⁵)	7/27	10/27	0/2	1/2

adrenaline, the predominant effect was I_M suppression (7/14 B-cells), whereas I_M was increased in only 1 cell and the remaining 6 B-cells were unresponsive. PE also had a similar selectivity in reducing the I_M (6/10 cells) and enhanced I_M in only 1 of 10 cells studied. However, there was no particular selectivity found upon the application of INA; I_M was increased in 7/27 cells, decreased in 10/27 and no effect was observed in the remaining 10 B-cells.

4. EFFECTS OF NPY ON GANGLION NEURONS.

NPY is usually co-localized with adrenaline or noradrenaline and when co-released it inhibits transmitter release from presynaptic terminals (Sundler et al, 1986). However, in frog sympathetic ganglia, NPY is not co-localized with adrenaline in B-neurons but is found in C-neurons (Horn et al, 1987). Furthermore, NPY blocks a Ca^{2+} current in bullfrog sympathetic C-cells, but not in B-cells (Schofield and Ikeda, 1988). Although there is no evidence for NPY release in the sympathetic ganglia, similar mechanisms that regulate neurotransmitter release from the terminals may also exist in the soma. Therefore, it was of interest to test whether there also exists a selective action on potassium conductances in these neurons.

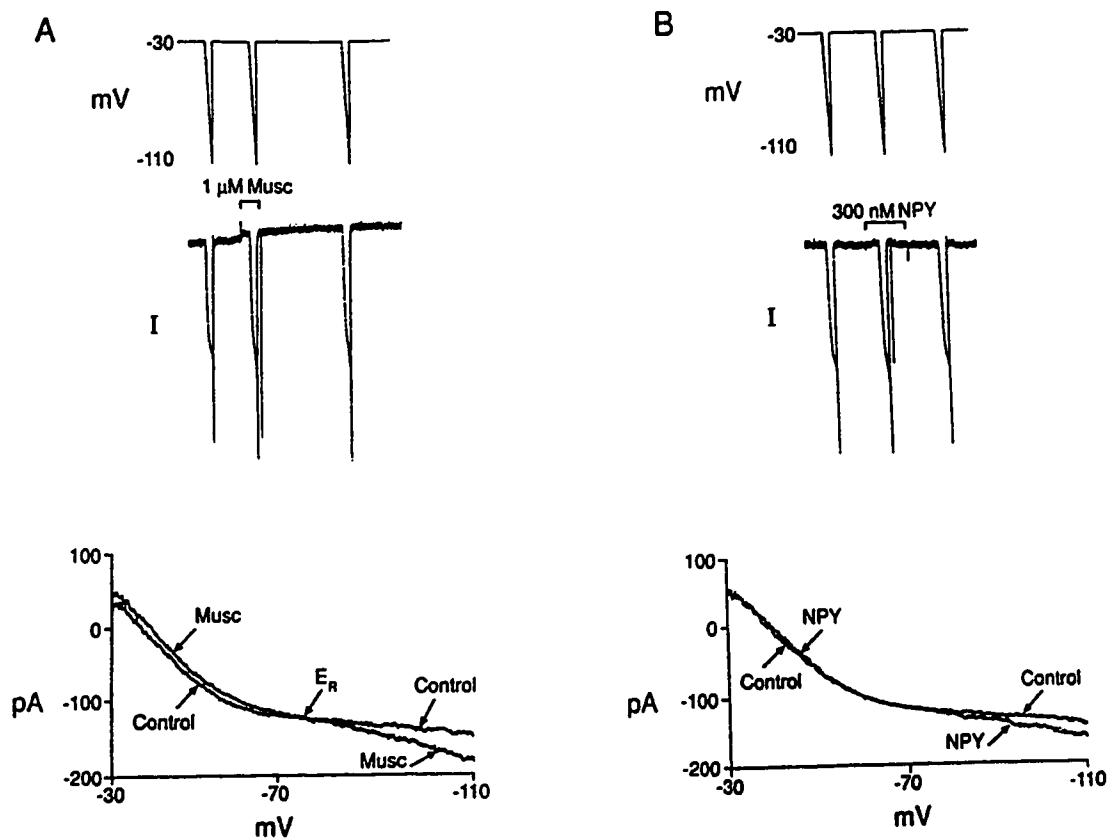


Figure 51. Similar effects of muscarine and NPY on a C-cell. Steady-state inwardly-rectifying currents induced by application of 10 μ M muscarine (A) and 300 nM NPY (B) on the same C-cell; $V_H = -30$ mV in 6 mM $[K^+]_o$. Bottom. Fast records of agonist-induced change in I/V characteristics obtained during 5 s voltage ramps, from V_H to -110 mV, by muscarine (bottom left) and NPY (bottom right). Upper traces from rectilinear pen recorder; lower traces from x-y plotter.

4.1. CHARACTERIZATION OF NPY EFFECTS ON B- AND C-CELLS.

The application of 300nM NPY to B-cells produced variable effects on I_M but did not produce any more than a 10% increase or decrease in I_M , in fact many B-cells were unresponsive. The effect NPY on C-cells was much more consistent; Figure 51 shows that NPY causes an outward current that is smaller than, but quite similar to that produced by 10 μ M muscarine in 6mM $[K^+]_o$. The reversal potential of the NPY effect is difficult to determine from this example because the amplitude of outward current at -30mV is small. However, the current appears to reverse between -50 and -75mV and inwardly rectifies at command potentials negative to -80mV.

The similarities between muscarine- and NPY-induced inward rectification on the same C-cell and the dependence on $[K^+]_o$ are shown in Figure 52. The amplitude of inward-rectification induced by both muscarine and NPY is significantly increased by the elevation of $[K^+]_o$ to 20mM. Moreover, the voltage where inward rectification is first observed shifts according to the calculated E_K (-43mV). This is consistent with the notion that a similar ionic mechanism may be involved.

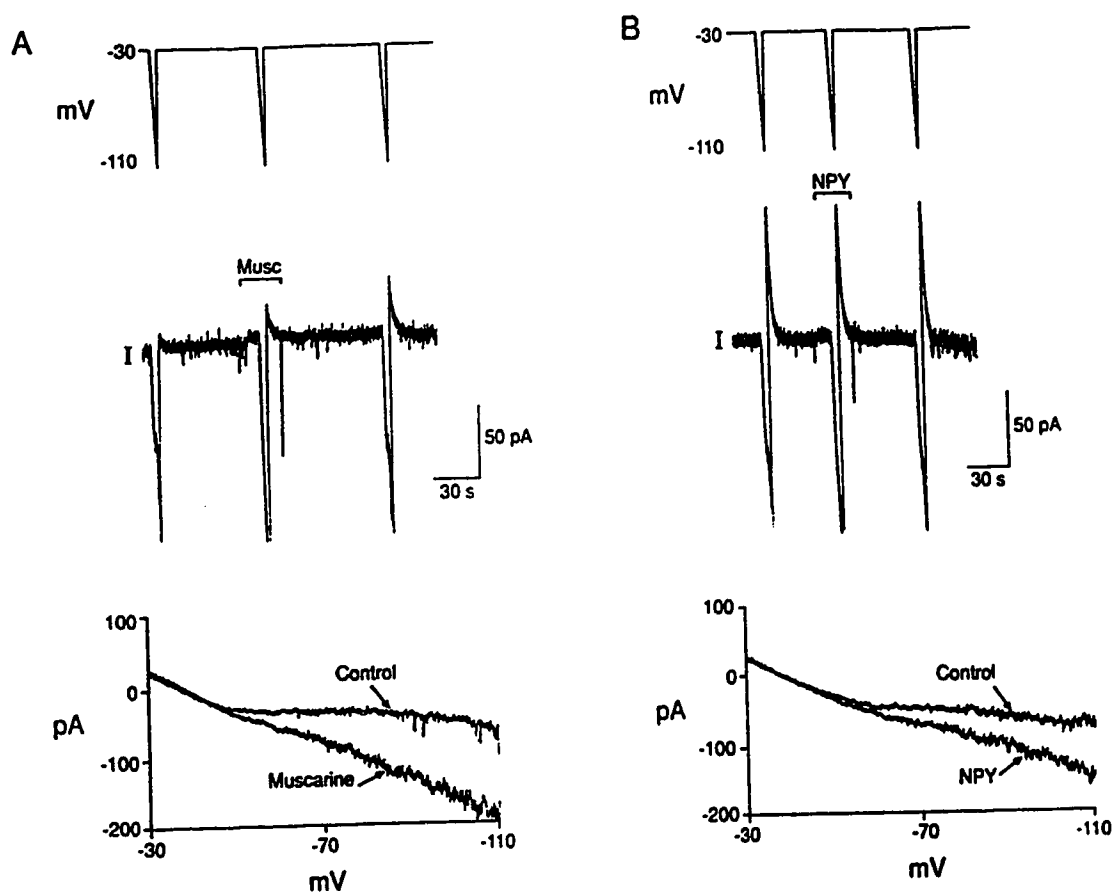
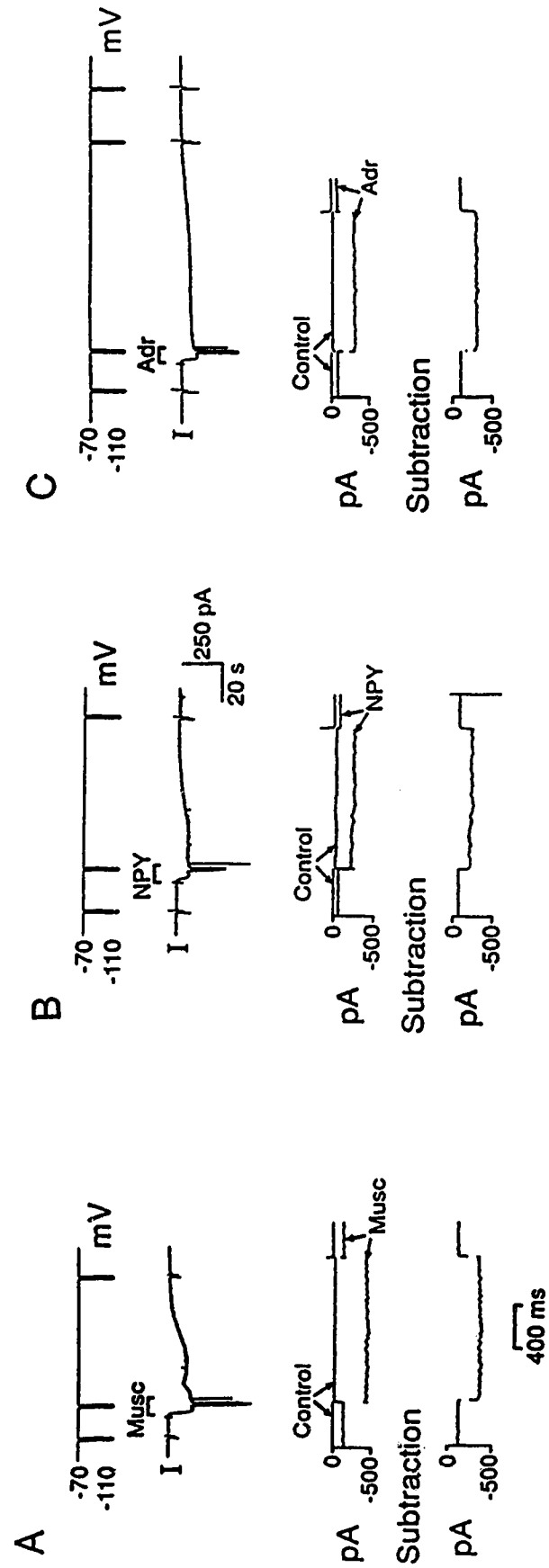


Figure 52. Elevation of $[K^+]_o$ causes increase in NPY- and muscarine-induced inward rectification in a C-cell. Upper traces. $[K^+]_o = 20 \text{ mM}$ ($E_K = -43 \text{ mV}$) and $V_H = -30 \text{ mV}$. Voltage protocol and steady-state currents before, during, and after application of $10 \mu\text{M}$ muscarine (A) and 300 nM NPY (B). Lower traces. I/V plots of conductance change during 5s voltage ramp from -30 to -110 mV induced by muscarine (lower left) and NPY (lower right). Upper records from rectilinear pen recorder lower records; x-y plots of computer stored data.

Figure 53. Similar effects of muscarine, adrenaline and NPY on the same C-cell. Top traces. Voltage protocol ($V_H = -70\text{mV}$ interrupted by 1s hyperpolarizing steps to -110mV). Steady-state currents observed to application of A, $2\mu\text{M}$ muscarine (Musc), B, 300nM NPY, and C, $100\mu\text{M}$ adrenaline (Adr) on the same C-cell; recorded in $[\text{K}^+]_o = 20\text{mM}$. Bottom traces. Current response during 1s steps to -110mV before and during the application of agonists. The subtractions, located directly below fast current responses, are the net agonist-induced inwardly-rectifying currents. Note the similar time course of activation. Top traces from rectilinear pen recorder and bottom traces from x-y plots of computer stored data.



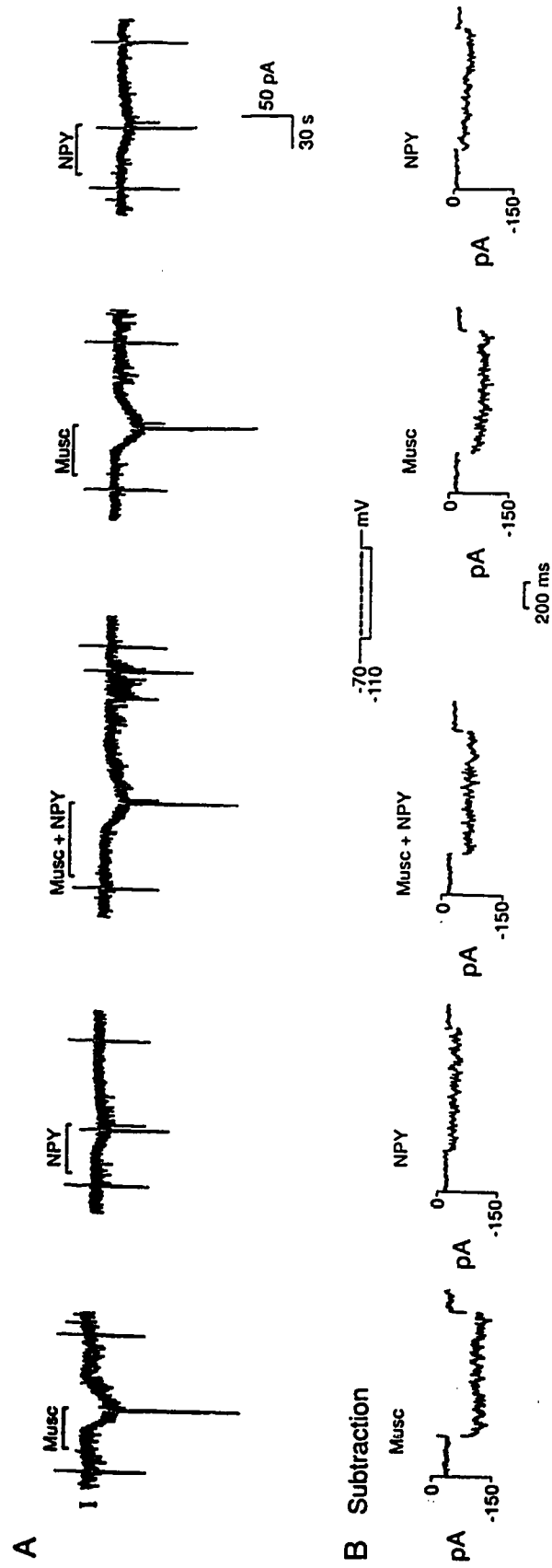
4.1.1. Activation Of NPY-Induced, Inwardly-Rectifying K⁺-Current In C-Cells.

The rate of activation was studied by holding a C-cell at a relatively negative holding potential (-70mV) so as to eliminate artifacts resulting from changes in space clamp (as a result of I_M deactivation, see Results: 3.1.3.). NPY produces an inward current at potentials negative to -43mV in 20mM[K⁺]_o. In this experiment, muscarine and adrenaline were also applied to the same C-cell for comparative purposes. Figure 53 shows that the rate of activation of the inwardly-rectifying K⁺ current induced by muscarine (10μM) in panel A, NPY (300nM) in panel B and adrenaline (100μM) in panel C, are strikingly similar. The time course of activation, obtained from subtraction of currents observed during step commands to -110mV before and during the application of each agonist illustrate that the inwardly-rectifying K⁺ current activates between 5 and 10ms (cf Williams et al, 1988a).

4.1.2. Does NPY Occlude The Muscarine Response In C-Cells?

These data are consistent with the possibility that the same population of K⁺ channels are involved in all three agonists responses. The muscarine- and adrenaline-induced inwardly-rectifying K⁺ currents are non-additive suggesting that both agonists act on the same population of channels (see above; Figure 45). Furthermore, occlusion of the effect of muscarine by NPY provides evidence for

Figure 54. NPY occludes the response to muscarine in a C-cell. **A.** Steady-state currents induced by the application of $2\mu\text{M}$ muscarine (Musc), 300nM NPY, and a solution containing both Musc and NPY; $V_H = -70\text{mV}$ in 20mM $[\text{K}^+]_o$. Brief interruptions are current responses to 1s voltage steps from V_H to -110mV (inset) so as to monitor the amplitude and rate of activation of agonist-induced inward rectification. **B.** The net increase in inward currents (subtractions), as measured at -110mV , show that net current induced by simultaneous application of Musc and NPY are not additive. Traces in **A** from rectilinear pen recorder; **B** are x-y plots of computer subtracted data.



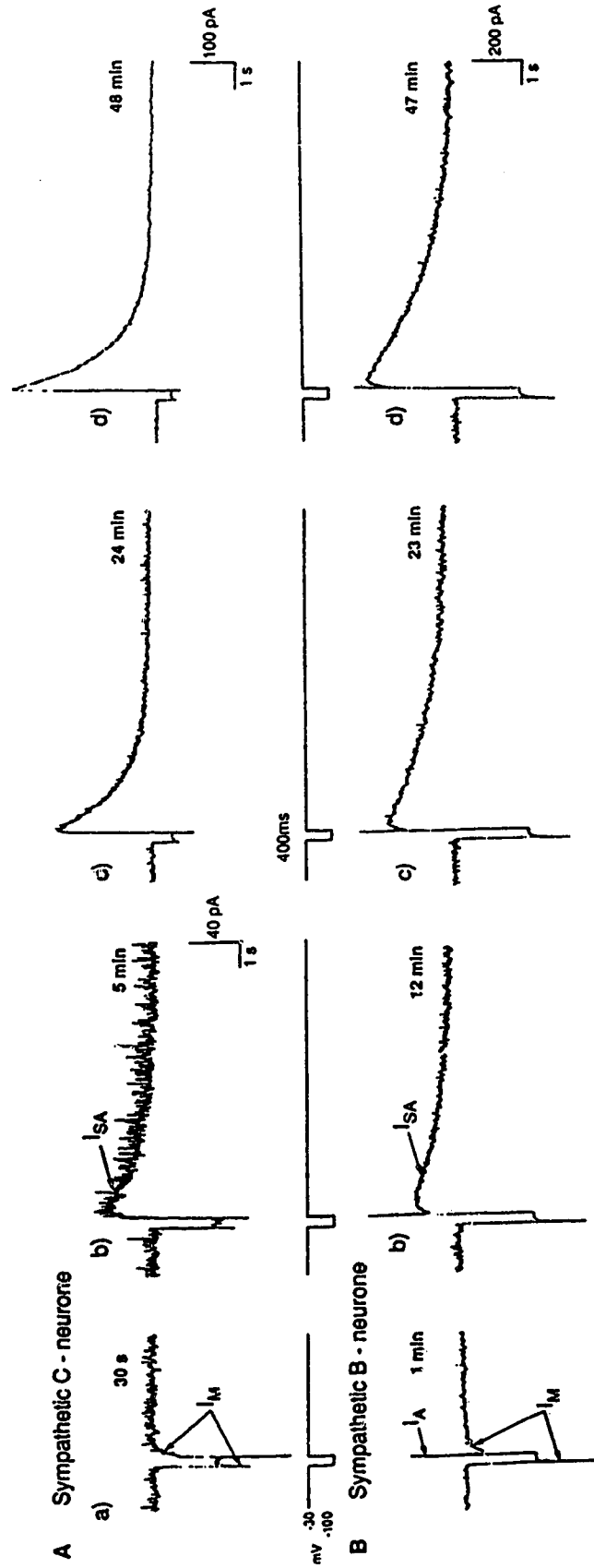
convergence of all three transduction mechanisms at some locus prior to activation of the inwardly-rectifying K^+ channel. Figure 54 shows that the inwardly-rectifying current evoked by simultaneous addition NPY (300nM) and muscarine (10 μ M) did not exceed the sum of currents observed when applied separately. The subtractions of control and agonist-induced currents (current measured during single command voltage jump from -70 to -110mV) are illustrated in panel B. These traces confirm that there is no additional net inwardly-rectifying K^+ current. Note that muscarine actually produces a larger current in the absence of NPY. One interpretation of this is that the transduction mechanism for the muscarinic receptor couples more strongly to the inwardly-rectifying K^+ channel than the NPY receptor does.

5. EXAMINATION OF A SLOW, TRANSIENT OUTWARD CURRENT REVEALED IN BOTH B- AND C-CELLS BY WCR.

5.1. GENERAL.

In a large number of figures presented, see Figures 21A, 27, 28B, 30A, 32A, 36A, 37A, 42A, 44A, and 52, a large, transient, outward current is observed upon return to -30mV from strongly hyperpolarized potentials. The electrophysiological and pharmacological properties of this response were studied for comparison with currents previously characterized in amphibian sympathetic ganglion neurons.

Figure 55. Time-dependent development of a slow, transient outward current in sympathetic neurons. Currents recorded in response to hyperpolarizing voltage commands from $V_H = -30\text{mV}$. **A.** C-neuron: Currents evoked by a 400ms hyperpolarizing command pulse to -100mV from V_H . a) 30s, b) 5 min, c) 24min and d) 48min after establishing WCR. Note appearance and progressive enlargement of slow, transient outward current which activated upon repolarization to -30mV . 40pA calibration refers to a) and b), 100pA refers to c) and d). **B.** B-neuron: Currents evoked by a 400ms hyperpolarizing voltage step to -110mV from V_H . a) 1 min after establishing WCR. Note interruption of I_M activation by a rapid, transient, outward I_A . b), c) and d) 12, 23, and 47 min after establishing WCR. 200pA calibration refers to all records. All traces from rectilinear pen recorder.



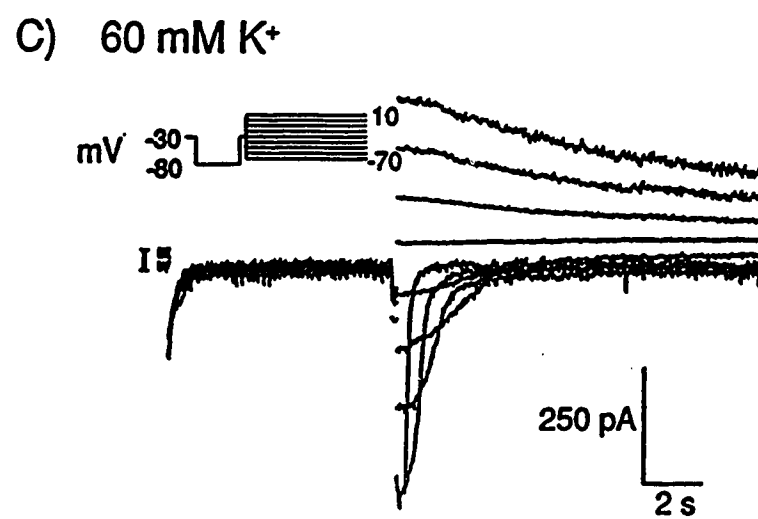
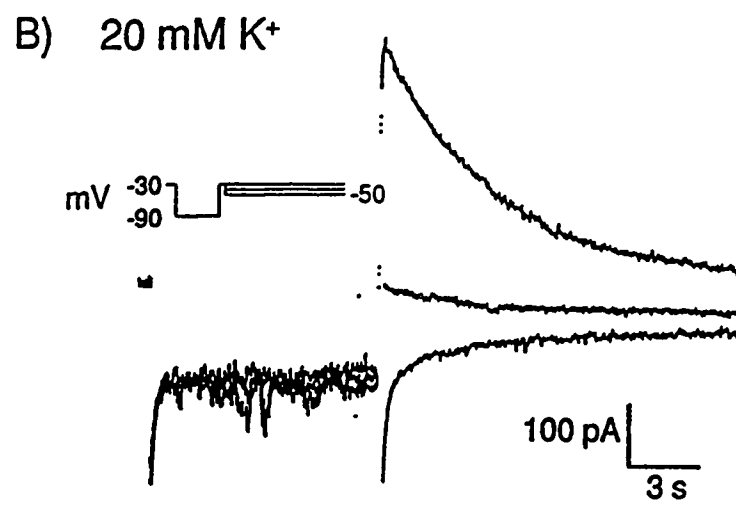
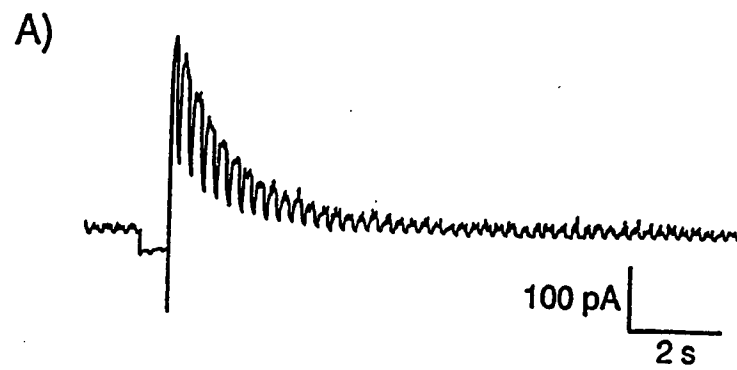
5.1.1. Analysis Of The Onset And Development Of The Slow, Transient Outward Current.

Upon the establishment of WCR, I_M was the predominant steady-state current (apart from voltage-insensitive leakage conductance, see Jones, 1989) which contributed to the whole cell conductance in the voltage range selected (-30 to -110mV). I_C , $I_{K(V)}$, and I_{AHP} are activated at potentials positive to the selected holding potential (-30mV) and I_A is a fast transient current that is inactivated at -30mV (see Introduction). However, as time proceeded, an additional slow, transient, outward current appeared and progressively increased in amplitude during recording. Figure 55 illustrates this effect in both a C- and a B-neuron, note that the magnitude of the slow, outward current increases to about 350pA and develops with a similar time course in both cells. Also, the brief activation of I_A in the B-neuron (Panel B) but not in the C-neuron (Panel A) is consistent with the notion that the slow, transient outward current is distinct current and not simply a prolongation of the inactivation kinetics of I_A .

5.1.2. Ionic Mechanism Of The Slow, Transient Outward Current.

Figure 56A shows that an increase in membrane conductance occurs during the slow, transient outward current. The magnitude of the current deflections are

Figure 56. Ionic mechanism of the slow, transient outward current. **A.** Small, transient inward currents result from brief, hyperpolarizing commands (10mV) elicited during the main clamp paradigm. The voltage commands produce larger deflections during the activation of the outward current, indicating an increase in conductance. **B & C.** Determination of reversal potential for the slow, transient outward current. Inactivation was removed by stepping to -90mV (**B**) or -80mV (**C**) and the transient current activated by returning the command potential to -30mV. The potential was then stepped to a series of voltages prior to the complete deactivation of the transient current so as to monitor the current reversal. This was repeated in different $[K^+]_o$. **B.** Experiment carried out in 20mM $[K^+]_o$; extrapolated $E_R = -43mV$. **C.** Experiment carried out in 60mM $[K^+]_o$; extrapolated $E_R = -14mV$. Experiments were carried out on two different C-cells. Record in **A** from rectilinear pen recorder. Records in **B & C** are x-y plots of digitally-stored data.



largest at the peak of the slow, transient outward current and decrease in amplitude as this current abates.

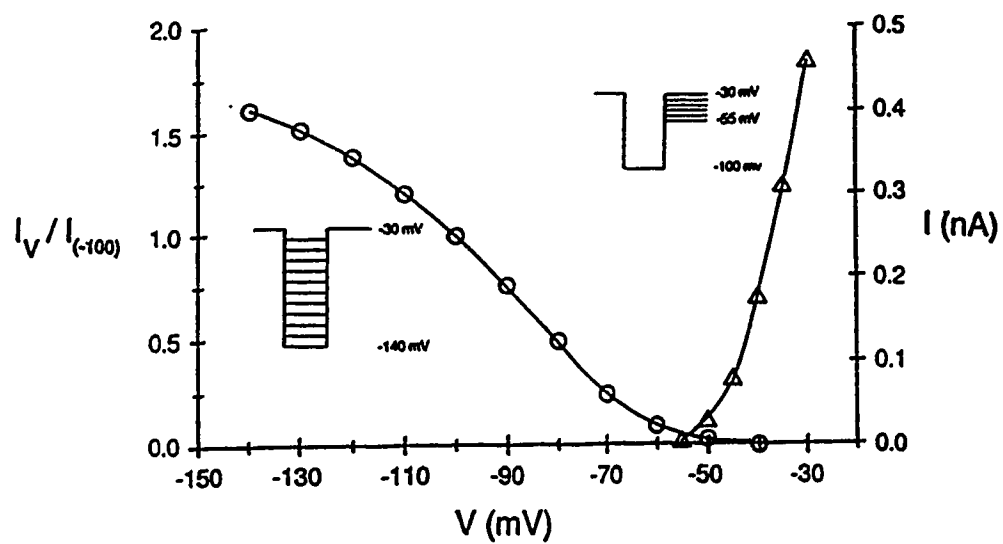
The slow inactivation can be exploited in determining the reversal potential. Prior to activation of the slow, transient outward current, the inactivation was removed by a long duration (> 5s) hyperpolarization to -110mV. Subsequent to activation, a series of hyperpolarizing post-pulse voltage commands were applied and the direction of the resulting current monitored to determine the current reversal potential. Figures 56B & C shows that the transient outward current reverses between -50 and -40mV in 20mM $[K^+]_o$ and between -20 and -10mV in 60mM $[K^+]_o$. The extrapolated E_R (data not shown) corresponded to -43 and -14mV, which was equal to and shifted according with the calculated E_K in 20 and 60mM $[K^+]_o$. Therefore, the appearance of the slow, transient outward current is due to the activation of a K^+ -selective channel.

5.1.3. Activation And Inactivation Kinetics Of The Slow, Transient Outward K^+ Current.

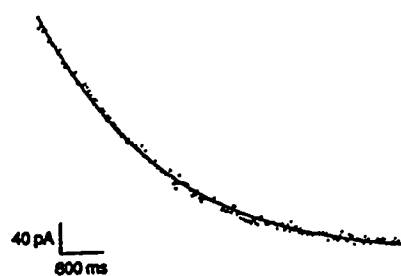
C-cells were chosen for the determination of activation and inactivation kinetics since they lack I_A . Also, these measurements were determined well after I_M had abated, thus minimizing the contribution of M-channel activation to the whole-cell currents as the command potential returned from hyperpolarized voltage commands.

Figure 57. Kinetics of the slow, transient outward current. **A.** Activation curve (Δ) obtained by measuring absolute currents evoked at the termination of 400ms hyperpolarizing command to -100mV and stepping to a range of postpulse potentials as shown in the inset (upper right). Curve for (the removal of) inactivation (\circ) obtained by stepping from a series of hyperpolarized potentials (from -140 to -40mV) and measuring the current upon repolarization to -30mV (see lower left inset). These currents were normalized to current produced from the -100mV command pulse. Note the small overlap between inactivation and activation curves. Data obtained from a C-cell following the abatement of I_M . **Plot B.** In this C-cell, a single exponential, computer-generated line best fits digitized points of the slow, transient current ($\tau=2.7s$). In some cases, however, such data was fit by two exponentials (see Table 1). **C.** Estimation of the time constant for removal of inactivation. The amplitude of normalized current responses (ordinate scale) to a series of hyperpolarizing steps from $V_H=-30mV$ to -110mV in which the duration of the steps was varied from 30ms to 20s (abscissa scale). Digitized points in B from x-y plot of computer stored data.

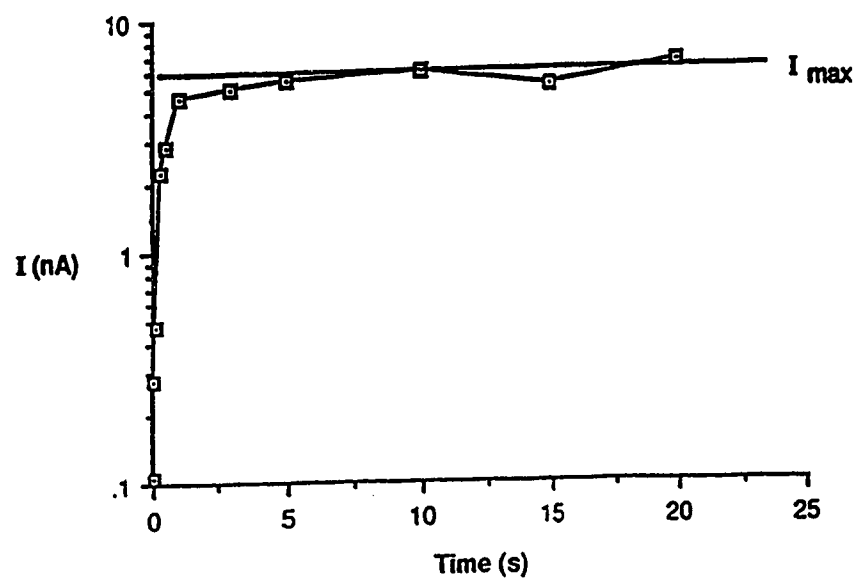
A



B



C



The activation and inactivation curves for the slow, transient outward current are shown in Figure 57A. These curves are very similar to those reported for I_A (Adams et al, 1982a), however the data shown were obtained from a C-cell (these cells do not have an I_A : see Results 1.2.2.). The two curves overlap very little; activation is observed at potentials positive to -60mV and is strongly voltage-dependent. The current is completely inactivated at -50mV. Therefore, the slow, transient outward current contributes little to the setting of the resting membrane potential.

In most of the C-cells studied, the rate of inactivation of the slow, transient outward K^+ current was best fit by a single exponential function ($\tau=3.58\pm0.35s$, $n=19$) (eg Figure 57B). In 7 other C-cells, two exponentials provided a significant improvement in the fit, however the second time constant ($4.04\pm0.73s$) was not significantly different from those C-cells that had one time constant.

Although the slow, transient outward K^+ current was strikingly similar to I_A in many respects, the main difference was that the inactivation time constant was about 80 fold slower than that of BFSG I_A (Adams et al, 1982a). Furthermore, since C-cells lack I_A , but have a robust slow, transient outward K^+ current, it suggests that this may be a novel K^+ current. The current was subsequently named the slow A current (I_{SA}).

τ for the removal of inactivation in C-cells was determined by varying the duration of a hyperpolarizing command to -110mV from 30ms to 12s and measuring

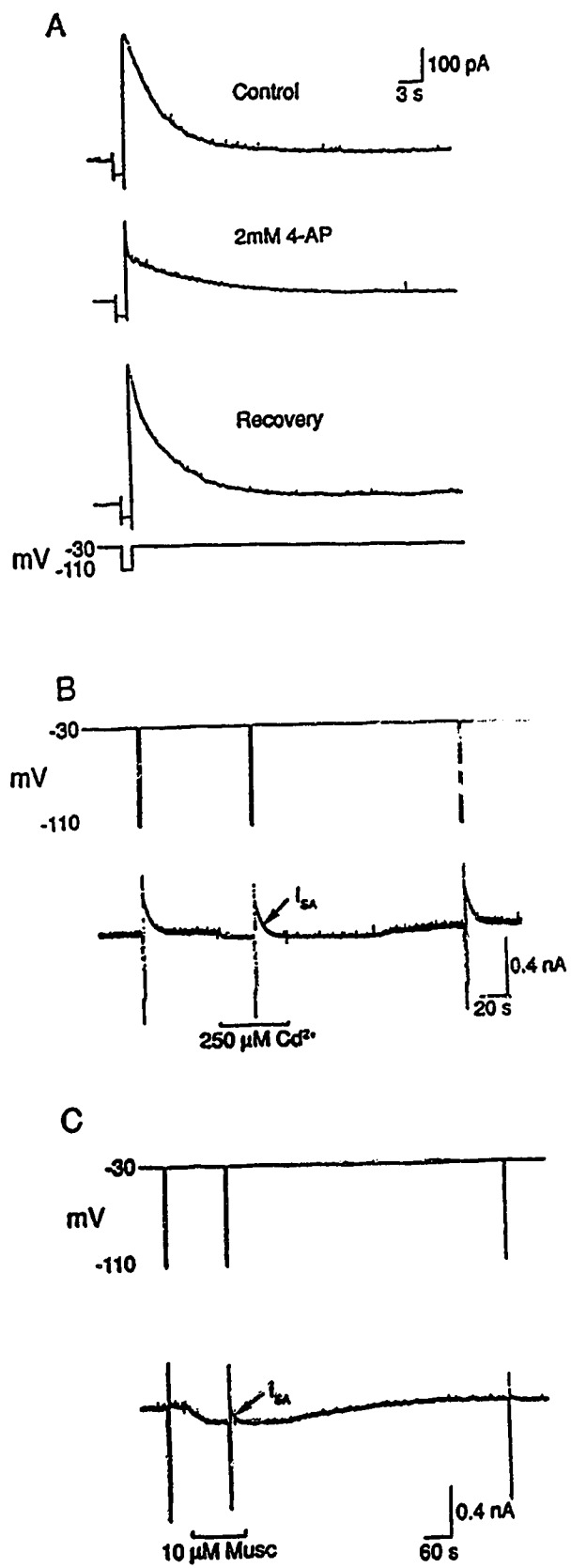
the amount of current upon repolarization to -30mV (as a percent of the maximally-activated current (I_{max})). Figure 57C shows the normalized slow, transient current measured versus command pulse duration at -110mV and τ for the removal of inactivation was 214 ± 36 ms, $n=2$.

5.2. PHARMACOLOGY OF I_{SA} .

5.2.1. K^+ Channel Blockers.

The most significant effect on I_{SA} by the various K^+ channel blockers tested was found using 4-AP. Figure 58A illustrates the reversible attenuation of the peak amplitude of I_{SA} by 2mM 4-AP. The rate of inactivation of I_{SA} in control ($\tau=7.7$ s), was dramatically altered by 4-AP where two distinct time constants were necessary to provide an appropriate fit ($\tau_{fast}=0.8$ s and $\tau_{slow}=13.2$ s). No significant effect (less than 10% block) of the I_{SA} was found in the presence of 2.5mM Ba^{2+} and 70 μ M dTC. Similarly, 3mM TEA usually had little effect, although a significant block of I_{SA} was elicited by 3mM TEA in 2 cells. However, in these particular cells, the baseline noise was strongly attenuated by TEA and also by 0.25mM cadmium (data not shown).

Figure 58. Pharmacology of I_{SA} . **A.** Effect 4-AP. Top. Control activation of I_{SA} following a 1.5 s voltage step from the holding potential of -30 to -110mV in a C-cell. Middle. Same response recorded in the presence of 2mM 4-AP. Note attenuation of peak amplitude of I_{SA} and biphasic decline of current. Bottom. Recovery of I_{SA} following 3 min 15s washout of 4-AP. **B.** Lack of effect of 250 μ M Cd^{2+} on I_{SA} evoked another C-cell following a 1s voltage step from -110 to -30mV. **C.** Muscarine-induced enhancement of I_{SA} in a B-cell. Initial voltage command from holding potential of -30mV to -110mV produces an inward current that is followed by a very small, transient I_{SA} . Application of 10 μ M muscarine produces an increase in steady-state inward current as a result of I_M suppression, but also markedly increases the amplitude of I_{SA} . Upon the removal of muscarine, the steady-state current recovers to its control level and I_{SA} becomes less prominent. All traces from rectilinear pen recorder.



5.2.2. Ca^{2+} -Dependence Of I_{SA} .

There was a possibility that I_{SA} was due to the entry of extracellular Ca^{2+} to activate a population of Ca^{2+} -sensitive K^+ channels. However, I_{SA} was not affected by the extracellular application of 2mM Mg^{2+} /0 Ca^{2+} or 0.25mM cadmium (illustrated in Figure 58B).

5.3. IS THE ONSET AND THE TIME-DEPENDENT DEVELOPMENT OF I_{SA} DUE TO A PROGRESSIVE LOSS OF SOME CYTOPLASMIC FACTOR ?

If the dilution of an intracellular factor underlies the activation of this current, perhaps the addition of various intracellular agents could prevent I_{SA} from appearing. The addition of ATP (1.5mM), GTP (1.5mM), cAMP (100 μM), IP₃ (0.5mM), GST (50 μM), or H-7 (50 μM) via the patch pipette or external application of PMA (2 μM) failed to prevent the development of the I_{SA} .

5.4. MODULATION OF I_{SA} BY MUSCARINE.

In several experiments, such as those illustrated by Figures 32A, 36A, 37A, 42A, 49B, 50A, and 58C, 10 μM muscarine reversibly induces I_{SA} . Table 7

Table 7

Effects of muscarine on I_{SA} in Rana pipiens sympathetic ganglion neurons.

	n	No effect	Increased I_{SA}	Decreased I_{SA}
B-cells	39	6	32	1
C-cells	37	8	23	6
All Neurons	76	14	55 ¹	7 ²

¹ Muscarine induced I_{SA} in 13 of these 55 cells where the current was previously absent (i.e. infinite potentiation). In the remaining cells, I_{SA} was potentiated by $203.6 \pm 11.8\%$ ($n=42$). There was no obvious difference in the ability of muscarine to induce I_{SA} in B-cells compared with C-cells.

² Muscarine reduced I_{SA} to $79.0 \pm 3.1\%$ of control ($n=7$).

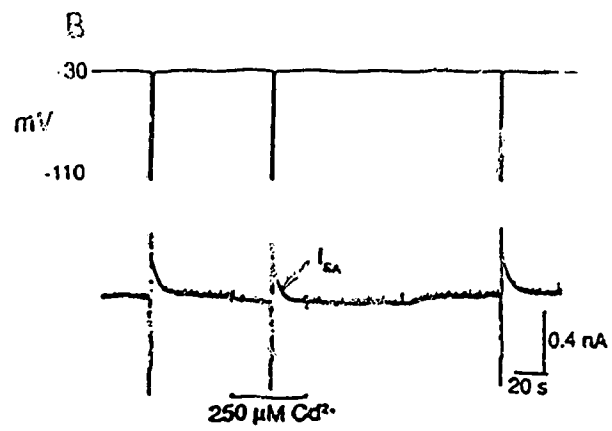
summarizes the effects of muscarine on I_{SA} in RPSG neurons. A muscarine-induced effect on I_{SA} was observed in 62 of 76 cells.

In 55 cells, muscarine induced an increase in I_{SA} . In 13/55 cells, I_{SA} was observed only in the presence of muscarine, in 42/55 cells muscarine increased I_{SA} by $203 \pm 11.8\%$ and no effect was observed in 14/55 cells. In the remaining 7 (of 76) cells, muscarine decreased I_{SA} amplitude, however the mean attenuation was only $79.0 \pm 3.1\%$ and 6 of the 7 observations occurred in C-cells.

5.5. IS THE MUSCARINE-INDUCED ENHANCEMENT OF I_{SA} DUE TO AN IMPROVEMENT OF THE SPACE CLAMP?

The muscarine-induced I_M suppression and subsequent increase in membrane resistance may improve the voltage control and shift the membrane potential into the activation range for the delayed rectifier current ($I_{K(V)}$). This is especially likely if $I_{K(V)}$ activation curve is shifted in the negative direction during WRC and I_{SA} could simply reflect a small amount of $I_{K(V)}$ activation. If this were the case, then blockade of I_M with Ba^{2+} (Adams et al, 1982b) should also induce I_{SA} . Attempts to evoke I_{SA} during I_M blockade by 5mM Ba^{2+} were unsuccessful. Figure 59A illustrates one of 9 trials performed on 6 B-cells. However, in 6 of 9 experiments (on 4 B-cells) where muscarine (10 μ M) was applied in the presence of Ba^{2+} , I_{SA} was still induced (an example is shown by Figure 59B) suggesting that muscarine-induced appearance of I_{SA} is entirely independent of I_M .

Figure 59. Muscarine-induced I_{SA} in the presence of Ba^{2+} . Current responses evoked in a B-cell voltage commands to -50 and -110mV from $V_H=-30mV$, before and during the application of drugs (recovery records omitted for clarity); $[K^+]_o=6mM$. **A.** The application of 5mM Ba^{2+} produces inward current (I_M suppression) yet fails to induce I_{SA} transients (bottom left current trace). The insets show current responses to -50 and -110mV step commands. Note suppression of I_M relaxations by Ba^{2+} . **B.** Effect of application of a solution containing 5mM Ba^{2+} and 10 μ M muscarine to the same B-cell. Bottom right trace. Strong inward current results from I_M suppression. This is also illustrated by middle insets. The small, transient I_{SA} which follows the command to -110mV is almost doubled in amplitude during the application of the Ba^{2+} /muscarine mixture. Top and bottom traces in A & B from rectilinear pen recorder (refer to 200pA-60s calibration bars) and insets are x-y plots (refer to 200pA-0.2s calibration) of computer stored data.



The observation that muscarine increased I_{SA} in 23/37 C-cells (see Table 7) also argues against an improvement in space clamp, since muscarine induces an increased K^+ conductance in these cells which would not be expected to improve the quality of the clamp.

5.6. IS THE BINDING OF MUSCARINE VOLTAGE-DEPENDENT?

The time course of I_{SA} inactivation and muscarine-induced I_M depression were often quite similar (see Figures 36A, 37A, 49B and 50A and 58C). There exists a possibility that muscarine binding may be voltage-dependent and hyperpolarization to -110mV and return to -30mV may cause muscarine to briefly unbind and rebind; hence a transient outward current would appear and abate according to the rate of re-binding. This hypothesis was tested by holding a cell at a potential negative to M-current activation ($V_H = -90mV$). I_M was activated by brief depolarizing voltage commands from V_H to -40mV. If muscarine binding is reduced by hyperpolarized potentials, the outward current observed at -40mV in the presence of muscarine should decrease with time as the drug rebinds to the receptor in a voltage-dependent manner. Figure 60 shows that application of muscarine at -90mV suppresses I_M activation throughout the entire voltage jump to -40mV. Therefore, the binding of muscarine to receptor governing I_M suppression was not particularly voltage-sensitive and likely does not account for the muscarine-induced appearance of the transient outward current, as exemplified in Figure 58C.

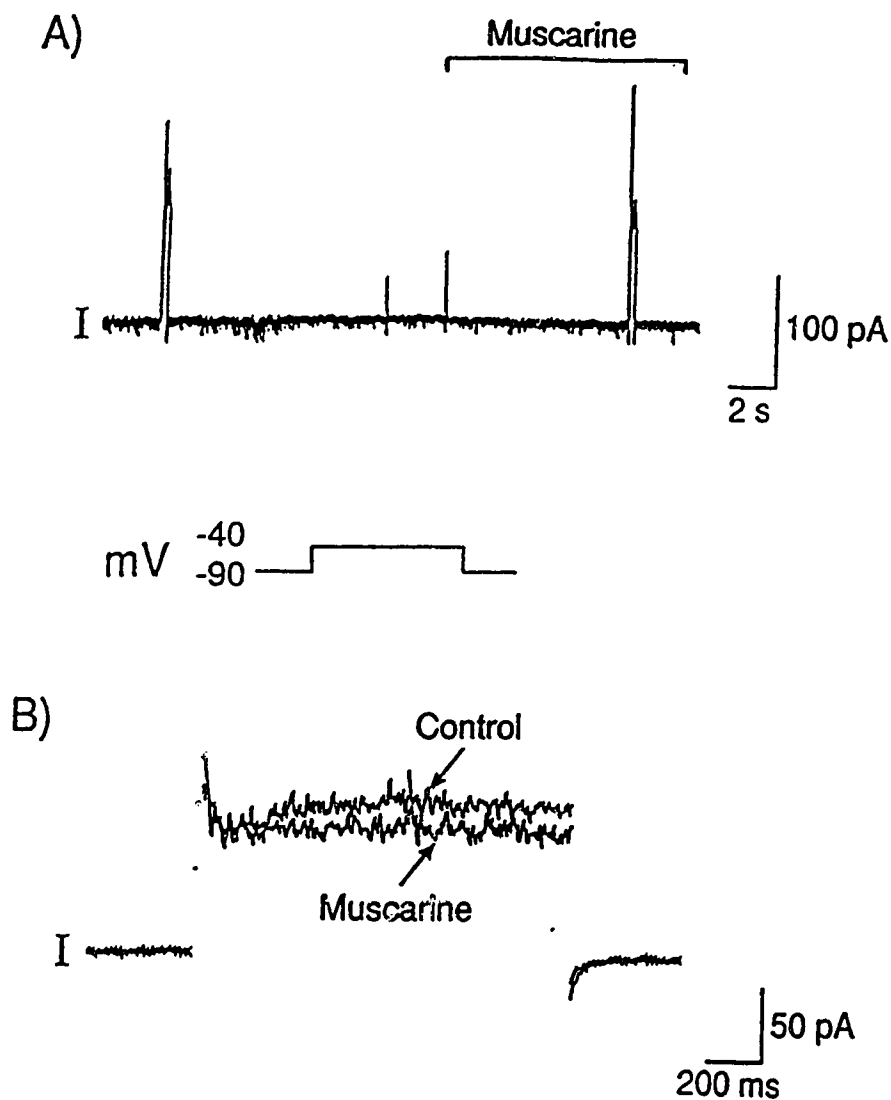


Figure 60. Effect of holding potential on the binding of muscarine and suppression of I_M in a B-cell. **A.** Steady-state current before and during application of $10\mu\text{M}$ muscarine; $V_H = -90\text{mV}$ and $[\text{K}^+]_o = 6\text{mM}$. Note that the application of muscarine at -90mV does not cause a change in steady-state current. **B.** The fast current records of outward currents generated by short step commands from -90mV to -40mV . Note that during the step to -40mV , muscarine reduces the amplitude of the outward current which results primarily from I_M activation. Traces in A from rectilinear pen recorder and B from x-y plot of computer stored data.

CHAPTER IV

DISCUSSION

1. GENERAL.

This investigation concentrated on determining the ionic and signal transduction mechanisms by which the same neurotransmitter generates completely opposite effects on neuronal excitability in amphibian sympathetic ganglia.

The whole cell patch-clamp technique (Hamill et al, 1981) is the method of choice for the study of voltage- and neurotransmitter-activated currents in neurons; particularly for small neurons that have had a limited amount of electrophysiological study at the single cell level. For example, reports on voltage-dependent currents occurring in frog C-cells (Jones, 1987a) has lagged well behind those in B-cells (Kuba and Koketsu, 1976; see Adams et al, 1986) since these cells are more susceptible to microelectrode impalement damage than B-cells (Rafuse et al, 1988).

One of the most important advantages of WCR is the utilization of the patch pipette to deliver various agents to the intracellular milieu (Neher, 1988). In the past, intracellular application of compounds was accomplished by intracellular iontophoresis or pressure injection. In other experiments, compounds were modified structurally so as to increase membrane permeability. One of the main problems with these methods was that the exact intracellular concentration of an agent could not be easily determined.

However, WCR method also has certain drawbacks that can complicate the interpretation of data. For example, 'rapid run-down' of membrane currents (Marty and Neher, 1983; Fernandez et al, 1984; Belles et al, 1988) and junction-potential

drift shifts voltage-activation curves to more negative potentials (Marty and Neher, 1983). These changes likely result from the exchange and dilution of intracellular contents with 'internal solution' contained in the patch pipette. Moreover, the dissociation of sympathetic ganglion neurons might be regarded as an enzymatic assault on the external membrane. Trypsin treatment may alter the externalized portion of membrane bound proteins, including receptors and channel proteins and thereby modify their functional integrity. Furthermore, the subsequent dialysis of neurons with artificial 'internal solution' via the patch pipette provides an equal, if not a greater, insult to neuronal biochemistry. Such alterations may modify homeostatic mechanisms that control cellular processes. For example, changes in phosphorylation of the cytoplasmic domain of membrane bound proteins could alter the conformation and function of channel proteins (Catterall, 1988; Horn and Marty, 1988; Simmons et al, 1990). One aspect of this study was to establish whether normal responses could be evoked following application of muscarine that mimicked postsynaptic potentials in amphibian sympathetic neurons.

In view of problems associated with WCR, alternate techniques should be utilized, where possible, to support WCR data. Furthermore, other techniques provide data which is not easily acquired using WCR. For example, in the present study, sucrose-gap recording was used for the determination of pA_2 values since it provides a high degree of recording stability as well as consistent and reproducible agonist-induced responses (Arunlakshana and Schild, 1959). Also, the independence

of adenylate cyclase inhibition and activation of adrenaline-induced hyperpolarization or outward currents was established using sucrose-gap and WCR.

2. CHARACTERIZATION OF DISSOCIATED SYMPATHETIC NEURONS.

2.1. ISOLATION OF CELLS FROM FROG PARAVERTEBRAL SYMPATHETIC GANGLIA.

The dissociation procedure for dispersion of Rana pipiens paravertebral sympathetic ganglia neurons was modified slightly from that used for bullfrog paravertebral sympathetic ganglia (Kuffler and Sejnowski, 1983; Schofield et al, 1988). Neurons isolated from RPSG were smaller and had less connective tissue than BFG. The enzyme treatment time, therefore, was reduced accordingly. Since the dissociation procedure removed axonal material, these cells could not be identified by means of their relative antidromic conduction velocities (Nishi et al, 1965; Dodd and Horn, 1983a). However, upon observation, cells generally consisted of two visually discernable groups: 1) Large neurons and 2) Small neurons.

2.1.1. Proposed Classification For Dissociated Sympathetic Ganglion Neurons.

It was necessary to establish criteria for the classification of dissociated amphibian sympathetic neurons. Although no significant difference between measured resting membrane potentials or input resistances of small and large cells were noted, there existed a sufficient number of clear disparities that form an adequate basis for classification of dissociated Rana pipiens sympathetic ganglion cells into putative B-and C-neurons. These are as follows:

- 1) Response to the application of muscarine.
- 2) Input capacitance.
- 3) Presence or absence of I_A .

The first two criteria will be discussed together due to their interdependence. Large and small cell responses to the application of muscarine ($10\mu\text{M}$) differed dramatically. A muscarine-induced inwardly-rectifying current (outward current at -30mV) was observed in all cells with $C_m < 18\text{pF}$, whilst all cells with $C_m > 40\text{pF}$ responded with inward current (@ -30mV). These results are consistent with earlier reports by Koketsu et al (1968), Weight and Padjen (1973b), Dodd and Horn (1983 a & b), and Smith and Weight (1986) who collectively showed that small C-cells are hyperpolarized and large B-cells are depolarized by muscarinic agonists. The mean C_m for those cells that responded with an outward current was $21.3 \pm 0.8\text{pF}$ ($n=70$) and was about half of that observed for cells that responded with inward current ($40.5 \pm 1.5\text{pF}$, $n=66$). Therefore, a clear dichotomy existed between large and small

dissociated Rana pipiens sympathetic ganglion neurons in terms of their response to muscarine.

The presence or absence of the fast transient A-current (I_A ; Adams et al, 1982a) is the third criterion for the proposed classification. Figure 15 E shows the probability of observing I_A was greatly increased in large cells. Furthermore, I_A was observed in approximately 91% of the large cells included in Table 2. Also, I_A was absent from current records in a paper by Jones (1987a) who studied bullfrog C-cells.

Although the proposed classification is not absolute, taken together, these three criteria should be sufficient to classify electrophysiologically large and small dissociated Rana pipiens sympathetic ganglion neurons as putative B- and C-cells respectively. Further confirmation of this categorization could be provided by employing histochemical techniques because NPY-immunoreactivity is evident in C-cells only (Horn et al, 1987; Horn and Stofer, 1988).

2.1.2. Voltage-Dependent Currents In Putative B- And C-Cells.

In the majority of experiments, the holding potential was set so as to maximize the M-current without activating other large neuronal currents such as I_C , $I_{K(V)}$ and I_{Na} . The kinetics for WCR I_M were determined for Rana pipiens B- and C-neurons for comparison with previous microelectrode characterizations of the same

neurons in BFSG (Adams et al, 1982a; Jones, 1987a). In addition, it was important to determine the stability of I_M as WCR proceeded.

Steady-state currents observed over the -30 to -110mV voltage range consisted, in part, of a voltage-dependent, non-inactivating, outward current that appeared similar to the I_M described in BFSG B- and C-neurons (Adams et al, 1982a; Jones, 1987a; see Table 1). However, other than comparable values for an e-fold shift in G_M and a similar trend in the rate of I_M deactivation, many of the quantitative voltage-dependent values obtained by WCR were negative to those obtained by microelectrode recording (see Table 1).

In this study, the WCR-recorded B-cell I_M activated at -75mV, the half maximal activation voltage occurred at -52mV and was fully activated at -30mV; these values are 15 mV, 17mV and 30mV negative (respectively) to those values reported for BFSG B-cells (Adams et al, 1982a). The negative shift in WCR data may be explained by differences in the two recording techniques; perhaps the increased input resistance combined with low series resistance enhanced the quality of the voltage-clamp during WCR as compared to that obtained during microelectrode voltage-clamp recording. However, a more likely explanation for these discrepancies is that they result from the loss or dilution of cytoplasmic contents due to intracellular perfusion with 'internal solution' contained in the patch pipette. This exchange often results in a drift in junction potential that can shift activation curves to more negative potentials (Marty and Neher, 1983). The RMP of a large number of B- and C-neurons often became more negative as recording

proceeded such that the steady-state (outward) holding current (measured @ -30mV) increased and attained a new level during the first 5-10 minutes after the establishment of WCR. In this regard, it is interesting to note that steady-state outward current, which appears to be due to an increase in I_M , often progressively increased irrespective of the content of the patch pipette. This phenomenon was not sensitive to inclusion of ATP, GTP, GTP- γ -S, IP₃, GST, H-7, or DPG in the patch pipette. It was not determined whether this phenomenon was dependent or even related to the exchange of solutions, however, such an effect is consistent with this notion. Alternatively, these observations may be symptomatic of more complex biochemical changes promoted by WCR technique.

The largest discrepancy evident in Table 1 is the maximum G_M measured from Rana pipiens B- and C-cells by means of WCR technique was only about 6% and 4% of those values reported from bullfrog B- and C-cells using conventional microelectrode techniques (Adams et al, 1982a; Jones, 1987a). This disparity may be explained in whole or part by the following factors: 1) Rana pipiens B- and C-cell bodies (converted from C_m measurements; $C_m = \pi d^2$) are about half the diameter of bullfrog B- and C-cell bodies (Dodd and Horn, 1983a). Therefore, the macroscopic I_M in RPSG neurons would be reduced assuming that similar M-channel density exists in both species. 2) Strong enzymatic and mechanical manipulations during the preparation of dissociated cells may damage the M-channels. 3) The insult of intracellular dialysis with the artificial 'internal solution'

could dilute, eliminate, or antagonize cytoplasmic agents that maintain channel function. 4) Brown et al (1989) reported that I_M in cultured SCG cells may be enhanced when the internal solution pH was lowered to 6.7. Perhaps a larger I_M would have been recorded in RPSG B- and C-cell under these conditions.

Recent reports on the amplitude of I_M and agonist-induced I_M suppression recorded by means of WCR from both BFSG and RPSG B-neurons concur well with the values reported in this thesis (300pA; Pfaffinger, 1988; Pfaffinger et al, 1988; Jones, 1989; Bosma and Hille, 1989; Bley and Tsien, 1990; Simmons et al, 1990), and also from toad smooth muscle cells (Sims et al, 1988) and cultured rat sympathetic neurons (Brown et al, 1989). Therefore, the WCR technique is quite amenable for the detailed studies required for the elucidation of ionic and signal transduction mechanisms involved in I_M suppression (Brown and Adams, 1987; Pfaffinger, 1988; Pfaffinger et al, 1988; Selyanko et al, 1990a; Bley and Tsien, 1990).

3. CELL-SPECIFIC AND NON-SPECIFIC RESPONSES.

The responses studied in this thesis can be grouped and discussed in three well defined groups:

- 3.1. Responses Occurring Only In C-Cells.
- 3.2. Responses Occurring Only In B-Cells.
- 3.3. Responses Occurring In Both B- And C-Cells.

3.1. RESPONSES OCCURRING ONLY IN C-CELLS.

The results showed a striking similarity in the C-cell response to the application of muscarine, adrenaline, or NPY (see Figure 53); these agonists promoted a similar small outward current at -30mV. When the characteristics of these currents were studied over a broad voltage range, the conductance was remarkably voltage-dependent at potentials negative to current reversal (see current subtractions in Figure 23). This figure also shows that the reversal potential shifted to more positive potentials and the slope of rectification increased in accordance to the elevation of external K^+ (cf Pfaffinger, 1985; Kurachi et al, 1986a). Therefore, the current activated by muscarine, adrenaline or NPY is consistent with an agonist-regulated flux through a population of inwardly-rectifying K^+ channels.

3.1.1. Nature Of The Agonist-Sensitive, Inwardly-Rectifying K^+ Channel.

The inwardly-rectifying current described in this thesis is similar, in many respects, to the agonist-induced inwardly-rectifying K^+ (I_{AIR}) current observed in frog atrial cells (Pfaffinger et al, 1985; Simmons and Hartzell, 1987). It is also similar to the 'background' or 'anomalous' inward-rectifier (I_{IR}) shown in other neuronal tissues: olfactory cortex (Constanti and Galvan, 1983), submucous plexus (Mihara et al, 1987), locus ceruleus (Osmanovic and Shefner, 1987; Williams et al, 1988a),

and dorsal raphe (Williams et al, 1988b) and in a variety of non-neuronal tissues: skeletal muscle (Adrian et al, 1970), egg cell (Hagiwara et al, 1976; Ohmori, 1978) and cardiac muscle (Hutter and Noble, 1960).

- a) Does I_{AIR} and I_{IR} flow through the same or distinct channel proteins?

A controversy exists as to whether the background and the agonist-induced, inwardly-rectifying currents utilize the same K^+ channel or distinct K^+ channels in cardiac myocytes such that dissimilarities between the two currents (see below) could be explained by an agonist-induced modulation of channel characteristics (for review see Löffelholz and Pappano, 1985).

Evidence supporting the involvement of one channel type is as follows: I_{AIR} and I_{IR} have identical single channel conductances (≈ 40 pS in 140mM K^+ ; Sakmann et al, 1983). Activation curves and inward rectification shifts according to changes in $[K^+]_o$ (Pfaffinger et al, 1985; Kurachi, 1985) and similar channel rectification mechanisms exist (Mg^{2+} and voltage-regulated; Kurachi, 1985; Matsuda et al, 1987; Ishihara et al, 1989). Furthermore, channel open time kinetics of resting I_{IR} in mammalian sino-atrial nodal cells are similar to those activated by ACh (Sakmann et al, 1983; Soejima and Noma, 1984; Kurachi et al, 1986a). Pharmacologically, both channels are sensitive to aminopyridines, cesium, and high concentrations of barium (Cook, 1988; Castle et al, 1989).

However, there is also evidence for the existence of distinct channel proteins. A second class of I_{IR} channels that are observed in nodal tissue have slower mean open time duration (50ms) than that measured for the ACh-sensitive channel (1.8ms) (Sukmann et al, 1983). The steady-state outward current via the I_{IR} reaches a maximal outward current at about 10mV positive to E_R and then deactivates as the membrane is stepped to more positive potentials (see Pennefather and Cohen, 1990), whereas steady-state ACh-induced current is constant at potentials positive to E_R (Kurachi et al, 1986a; Simmons and Hartzell, 1987). The only pharmacological evidence for distinct channel proteins is reflected by a differential sensitivity to low concentrations of barium where $5\mu M Ba^{2+}$ evokes a time-dependent blocking effect on the I_{IR} but a time-independent block on the ACh-induced I_{AIR} (Carmeliet and Mubagawa, 1986).

The main problem which has lead to this controversy is the fact that these two currents do not co-exist in mammalian cardiac tissue to an extent which would permit a clear study to be performed. However, a very recent paper by Clark and coworkers (1990) have reported that a large I_{IR} and an ACh-activated I_{AIR} co-exist in dissociated bullfrog atrial myocytes. These authors convincingly showed that I_{AIR} was not simply a modulated I_{IR} by showing differences in conductance measurements, mean open channel time, sensitivities to N-ethylmaleimide, GTP and GTP- γ -S. Furthermore, I_{AIR} required the presence of GTP, whereas I_{IR} was observed in the absence of GTP in inside-out patches. This may explain why Pfaffinger et al

(1985) reported an absolute requirement for GTP in inside-out patches to observe an ACh-induced I_{ACh} in atrial cells, whereas in the present experiments a GTP-fortified internal solution was not required to observe muscarine-induced I_{AIR} via WCR in intact neurons (see Results).

b) The nature of agonist-sensitive inwardly-rectifying K^+ current.

The I_{AIR} induced by the application of muscarine, adrenaline or NPY appear to flow through the same population of inwardly-rectifying K^+ channels. These channels, like I_{AIR} channels in the heart, cannot be opened by voltage in the absence of an appropriate agonist. This is exemplified by the lack of rectification observed in control I/V plots at very negative potentials (see Figures 21, 27, 28, 29 & 30) and argues against an I_{IR} existing in RPSG neurons.

The mechanism for agonist-induced inward rectification is not well understood. Matsuda et al (1987) and Ishihara et al (1989) suggested that both a voltage-dependent Mg^{2+} block and a voltage-dependent gating mechanism regulate I_{IR} . Although, a similar effect of Mg^{2+} is reported for the muscarine-induced I_{AIR} in guinea pig heart cells, the effect of Mg^{2+} on C-cell inward rectification was not addressed in the present study. However, the rate of activation of muscarine-induced I_{AIR} appears to depend on the holding potential. Figure 24 shows the muscarine-induced I_{AIR} activated slowly ($\tau=172ms$) when V_H was $-30mV$ ($\tau > 100ms$; cf Simmons and Hartzell, 1987; Breitwieser and Szabo, 1988; Tatsumi et al, 1990)

and was virtually instantaneous when $V_H = -70\text{mV}$ ($\tau < 10\text{ms}$; cf Simmons and Hartzell, 1987; Breitwieser and Szabo, 1988; Williams et al, 1988 a & b; Tatsumi et al, 1990). These observations are consistent with the notion that hyperpolarization reduces the Mg^{2+} block of inwardly-rectifying K^+ channels. Another mechanism suggested for the voltage-dependent change in activation kinetics is that the binding of activated G-protein to the inwardly-rectifying K^+ channel may be enhanced by hyperpolarization (Horie and Irisawa, 1987 & 1989). It is also possible that both mechanisms co-exist to control the K^+ flux through these inwardly rectifying channels; Mg^{2+} -block to limit outward current at positive potentials and voltage-dependent G-protein-channel interaction to maximize current at hyperpolarized potentials.

c) Agonist-sensitive inwardly-rectifying K^+ channels.

Prior to this study, the K^+ channels involved in the generation of the muscarine-induced hyperpolarization had not been quantitatively described in frog sympathetic ganglion C-neurons. Evidence obtained from a variety of neuronal preparations suggests that the activation of a similar population of agonist-sensitive inwardly-rectifying K^+ channels is likely a common mechanism for the generation of all neuronal s-IPSPs (North, 1989). However, the physiological neurotransmitter governing slow synaptic potentials vary from tissue to tissue. For example, the s-IPSP occurring in rat locus ceruleus neurons is governed by noradrenaline activating

α_2 -adrenoceptors (Egan, 1983; North et al, 1987; Williams et al, 1988a; North, 1989), by ACh stimulation of muscarinic receptors in mudpuppy heart ganglion (Hartzell et al, 1977) and by serotonin activation of 5-HT_{1A} receptors in guinea pig prepositus hypoglossi (Bobker and Williams, 1990).

Studies on synaptic transmission often include additional reports of postsynaptic inhibitory effects that are induced by exogenous application of chemically and structurally unrelated neurotransmitters or neurotransmitter-like substances. For example, synaptically-released noradrenaline induces a s-IPSP in guinea pig submucous neurons (Surprenant, 1984), however a similar effect was elicited by exogenous application of opiates or somatostatin (Tatsumi et al, 1990). A similar opiate action was reported to occur in rat locus ceruleus neurons (North et al, 1987). In the present study muscarine, NPY and adrenaline all produced a similar response whereas, of these three agonists, only ACh release from pre-ganglionic terminals has been unequivocally demonstrated.

It is possible that circulating hormones, neurotransmitters and drugs modulate cellular excitability through a variety of cell surface receptors, independent of synaptically-released neurotransmitter. This could perhaps address the question of why such an abundance of distinct receptor types exist on neurons. Is this wide spread phenomenon merely a redundant synthesis and maintenance of a wide variety of receptors to react under unusual or abnormal physiological conditions? Alternatively, does the cell produce a universal means for altering excitability such that specialized cellular functions are governed, and transduction mechanisms

reinforced, by the particular neurotransmitter released from the presynaptic terminal? If the later possibility is valid, do neurons display a degree of plasticity to respond to other synaptically released neurotransmitters, for example in cell culture or in transplantation experiments?

3.1.2. Examination Of The Transduction Mechanism For The Activation Of I_{AIR} .

a) General observations.

The application of muscarine, adrenaline, or NPY likely utilizes a very similar, if not the same, transduction mechanism in the generation of I_{AIR} in dissociated C-cells. The striking similarities of the ionic mechanism, time course, voltage-dependence, latency and magnitude of the current induced by all three agonists is consistent with the possibility that the only distinction between these responses occurs at the receptor level. Occlusion experiments supported this notion (see Figures 45 & 54).

b) Evidence for G-protein involvement.

The irreversible activation of the inwardly-rectifying K^+ current by the inclusion of a non-hydrolyzable GTP analogue, GTP- γ -S, in the patch pipette

confirmed that I_{AIR} was G-protein coupled. One interesting aspect of this study was the necessity of agonist application prior to a definable onset of irreversible current activation. In contrast, GTP- γ -S is reported to cause a relatively slow activation of I_{AIR} independent of agonist addition in mammalian atrial myocytes (Kurachi et al, 1986a), CNS neurons (Trussel and Jackson, 1987) and submucous plexus neurons (Tatsumi et al, 1990). This effect is not a consequence of slow diffusion of GTP- γ -S from the pipette into the cell, since flash photolysis of caged GTP- γ -S evoked a similar slow onset (Dolphin et al, 1987). It is known that a slow GTP/GDP exchange rate at the G-protein occurs in the absence of an appropriate agonist, and receptor activation markedly increases this exchange to account for the rapid effect of GTP- γ -S subsequent to agonist application (Breitwiesser and Szabo, 1988). In the present study, however, there appeared to be an absolute requirement for an appropriate receptor stimulation of C-cells, since GTP- γ -S did not concomitantly suppress C-cell I_{AIR} . This current was clearly suppressed by addition of either LHRH or PMA. Irreversible activation of C-cell LHRH induced I_{AIR} suppression was not tested in the presence of a non-hydrolyzable GTP analogue in present study.

It is possible that the use of higher concentrations of GTP- γ -S would produce a slow activation of I_{AIR} . However, use of data obtained from such experiments would be questionable since any mechanism that is G-protein coupled would also be irreversibly activated by GTP- γ -S. It therefore seemed more reasonable to examine the effect of GTP- γ -S under receptor-activated conditions.

One aspect in which I_{AIR} in frog sympathetic neurons differs from that occurring in mammalian neuronal and cardiac tissue is that mammalian I_{AIR} is PTX-sensitive (Pfaffinger et al, 1985; Kurachi, 1986a; North et al, 1987; Williams et al, 1988a). In the present study, electrophysiological methods showed a lack of an effect of PTX on a variety of synaptic and drug responses (see Figure 26). These responses included muscarinic and adrenergic hyperpolarization and s-IPSP that are generated by activation of agonist-sensitive inwardly-rectifying K^+ channels (North, 1989). Similarly, no ADP-ribosylation of PTX treated RPSG membranes was reported by Pfaffinger (1988) in his detailed biochemical and electrophysiological study of the M-current. Perhaps a slightly different G-protein exists in the frog ganglia which functions in a similar manner to that observed in mammalian tissue but lacks the PTX-sensitive cysteine ribosylation site.

c) Analysis of the involvement of various signal transduction pathways in the generation of I_{AIR} .

Phosphatidylinositide pathway. Direct delivery of IP_3 via the patch pipette or bath application a phorbol ester (PMA) did not mimic the C-cell I_{AIR} . Since the 'assay' for a direct involvement was simply whether or not an inwardly-rectifying K^+ current appeared (in the absence of an agonist) these results argue strongly against any direct involvement of the phosphatidylinositol pathway in the generation of muscarine-, adrenaline- or NPY-induced I_{AIR} .

Evaluation of the role of Ca^{2+} -dependence in the generation of C-cell responses. Experiments performed prior to the characterization of I_{AIR} by WCR, tested the possibility that the muscarine-induced hyperpolarization was mediated by a Ca^{2+} -activated K^+ conductance (Cole and Shinnick-Gallagher, 1984).

Sucrose-gap experiments showed a lack of direct Ca^{2+} involvement in the generation of muscarine-induced hyperpolarization in RPSG. Ca^{2+} -sensitive K^+ channel blockers (apamin or dTC) or blockers of Ca^{2+} release (dantrolene) did not significantly attenuate the muscarine-induced hyperpolarization in isolated RPSG (see Table 3). Interestingly, the strong effect of 4-AP is consistent with the blockade of agonist-sensitive, inwardly-rectifying K^+ channels (see Cook, 1988; Castle et al, 1989) and also with the strong attenuation of adrenaline-induced hyperpolarization reported in isolated RPSG (Rafuse, 1985).

Evaluation of the role of adenylate cyclase inhibition in C-cell responses. The α_2 -adrenoceptor is thought to be negatively coupled to adenylate cyclase via G_i and a reduction in $[\text{cAMP}]_i$ has been proposed to lead to physiological responses observed in CNS neurons (Andrade and Aghajanian, 1985; Aghajanian and Wang, 1987; Wang and Aghajanian, 1987). This hypothesis was re-evaluated using WCR and sucrose-gap recording where the results were compared to those obtained from a concurrent biochemical study. This permitted functional studies to be conveniently correlated with actual drug-induced effects on $[\text{cAMP}]_i$ as measured by RIA.

There was no evidence for a positive correlation between the ability of drugs to elevate $[cAMP]_i$ (measured biochemically) and in their ability to attenuate the adrenaline-induced hyperpolarization measured via the sucrose-gap technique.

Chronic and acute PTX-exposure on isolated ganglia failed to attenuate adrenaline- or muscarine-induced hyperpolarizations (see [Table 5](#) and [Figure 25](#)). However, PTX-sensitivity of G_i determined by RIA was somewhat more difficult to interpret. In [Figure 46](#), the addition of adrenaline reduced forskolin-induced cAMP accumulation. If the same experiment was performed in the presence of PTX, adrenaline was apparently ineffective in reducing cAMP content. These results, taken alone, would be consistent with PTX-sensitivity. However, further examination of the data questioned this interpretation because PTX pre-treatment alone reduced the accumulation cAMP to a similar value as forskolin-adrenaline or forskolin-adrenaline-PTX. This would mean that the G-protein was PTX-insensitive and is in agreement with results reported by Pfaffinger (1988) who could not identify a PTX-sensitive substrate in the frog ganglia membranes (although a substrate in frog brain membranes was found and used as a control).

WCR experiments provided another line of evidence to argue against any involvement of adenylate cyclase inhibition in the generation of inhibitory responses in frog ganglia. The inclusion of cAMP ($100\mu M$) in the internal solution failed to prevent muscarine- and adrenaline-induced outward currents in C-cells. Moreover, the inclusion of cAMP in the patch pipette markedly increased the likelihood of

r controlling an I_{AIR} in a given C-cell (see Table 2); to the extent that cAMP was routinely used in all experiments where agonist-induced effects were studied.

Evidence is currently accumulating which suggesting that cyclic nucleotides are required to maintain proper ion channel function (Catterall, 1988). For example, cAMP-dependent phosphorylation sites have been identified and their functional significance accessed by site-directed mutagenesis of Ca^{2+} channels. Such findings bring to rise the important role that the intracellular environment plays in the maintenance and control of cellular physiology. Moreover, results from such studies may help explain the phenomena of receptor desensitization, affinity, efficacy, or why channel kinetics are slower when, for instance, cloned delayed rectifier K^{+} channels are expressed in artificial systems (Christie et al, 1990; Koren et al, 1990). These are obviously important matters that need to be addressed in the future in the interpretation of reports of transduction mechanisms obtained using the patch clamp recording technique.

Other possible second messengers not likely involved in the generation of C-cell I_{AIR} .

ATP. Recently, an ATP-sensitive inwardly-rectifying K^{+} channel ($K_{(ATP)}$) has been described in cardiac muscle, pancreatic β -cells, cortical neurons and arterial smooth muscle (Stanfield, 1987; Quast and Cook, 1989). Since $K_{(ATP)}$ channels are blocked by $[ATP]_i$, they tend to open when intracellular ATP reaches low levels. A

suggested physiological role in cardiac tissue for this current is to shorten the cardiac action potential and hyperpolarize myocytes during ischemic conditions. Perhaps the most important role for $K_{(ATP)}$ channels is the control of insulin release from pancreatic β -cells where, unlike in cardiac tissue or neurons, these channels contribute to the resting membrane potential (De Weille et al, 1989; Peterson and Dunne, 1989).

It is therefore conceivable that muscarine somehow reduces $[ATP]_i$ and thereby activates an $I_{K(ATP)}$. However, this is unlikely because inward rectification did not spontaneously develop in cells that were studied without ATP included in the patch pipette. Furthermore, single channel analysis of ATP-sensitive inwardly-rectifying channels showed that these channels were distinct from those that generate I_{AIR} in bullfrog atrial myocytes (Clark et al, 1990).

cGMP. A large amount of electrophysiological data exists to argue against any involvement of cGMP in the generation of s-IPSP, or other slow postsynaptic potentials in mammalian or amphibian sympathetic ganglia (Dunn et al, 1977; Gallagher and Shinnick-Gallagher, 1978; Busis et al, 1978; Weight et al, 1978; Smith et al, 1979; see Weight, 1983). These authors did not deny that a measurable elevation of ganglionic cGMP or increased protein phosphorylation occurred in postsynaptic neurons subsequent to synaptically-released ACh (Greengard, 1976), but that the two phenomena are likely not related. The elevation of cGMP probably has other functions independent of slow postsynaptic potentials (see Hille,

1989). For example, a second messenger role for cGMP-mediated inhibition of Na^+ channels has been recently reported in renal inner medullary collecting duct cells, where external application of atrial natriuretic factor or dibutyl-cGMP to outside-out patches mimicked cGMP application to inside-out patches (Light et al, 1989).

Arachidonic acid (AA) or its metabolites. Recently, interest has been generated due to reports that external application of AA opens inwardly-rectifying K^+ channels in mammalian atrial myocytes (Kim et al, 1989; Kurachi et al, 1989). Furthermore, these authors showed that application of AA to inside-out patches could not evoke a response but metabolites of the lipoxygenase pathway (H-PETEs, LTC_4 and LTA_4) could, even subsequent to PTX pre-treatment. Moreover, Kim and coworkers (1989) reported direct activation of this current by application of purified $\text{G}_{\beta\gamma}$ subunit. These authors also showed that a phospholipase A_2 antibody blocked the AA-induced effect but not the ACh- or $\text{GTP-}\gamma\text{-S}$ -induced current activation. These data seemingly provide support for the involvement of AA in the generation of I_{AIR} . However, a second messenger role for AA in the generation of a muscarine-induced inhibition (latency of current onset 0.2s; see Results) is unlikely for the following reasons. Kim and co-workers (1989) reported that: 1) The effect of bath-applied AA appeared after minutes (up to 5 minutes) of application. 2) Bath-application of AA activated single channel recordings were obtained using the cell-attached mode. These results imply a remote stimulus site for AA relative to the ion channel, 3) No effect on channel activity was observed

when AA was included in the patch pipette, and 4) AA-induced I_{AIR} is not PTX-sensitive whereas ACh-induced I_{AIR} is sensitive to this toxin in mammalian heart cells (Kurachi et al, 1986). These results clearly deviate from the intimate coupling which the ACh- or adenosine-activated I_{AIR} displays (Pfaffinger et al, 1985; Kurachi et al, 1986a). Therefore, AA produces an interesting effect which might be involved in a long term modulation of I_{AIR} , however a direct involvement in the generation of the muscarine-, adrenaline- or NPY-induced effect in Rana pipiens C-cell would be unlikely.

Evaluation of a direct coupling transduction mechanism for C-cell I_{AIR} . The activation of I_{AIR} by the addition of GTP- γ -S confirmed the hypothesis that muscarinic responses, in general, are mediated by G-proteins (Gilman, 1987; Pfaffinger, 1988; Brown et al, 1989; North, 1989). However, I_{AIR} could not be mimicked or attenuated by pharmacological intervention at loci subsequent to the G-protein level. This current was not attenuated by protein kinase inhibitors H-7 and GST (at about 10X's K_i ; Hidaka et al, 1984; Parente et al, 1989), by elevation of cAMP, nor was it mimicked by the addition of IP, or PMA. The elevation of cGMP, ATP, or activation of AA pathway are also unlikely candidates (see above). There are, however, a few other remaining possibilities which could adequately explain these observations: 1) A direct activation of inwardly-rectifying K^+ channels that is similar in many respects to the ACh- or adenosine I_{AIR} current in mammalian atrial cells (Pfaffinger et al, 1985; Kurachi et al, 1986a; Logothetis et al, 1987;

Yatani et al, 1987; Breitwieser and Szabo, 1988), 2) Utilization of a yet unidentified soluble second messenger, or 3) A dephosphorylation mechanism involving a phosphatase rather than a kinase (Pfaffinger et al, 1988). These questions remain to be resolved, however, striking similarities exist between the activation kinetics of C-cell I_{AIR} with those reported for I_{AIR} in atrial cells (Simmons and Hartzell, 1987) and rat locus ceruleus neurons (Williams et al, 1988a; Miyake et al, 1989). Furthermore, single channel studies on atrial and locus ceruleus cells indicate that similar direct coupling mechanisms exist and likely govern inhibition observed in both of these tissues (Pfaffinger et al, 1985; Miyake et al, 1989). Although this aspect was not tested by single channel analysis on C-cells in this study, the evidence presented is most consistent with direct G-protein coupling to the inwardly-rectifying K^+ channel.

It is well documented that a variety of neurotransmitters are capable of opening the same population of inwardly-rectifying K^+ channels. For example, in rat locus ceruleus and submucous plexus neurons, the addition of noradrenaline initiates an inhibitory that mimics synaptic inhibition (see North et al, 1987; Williams et al, 1988a; Miyake et al, 1989). However, these authors also showed that exogenous application of somatostatin or opiates mimic the noradrenaline effect and occlusion experiments were consistent with the activation of the same population of ion channels by the three agonists. Similar results were found on C-cells in the present study, where muscarine, adrenaline and NPY were all effective in activating an I_{AIR} . One aspect which appeared consistent among the C-cells studied was the relative

ability for each of these agonists to produce current. One might then ask, how do these observations relate to the efficacy of the coupling mechanism? Of these three agonists tested, muscarine always produced the largest and most consistent I_{AIR} . However, all three agonist-induced currents activated with a comparable time course. This might suggest an equivalent proximity of each of the receptors to G-protein and the inwardly-rectifying channel. Although convergence of agonist-induced I_{AIR} was demonstrated by occlusion experiments (Figures 45 & 54), it could not be determined whether the effect occurred at the level of the G-protein or at the level of the ion channel. Therefore, it is plausible that coupling could occur via a highly mobile G-protein that is capable of interacting with each of the three receptors, or alternatively through distinct G-proteins that are specific to each receptor. Although this particular model would be classified as a 'remote sensor' by definition (Hille, 1984), the rapid activation these responses (likely facilitated by the close association of the receptor, G-protein and ion channel) combined with the lack of involvement of soluble second messengers suggests that a term such as an 'associate' or 'proximate' sensor might be more appropriate to describe a directly-coupled transduction mechanism.

3.1.3. Examination Of The Muscarinic Receptor Subtype Governing The C-Cell I_{AIR} .

Pirenzepine. The M_1 antagonist pirenzepine exhibited an unexpected selectivity for the muscarine-induced hyperpolarization in BFSG (see Figure 19). In much of the previous literature, pirenzepine selectively blocked muscarinic depolarization (Brown et al, 1980; Newberry et al, 1985) and the s-EPSP (Ashe and Yaroshi, 1984). This led to a hypothesis that M_1 receptors mediated depolarizing responses in ganglia. Conversely, a recent study in BFSG showed that the s-IPSP was more sensitive to pirenzepine than the s-EPSP (Yavari and Weight, 1987).

The pA_2 value for pirenzepine antagonism of the muscarine-induced hyperpolarization was 7.98 ($K_d = 10.58\text{nM}$, geometric range $5.64 \leq x \leq 15.52 \text{ nM}$, slope: 1.02 ± 0.06 , $n=7$). Therefore, the receptor that initiated this response would be classified as an M_1 receptor by the existing nomenclature.

AF-DX 116 is a tricyclic compound which differs slightly from pirenzepine in structure that discriminates between M_2 and M_3 muscarinic receptors in binding studies (Hammer et al, 1986; Engel et al, 1987). The characterization of muscarinic receptors by functional studies usually include the antagonism of atropine with either AF-DX 116 or pirenzepine, but very few studies quantitate the antagonism of both AF-DX 116 and pirenzepine on the same response.

In the present study, AF-DX 116 attenuated the muscarine-induced hyperpolarization at nanomolar concentrations ($pA_2=7.78$, $K_D=17.1\text{nM}$; geometric range $9.9 \leq x \leq 28.6\text{nM}$, $n=7$). However, the antagonism was non-competitive

since $pA_2 - pA_{10} = 1.15 \pm 0.05$ ($n=7$) is statistically different from the desired value of 0.95 (Schild, 1947). Therefore, the apparent high affinity value should be regarded with some caution in frog sympathetic ganglia or in other tissues where competitiveness is not reported.

The nature of the apparent non-competitive action of AF-DX 116 remains to be determined. However, the non-competitive effect of gallamine in cardiac tissue is well established (Stockton et al, 1983; Dunlap and Brown, 1983; Nedoma et al, 1985; Jagadeesh and Sulakhe, 1985; Birdsall et al, 1987). In this study, $10\mu\text{M}$ gallamine reversibly reduced the muscarine-induced hyperpolarization to about 20% of control and $50\mu\text{M}$ gallamine totally blocked this response. Gallamine is thought to bind allosterically to the muscarinic receptor (Birdsall et al, 1988). However, it is conceivable that gallamine could render its effect by acting directly on the inwardly-rectifying K^+ channel. This notion would be consistent with results obtained from this study and with previous reports where gallamine consistently and selectively blocked the s-IPSP in both amphibian and mammalian sympathetic ganglia. This contrasts with the different effects of the competitive antagonist pirenzepine has on slow PSPs in mammalian and amphibian ganglia (Ashe and Yarosh, 1984; Newberry et al, 1985; Newberry, 1988; Yavari and Weight, 1987).

3.2. RESPONSES OCCURRING ONLY IN B-CELLS.

The agonist-induced response that warranted the most detailed study in B-cells was the muscarine-induced I_M inhibition since suppression of this current by synaptically-released ACh contributes to the generation of B-cell s-EPSP in frog ganglia (Tosaka et al, 1968; Nishi et al, 1969; Weight and Votova, 1970; Kuba and Koketsu, 1976; Adams and Brown, 1980). Therefore, experiments performed on dissociated B-cells attempted to mimic this ACh-induced response and elucidate its transduction mechanism.

3.2.1. Examination Of The Transduction Mechanism For I_M Suppression.

a) Ionic mechanism.

The suppression of the outward flux of K^+ by muscarine in Rana pipiens B-cells was verified (Adams et al, 1982a) by showing a Nernstian shift in reversal potential as $[K^+]_o$ was elevated (see Figure 22; open circles).

b) Examination the involvement of various second messengers in I_M suppression.

Although the ionic mechanism for I_M suppression is well established, the exact nature of the transduction mechanism that links the activation of the muscarinic receptor to the suppression of current through these channels has remained elusive (Pfaffinger, 1988; Pfaffinger et al, 1988; Brown et al, 1989; Hille, 1989; Selyanko et al, 1990a). Biochemical studies have shown that various second messengers may be altered following treatment of ganglia with muscarinic agonists. For example, $[cGMP]_i$ is elevated (Kebabian et al, 1975), adenylate cyclase is inhibited leading to a reduction in $[cAMP]_i$ (Hulme et al, 1981), phosphatidylinosotide turnover is increased (Paterson and Volle, 1984; Bone et al, 1984; Pfaffinger, 1988) and the generation of IP_3 leads to an increase in $[Ca^{2+}]_i$ (Pfaffinger et al, 1988).

cGMP or cAMP. Microelectrode studies previously performed on ganglia showed that iontophoretically injected cAMP or cGMP, or bath application of membrane permeable c-AMP analogues (8-Br-cAMP or 8-Br-cGMP), forskolin, or phosphodiesterase inhibitors failed to mimic the effect of muscarine and argues strongly against the direct involvement these two cyclic nucleotides in I_M suppression, membrane depolarization or s-EPSP (Dun et al, 1977; Gallagher and Shinnick-Gallagher, 1978; Busis et al, 1978; Weight et al, 1978; Adams et al, 1982b; Brown and Adams, 1987; Brown et al, 1989). In view of this vast amount of negative data, the inclusion of cGMP was not attempted in the present study. However, the inclusion of $100\mu M$ cAMP in the patch pipette clearly showed that

this relatively high concentration of cAMP did not affect the ability of muscarine to suppress I_M (see Table 2).

Phosphatidylinositol pathway. The generation of two distinct second messengers, IP_3 and DAG, would provide a simple explanation for muscarinic depolarization and hyperpolarization in mammalian ganglion neurons. Higashida and Brown (1986) showed that bradykinin induced a biphasic response in neuroblastoma cells; depolarization (attributed to I_M suppression) was mimicked by the addition of phorbol dibutyrate (PDBu) and hyperpolarization was imitated by iontophoretic injection of IP_3 . Conversely, PKC activation was not involved with I_M suppression in hippocampal CA_1 pyramidal neurons, although a PDBu-induced membrane depolarization was observed (Malenka et al, 1986).

Results from the present study confirmed an irreversible phorbol ester-induced I_M suppression that is consistent with Higashida and Brown's findings in neuroblastoma cells. However, the actual involvement of PKC activation was assessed more rigorously here by testing whether muscarine- or PMA-induced effects were blocked when protein kinase inhibitors (PKIs; H-7 or GST) were included in the patch pipette. Figures 35 and 36 show that the absence or presence of GST did not affect the ability of muscarine or PMA to suppress I_M . This argues against any direct involvement of PKC activation in I_M suppression by either muscarine or PMA. These findings are consistent with other studies on frog B-cells where an irreversible phorbol ester-induced I_M suppression was observed but

the ability of LHRH or Substance P (SP) to suppress I_M was unaffected (Brown and Adams, 1987; Pfaffinger et al, 1988; Bosma and Hille, 1989). Although both series of experiments argued against direct PKC involvement in agonist-induced I_M suppression, there was an inconsistency between results from the present study and those of Bosma and Hille (1989) who reported that staurosporine (Tamaoki et al, 1986), PKC pseudosubstrate peptide (House and Kemp, 1987) and H-7 attenuated phorbol ester-induced I_M suppression. These effects of PKIs were not confirmed in the present study and remain to be resolved. However, the observation of a muscarine-induced I_M suppression in the presence of PKIs (at $10 \times K_i$) indicated that PKC activation was not directly involved in the suppression of this current.

IP_3 promotes Ca^{2+} release from intracellular stores (Berridge and Irvine, 1984 & 1989) and if applied intracellularly, leads to membrane hyperpolarization presumably via the activation of Ca^{2+} -sensitive K^+ channels (Higashida and Brown, 1986; Sawada et al, 1987; Brown et al, 1989). By contrast, Dutar and Nicoll (1988) showed that IP_3 suppressed I_M in hippocampal CA_1 pyramidal neurons when BAPTA or EGTA was included in the microelectrodes, these authors therefore suggested that this effect was independent of Ca^{2+} release. In the present study, the effect of intracellular application of IP_3 or the elevation of $[Ca^{2+}]_i$ were examined. There was no difference in the ability of muscarine to suppress I_M nor was the whole-cell I_M current (@ -30mV) significantly reduced whilst recording under either

condition (see Figures 38, 39 & 40). The lack of effect on I_M in IP_3 loaded cells argues against a direct action of IP_3 on ion channels (Kuno and Gardner, 1987) or IP_3 -induced Ca^{2+} release from intracellular stores to suppress this current. The ability of muscarine to suppress I_M in elevated Ca^{2+} also argues against the involvement of Ca^{2+} -dependent processes.

It could be suggested that the routine inclusion of EGTA in the internal solution might buffer IP_3 -induced release of Ca^{2+} from its stores. However, this did not appear to be the case since spontaneous miniature outward currents ('smocs') were observed in a large number of neurons under study (see Figure 31B) 'Smocs' are thought to result from the activation of Ca^{2+} -sensitive K^+ channels by transient intracellular Ca^{2+} release (Satin and Adams, 1987). Therefore, the presence of 'smocs' indicated that the concentration of EGTA used in these experiments did not completely buffer rapid Ca^{2+} transients.

Similar findings of a lack of IP_3 involvement in I_M suppression was recently reported in rat fetal SCG neurons (Brown et al, 1989). The IP_3 -induced suppression of I_M observed by Dutar and Nicoll (1988) may be specific for hippocampal pyramidal neurons, although it should be verified using the patch-slice technique (Blanton et al, 1989; Hestrin et al, 1990) so as to deliver a known concentration of the drug to the intracellular milieu rather than rely on the slow intracellular delivery of IP_3 through the small microelectrode tip opening.

Presently, biochemical experiments that have implicated the direct involvement of phosphatidylinositol turnover in a variety of physiological responses are

undergoing functional scrutiny which in most cases, including the present study, fail to reveal a causal relationship. It is increasingly obvious that application of agonists are capable of producing a co-ordinated array of biochemical changes, recently termed a 'pleiotropic' agonist effect by Hille (1989). Therefore, it must be established whether a biochemical change is directly related to the physiological response by functional studies to confirm or deny whether a direct relationship exists (see Pfaffinger et al, 1988; Zidichouski et al, 1989a; Hille, 1989; Brown, 1989).

- c) Other more speculative possibilities for the transduction mechanism for I_M suppression.

Phosphorylation/dephosphorylation mechanism. Intracellular application of the phosphatase inhibitor DPG (1mM) did not affect the amplitude or the duration of muscarine-induced I_M suppression (see Figure 41). This result not only argues against the possibility that I_M suppression involves a dephosphorylation mechanism (cf Pfaffinger, 1988) but also questions the whole concept of whether a phosphorylation/dephosphorylation mechanism is involved in agonist-mediated modulation of I_M . If the channels were closed by phosphorylation, recovery from I_M suppression would involve the removal of a phosphate group by a phosphatase. Therefore, application of muscarine in the presence of a phosphatase inhibitor might be expected to produce an irreversible suppression of I_M ; however the

experiments with DPG included in the patch pipette show that this does not happen. This conclusion is also supported by the lack of effect of H-7 and GST on agonist-induced I_M suppression because these substances also inhibit other kinases (Hidaka et al, 1984; Parente et al, 1989) that may be involved if this process involved a dephosphorylation/phosphorylation mechanism.

Two other recent experiments from this laboratory have raised further doubts as to the role of phosphorylation/dephosphorylation in agonist-induced I_M suppression. Firstly, the effect of muscarine on I_M is unchanged when alkaline phosphatase (100 μ g/ml) is included in the patch-pipette (H. Chen, unpublished observations). Secondly, the percentage depression of I_M by muscarine is unaffected by intracellular application of ATP- γ -S (1mM) (H. Chen, unpublished observations). This substance forms a stable protein thio-phosphate and promotes rapid run-down of the resting I_M (cf Simmons et al, 1990) but does not affect the ability of muscarine to reduce the same proportion of the remaining I_M .

Direct coupling via a G-protein. Agonist-induced I_M suppression in frog and rat sympathetic ganglion neurons are both mediated by a PTX-insensitive G-protein (Pfaffinger, 1988; Brown et al, 1989). The present study confirmed these results by showing that GTP- γ -S irreversibly suppressed B-cell I_M (see [Figure 35](#)) and PTX-insensitivity of the methacholine-induced depolarization in isolated BFSG (see [Figure 26](#)). In contrast to the short latency (0.2s @ -30mV) of the muscarine-induced I_{AIR} in C-cells, the rather long latency (2.2s @ -30mV) of the muscarine-

induced I_M suppression observed in B-cells is consistent with the possibility that another biochemical step, or steps, subsequent to G-protein activation may occur. However, a direct coupling of a G-protein to M-channels remains an attractive hypothesis due to recent reports of the very low single channel conductance of M-channels in rat SSG (1-2 pS; Owen et al, 1989). The slow onset of agonist-induced I_M suppression could be accounted if the G-protein has to block the conductance of a substantial number of M-channels prior the observation of a discernable effect.

3.2.2. Effects Of Adrenaline On B-Cells.

The application of adrenaline induced two distinct responses in Rana pipiens B-cells; an inward current and an outward current (independent of I_{AIR}), both of which were due to effects on I_M . In Figure 49, independent application of muscarine and adrenaline reduced steady-state currents at potentials corresponding to I_M activation range. In another B-cell, adrenaline clearly increased I_M (see Figure 50).

a) Adrenaline-induced I_M suppression in B-cells

Adrenaline is known to depolarize sympathetic ganglion neurons and this effect has been attributed to stimulation of β -adrenergic receptors (Brown and Dunn, 1983; Akasu and Koketsu, 1987; Akasu, 1988a). Akasu (1988b) showed that

adrenaline attenuated I_M , the s-EPSP and the muscarine-induced postsynaptic effect in BFSG B-cells.

In the present experiments, adrenaline also suppressed I_M but always to a much lesser extent than the muscarine-induced effect when tested on the same cell. However, the sum of the muscarine- and adrenaline-induced I_M suppression exceeded 100% (eg [Figure 40](#)). This indicated that some M-channels were sensitive to both agonists. I_M is inhibited by a variety of neurotransmitters, peptides and drugs (see Introduction). Furthermore, much of the recent data obtained from frog ganglia suggests that the transduction mechanism is likely the same subsequent to independent receptor activation (Pfaffinger et al, 1988; Pfaffinger, 1988; Bosma and Hille, 1989). If this were the case then the adrenaline-induced depression of s-EPSP reported by Akasu (1988b) could be construed as an occlusion effect. This notion is consistent with the results obtained in the present study where inward current evoked by 100 μ M adrenaline was always much smaller (for example see [Figure 49](#)) and occurred much less frequently than inward current evoked by 10 μ M muscarine (see [Figure 15B](#)).

The adrenoceptor subtype(s) governing adrenaline-induced I_M inhibition were not unequivocally determined in the present study. However, from the limited results obtained it is quite conceivable that both α - and β -adrenoceptors mediate I_M suppression in B-cells. Phenylephrine (PE) suppressed I_M in 60% of B-cells tested (6/10). These results concur with the α_1 -mediated depolarization in BFSG recently reported by Smith and coworkers (1990). However, the non-selective β -agonist

isoprenaline (INA) was also effective in reducing I_M (10/27) confirming Akasu's findings (1988a). These observations require further study with specific adrenoceptor blockers since INA also augmented I_M in 7/27 B-cells (see Table 6 and below). Unfortunately, antagonist experiments using WCR were difficult to perform since adrenaline responses in B-cells were usually small and not particularly robust. Furthermore, the chamber design and drug application system were not conducive to such studies.

b) Adrenaline-induced I_M augmentation in B-cells.

The application of adrenaline, INA and PE caused an increase in B-cell I_M . (see Figure 50 and Table 6). These findings are believed to be one of the first documented cases whereby adrenaline increases neuronal I_M . This effect may not be particularly novel since somatostatin increased I_M in hippocampal and solitary tract neurons (Moore et al, 1988; Jacquin et al, 1988). In the present study, the adrenoceptor subtype that mediated the adrenaline-induced I_M enhancement is most likely a β -subtype. The application of INA augmented I_M in 7 of 27 B-cells tested, whereas PE increases I_M in only 1 of 10 B-cells. Again, further studies using specific adrenoceptor antagonists are necessary to unequivocally identify the receptor.

- c) Are sympathomimetic-induced I_M augmentation, I_M over-recovery and the slow development of I_M upon establishment of WCR related phenomena?

The transient nature of the over-recovery and the adrenaline-induced augmentation of I_M were very similar in time course and might therefore be related (see Figures 32 & 50). However, both of the transient effects were evident after the early development of I_M . Although I_M augmentation was mimicked by application of 8-Br-cAMP in smooth muscle cells (Sims et al, 1988), it seems unlikely that the agonist-induced or over-recovery effects are due to an elevation of cAMP in RPSG neurons since cells were dialyzed with 100 μ M cAMP at the time of agonist application. However, one cannot rule out the possibility that the early development of I_M is due to cAMP loading such that quiescent M-channels become functional channels due to some cAMP-dependent process.

The phenomenon of over-recovery which occurs subsequent to agonist-induced I_M suppression by muscarine, teleost-LHRH, and Substance P in BFSG B-cells are briefly mentioned in previous studies (Pfaffinger, 1988; Bosma and Hille, 1989; Bley and Tsien, 1990). In the present study, LHRH-induced I_M suppression recovered very slowly (see Figure 42) and in some cells no recovery was observed. Furthermore, a LHRH-induced over-recovery effect was never observed in any B- or C-cells tested (Substance P was not tested). These differences might be explained by the fact that chicken-II-LHRH was used here whereas teleost-LHRH was used

in other studies where a strong over-recovery effect was observed (Pfaffinger, 1988; Bosma and Hille, 1989). Chicken-II-LHRH was used in the present study because it was shown to be the most potent form of LHRH to suppress I_M in BFSG B-cells (Jones, 1987c); however, it may be ineffective in causing I_M over-recovery.

Since Pfaffinger and coworkers (1988) found that LHRH caused a transient increase in $[Ca^{2+}]_i$, it could be suggested that the over-recovery effect is a calcium-dependent process. However, these authors eliminated the involvement of Ca^{2+} by showing that both I_M suppression and over-recovery were still evident when a high concentration of the calcium chelator BAPTA was included in the patch pipette. A similar lack of effect in the presence of BAPTA was found for the muscarine-induced over-recovery in rat SCG neurons (personal communication, N.V. Marrion and T.G. Smart).

It is possible that the mechanism by which agonists increase the M-current is a novel inhibitory neuromodulatory action that occurs subsequent to periods of intense ganglionic transmission. Therefore, it is important to characterize this effect since such a phenomenon could be regarded as a ganglionic late slow-IPSP. This concept may not be entirely novel since a small hyperpolarization sometimes follows the ganglionic ls-EPSP recorded by the use of the sucrose-gap technique (P.A Smith and F.F. Weight, unpublished observations). Although data presented in Figure 50 shows that the changes in the noise levels (from control) observed during the maximal muscarine and adrenaline responses are consistent with an increase and decrease in membrane resistance respectively. It can not be

determined directly if these effects are due an alteration in the number of functional M-channels or the K^+ flux through the existing pool of functional M-channels, since changes in K^+ flux or the number of functional low conductance M-channels would result in similar effects on the whole cell noise. This question would be best resolved using single channel analysis to see if the conductance changes occur in a step-wise or a graded manner.

3.3. EFFECTS OCCURRING IN BOTH B- AND C-CELLS.

The previous sections of this discussion focused primarily on differences that exist between sympathetic B- and C- neurons. However, in many instances, similar effects occur in the two cell types. For example, voltage-dependent currents such as I_{Na} , $I_{K(V)}$, I_C and I_M , pump currents such as Na^+/K^+ electrogenic pump, ACh-mediated f-EPSP, and LHRH mediated ls-EPSP occur in frog B- and C-cells.

3.3.1. I_M inhibition by LHRH.

LHRH-like peptide is synaptically-released from C-fiber terminals and initiates the ls-EPSP in both B- and C-neurons (Jan and Jan, 1982). In the present study, c-II-LHRH suppressed I_M in both cell types whereas muscarine suppressed I_M in B-cells only. However, LHRH and PMA suppressed I_M to about the same extent in both cell types. This suggests that transduction mechanisms for I_M

suppression exist in both cell types and that C-cell muscarinic receptors are not capable of coupling to C-cell M-channels. This notion is supported by the fact that an ACh-activated s-EPSP is evident in B-cells only (see Introduction).

3.3.2. I_{SA} .

Many characteristics of I_{SA} were similar to I_A (cf Adams et al, 1982a). For example, the activation and inactivation curves are virtually identical, the time constants for removal of inactivation are similar, reversal potentials are both dependent on $[K^+]_o$, voltage for half-inactivation occurs at -100mV, and both are Ca^{2+} -independent currents. However, I_{SA} inactivation rate was about 80-fold slower than I_A , I_{SA} was sensitive to 4-AP whereas I_A in frog ganglia is not sensitive to this blocker (Adams et al, 1982a), I_{SA} appeared in a number of C-cells that did not exhibit I_A , and both currents were recorded simultaneously in B-cells (see [Figure 55B](#)), this suggested that I_{SA} is not a consequence of the deterioration or modification of I_A .

Since I_{SA} was not reduced by Cd^{2+} and was Ba^{2+} -insensitive, it was not likely generated as a result of the activation of I_C or I_M . However, TEA (3mM) produced variable effects on I_{SA} ; in some experiments no change in I_{SA} was observed and in other experiments TEA decreased the amplitude of I_{SA} . The attenuation by TEA was thought to reflect an action of the drug on I_C since TEA-sensitive noise was also reduced. These observations concur with recent reports of 4-AP sensitive,

TEA-insensitive, Ca^{2+} -independent transient outward K^+ currents with similar slow inactivation characteristics to I_{SA} described in rat hypothalamic neurons (Greene et al, 1990), rat hippocampal CA_1 neurons (Storm, 1988) and salamander retina ganglion cells (Lukasiewicz and Werblin, 1988).

Since I_{SA} increased in amplitude as recording time progressed, this may coincide with time of intracellular perfusion with internal solution. Therefore, it was possible that the slow development of I_{SA} in both B- and C-cells was due to the loss or dilution of some intracellular factor or component, that under normal circumstances, prevents the activation of this current. However, attempts to prevent the appearance of I_{SA} by the inclusion of ATP, GTP, cAMP, IP_3 , GST, H-7 or DPG in the patch pipette were unsuccessful. An interesting correlate to this hypothesis is that it was recently shown that cloned rat brain and rat muscle I_{KV} channels expressed in frog oocytes and studied by whole-cell or single channel recording exhibited very slow inactivation kinetics lasting seconds in duration (Christie et al, 1990; Koren et al, 1990). Conceivably the expression of these channels in oocytes cannot mimic the normal environment that these channel ordinarily reside.

Perhaps the most interesting electrophysiological aspect of the I_{SA} was that it was reversibly augmented by muscarine in freshly patched B- and C-cells (see Figure 58C). The phenomena of agonist-induced modulation of voltage-dependent currents was originally thought be quite a novel concept when the M-current was initially described (Adams and Brown, 1980). However, in recent years, a number of other voltage-dependent K^+ -currents are reported to be agonist-sensitive. For

example, adrenoceptor activation via β -receptor enhanced $I_{K(V)}$ in atrial myocytes (Tsien et al, 1972; Reuter, 1974; Kass and Tsien, 1976; Giles et al, 1989), and α_1 -receptor activation reduced cardiac transient outward current (Fedida et al, 1990) whilst β -adrenoceptor activation enhanced this same current (Nakayama et al, 1989). Muscarinic receptor stimulation is reported to shift i_f activation curve to more negative potentials in sino-atrial node myocytes (DiFrancesco and Tromba, 1988 a & b) and to enhance I_A in neostriatal neurons (Akins et al, 1990).

The muscarine-induced augmentation reported in the present study was not simply due to an improvement in space clamp since I_{SA} was not observed in the presence of Ba^{2+} alone but could be induced by the addition of muscarine (in Ba^{2+} Ringer's) (see [Figure 59](#)). Since muscarine receptor binding was not decreased by hyperpolarization, it argues against the possibility that muscarine unbinds during the step to -110mV and that the apparent I_{SA} enhancement results from a transient increase in I_M until muscarine re-binds to re-suppress I_M .

It remains possible that the activation of the delayed rectifier ($I_{K(V)}$) might explain the appearance of this transient outward K^+ current. It was originally not considered a possibility since precautions were taken so as to hold cells at potentials negative to the activation of $I_{K(V)}$ and only step in the negative direction. In view of the intermittent sensitivity of $I_{K(V)}$ to TEA observed in the present study and a recent report of a sensitivity of the delayed rectifier to aminopyridines in BFG B-cells (Goh and Pennefather, 1989), it remains possible that $I_{K(V)}$ might

activate under WCR conditions. Since internal perfusion with patch pipette solution during WCR is thought to cause a shift in activation curves to more negative potentials (Marty and Neher, 1983), it is conceivable that voltage commands from negative potentials to -30mV may have slightly activated this large outward K^+ current. Note that the activation curve for I_M in B-cells was shifted by about -15mV (cf Adams et al, 1982a; see Figure 17 and Table 1). If a similar shift occurred for $I_{K(V)}$, the current would activate at -40mV and could account for the appearance of a slow transient outward K^+ current observed at -30mV. Furthermore, I_{SA} and $I_{K(V)}$ have similar slow inactivation kinetics.

An alternative interpretation of the slow inactivation kinetics of $I_{K(V)}$ might be due to a co-activation of I_{SA} and $I_{K(V)}$. A recent report by Clark et al (1990) showed that the threshold for $I_{K(V)}$ activation in bullfrog parasympathetic neurons was about -50mV and once activated, the current slowly inactivated. However, if the command was stepped to negative potentials within a few hundred milliseconds of $I_{K(V)}$ activation, an instantaneous reduction of outward current is followed by a slowly inactivating outward tail current but if the cell is held at depolarized potentials for a number of seconds subsequent to $I_{K(V)}$ activation and then returned to negative potentials, the tail current was not evident. This may reflect the activation of two currents and the deactivation of one or two currents depending on the time held at depolarized potentials. It would be interesting to test the degree to which $I_{K(V)}$ inactivates in freshly patched cells since I_{SA} gradually increases as recording time proceeds.

In summary, some interesting effects on this transient outward current were shown but it remains to be resolved if I_{SA} and $I_{K(v)}$ are distinct currents. Regardless of whether I_{SA} and $I_{K(v)}$ co-exist or if $I_{K(v)}$ is simply modified by WCR conditions, the fact remains that muscarine was capable of inducing a transient outward K^+ current in freshly patched RPSG B- and C-cells and should therefore be included when describing cholinergic mechanisms occurring in frog sympathetic ganglia.

4. SOME QUESTIONS FOR FUTURE STUDY.

4.1. I_{AIR} IN C-CELLS.

Evidence presented in this thesis is consistent with the notion that C-cell I_{AIR} , which was activated by muscarine, adrenaline and NPY, is governed by a direct coupling mechanism. The next logical step would be to verify this belief using single channel patch clamp recording methods. Cell-attached patch configuration (Hamill et al, 1981) with and without muscarine contained in the patch electrode and the monitoring channel activity in the cell-attached mode during application of muscarine to the cell body would resolve this question. Providing I_{AIR} is indeed directly-coupled, isolated membrane patches should then be used to fully characterize their single channel conductance and also examine the means by which the transduction occurs. For example, application of various preactivated G-proteins or a series of recombinant G_α subunits could be easily administered to inside-out

patches to determine which G-proteins are capable of activating the channel (see VanDongen et al, 1988). An outside-out configuration could perhaps address how muscarine, adrenaline and NPY were all capable of activating the I_{AIR} with a similar latency. Does this indicate that the three receptors are similarly located with respect to the G-protein and channel proteins? If so, can two or more agonists activate I_{AIR} in the same outside-out membrane patch with the same latency? This type of study would be useful in the characterization of the 'proximate' or 'associate' sensor that was introduced in the discussion. It is known that ion channels and G-protein-coupled receptors span the entire membrane and the G-protein, which is not membrane spanning, transduces the external signal to the channel protein. Therefore, topographically, it would be interesting to determine the location of the receptors relative to the ion channel and how this relates to the fact that three distinct agonists generate I_{AIR} with a similar latency in WCR.

Another series of experiments which require serious consideration would be to attempt to use intact ganglia for patch clamp recording of synaptic events since the dissociation procedure abolished the possibility of recording synaptically-evoked s-IPSPs from C-cells. Results from such experiments could address whether the muscarine-induced I_{AIR} and current observed during a synaptically-evoked s-IPSP are due to the activation of the same population of inwardly rectifying K^+ channels involved in neuronal inhibition as suggested by North (1989).

4.2. I_M .

One of the most important questions which remains to be determined is the transduction mechanism for the suppression of I_M since it does not appear to be mediated by any of the presently described signal transduction mechanisms that were tested in the present study. Muscarine-sensitive, whole-cell noise recorded and analyzed from both frog and rat sympathetic ganglion neurons indicate that M-channel conductance was about 1-2 pS (Marsh et al, 1989; Owen et al, 1989). The next logical step would be to determine whether these channels are directly-coupled. However, the recording of single M-channels in membrane patches likely requires the refinement of single-channel recording technique to properly address this question.

The present study reported that a typical voltage-sensitive I_M existed in both B- and C-cells and that muscarinic agonists were capable of suppressing this current in B-cells only (cf Adams et al, 1982a; Jones, 1987a). However, the application of other drugs (LHRH and PMA) suppressed I_M in both cell types. This observation in C-cells could therefore be used to determine the role which receptor activation plays in the irreversible effect of membrane currents by intracellular application of GTP- γ -S. The definitive experiment would be to determine whether the C-cell I_M is irreversibly suppressed by LHRH without a concomitant activation of I_{AIR} .

The nature of the receptors governing sympathomimetic augmentation and inhibition of I_M in B-cells should be examined. Particular attention should be

devoted to the rather novel transient isoprenaline-induced I_M enhancement and whether a relationship exists with the transient increase of I_M (over-recovery phenomenon) that sometimes occurs subsequent to the application of muscarine. Furthermore, it should be determined whether the transient over-recovery is a novel late-slow IPSP; again, the use of the patch-clamp technique on intact ganglia would be the most useful technique to examine this notion.

4.3. I_{SA} .

It remains to be determined whether the I_{SA} observed in amphibian sympathetic ganglion neurons is a novel K^+ current or a WCR-induced modification of I_{KV} . These experiments should therefore be repeated in TEA Ringer's solution to attenuate I_{KV} . The modulation of this transient outward K^+ current by other neurotransmitters or neurotransmitter-like substances should be evaluated since muscarine clearly increased the amplitude I_{SA} independent of an alteration of the space clamp. Although the activation of this current is too slow to affect the shape of the action potential in these neurons, it should be determined whether this current is evident in damaged cells or in neurons that have been repetitively stimulated so as to allow for electrogenic and metabolic recovery to occur. Such a mechanism might be important in the alteration of ganglionic transmission and the coding of information to the periphery.

SUMMARY.

- 1) Whole-cell patch clamp recording, sucrose-gap recording and radioimmunoassay were used to investigate the mechanism of action of various neurotransmitters and peptides on neurons in amphibian paravertebral sympathetic ganglia.
- 2) An enzymatic dissociation procedure was developed to obtain viable Rana pipiens neurons for whole-cell recording (WCR).
- 3) Dissociated neurons were classified as B-neurons or C-neurons based on differences in their responses to application of muscarine, differences in cell body size as measured by whole-cell capacitance (C_m) and the presence or absence of a rapid transient outward current (A-current; I_A).
- 4) C-cells were small in size (mean $C_m = 21.3 \pm 0.8 \text{ pF}$, $n=70$) and lacked I_A . Application of muscarine induced a rapid, reversible inwardly-rectifying K^+ current (I_{AIR}). B-cells were larger (mean $C_m = 40.5 \pm 1.5 \text{ pF}$, $n=66$) and exhibited I_A . Application of muscarine produced inward current which was entirely attributable to the slow and reversible suppression of a non-inactivating K^+ current (I_M).

- 5) I_M was present in both cell types and was suppressed by chicken-II-luteinizing hormone releasing hormone (c-II-LHRH) and phorbol myristate-13-acetate (PMA). However, muscarine was ineffective in suppressing this current in C-cells. I_M activated at -75mV, was half activated at -52mV and the activation curve was sigmoidal reaching a maximal conductance at about -30mV. The total G_M per unit area was greater in C-cells ($1495\mu S/cm^2$) than in B-cells ($1034\mu S/cm^2$).
- 6) Agonist-induced activation of I_{AIR} and suppression of I_M involve pertussis toxin- (PTX-) insensitive GTP-binding proteins. However, inclusion of protein kinase inhibitors failed to antagonize either muscarine-induced current. Inclusion of inositol trisphosphate (IP_3) in the patch pipette failed to mimic either muscarine-induced current. B-cell I_M was not suppressed when intracellular Ca^{2+} was increased from 0.1 to $1\mu M$.
- 7) The inhibition of adenylate cyclase was not involved in the C-cell agonist-induced responses observed at the single cell level (determined by WCR) or in intact isolated ganglia, as determined by sucrose-gap recording and radioimmunoassay methods.

- 8) In view of the general lack of effect of drugs which mimic or perturb the actions of cytosolic second messengers, it is likely that both responses are mediated by direct-coupling between the receptor, G-protein and ion channel, even though the latency for agonist-induced I_M suppression (about 2s) was 10 times greater than that for activation of I_{AIR} .
- 9) In C-cells, I_{AIR} was evoked by muscarine, adrenaline and neuropeptide Y (NPY). Moreover, occlusion experiments indicated that some I_{AIR} channels were sensitive to all three agonists. In B-cells, I_M was suppressed by adrenaline, LHRH and PMA. The sum of current suppressed by independent addition of two agonists exceeded the total available I_M . Therefore, some M-channels are sensitive to more than one agonist.
- 10) Adrenaline enhanced I_M in a few (< 10%) B-cells and experiments with isoprenaline suggested this effect might be mediated by a β -receptor. Attempts to determine the identity of the adrenoceptor subtype involved in I_M suppression were not conclusive.
- 11) A slowly inactivating, transient outward K^+ current, (I_{SA}) progressively developed during WCR from B- and C-neurons. The activation and inactivation curves for I_{SA} overlapped to a very limited degree at about -55mV; therefore I_{SA} can not contribute to the setting of the resting

membrane potential. These curves were similar to those reported for I_A ; however, I_{sA} inactivated about 80 times slower than I_A . The current was attenuated by 4-AP and was Ca^{2+} -insensitive whilst the sensitivity to TEA was variable. Although I_{sA} was easily distinguished from I_A , it could not be clearly separated from the outward rectifier ($I_{K(V)}$).

- 12) Muscarine reversibly induced a I_{sA} in freshly patched cells. This effect was not due to alterations in the space clamp or to a voltage-dependent unbinding and re-binding of muscarine during hyperpolarizing voltage steps. Effects of agonists on I_{sA} (or $I_{K(V)}$) must be considered when attempting to understand neuromodulatory mechanisms in autonomic ganglia.

CHAPTER V

REFERENCES

ADAMS, P.R. The calcium current of a vertebrate neurone. In Advances in Physiological Science. Vol. 4, The physiology of excitable membranes. Ed. J. Salanki, Pergamon Press, New York, 135-138, 1981.

ADAMS, P.R. and BROWN, D.A. Ionic basis of the slow excitatory post-synaptic current in voltage-clamped bullfrog sympathetic neurones. *J. Physiol. (Lond.)*, 303, 66P, 1980.

ADAMS, P.R. and BROWN, D.A. Luteinizing hormone-releasing factor and muscarinic agonists act on the same voltage-sensitive K^+ -current in bullfrog sympathetic neurones. *Br. J. Pharmacol.*, 68, 353-355, 1980.

ADAMS, P.R. and BROWN, D.A. Synaptic inhibition of the M-current: slow EPSP mechanism in bullfrog sympathetic neurones. *J. Physiol. (Lond.)*, 332, 263-272, 1982.

ADAMS, P.R., BROWN, D.A. and CONSTANTI, A. M-currents and other potassium currents in bullfrog sympathetic neurones. *J. Physiol. (Lond.)*, 330, 537-572, 1982a.

ADAMS, P.R., BROWN, D.A. and CONSTANTI, A. Pharmacological inhibition of the M-current. *J. Physiol. (Lond.)*, 332, 223-262, 1982b.

ADAMS, P.R., CONSTANTI, A., BROWN, D.A. and CLARK, R.B. Intracellular Ca^{2+} activates a fast voltage-sensitive K^+ current in vertebrate sympathetic neurones. *Nature*, 296, 746-749, 1982c.

ADAMS, P.R., BROWN, D.A. and JONES, S.W. Substance P inhibits the M-current in bullfrog sympathetic neurones. *Br. J. Pharmacol.*, 79, 330-333, 1983.

ADAMS, P.R. and GALVAN, M. Voltage-dependent currents of vertebrate neurons and their role in membrane excitability. In Advances in Neurology, Eds. A.A. Ward Jr., D.M. Woodbury and R.J. Porter, Raven Press, New York, 44, 137-170, 1986.

- ADAMS, P.R., JONES, S.W., PENNEFATHER, P., BROWN, D.A., KOCH, C. and LANCASTER, B. Slow synaptic transmission in frog sympathetic ganglia. *J. Exp. Biol.*, 124, 259-285, 1986.
- ADRIAN, R.H., CHANDLER, W.K. and HODGKIN, A.L. Slow changes in potassium permeability in skeletal muscle. *J. Physiol. (Lond.)*, 208, 645-668, 1970.
- AGHAJANIAN, G.K. and WANG, Y.Y. Pertussis toxin blocks outward currents evoked by opiate and α_2 -agonists in locus coeruleus neurons. *Brain Res.*, 371, 390-394, 1986.
- AGHAJANIAN, G.K. and WANG, Y.Y. Common α_2 - and opiate mechanisms in the locus coeruleus: Intracellular studies in brain slices. *Neuropharmacol.*, 26, 793-799, 1987.
- AKASU, T. Adrenaline depolarization in paravertebral sympathetic neurones of bullfrogs. *Pflugers Arch.*, 411, 80-87, 1988a.
- AKASU, T. Adrenaline inhibits muscarinic transmission in bullfrog sympathetic ganglia. *Pflugers Arch.*, 413, 616-621, 1988b.
- AKASU, T., GALLAGHER, J.P., KOKETSU, K. and SHINNICK-GALLAGHER, P. Slow excitatory post-synaptic currents in bullfrog sympathetic neurones. *J. Physiol. (Lond.)*, 351, 538-593, 1984.
- AKASU, T. and KOKETSU, K. Modulation of voltage-dependent currents by muscarinic receptor in sympathetic neurones of bullfrog. *Neurosci. Lett.*, 29, 41-45, 1982.
- AKASU, T. and KOKETSU, K. Evidence for epinephrine-induced depolarization in neurons of bullfrog sympathetic ganglia. *Brain Res.*, 405, 375-379, 1987.

- AKASU, T., NISHIMURA, T. and KOKETSU, K. Substance P inhibits the action potentials in bullfrog sympathetic ganglion neurones. *Neurosci. Lett.*, 41, 161-166, 1983.
- AKINS, P.T., SURMEIER, D.J. and KITAI, S.T. Muscarinic modulation of a transient K^+ conductance in rat neostriatal neurons. *Nature*, 344, 240-242, 1990.
- ANDRADE, R. and AGHAJANIAN, G.K. Opiate and alpha-2-adrenoceptor-induced hyperpolarizations of locus ceruleus neurons in brain slices: Reversal by cyclic adenosine 3':5'-monophosphate analogues. *J. Neurosci.*, 5, 2359-2364, 1985.
- ARANLAKSHANA, A.D. and SCHILD, H.O. Some quantitative uses of drug antagonists. *Br. J. Pharmacol.*, 14, 48-58, 1959.
- ASHE, J.H. and YAROSH, C.A. Differential and selective antagonism of the slow-inhibitory postsynaptic potential and slow-excitatory postsynaptic potential by gallamine and pirenzepine in the superior cervical ganglion of the rabbit. *Neuropharmacol.*, 23, 1321-1329, 1984.
- BALUK, P. Scanning electron microscope studies on bullfrog sympathetic neurons exposed by enzymatic removal of connective elements and satellite cells. *J. Neurocytol.*, 15, 85-95, 1986.
- RANKS, B.G.C., BROWN, C., BURGESS, G.M., BURNSTOCK, G., CLARET, M., COCKS, T.M. and JENKINSON, D.H. Apamin reduces certain neurotransmitter-induced increases in potassium permeability. *Nature*, 283, 415-417, 1979.
- BELLES, B., MALECOT, C.O., HESCHELER, J. and TRAUTWEIN, W. "Run-down" of the Ca current during long whole-cell recordings in guinea pig heart cells: role of phosphorylation and intracellular calcium. *Pflügers Arch.*, 411, 353-360, 1988.

BERRIDGE, M.J. Inositol trisphosphate and diacylglycerol as second messengers. *Biochem. J.*, 220, 345-360, 1984.

BERRIDGE, M.J. and IRVINE, R.F. Inositol trisphosphate, a novel second messenger in cellular signal transduction. *Nature*, 312, 315-321, 1984.

BERRIDGE, M.J. and IRVINE, R.F. Inositol phosphates and cell signalling. *Nature*, 341, 197-205, 1989.

BIRDSALL, N.J.M., HULME, E.C., KROMER, W. and STOCKTON, J.M. A second drug-binding site on muscarinic receptors. *Fed. Proc.*, 46, 2525-2527, 1987.

BLACKMAN, J.G. Ganglionic transmission. *Proc. Australian Phys. and Pharmacol. Soc.*, 12, 64-68, 1981.

BLACKMAN, J.G., GINSBORG, B.L. and RAY, C. Synaptic transmission in the sympathetic ganglion of the frog. *J. Physiol. (Lond.)*, 167, 355-373, 1963.

BLANTON, M.G., LO TURIO, J.J. and KRIEGSTEIN, A.R. Whole cell recordings from neurons in slice of reptilian and mammalian cerebral cortex. *J. Neurosci.*, 30, 203-210, 1989.

BLATZ, L.A. and MAGLEBY, K.L. Single apamin-blocked Ca-activated K⁺ channels of small conductance in cultured rat skeletal muscle. *Nature*, 323, 718-720, 1986.

BLEY, K.R. and TSIEN, R.W. Inhibition of Ca²⁺ and K⁺ channels in sympathetic neurons by neuropeptides and other ganglionic transmitters. *Neuron*, 2, 379-391, 1990.

BOBKER, D.H. and WILLIAMS, J.T. Serotonin-mediated inhibitory postsynaptic potential in guinea-pig prepositus hypoglossi and feedback inhibition by serotonin. *J. Physiol. (Lond.)*, 422, 447-462, 1990.

- BONE, E.A., FRETTE, P., PALMER, S., KIRK, C.J. and MITCHELL, R.H. Rapid accumulation of inositol phosphates in isolated rat superior cervical ganglia exposed to V₁-vassopressin and muscarinic cholinergic stimuli. *Biochem. J.*, 221, 803-811, 1984.
- BOSMA, M.M. and HILLE, B. Protein kinase C is not necessary for peptide-induced suppression of M current or for desensitization of the peptide receptors. *Proc. Nat. Acad. Sci. (USA)*, 86, 2943-2947, 1989.
- BREITWEISER, G.E. and SZABO, G. Mechanism of muscarinic-receptor-induced K⁺ channel activation as revealed by hydrolysis-resistant GTP analogues. *J. Gen. Physiol.*, 91, 460-493, 1988.
- BROWN, D.A. Slow cholinergic excitation- a mechanism for increasing neuronal excitability. *Trends in Neurosci.*, 6, 302-307, 1983.
- BROWN, D.A. M-currents: an update. *Trends in Neurosci.*, 11, 294-299, 1988.
- BROWN, D.A. and ADAMS, P.R. Muscarinic suppression of a novel voltage-sensitive K⁺ current in a vertebrate neurone. *Nature*, 283, 673-676, 1980.
- BROWN, D.A. and ADAMS, P.R. Effects of phorbol dibutyrate on M-currents and M-current inhibition in bullfrog sympathetic neurons. *Cell. Mol. Neurobiol.*, 7, 255-269, 1987.
- BROWN, D.A., CAULFIELD, M.P. and KIRBY, P.J. Relationship between catecholamine-induced cyclic AMP changes and hyperpolarization in isolated rat sympathetic ganglia. *J. Physiol. (Lond.)*, 290, 441-451, 1979.
- BROWN, D.A., CONSTANTIN, A. and ADAMS, P.R. Slow cholinergic and peptidergic transmission in sympathetic ganglia. *Fed. Proc.*, 40, 2625-2636, 1981.

- BROWN, D.A. and DUNN, P.M. Depolarization of rat isolated superior cervical ganglia mediated by β_2 -adrenoceptors. *Br J. Pharmacol.*, 79, 429-439, 1983.
- BROWN, D.A., FORWARD, A. and MARSH S. Antagonist discrimination between ganglionic and ileal muscarinic receptors. *Br. J. Pharmacol.*, 14, 723-736, 1980.
- BROWN, D.A. and GRIFFITH, W.H. Calcium-activated outward current in voltage clamped hippocampal neurones of the guinea-pig. *J. Physiol. (Lond.)*, 337, 287-310, 1983.
- BROWN, D.A. and HIGASHIDA, H. Inositol-1,4,5-trisphosphate and diacylglycerol mimic bradykinin effects on mouse neuroblastoma X glioma hybrid cells. *J. Physiol. (Lond.)*, 397, 185-207, 1988.
- BROWN, D.A., MARRION, N.V., and SMART, T.G. On the transduction mechanism for muscarine-induced inhibition of the M-current in cultured rat sympathetic neurones. *J. Physiol. (Lond.)*, 413, 469-488, 1989.
- BROWN, D.A. and SELYANKO, A.A. Two components of muscarine-sensitive membrane currents in rat sympathetic neurones. *J. Physiol. (Lond.)*, 358, 335-363, 1985.
- BUSIS, N.A., WEIGHT, F.F. and SMITH, P.A. Synaptic potentials in sympathetic ganglia: Are they mediated by cyclic nucleotides? *Science*, 200, 1079-1081, 1978.
- CARMALIET, E. and MUBAGWA, K. Characterization of the acetylcholine-induced potassium current in rabbit cardiac purkinje fibres. *J. Physiol. (Lond.)*, 371, 219-237, 1986.
- CASTLE, N.A., HAYLETT, D.G. and JENKINSON, D.H. Toxins in the characterization of potassium channels. *Trends Neurosci.*, 12, 59-65, 1989.

CATTERALL, W.A. Structure and function of voltage-sensitive ion channels. *Science*, 242, 50-61, 1988.

CHRISTIE, M.J. and NORTH, R.A. Control of ion conductances by muscarinic receptors. *Trends Pharmacol. Sci. (suppl)*, 30-34, 1988.

CHRISTIE, M.J., NORTH, R.A., OSBOURNE, P.B., DOUGLASS, J. and ADELMAN, J.P. Heteropolymeric potassium channels expressed in xenopus oocytes from cloned subunits. *Neuron*, 2, 405-411, 1990.

CLARK, R.B., NAKAJIMA, T., GILES, W., MOMOSE, K.Y. and SZABO, G. Two distinct types of inwardly rectifying K⁺ channels in bull-frog atrial myocytes. *J. Physiol. (Lond.)*, 424, 229-251, 1990.

CODINA, J., YATANI, A., GRENET, D., BROWN, A.M. and BIRNBAUMER, L. The alpha-subunits of G_K opens atrial K⁺ channels. *Science*, 238, 442-445, 1987.

COLE, A.E. and SHINNICK-GALLAGHER, P. Alpha-adrenoceptor and dopamine receptor antagonists do not block the slow inhibitory postsynaptic potential in sympathetic ganglia. *Brain Res.*, 187, 226-230, 1980.

COLE, A.E. and SHINNICK-GALLAGHER, P. Muscarinic inhibitory transmission in mammalian sympathetic ganglia is mediated by increased potassium conductance. *Nature*, 307, 270-271, 1984.

CONNOR, J.A. and STEVENS, C.F. Voltage clamp studies of a transient outward membrane current in gastropod neural somata. *J. Physiol. (Lond.)*, 212, 21-30, 1971.

CONSTANTI, A. and BROWN, D.A. M-currents in voltage-clamped olfactory cortex neurones. *Neurosci. Lett.*, 24, 289-294, 1981.

- CONSTANTI, A. and GALVAN, M. Fast inward rectifying current accounts for anomalous rectification in olfactory cortex neurones. *J. Physiol. (Lond.)*, **335**, 153-178, 1983.
- COOK, N.S. The pharmacology of potassium channels and their therapeutic potential. *Trends Pharmacol. Sci.*, **9**, 21-28, 1988.
- COREY, D.P. and STEVENS, C.F. Science and Technology of Patch-Recording Electrodes in Single-Channel Recording, eds. B. Sakmann and E. Neher, Plenum Press, New York, 53-68, 1983.
- DAIL, W., CHOUDARY, S., BARROZA, C., MURRAY, H. and BRADLEY, C. The fate of adrenergic fibres which enter superior cervical ganglion in Histochemistry and Cell Biology of Autonomic Neurons, SIF Cells, and Paraneurons, eds. O. Eranko, S. Soinila, and H. Paivarinta, Raven Press, New York, 287-297, 1980.
- DE WEILLE, J.R., FOSSET, M., MOURRE, C., SCHMID-ANTOMARCHI, H., BERNARDI, H. and LAZDUNSKI, M. Pharmacology and regulation of ATP-sensitive K⁺ channels. *Pflugers Arch.*, **414**, (suppl. 1), S80-87, 1989.
- DIFRANCESCO, D. A study of the ionic nature of the pace-maker current in calf Purkinje fibres. *J. Physiol. (Lond.)*, **314**, 359-376, 1981a.
- DIFRANCESCO, D. Characterization of the pace-maker current kinetics in calf Purkinje fibres. *J. Physiol. (Lond.)*, **314**, 377-393, 1981b.
- DIFRANCESCO, D., FERRONI, A., MAZZANTI, M. and TROMBA, C. Properties of the hyperpolarizing-activated current (i_h) in cells isolated from the rabbit sino-atrial node. *J. Physiol. (Lond.)*, **377**, 61-68, 1986.
- DIFRANCESCO, D. and TROMBA, C. Acetylcholine inhibits activation of the cardiac hyperpolarizing-activated current, i_h. *Pflugers Arch.*, **410**, 139-142, 1987.

- DIFRANCESCO, D. and TROMBA, C. Inhibition of the hyperpolarization-activated current (i_h) induced by acetylcholine in rabbit sino-atrial node myocytes. *J. Physiol. (Lond.)*, 405, 477-491, 1988a.
- DIFRANCESCO, D. and TROMBA, C. Muscarinic control of the hyperpolarization-activated current (i_h) in rabbit sino-atrial node myocytes. *J. Physiol. (Lond.)*, 405, 493-510, 1988b.
- DODD, J. and HORN, J.P. A reclassification of B- and C-neurons in the ninth and tenth paravertebral sympathetic ganglion of the bullfrog. *J. Physiol. (Lond.)*, 334, 255-269, 1983a.
- DODD, J. and HORN, J.P. Muscarinic inhibition of sympathetic C-cells in the bullfrog. *J. Physiol. (Lond.)*, 334, 271-291, 1983b.
- DOLPHIN, A.C., SCOTT, R.H., TRENTAM, D.R. and WOOTTON, J.F. Photoactivation of a GTP analogue differentially inhibits the transient component of the calcium current in rat sensory neurons. *J. Physiol. (Lond.)*, 390, 87P, 1987.
- DUN, N. Ganglionic transmission: electrophysiology and pharmacology. *Fed. Proc.*, 39, 2982-2989, 1980.
- DUN, N.J., KAIBARA, K. and KARCZMAR, A.G. Direct postsynaptic membrane effects of dibutyryl cyclic GMP on mammalian sympathetic neurons. *Neuropharmacol.*, 16, 715-717, 1977.
- DUN, N.J. and KARCZMAR, A.G. A comparative study of the pharmacological properties of the positive potential recorded from the superior cervical ganglia of several species. *J. Pharmac. Exp. Ther.*, 215, 455-460, 1980.
- DUNLAP, J. and BROWN, J.H. Heterogeneity of binding sites on cardiac muscarinic receptors induced by the neuromuscular blocking agents gallamine and pancuronium. *Mol. Pharmacol.*, 24, 15-22, 1983.

- DUNMAN, R.S. and ENNA, S.J. A procedure for measuring alpha-adrenergic phenomena. *Am. J. Physiol.*, 248, E633-E647, 1985.
- DUTAR, P. and NICOLL, R.A. Stimulation of phosphatidylinositol (PI) turnover may mediate the muscarinic suppression of the M-current in hippocampal pyramidal cells. *Neurosci. Letters*, 85, 89-94, 1988.
- ECCLES, J.C. Synaptic potentials and transmission in sympathetic ganglion. *J. Physiol. (Lond.)*, 101, 465-483, 1943.
- ECCLES, R.M. and LIBET, B. Origin and blockade of the synaptic responses of curarized sympathetic ganglia. *J. Physiol. (Lond.)*, 157, 484-503, 1961.
- EGAN, T.M., HENDERSON, G., NORTH, R.A. and WILLIAMS, J.T. Noradrenaline-mediated synaptic inhibition in locus coeruleus neurones. *J. Physiol. (Lond.)*, 345, 477-488, 1983.
- ENGEL, W., EBERLEIN, G., TRUMMLITZ, G. and MIHN G. Pirenzepine and AF-DX 116, two structurally related antimuscarinics with opposite receptor selectivity. *Federation Proc.*, 46, 2528-2529, 1987.
- FEDIDA, D., SHIMONI, Y. and GILES, W.R. α -Adrenergic modulation of the transient outward current in rabbit atrial myocytes. *J. Physiol. (Lond.)*, 423, 257-277, 1990.
- FERNANDEZ, J.M., NEHER, E. and GOMPERTS, B.D. Capacitance measurements reveal stepwise fusion events in degranulating mast cells. *Nature*, 312, 453-455, 1984.
- FRANDSEN, E.K. and KRISHNA, G. A simple ultrasensitive method for the assay of cyclic AMP and cyclic GMP in tissues. *Life Sciences*, 18, 529-541, 1976.

GALLAGHER, J.P. and SHINNICK-GALLAGHER, P. Electrophysiological effects of nucleotides injected into rat sympathetic ganglion cells. In Iontophoresis and transmitter mechanisms in the mammalian central nervous system. Eds. R. Ryall and J. Kelly. Elsevier/North Holland Biomedical Press, 152-154, 1978.

GALLAGHER, J., SHINNICK-GALLAGHER, P., COLE, A., GRIFFITH, W. and WILLIAMS, B. Current hypothesis for the slow inhibitory postsynaptic pathway in sympathetic ganglia. *Fed. Proc.*, 39, 3009-3013, 1980.

GALVAN, M. and BEHREND, J. Apamin blocks calcium-dependent spike afterhyperpolarization in rat sympathetic neurones. *Pflugers Arch.*, 403, (suppl.), R50, 1985.

GILES, W., NAKAJIMA, T., ONO, K. and SHIBATA, E.F. Modulation of the delayed rectifier K^+ current by isoprenaline in bull-frog atrial myocytes. *J. Physiol. (Lond.)*, 415, 233-249, 1989.

GILMAN, A.G. G- proteins: transducers of receptor generated signals. *Ann Rev. Biochem.*, 56, 615-649, 1987.

GOH, J.W., KELLY, M.E.M. and PENNEFATHER, P.S. Electrophysiological function of the delayed rectifier (I_K) in bullfrog sympathetic ganglion neurones. *Pflugers Arch.*, 413, 482-486, 1989.

GOH, J.W. and PENNEFATHER, P.S. Pharmacological and physiological properties of the after-hyperpolarization current of bullfrog ganglion neurones. *J. Physiol. (Lond.)*, 394, 314-330, 1987.

GREENE, R.W., HAAS, H.L. and REINER, P.B. Two transient outward currents in histamine neurons of the rat hypothalamus in vitro. *J. Physiol. (Lond.)*, 420, 149-163, 1990.

- GREENGARD, P. Possible role for cyclic nucleotides and phosphorylated membrane proteins in postsynaptic actions of neurotransmitters. *Nature*, 260, 101-108, 1976.
- GROB, B. In Basic electronics, McGraw-Hill, New York, 1977.
- GRUNER, W., MARRION, N.V. and ADAMS, P.R. Three kinetic components to M-currents in bullfrog sympathetic neurons. *Soc. Neurosci. Abs.*, 15, 990, 1989.
- HABERMANN, E. Apamin. *Pharmacol. Ther.*, 25, 255-270, 1984.
- HAGIWARA, S., MIYAZAKI, S. and ROSENTHAL, N.P. Potassium current and the effect of cesium on this current during anomalous rectification of the egg cell membrane of the starfish. *J. Gen. Physiol.*, 67, 621-638, 1976.
- HALLIWELL, J.V. M-currents in human neocortical neurones. *Neurosci. Lett.*, 67, 1-6, 1986.
- HALLIWELL, J.V. and ADAMS, P.R. Voltage-clamp analysis of muscarinic excitation in hippocampal neurons. *Brain Res.*, 250, 71-92, 1982.
- HAMILL, O.P., NEHER, E., SAKMANN, B. and SIGWORTH, F.J. Improved patch-clamp techniques for high resolution current recording from cells and cell-free membrane patches. *Pfugers Arch.*, 391, 85-100, 1981.
- HAMMER, R., GIRALDO, E., SCHIAVI, G.B., MONFERINI, E. and LADENSKY, H. Binding profile of a novel cardioselective muscarine receptor antagonist, AF-DX 116, to membranes of peripheral tissues and brain in the rat. *Life Sci.*, 38, 1653-1662, 1986.
- HARTZELL, H.C., KUFFLER, S.W., STICKGOLD, R. and YOSHIKAMI, D. Synaptic excitation and inhibition resulting from direct action of acetylcholine

on two types of chemoreceptors on individual amphibian parasympathetic neurones. *J Physiol. (Lond.)*, 271, 817-846, 1977.

HESTRIN, S., NICOLL, R.A., PERKELL, D.J. and SAH, P. Analysis of excitatory synaptic action in pyramidal cells using whole-cell recording from rat hippocampal slices. *J. Physiol. (Lond.)*, 422, 203-225, 1990.

HIDAKA, H., INAGAKI, M., KAWAMOTO, S. and SASAKI, Y. Isoquinoline-sulfonamides, novel and potent inhibitors of cyclic nucleotide dependent protein kinase and protein kinase C. *Biochem.*, 23, 5036-5041, 1984.

HIGASHIDA, H. and BROWN, D.A. Two polyphosphoinositide metabolites control two K^+ currents in a neuronal cell. *Nature*, 323, 333-335, 1986.

HILLE, B. Ionic Channels of Excitable Membranes, Saunauer and Associates, Sunderland, Mass., 1984.

HILLE, B. Ionic channels: evolutionary origins and modern roles. *Quart. J. Expl. Physiol.*, 74, 785-804, 1989.

HODGKIN, A.L. and HUXLEY, A.F. A quantitative description of membrane current and its application to conduction and excitation in nerve. *J. Physiol. (Lond.)*, 117, 500-544, 1952.

HOKFELT, T., JOHANSSON, O., LUNDBERG, J.M. and SCHULTZBERG, J.M. Peptidergic neurones. *Nature*, 284, 515-521, 1980.

HOLZ, G.G.^{4a}, SHEFNER, S.A. and ANDERSON, E.G. Serotonin decreases the duration of action potentials recorded from tetraethylammonium-treated bullfrog dorsal root ganglion cells. *J. Neurosci.*, 6, 620-626, 1986.

HONMA, S. Functional differentiation in sB and sC neurons of toad sympathetic ganglia. *Jap. J. Physiol.*, 20, 281-295, 1970.

- HORIE, M. and IRISAWA, H. Rectification of muscarinic K^+ current by magnesium ion in guinea pig atrial cells. *Am. J. Physiol.*, 253, H210-H214, 1987.
- HORIE, M. and IRISAWA, H. Dual effects of intracellular magnesium on muscarinic potassium channel current in single guinea-pig atrial cells. *J. Physiol. (Lond.)*, 408, 313-332, 1989.
- HORN, J.P. and DODD, J. Monosynaptic muscarinic activation of K^+ conductance underlies the slow inhibitory postsynaptic potential in sympathetic ganglia. *Nature*, 292, 625-627, 1981.
- HORN, J.P. and DODD, J. Inhibitory cholinergic synapses in autonomic ganglia. *Trends Neurosci.*, 6, 180-184, 1983.
- HORN, J.P., FATHERAZI S. and STOFER, W.D. Selective innervation of blood vessels in the bullfrog by sympathetic C neurons that contain neuropeptide-Y-like immunoreactivity. *Soc. Neurosci. Abs.*, 12, 542, 1986.
- HORN, J.P., FATHERAZI, S. and STOFER, W.D. Differential projections of B and C sympathetic axons in peripheral nerves of the bullfrog. *J. Comp. Neurol.*, 278, 570-580, 1988.
- HORN, J.P. and STOFER, W.D. Double-labelling of the paravertebral sympathetic C system in the bullfrog with antisera to LHRH and NPY. *J. Auton. Nerv. Syst.*, 23, 17-24, 1988.
- HORN, J.P., STOFER, W.D. and FATHERAZI, S. Neuropeptide-Y-like immunoreactivity in bullfrog sympathetic ganglia is restricted to C-cells. *J. Neurosci.*, 7, 1717-1727, 1987.
- HORN, R. and MARTY, A. Muscarinic activation of ionic currents measured by new whole-cell recording method. *J. Gen. Physiol.*, 92, 145-159, 1988.

- HOSS, W. and MESSER, W. Jr. Multiple muscarinic receptors in the CNS. *Mol. Pharmacol.*, 35, 3895-3901, 1986.
- HOUSE, C. and KEMP, B. Protein kinase C contains pseudosubstrate prototope in its regulatory domain. *Science*, 238, 1726-1728, 1987.
- HUGHES, M., SCHMID, H., ROME, G., DUVAL, D., FRELIN, C. and LADZDUNSKI, M. The Ca^{2+} -dependent slow K^+ conductance in cultured rat muscle cells: characterization with apamin. *EMBO J.*, 1, 1039-1042, 1982.
- HULME, E.C., BERRIE, C.P., BIRDSALL, N.J. and BURGEN, A.S.V. Interaction of muscarinic receptor with guanine nucleotides and adenylate cyclase. In Drugs Receptors and Their Effectors. Ed. N.J.M. Birdsall, MacMillan, London, 23-24, 1981.
- HUTTER, O.F. and NOBLE, D. Rectifying properties of heart muscle. *Nature*, 188, 495, 1960.
- IYENGAR, R. and BIRNBAUMER, L. Signal transduction by G-proteins. In ISI Atlas of Science: Pharmacology, 213-221, 1987.
- ISHIHARA, K., MITSUIYE, T., NOMA, A. and TAKANO, M. The Mg^{2+} block and intrinsic gating underlying inward rectification of the K^+ current in guinea-pig cardiac myocytes. *J. Physiol. (Lond.)*, 419, 297-320, 1989.
- JACK, J.J.B., NOBLE, D. and TSIEN, R.W. In Electrical Current Flow in Excitable Cells, Clarendon Press, Oxford, 1975.
- JACQUIN, T., CHAMPAGNAT, J., DENAVIT-SAUBIE, M. and SIGGINS, G.R. Somatostatin depresses excitability in neurons of the solitary tract complex through hyperpolarization and augmentation of I_M , a non-inactivating voltage-dependent outward current blocked by muscarinic agonists. *Proc. Nat. Acad. Sci. (USA)*, 85, 948-952, 1988.

- JAGADEESH, G. and SULAKHE, P.V. Gallamine binding to heart M₂ cholinergic receptors does not antagonize cholinergic inhibition of adenylate cyclase in isolated plasma membrane. *Eur. J. Pharmacol.*, 109, 311-313, 1985.
- JAN, L.Y., JAN, Y.N. and BROWNFIELD, M.S. Peptidergic transmitters in synaptic boutons of sympathetic ganglia. *Nature*, 288, 380-382, 1980a.
- JAN, Y.N. and JAN, L.Y. Peptidergic transmitters in sympathetic ganglia of the frog. *J. Physiol. (Lond)*, 327, 219-246, 1982.
- JAN, Y.N., JAN, L.Y. and KUFFLER, S.W. Further evidence for peptidergic transmission in sympathetic ganglia. *Proc. Nat. Acad. Sci. USA*, 77, 5008-5012, 1980b.
- JONES, S.W. Muscarinic and peptidergic excitation of bullfrog sympathetic neurones. *J. Physiol. (Lond.)*, 366, 63-87, 1985.
- JONES, S.W. A muscarine-resistant M-current in C cells of bullfrog sympathetic ganglia. *Neurosci. Lett.*, 74, 309-314, 1987a.
- JONES, S.W. Sodium currents in dissociated bullfrog sympathetic ganglion neurons. *J. Physiol. (Lond.)*, 389, 605-627, 1987b.
- JONES, S.W. Chicken II luteinizing-hormone releasing hormone inhibits the M-current of bullfrog sympathetic neurons. *Neurosci. Lett.*, 80, 180-184, 1987c.
- JONES, S.W. On the resting potential of isolated frog sympathetic neurons. *Neuron*, 3, 153-161, 1989.
- JONES, S.W., ADAMS, P.R., BROWNSTEIN, M.J. and RIVIER, J.E. Teleost luteinizing hormone-releasing hormone: action on bullfrog sympathetic ganglia is consistent with role as neurotransmitter. *J. Neurosci.*, 4, 420-429, 1984

- KACZMAREK, L.K. and LEVITAN, I.B. In Neuromodulation: the biochemical control of neuronal excitability. Eds. L. Kaczmarek and I. Levitan, Oxford Univ. Press, New York, 1-248, 1987.
- KASS, R.S. and TSIEN, R.W. Control of action potential duration by calcium ions in cardiac Purkinje fibres. *J. Gen. Physiol.*, 67, 599-617, 1976.
- KATADA, T., GILMAN, A.G., WATANABE, Y., BAUER, S. and JACOBS, K.H. Protein kinase C phosphorylates the inhibitory guanine-nucleotide-binding regulatory component and apparently suppresses its function in hormonal inhibition of adenylate cyclase. *Eur. J. Biochem.*, 151, 431-437, 1985.
- KEBABIAN, J.W., STEINER, A.L. and GREENGARD, P. Muscarinic cholinergic regulation of guanosine-3, 5-monophosphate in autonomic ganglia: possible role in synaptic transmission. *J. Pharmacol. Exptl. Ther.*, 193, 474-488, 1975.
- KIKKAWA, U. and NISHIZUKA, Y. The role of protein kinase C in transmembrane signalling. *Ann. Rev. Cell Biol.*, 2, 149-178, 1986.
- KIM, D., LEWIS, D.L., GRAZIADEI, L., NEER, E.J., BAR-SAGI, D. and CLAPHAM, D.E. G-protein beta-gamma subunits activate the cardiac muscarinic K⁺-channel via phospholipase A₂. *Nature*, 337, 557-560, 1989.
- KOKETSU, K. and NAKAMURA, M. The electrogenesis of adrenaline-hyperpolarization of sympathetic ganglion cells in bullfrog. *Jap. J. Physiol.*, 26, 63-77, 1976.
- KOKETSU, K., NISHI, S. and SOEDA, H. Acetylcholine-potential of sympathetic ganglion cell membrane. *Life Sci.*, 7, 741-749, 1968.
- KOREN, G., LIMAN, E.R., LOGOTHETIS, D.E., NADAL-GINARD, B. and HESS, P. Gating mechanism of a cloned potassium channel expressed in frog oocytes and mammalian cells. *Neuron*, 2, 39-51, 1990.

- KOSTYUK, P.G. and KRISHTAL, O.A. Separation of sodium and calcium currents in the somatic membrane of mollusc neurones. *J. Physiol. (Lond.)*, 117, 500-544, 1977.
- KOSTYUK, P.G., KRISHTAL, O.A. and DOROSHENKO, P.A. Calcium currents in snail neurones. I. Identification of calcium current. *Pflugers. Arch.*, 348, 83-93, 1974.
- KRISHTAL, O.A. and PIDOPLICHKO, V.I. A receptor for protons in the nerve cell membrane. *Neuroscience* 5, 2325-2327, 1980.
- KUBA, K. Release of calcium ions linked to the activation of potassium conductance in a caffeine-treated sympathetic neurone. *J. Physiol., (Lond.)*, 298, 251-269, 1980.
- KUBA, K., KATO, E., KUMAMOTO, E., KOKETSU, K. and HIRAI, K. Sustained potentiation of transmitter release by adrenaline and dibutyl cyclic AMP in sympathetic ganglia. *Nature*, 291, 654-656, 1981.
- KUBA, K. and KOKETSU, K. Synaptic events in sympathetic ganglia. *Progress in Neurobiol.*, 11, 77-169, 1978.
- KUBA, K. and NISHI, S. Rhythmic hyperpolarizations and depolarizations of sympathetic ganglion cells induced by caffeine. *J. Neurophysiol.*, 39, 547-563, 1976.
- KUFFLER, S.W. and SEJNOWSKI, T.J. Peptidergic and muscarinic excitation at amphibian sympathetic synapses. *J. Physiol.*, 341, 257-278, 1983.
- KUNO, M. and GARDNER, P. Ion channels activated by inositol 1,4,5-triphosphate in plasma membrane human T-lymphocytes. *Nature*, 320, 631-634, 1987.

- KURACHI, Y. Voltage-dependent activation of the inward rectifier potassium channel of guinea pig heart. *J. Physiol. (Lond.)*, 366, 365-385, 1985.
- KURACHI, Y., ITP, H., SUGIMOTO, T., SHIMIZU, T., MIKI, I. and UI, M. Arachidonic acid metabolites as intracellular modulators of the G protein-gated cardiac channel. *Nature*, 337, 555-557, 1989.
- KURACHI, Y., NAKAJIMA, T. and SUGIMORO, T. On the mechanism of activation of muscarinic and cardiac channels by adenosine in isolated atrial cells involvement of GTP-binding proteins. *Pflugers Arch.*, 407, 264-274, 1986a.
- LANCASTER, B. and PENNEFATHER, P. Potassium currents in bullfrog ganglion cells evoked by brief depolarizations. *J. Physiol. (Lond.)*, 387, 519-548, 1987.
- LANGLEY, J.N. and ORBELI, L.A. Observations on the sympathetic and sacral autonomic system of the frog. *J. Physiol. (Lond.)*, 41, 450-480, 1910.
- LAPORTE, Y. and LORENTE DE NO, R. Potential changes evoked in a curarized sympathetic ganglion by presynaptic volleys of impulses. *J. Cell. Comp. Physiol.*, (Suppl. 2), 61-106, 1950.
- LEE, K.S. and TSIEN, R.W. High selectivity of calcium channels in single dialysed heart cells of the guinea pig. *J. Physiol. (Lond.)*, 354, 253-272, 1984.
- LIBET, B. and KOBAYASHI, H. Adrenergic mediation of slow inhibitory postsynaptic potential in sympathetic ganglia of the frog. *J. Neurophysiol.*, 37, 805-814, 1974.
- LIGHT, D.B., SCHWIEBERT, E.M., KARLSON, K.H. and STANTON, B.A. Atrial natriuretic peptide inhibits a cation channel in renal inner medullary collecting duct cells. *Science*, 243, 383-385, 1989.

LOFFELHOLZ, K. and PAPPANO, A.J. The parasympathetic neuroeffector junction of the heart. *Pharmacol. Rev.*, 37, 1-24, 1985.

LOGOTHETHIS, D.E., KURACHI, Y., GALPER, J., NEER, E.J. and CLAMPHAM, D.E. The beta-gamma-subunit of GTP-binding proteins activate the muscarinic K⁺ channel in heart. *Nature*, 325, 321-326, 1987.

LOWRY, O.H., ROSEBROUGH, N.J., FARR, A.L. and RANDALL, R.J. Protein measurement with the Folin phenol reagent, *J. Biol. Chem.*, 193, 265-275, 1954.

LUKASIEWICZ, P. and WERBLIN, F. A slowly inactivating potassium current truncates spike activity in ganglion cells of the tiger salamander retina. *J. Neurosci.*, 8, 4470-4481, 1988.

LUNDBERG, J.M., TERENIUS, L., HOKFELT, T., MARTLING, C.R., TATEMOTO, K., MUTT, V., POLAK, J., BLOOM, S. and GOLDSTEIN, M. Neuropeptide Y (NPY)-like immunoreactivity in peripheral noradrenergic neurons and effects of NPY on sympathetic function. *Acta. Physiol. Scand.*, 116, 477-480, 1982.

MALENKA, R.C., MADISON, D.V., ANDRADE, R. and NICOLL, R.A. Phorbol esters mimic some cholinergic actions in hippocampal pyramidal neurons. *J. Neurosci.*, 6, 475-480, 1986.

MARSHALL, L.M. Synaptic localization of alpha-bungarotoxin binding which blocks nicotinic transmission at frog sympathetic neurones. *Proc. Nat. Acad. Sci. USA*, 78, 1948-1952, 1981.

MARTY, A. Ca-dependent K channels with large unitary conductance in chromaffin cell membranes. *Nature*, 291, 497-500, 1981.

MARTY, A. and NEHER, E. Tight-Seal Whole-Cell Recording. In Single-Channel Recording, Ed. by B. Sakmann and E. Neher, Plenum Press, New York, 107-121, 1983.

- MATSUDA, H., SAIGUSA, A. and IRISAWA, H. Ohmic conductance through the inwardly rectifying channel and blocking by Mg^{2+} . *Nature*, 325, 156-159, 1987.
- MAYER, M.L. and WESTBROOK, G.L. A voltage-clamp analysis of inward (anomalous) rectification in mouse spinal sensory ganglion cells. *J. Physiol. (Lond.)*, 340, 19-45, 1983.
- M'AFEE D.A. Superior cervical ganglion: physiological considerations. In Progress in Cholinergic Biology: Model Cholinergic Synapses, Ed. by I. Hanin and A.M. Goldberg, Raven Press, New York, 191-211, 1982.
- MIHARA, S., NORTH, R.A. and SUPRENANT, A. Somatostatin increases an inwardly rectifying potassium conductance in guinea-pig submucous plexus neurons. *J. Physiol. (Lond.)*, 390, 335-356, 1987.
- MILLER, C., MOCZYDLOWSKI, E., LATORRE, R. and PHILLIPS, M. Charybdotoxin, a protein inhibitor of single Ca^{2+} -activated channels from mammalian skeletal muscle. *Nature*, 313, 316-318, 1985.
- MIYAKE, M., CHRISTIE, R.A. and NORTH, R.A. Single potassium channels opened by opioids in rat locus ceruleus. *Proc. Nat. Acad. Sci. (USA)*, 86, 3419-3422, 1989.
- MOORE, S.D., MADAMBA, S.J., JOELS, M. and SIGGINS, G.R. Somatostatin augments the M-current in hippocampal neurones. *Science*, 239, 278-280, 1988.
- MOSS J., STANLEY S.J., BURNS D.L., HSAI J.A., YOST D.A., MYERS G.A. and HEWLETT, E.L. Activation by thiol of the latent NAD glycohydrolase and ADP-ribosyltransferase activities of Bordetella pertussis toxin (Islet-activating protein). *J. Biol. Chem.*, 258, 11879-11882, 1983.

- MURASE, K., RYU, P.D. and RANDIC, M. Substance P augments a persistent slow inward calcium-sensitive current in voltage-clamped spinal dorsal horn neurone of the rat. *Brain Res.*, 346, 203-217, 1986.
- NAKAYAMA, T., PALFREY, C. and FOZZARD, H.A. Modulation of the cardiac transient outward current by catecholamines. *J. Mol. Cell. Cardiol.*, 21 (Supp. 1), 109-118, 1989.
- NATHANSON, N.M. Molecular properties of the muscarinic acetylcholine receptor. *Ann. Rev. Neurosci.*, 10, 195-236, 1987.
- NEDOMA, J., DOROFEEVA, N.A., TUCEK, S., SHELKOVNIKOV, S. and DANILOV, A.F. Interaction of the neuromuscular blocking drugs alcuronium, decamethonium, gallamine, pancuronium, ritebronium, tercuronium and d-tubocurarine with muscarinic acetylcholine receptors in the heart and ileum. *Naunyn-Schmiedeberg's Arch. Pharmacol.*, 329, 176-181, 1985.
- NEHER, E. Two fast transient current components during voltage clamp on snail neurons. *J. Gen. Physiol.*, 58, 36-53, 1971.
- NEHER, E. The use of the patch clamp technique to study second messenger mediated cellular events. *Neurosci.*, 26, 727-734, 1988.
- NEHER, E., MARTY, A., FUDUKA, K., KUBO, T. and NUMA, S. Intracellular calcium release mediated by two muscarinic receptor subtypes. *FEBS Lett.*, 240, 9988-9994, 1988.
- NEHER, E. and SAKMANN, B. Single channel currents recorded from membrane of denervated frog muscle. *Nature*, 260, 799-802, 1976.
- NEWBERRY, N.R. M_1 and M_2 receptors mediate different effects on synaptically evoked potentials of the rat superior cervical ganglion. *Neurosci. Letts.*, 88, 100-106, 1988.

- NEWBERRY, N.R., PRIESTLEY, T. and WOODRUFF, G.N. Pharmacological distinction between two muscarinic responses in the isolated superior cervical ganglion of the rat. *Eur. J. Pharmacol.*, 116, 191-192, 1985.
- NISHI, S. and KOKETSU, K. Electrical properties and activities in single sympathetic neurones in frogs. *J. Cell. Comp. Physiol.*, 55, 15-30, 1960.
- NISHI, S. and KOKETSU, K. Late after-discharge of sympathetic postganglionic fibers. *Life Sci.*, 5, 1991-1997, 1966.
- NISHI, S. and KOKETSU, K. Analysis of slow inhibitory postsynaptic potentials in bull frog sympathetic ganglion. *J. Neurophysiol.*, 31, 109-121, 1968.
- NISHI, S., SOEDA, H. and KOKETSU, K. Studies on sympathetic B and C neurons and patterns of preganglionic innervation. *J. Cell Comp. Physiol.*, 66, 19-32, 1965.
- NISHI, S., SOEDA, H. and KOKETSU, K. Unusual nature of ganglionic slow EPSP studied by voltage clamp method. *Life Sci.*, 8, 33-42, 1969.
- NISHIZUKA, Y. The role of protein kinase C in cell surface signal transduction and turnover promotion. *Nature*, 308, 693-698, 1984.
- NOHOMI, M. and KUBA, K. (+)-Tubocurarine blocks the Ca^{2+} -dependent K^{+} -channel of the bullfrog sympathetic ganglion cell. *Brain Res.*, 301, 146-148, 1984.
- NORTH, R.A. Receptors on individual neurones. *Neuroscience*, 4, 899-907, 1986.
- NORTH, R.A. Drug receptor and inhibition of nerve cells. *Br. J. Pharmacol.*, 98, 13-28, 1989.

- NORTH, R.A. and TOKIMASA, T. Persistent calcium-sensitive potassium current and the resting properties of guinea-pig myenteric neurons. *J. Physiol. (Lond.)*, 386, 333-353, 1987.
- NORTH, R.A., WILLIAMS, J.T., SURPRENANT, A. and CHRISTIE, M.J. Mu and delta receptors belong to a family of receptors that are coupled to potassium channels. *Proc. Nat. Acad. Sci. USA*, 84, 5487-5491, 1987.
- OHMORI, H. Inactivation kinetics and steady-state current noise in the anomalous rectifier of tunicate egg cell membrane. *J. Physiol. (Lond.)*, 281, 77-99, 1978.
- OSMANOVIC, S.S. and SHEFNER, S.A. Anomalous rectification in rat locus coeruleus neurons. *Brain Res.*, 417, 161-166, 1987.
- OWEN, D.G., MARSH, S.J. and BROWN, D.A. M-current noise in rat sympathetic neurones. *Soc. Neurosc. Abs.*, 15, 990, 1989.
- PALLOTTA, B.S., MAGLEBY, K.L. and BARRETT, J.N. Single channel recordings of Ca^{2+} -activated K^{+} currents in rat muscle cell culture. *Nature*, 293, 471-474, 1981.
- PARENTE, J.E., WALSH, M.P., GIRARD, P.R., KUO, J.F., NG, D.S. and WONG, K. Effects of gold co-ordination complexes on neutrophil function are mediated via inhibition of protein kinase C. *Mol. Pharmacol.*, 35, 26-33, 1989.
- PATTERSON, D.A. and VOLLE, R.L. Muscarinic receptors and [^3H]inositol incorporation in a rat sympathetic ganglion. *J. Auton. Nerv. Sys.*, 10, 69-72, 1984.
- PENNEFATHER, P. and COHEN, I.S. Molecular mechanisms of cardiac K^{+} -channels regulation. In Cardiac electrophysiology and arrhythmias: from cell to bedside, Eds. D.P. Zipes and J. Jalife, W.B Saunders, 1990 (in press).

- PENNEFATHER, P., LANCASTER, B., ADAMS, P.R. and NICOLL, R.A. Two distinct Ca-dependent K currents in bullfrog sympathetic ganglion cells. *Proc. Nat. Acad. Sci.*, 82, 3040-3044, 1985.
- PETERSON, O.H. and DUNNE, M.J. Regulation of K⁺ channels plays a critical role of insulin secretion. *Pflugers Arch.*, 414, (Supp. 1), S115-S120, 1989.
- PFAFFINGER, P.J. Muscarine and LHRH suppress M-current by activating an IAP-insensitive G-protein. *J. Neurosci.*, 8, 3343-3353, 1988.
- PFAFFINGER, P.J., LEIBOWITZ, M.D., SUBERS, E.M., NATHANSON, N.M., ALMERS, W. and HILLE, B. Agonists that suppress M-current elicit phosphoinositide turnover and Ca²⁺ transients, but these events do not explain M-current suppression. *Neuron*, 1, 477-484, 1988.
- PFAFFINGER, P.J., MARTIN, J.M., HUNTER, D.D., NATHANSON, N.M. and HILLE, B. GTP-binding proteins couple cardiac muscarinic receptors to a K_v channel. *Nature*, 317, 536-538, 1985.
- PORTZEHL, H., CALDWELL, P.C. and RUEGG, J.C. The dependence of contraction and relaxation of muscle fibres from the crab maia squinada on the internal concentration of free calcium ions. *Biochemica et Biophysica Acta.*, 79, 581-591, 1964.
- PUSCH, M. and NEHER, E. Rates of diffusional exchange between small cells and a measuring patch pipette. *Pflugers Arch.*, 411, 204-211, 1988.
- QUAST, U. and COOK, N.S. In vitro and in vivo comparison of two K⁺ channel blockers, diazoxide and cromakalim, and their inhibition by glibenclamide. *J. Pharm. Exp. Ther.*, 250, 261-271, 1989.
- RAFUSE, P.E. Examination of the adrenaline-induced hyperpolarization in the postganglionic neurones of amphibian sympathetic ganglia. In Ph.D. thesis, 1985.

- RAFUSE, P.E. and SMITH, P.A. Alpha₂-adrenergic hyperpolarization is not involved in slow synaptic inhibition in amphibian sympathetic ganglia. *Br. J. Pharmacol.*, 87, 409-416, 1986.
- RAFUSE, P.E., SMITH, P.A. and ZIDICHOUSKI, J.A. Examination of the role of calcium in the adrenaline-induced hyperpolarization of bullfrog sympathetic neurons. *Neurosci.*, 25, 671-678, 1988.
- REUTER, H. Localization of beta adrenergic receptors, and the effects of noradrenaline and cyclic nucleotides on action potentials, ionic currents and tension in mammalian cardiac muscle. *J. Physiol. (Lond.)*, 242, 429-451, 1974.
- ROMEY, G. and LAZDUNSKI, M. The coexistence in rat muscle cells of two distinct classes of Ca²⁺-dependent K⁺ channels with different pharmacological properties and different physiological functions. *Biochem. Biophys. Res. Comm.*, 118, 669-674, 1984.
- ROSS, E.M. Signal sorting and amplification through G protein-coupled receptors. *Neuron*, 3, 141-152, 1989.
- RUDY, B. Diversity and ubiquity of K⁺ channels. *Neurosci.*, 25, 729-749, 1988.
- SAKMANN, B., NOMA, A. and TRAUTWEIN, W. Acetylcholine activation of single muscarinic K⁺ channels in isolated pacemaker cells of the mammalian heart. *Nature*, 303, 250-253, 1983.
- SARGENT, P.B. The number of synaptic boutons terminating on *Xenopus* cardiac ganglion cells is directly correlated with size. *J. Physiol. (Lond.)*, 343, 85-104, 1983.
- SATIN, L.S. and ADAMS, P.R. Spontaneous miniature outward currents in cultured bullfrog sympathetic neurones. *Brain Res.*, 401, 331-339, 1987.

- SAWADA, M., ICHINOSE, M. and MAENO, T. Ionic mechanism of the outward current induced by intracellular injection of inositol triphosphate into Aplysia neurons. *J. Neurosci.*, 7, 1470-1483, 1987.
- SCHILD, H.O. pA_2 , A new scale for the measurement of drug antagonism. *Br. J. Pharmacol.*, 2, 189-206, 1947.
- SCHOFIELD, G.G. and IKEDA, S.R. Neuropeptide Y blocks a calcium current in C cells of bullfrog sympathetic ganglia. *European J. Pharmacol.*, 151, 131-134, 1988.
- SCHOFIELD, G.G., WEIGHT, F.F. and IKEDA, S.R. The effect of pumiliotoxin-B on the excitability of bullfrog sympathetic neurons. *European J. Pharmacol.*, 147, 39-48, 1988.
- SCHULMAN, J.A. and WEIGHT, F.F. Synaptic transmission: long lasting potentiation by a postsynaptic mechanism. *Science*, 194, 1437-1439, 1976.
- SELYANKO, A.A., SMITH, P.A. and ZIDICHOUSKI, J.A. Effects of muscarine and adrenaline on neurones from *Rana pipiens* sympathetic ganglia. *J. Physiol. (Lond.)*, 425, 471-500, 1990a.
- SELYANKO, A.A., ZIDICHOUSKI, J.A. and SMITH, P.A. A muscarine-sensitive, slow, transient outward current in frog autonomic neurones. *Brain Res.*, 524, 236-243, 1990b.
- SHERWOOD, N.L., EIDEN, L., BROWNSTEIN, M., SPEISS, J., RIVIER, J. and VALE, W. Characterization of a teleost gonadotropin-releasing hormone. *Proc. Nat. Acad. Sci. USA*, 80, 2794-2798, 1983.
- SIGWORTH, F.J. Electronic design of the patch clamp. In *Single-Channel Recording*, Ed. by B. Sakmann and E. Neher, Plenum Press, New York, 3-35, 1983.

- SIGWORTH, F.J. and NEHER, E. Single Na^+ channel currents observed in cultured rat muscle cells. *Nature*, 287, 71-73, 1980.
- SIMMONS, M.A. and HARTZELL, H.C. A quantitative analysis of the acetylcholine-activated potassium current in single cells from frog atrium. *Pflugers Arch.*, 409, 454-461, 1987.
- SIMMONS, M.A., BECKER, J.B. and MATHER, R.J. Desensitization of the inhibition of the M-current in sympathetic neurons: effects of ATP analogs, polyanions, and multiple agonist applications. *Neuron*, 4, 557-562, 1990.
- SIMS, S.M., SINGER, J.J. and WALSH, J.V.Jr. Cholinergic agonists suppress a potassium current in freshly dissociated smooth muscle cells of the toad. *J Physiol. (Lond.)*, 367, 503-529, 1985.
- SKOK, V.I. Conduction in tenth ganglion of the frog sympathetic trunk. *Fed. Proc.*, 24 (Transl. Supp.), T363-T367, 1965.
- SMITH, P.A., GORDON, T., KEHOE, M.P. and MARSHALL, K.C. Alpha-1-adrenoceptor, alpha-2-adrenoceptor and muscarinic responses in normal and axotomized bullfrog sympathetic ganglia. *Can. J. Phys. Pharmacol.*, (in press, 1990).
- SMITH, P.A. and PANT, K.K. Atrial natriuretic factor suppresses M-current in frog but not in rat sympathetic neurones. *Neurosci. Lett.*, 100, 243-248, 1989.
- SMITH, P.A. and WEIGHT, F.F. Evidence for generation of the slow IPSP by direct muscarinic hyperpolarizing action of acetylcholine in bullfrog sympathetic ganglia. *Neurosci. Abst.*, 7, 807, 1981.
- SMITH, P.A. and WEIGHT, F.F. The pathway for the slow inhibitory post synaptic potential in bullfrog sympathetic ganglia. *J. Neurophysiol.*, 56, 823-834, 1986.

- SMITH, P.A., WEIGHT F.F. and LEHNE, R.A. Potentiation of Ca^{2+} dependent K^+ activation by theophylline is independent of cyclic nucleotide elevation. *Nature*, 280, 400-402, 1979.
- SOEJIMA, M.A. and NOMA, A. Mode of regulation of the ACh-sensitive K-channel by the muscarinic receptor in rabbit atrial cells. *Pflugers Arch.*, 400, 424-431, 1984.
- STAMPFLI, R. A new method for measuring potentials with external electrodes. *Experientia*, 10, 508-509, 1954.
- STANFIELD, P.R. Nucleotides such as ATP may control the activity of ion channels. *Trends Neurosci.*, 10, 335-339, 1987.
- STOCKTON, J.M., BIRDSALL, N.J.M., BURGEN, A.S.V. and HULME, E.C. Modification of the binding properties of muscarinic receptors by gallamine. *Mol. Pharmacol.*, 23, 551-557, 1983.
- STORM, J.F. Action potential repolarization and a fast after-hyperpolarization in rat hippocampal pyramidal cells. *J. Physiol. (Lond.)*, 385, 733-759, 1988.
- STORM, J.F. Temporal integration by a slowly inactivating K^+ current in hippocampal neurons. *Nature*, 336, 379-381, 1988.
- SURPRENANT, A. Slow excitatory synaptic potentials recorded from neurons of guinea-pig submucous plexus. *J. Physiol. (Lond.)*, 351, 343-361, 1984.
- TAMAOKI, T., NOMOTO, H., TAKAHASHI, I., KATO, Y., MORIMOTO, M. and TOMITA, F. Staurosporine, a potent inhibitor of phospholipid/ Ca^{++} dependent protein kinase. *Biochem. Biophys. Res. Commun.*, 135, 397-402, 1986.
- TATSUMI, H., COSTA, M., SCHIMERLIK, M. and NORTH, R.A. Potassium conductance increased by noradrenaline, opioids, somatostatin, and G-

proteins: whole-cell recording from guinea-pig submucous neurons. *J. Neurosci.*, 10, 675-682, 1990.

TAXI, J. Morphology of the autonomic nervous systems. In *Frog Neurobiology*, Eds. R. Llinas and W. Precht, Springer-Verlag press, New York, 93-150, 1976.

THOMPSON, S.H. Three pharmacologically distinct potassium channels in molluscan neurones. *J. Physiol. (Lond.)*, 265, 465-488, 1977.

THOMPSON, S.H. Aminopyridine block of transient potassium current. *J. Gen. Physiol.*, 80, 1-18, 1982.

TOKIMASA, T. Muscarinic agonists depress calcium-dependent G_K in bullfrog sympathetic neurones. *J. Aut. Nerv. Sys.*, 10, 107-116, 1984.

TOKIMASA, T. Intracellular Ca^{2+} -ions inactivate K^+ current in bullfrog sympathetic neurons. *Brain Res.*, 337, 386-391, 1985.

TOKIMASA, T. and AKASU, T. Cyclic AMP regulates an inwardly rectifying sodium-potassium current in dissociated bull-frog sympathetic neurones. *J. Physiol. (Lond.)*, 420, 409-429, 1990.

TOSAKA, T., CHICHUBU, S. and LIBET, B. Intracellular analysis of slow inhibitory and excitatory postsynaptic potentials in sympathetic ganglia of the frog. *J. Neurophysiol.*, 31, 396-343, 1968.

TOSAKA, T., TASAKA, J., MIYAZAKI, T. and LIBET, B. Hyperpolarization following activation of K^+ channels by excitatory postsynaptic potentials. *Nature*, 305, 148-150, 1983.

TRUSSELL, L.O. and JACKSON, M.B. Dependence of an adenosine-activated potassium current on a GTP-binding protein in mammalian central neurones. *J. Neurosci.*, 7, 3306-3316, 1987.

TSIEN, R.W., GILES, W. and GREENGARD, P. Cyclic AMP mediates the effects of adrenaline of cardiac Purkinje fibres. *Nature*, 240, 181-183, 1972.

UI, M. Islet-activating protein, pertussis toxin: as a probe for functions of the inhibitory guanine nucleotide regulatory component of adenylate cyclase. *Trends Physiol. Sci.*, 5, 277-279, 1984.

VANDONGEN, A.M.J., CODINA, J., OLATE, J., MATTERA, R., JOHO, R., BIRNBAUMER, L. and BROWN, A.M. Newly identified brain potassium channels gated by the guanine nucleotide binding protein G_o . *Science*, 242, 1433-1437, 1988.

VAN WINKLE, W.B. Calcium release from skeletal muscle sarcoplasmic reticulum: Site of action of dantrolene sodium. *Science*, 193, 1130-1131, 1976.

WALLIS, D.I., LEES, G.M. and KOSTERLITZ, H.W. Recording resting and action potentials by the sucrose gap method. *Comp. Biochem. Physiol.*, 50C, 199-216, 1975.

WANG, Y.Y. and AGHAJANIAN, G.K. Intracellular GTP- γ -S restores the ability of morphine to hyperpolarize rat locus coeruleus neurones after blockade by pertussis toxin. *Brain, Res.*, 436, 396-401, 1987.

WANTANABE, H. Ultrastructural study of the frog sympathetic ganglia. In Histochemistry and cell biology of autonomic neurons, SIF cells, and paraneurons. Ed. by O. Eranko, et al., Raven Press, New York, 153-171, 1980.

WEIGHT, F.F. Physiological mechanisms of synaptic modulation. In The Neurosciences: Third Study Program. Ed. by F.O. Schmitt and F.G. Worden, 929-941, MIT press, Cambridge, MA., 1974.

WEIGHT, F.F. Synaptic mechanisms in amphibian sympathetic ganglia. In Autonomic Ganglia. Ed. Lars-Gosta Elfvin, John Willey and Sons Ltd., 309-344, 1983.

WEIGHT, F.F. and MACDERMOTT, A.B. Postsynaptic mechanisms in synaptic plasticity. *Adv. Physiol. Sci.*, 36, 243-251, 1981.

WEIGHT, F.F. and PADJEN, A. Slow synaptic inhibition: Evidence for synaptic inactivation of sodium conductance in sympathetic ganglion cells. *Brain Res.*, 55, 219-224, 1973a.

WEIGHT, F.F. and PADJEN, A. Acetylcholine and slow synaptic inhibition in frog sympathetic ganglion cells. *Brain Res.*, 55, 225-228, 1973b.

WEIGHT, F.F., SCHULMAN, J.A., SMITH, P.A. and BUSIS, N.A. Long-lasting synaptic potentials and the modulation of synaptic transmission. *Fed. Proc.*, 38, 2084-2094, 1979.

WEIGHT, F.F. and SMITH, P.A. Small Intensely Fluorescent Cells and the Generation of Slow Postsynaptic Inhibition. In Sympathetic Ganglia, Histochemistry and Cell Biology of Autonomic Neurons, SIF Cells and Paraneurons, Ed. O. Eranko, et al, Raven Press, New York, 159-171, 1980.

WEIGHT, F.F., SMITH, P.A. and SCHULMAN, J.A. Postsynaptic potential generation appears independent of synaptic elevation of cyclic nucleotides in sympathetic neurons. *Brain Res.*, 158, 197-202, 1978.

WEIGHT, F.F. and VOTAVA, J. Slow synaptic excitation in sympathetic ganglion cells: evidence for synaptic inactivation of potassium conductance. *Science*, 170, 755-757, 1970.

WEIGHT, F.F. and WEITSEN, H.A. Identification of small intensely fluorescent (SIF) cells in the bullfrog. *Brain Res.*, 128, 197-211, 1977.

WEITSEN, H.A. and WEIGHT, F.F. Synaptic innervation of sympathetic ganglion cells in the bullfrog. *Brain Res.*, 128, 197-211, 1977.

- WILLIAMS, J.T., COLMERS, W.F. and PAN, Z.Z. Voltage- and ligand-activated inwardly rectifying currents in dorsal raphe neurons in vitro. J. Neurosci., 8, 3499-3506, 1988b.
- WILLIAMS, J.T., NORTH, R.A. and TOKIMASA, T. Inward rectification of resting and opiate-activated potassium currents in rat locus coeruleus neurons. J. Neurosci., 8, 4299-4306, 1988a.
- YALOW, R.S and BERSON, S.A. In Principles of competitive protein binding assays, Eds. Odell, W.D. and Daughaday, W.H., J.B. Lippincott Co., Philadelphia, Pa., USA, Ch. 1, 1971.
- YANAGIHARA, K. and IRISAWA, H. Inward current activated during hyperpolarization in the rabbit sinoatrial node cell. Pflugers Arch., 385, 11-19, 1980.
- YATANI, A., CODINA, J., BROWN, A.M. and BIRNBAUMER, L. Direct activation of mammalian atrial muscarinic channels by GTP regulatory protein G_r. Science, 235, 207-211, 1987.
- YAVARI, P. and WEIGHT, F.F. Effect of phentolamine on synaptic transmission in bullfrog sympathetic ganglia. Soc. Neurosc. Abs., 7, 807, 1981.
- YAVARI, P. and WEIGHT, F.F. Antagonists discriminate muscarinic excitation and inhibition in sympathetic ganglion. Brain Res., 400, 133-138, 1987.
- YAVARI P. and WEIGHT, F.F. Pharmacological studies in frog sympathetic ganglion: support for the cholinergic monosynaptic hypothesis for slow IPSP mediation. Brain Res., 452, 175-183, 1988.
- YEH, J.Z., OXFORD, G.S., WU, C.H. and NARAHASHI, T. Dynamics of aminopyridine block of potassium channels in squid axon membranes. J. Gen. Physiol., 68, 519-539, 1976.

- YOSHIMURA, M. Tonic and reflex discharges of sympathetic ganglion cells. J. Kurume Med. Assoc., 42, 1221-1238, 1979.
- ZIDICHOUSKI, J.A., CHEN, H. and SMITH, P.A. Neuropeptide Y activates inwardly-rectifying K⁺ channels in C-cells of amphibian sympathetic ganglia. Neurosci. Letts., (in press), 1990.
- ZIDICHOUSKI, J.A., KEHOE, M.P. and SMITH, P.A. Comparison of muscarinic and alpha₂-adrenergic hyperpolarizations in amphibian sympathetic ganglia. Proc. Can. Fed. Soc. Exptl. Biol., 30, 110 (1987).
- ZIDICHOUSKI, J.A., KEHOE, M.P., WONG, K. and SMITH, P.A. Elevation of intracellular cyclic AMP concentration fails to inhibit adrenaline-induced hyperpolarization in amphibian sympathetic neurones. Br. J. Pharmacol., 96, 779-784, 1989a.
- ZIDICHOUSKI, J.A., SELYANKO, A.A., KEHOE, M.P., RAFUSE, P.E. and SMITH, P.A. Three effects of adrenaline on sympathetic neurones. Proc. Can. Fed. Exptl. Biol., 32, 157, 1989b.
- ZIDICHOUSKI, J.A., SMITH, P.A., SELYANKO, A.A. and WONG, V. Analysis of muscarinic cholinergic inhibition. Can. J. Physiol. Pharmacol., 67, A42, 1989c.